ENGINE POWER FOR AGRICULTURAL MACHINES

2

INTRODUCTION

The earliest farm equipment made use of human power and, for a period in the 19th and 20th centuries, animals supplied the power needs of farm equipment. Modern agricultural equipment, however, is powered by *internal combustion (IC) engines* and, since the 1970s, nearly all new agricultural engines have been *compression ignition (CI) engines* that burn diesel fuel. The engine can be a part of the machine itself, as on a self-propelled combine, or can provide the power for an agricultural tractor.

Engines consume fuel to produce power. The power is delivered to some load through the crankshaft and flywheel of the engine. Much of the energy in the fuel is lost before it is converted to useful power. The purpose of this chapter is to clarify the processes by which an IC engine produces power and to provide insights into how engines may be made to operate efficiently. By reading this chapter, you will also learn the important terminology of diesel engines.

2.1 THE POWER IN FUEL

Liquid fuels are a highly concentrated form of chemical energy storage. Burning the fuel at even a modest rate releases a large amount of energy that can be calculated using Equation 2.1:

$$P_{fe} = \frac{H_g \dot{m}_f}{3600} \tag{2.1}$$

where P_{fe} = fuel equivalent power, kW

H_g = gross heating value of the fuel, kJ/kg

$\dot{m}_f$ = fuel consumption rate, kg/h

The heating values are measured by burning a sample of fuel in a calorimeter. The heating values are defined as gross (H_g) or net (H_n) depending on whether the water created in combustion is recovered as liquid or vapor, respectively. The terms higher

P_{fe} = Fuel Equivalent Power, kW
P_i = Indicated Power, kW
P_f = Friction Power, kW
P_b = Brake Power, kW
η_{it} = Indicated Thermal Efficiency, decimal
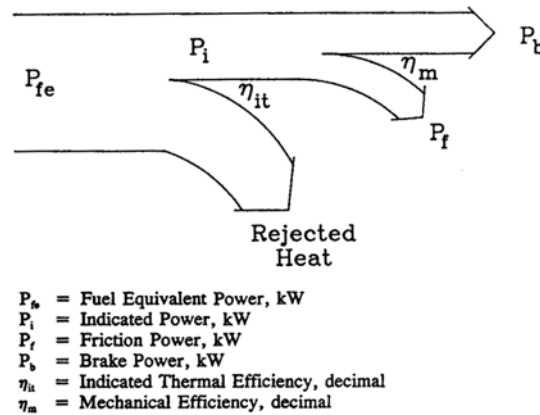η_m = Mechanical Efficiency, decimal

Figure 2.1 – Energy flows through an engine.

and lower are sometimes used instead of gross and net, respectively. Heating values tabulated in books (see Table 2.1) are gross values unless otherwise indicated. Less than half of the fuel equivalent power is available for useful work at the flywheel of an engine (see Figure 2.1). In the remainder of this chapter, the various power losses are identified.

2.2 COMBUSTION

Combustion is a very complex process, particularly in a CI engine. The fuel must vaporize and mix with air to form a combustible mixture. Burning of the fuel-air mixture generates exhaust emissions, but also generates increased pressure to drive the pistons. The rate of pressure rise affects engine performance and durability.

2.2.1 Combustion chemistry

Insights that are very useful in understanding engines can be obtained by making two simplifying assumptions regarding *combustion chemistry*. The first is that all of the hydrogen in the fuel links with oxygen to form water. The second is that all of the carbon in the fuel is converted to carbon dioxide (CO_2) and carbon monoxide (CO), so that no free carbon appears in the combustion products. Most conventional, petroleum-based engine fuels are mixtures of a variety of hydrocarbon molecules, but representative molecules are given in Table 2.1 for each of the common petroleum-based fuels. Alcohols, which may become engine fuels of the future, are also listed. Atomic weights of 12 for carbon, 1 for hydrogen, 16 for oxygen and 14 for nitrogen may be used in the combustion calculations. Although various gases are in the earth's atmosphere, it is common practice in combustion calculations to neglect all gases except oxygen and nitrogen. The composition of earth's atmosphere is such that 3.76 molecules of nitrogen (N_2) accompany every molecule of oxygen (O_2). Combustion chemistry then becomes a simple matter of counting atoms, as indicated in Example Problem 2.1.

Table 2.1. Comparison of properties of several fuels.

Fuel	API Gravity, degrees	Density, kg/m^3	Higher Heating Value, kJ/kg	Research Octane Number	Boiling Range, °C	Formula	Stoichio-metric Air-Fuel Ratio
Butane	112	580	49.500	98	0	C_4H_{10}	15.5
Propane	146	509	50,300	111	– 42	C_3H_8	15.7
Reg.gasoline	61	735	47,600	93	30 - 230	C_6H_{18}	15.2
No. 1 diesel	40	823	45,700	40[a]	160 - 260	$C_{12}H26$	15.0
No. 2 diesel	38	834	45,500	40[a]	200 - 370	$C_{16}H_{34}$	15.0
Methanol	---	792	22,700	110	65	CH_4O	6.49
Ethanol	---	785	29,700	110	78	C_2H_6O	9.03
Methyl soyate	---	885	38,379	51[b]		$C_{19}H_{36}O_2$	12.5

[a] Minimum cetane rating for diesel fuel
[b] Cetane rating

Example Problem 2.1

Calculate the *stoichiometric* (chemically correct) air/fuel ratio when diesel fuel is burned with air. Also analyze the products of combustion when No. 2 diesel is burned.

Solution

From Table 2.1, the cetane molecule ($C_{16}H_{34}$) is used to represent diesel fuel. Under the standard simplifying assumptions, the complete combustion reaction becomes:

$$C_{16}H_{34} + 24.5\ O_2 + 92.12\ N_2 \rightarrow 92.12\ N_2 + 16\ C0_2 + 17\ H_2O$$
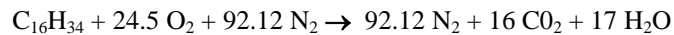
The reaction is balanced on the basis of one molecule of fuel. The hydrogen balance determines the amount of water in the combustion products, while the carbon balance determines the amount of CO_2. Then enough O_2 must be supplied to form the CO_2 and H_2O; each mole of O_2 is accompanied by 3.76 moles of N_2. The nitrogen is nearly inert and simply appears in the combustion products. The *stoichiometric air/fuel ratio* is:

$$A/F = (24.5 \times 32 + 92.12 \times 28) / 226 = 14.9$$

Note that 17 moles of water appear in the exhaust for each mole of fuel burned or, on a mass basis, 1.35 kg of water appear per kilogram of fuel burned. The difference between the gross and net heating values of the fuel is exactly equal to the latent energy of the water produced by combustion, i.e., the energy needed to convert that liquid water to vapor. A major reason why quick warm up of engines is important is to cause the combustion water to exit the engine as vapor rather than liquid. If the fuel contains sulphur impurities, the sulphur compounds created in combustion can react with liquid water to form sulfuric acid and corrode the engine.

Engine exhaust gases are normally analyzed on a dry, volume basis. Since the exhaust gases are intermingled at the same temperature and pressure, each molecule occupies the same volume according to Avogadro's Law. Thus, the analysis of the dry exhaust gases in Example Problem 2.1 is:

$92.12 / (92.12 + 16) = 0.852$ volume fraction (85.2%) is occupied by N_2,

and $16 / (92.12 + 16) = 0.148$ volume fraction (14.8%) is occupied by CO_2.

The equivalence ratio, ϕ, is a measure of mixture richness. It is defined as follows:

$$\phi = \frac{(F/A)_{actual}}{(F/A)_{stoichiometric}} \tag{2.2a}$$

or

$$\phi = \frac{(A/F)_{stoichiometric}}{(A/F)_{actual}} \tag{2.2b}$$

Note that the F/A ratio is just the inverse of the A/F ratio. Thus, in Example Problem 2.1, the stoichiometric ratios were A/F = 14.9 or F/A = 0.0671. An air-fuel mixture is rich if $\phi > 1$, stoichiometric if $\phi = 1$, or lean if $\phi < 1$. A rich mixture contains more fuel than the available oxygen can combust, while a lean mixture contains more oxygen than is theoretically needed to combust all the fuel. When $\phi > 1$, not enough oxygen is available to convert all the carbon in the fuel to CO_2; consequently, CO appears in the exhaust. When $\phi < 1$, not all of the oxygen is needed in combustion and free oxygen appears in the exhaust products. For a spark ignition engine, ϕ must be reasonably close to unity to sustain combustion. For a compression ignition engine, ϕ should not exceed 0.7 to prevent engine damage.

The following *generalized combustion reaction* is valid for any air-fuel mixture under the two simplifying assumptions given earlier:

$$C_x H_y O_z + \frac{\psi_1}{\phi} O_2 + 3.76 \frac{\psi_1}{\phi} N_2 \rightarrow$$
$$3.76 \frac{\psi_1}{\phi} N_2 + \psi_2 CO_2 + \psi_3 CO + \psi_4 O_2 + \frac{y}{2} H_2 O \tag{2.3}$$
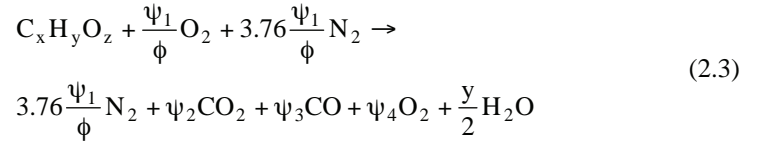
where x = number of carbon atoms in fuel molecule
   y = number of hydrogen atoms in fuel molecule
   z = number of oxygen atoms in fuel
   $\Psi_1 = x + y/4 - z/2$
   $\Psi_2 = x$ for $\phi \leq 1$
        $x - 2\Psi_1 (1 - 1/\phi)$ for $\phi > 1$
   $\Psi_3 = 0$ for $\phi \leq 1$
        $2\Psi_1 (1 - 1/\phi)$ for $\phi > 1$
   $\Psi_4 = \Psi_1 (1/\phi - 1)$ for $\phi < 1$
        0 for $\phi \geq 1$

Note that the Combustion Reaction 2.3 accommodates *oxygenated fuels*, such as the alcohols in Table 2.1. The number of carbon, hydrogen, and oxygen atoms need not be integer numbers. The stoichiometric air/fuel ratio for the combustion is:

$$A/F = \frac{137.3\psi_1}{\phi(12x + y + 16z)} \qquad (2.4)$$

The theoretical concentrations of the *dry* exhaust products on a volume basis are:

$$\text{Conc. } N_2 = 3.76\ \Psi_1/(\phi\ T) \qquad (2.5a)$$

$$\text{Conc. } CO_2 = \Psi_2/T \qquad (2.5b)$$

$$\text{Conc. } CO = \Psi_3/T \qquad (2.5c)$$

$$\text{Conc. } O_2 = \Psi_4/T \qquad (2.5d)$$

where $T = \Psi_2 + \Psi_3 + \Psi_4 + 3.76\Psi_1/\phi$.

Equations 2.5a through 2.5d give good approximations to actual exhaust emissions, except that minute amounts of other gases also appear. A small amount of oxygen and nitrogen react with each other to form oxides of nitrogen, i.e., NO and NO_2. The combined NO and NO_2 gases are commonly referred to as NO_x. Also, ϕ is typically not uniform throughout all of the combustion chambers of an actual engine. Thus, small amounts of CO and O_2 may appear in the exhaust whether the overall ϕ is less than or greater than one. Some free carbon may also appear, as well as trace amounts unburned hydrocarbons (HC), hydrogen, and other gases.

2.2.2 Energy release in combustion

The purpose of the combustion reaction is to release energy to drive the pistons. A cross section of a typical diesel engine is shown in Figure 2.2. The combustion process can be carried out in either two or four strokes of the piston, but the four-stroke cycle is most common. Unless otherwise indicated, all engines discussed in this book will be assumed to use the four-stroke cycle.

Through a combined experimental and analytical technique, it is possible to infer the *rate of energy release* throughout the combustion process. The technique relies on measurement of combustion chamber pressures in a running engine while simultaneously measuring the crankshaft rotation, and computing the volume within the combustion chamber. The spatially averaged temperature in the combustion chamber can be calculated from the pressure and volume. Then, from changes in pressure, volume, and temperature, the heat loss through the chamber walls, work done on the piston, and changes in internal energy of the mixture in the combustion chamber can be calculated. The energy released from the fuel is equal to the sum of the heat loss, work, and increases in internal energy. Figure 2.3 shows a typical energy release diagram for a diesel engine; the rate of energy release is plotted versus crankshaft position.
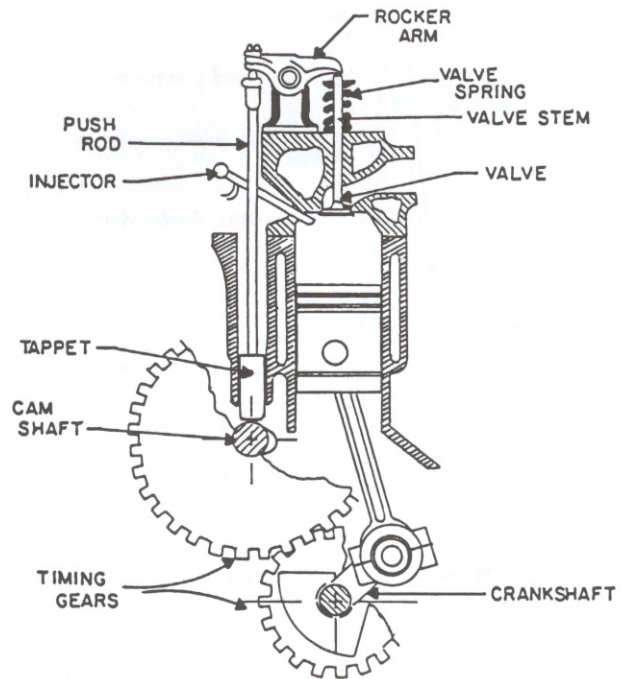
Figure 2.2 – Cross section of a typical diesel engine.
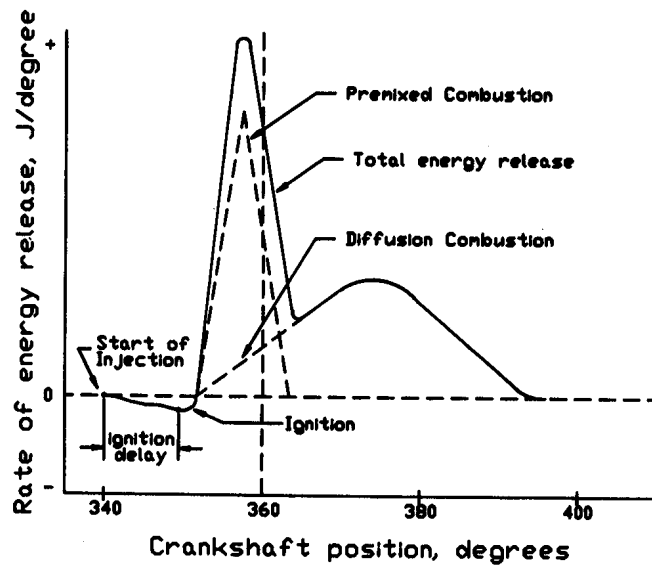

Figure 2.3 – Rate of energy release from fuels in a compression ignition engine.

In a diesel engine, air without fuel is taken in during the intake stroke and compressed. Late in the compression stroke, at approximately 20° before HDC (Head Dead Center), injection of fuel into the combustion chamber begins. An apparent negative energy release rate appears initially as energy is withdrawn from the chamber to evaporate the injected fuel. The evaporated fuel mixes with air and undergoes certain pre-reactions during an ignition delay period. Then ignition occurs and all of the air-fuel mixture prepared during the ignition delay burns suddenly to produce a sharp, triangular-shaped energy release pattern identified as *premixed combustion*. For combustion to continue, fuel vapor and air must diffuse toward each other across the regions burned out in the premixed combustion. The rate of diffusion limits the latter combustion, which is identified as *diffusion combustion*. The total energy release is the sum of the premixed and diffusion combustion. Premixed combustion is efficient and, except for the production of NO_x, is also clean combustion. However, the rapid release of energy produces the greatest stress on the engine and also most of the combustion noise. The slower diffusion burning is quieter and less stressful on the engine, but produces exhaust smoke and most of the CO emissions and is less efficient. Using fuels of higher cetane rating and less-advanced injection timing shifts more of the combustion from the premixed to the diffusion mode; the converse is also true.

In a diesel engine, the air supply is never throttled to control the engine speed. Rather, control is achieved by controlling only the fuel delivery rate. Consequently, ϕ is close to zero when the engine is idling without load and increases as more fuel is injected with increasing load. To limit smoke emissions and avoid excessive engine temperatures, it is necessary to operate a diesel engine with ϕ below approximately 0.7. As Reaction 2.3 and Equation 2.5d would show, considerable free oxygen appears in the exhaust when $\phi = 0.7$ or less. Engine users sometimes increase the fueling rate to diesel engines to take advantage of the extra oxygen and boost the power output of the engine, but at the cost of reduced engine life. For their own protection, engine manufacturers put a seal on the injector pumps of their engines; if the seal is broken to increase the fueling rate, the engine warranty is automatically voided.

2.3 THERMODYNAMIC LIMITS TO ENGINE PERFORMANCE

The effective pressure that can be obtained from fuel to drive the pistons and also the combustion efficiency have thermodynamic limits which are defined in this section. The engine is designed to carry out the combustion cycle in four strokes of the piston. As is required in an engine with a *four-stroke cycle*, the timing gears in Figure 2.2 are arranged such that the crankshaft makes two revolutions for each revolution of the camshaft. Valve timing in a four-stroke cycle is shown on a valve-timing spiral, as illustrated in Figure 2.4. Valve timing is designed to maximize airflow through the engine and may differ somewhat from that shown in Figure 2.4. The cycle begins just before *HDC (Head Dead* Center) with the opening of the intake valve, and the air intake process ends well after *CDC (Crank Dead Center)* with the closing of the intake valve. As the piston approaches HDC on the compression stoke, fuel is injected and, after a short delay, ignites and forces the piston down on the power stroke. The

exhaust process begins with the opening of the intake valve late in the power stroke and ends with the closing of the exhaust valve soon after HDC. Thus, the four strokes of the cycle are intake, compression, power, and exhaust. Note that there is valve overlap, i.e., both valves are open simultaneously during a brief part of the cycle. Alternate terms used in the literature are TDC (Top Dead Center) instead of HDC and BDC (Bottom Dead Center) instead of CDC.

The *dual cycle* of Figure 2.5 is the best thermodynamic model of the modern diesel engine. It illustrates the theoretical variations in combustion gas pressure and cylinder volume during an engine cycle. The dual cycle is a combination of the Otto cycle, which represents spark ignition engines, and the original Diesel cycle that Dr. Rudoph Diesel proposed to represent his engine. Parameter γ defines the relative proportion of energy input to the dual cycle at constant pressure, i.e.:

$$\gamma = \frac{q_p}{q_p + q_v} \tag{2.6}$$

where q_p = energy input at constant pressure
        q_v = energy input at constant volume

C   = COMPRESSION
E   = EXHAUST
P   = POWER
I   = INTAKE
IVO = INTAKE VALVE OPENS
IVC = INTAKE VALVE CLOSES
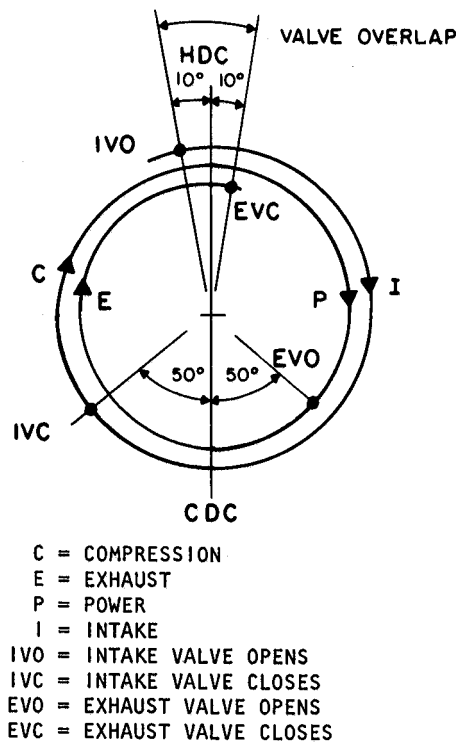EVO = EXHAUST VALVE OPENS
EVC = EXHAUST VALVE CLOSES

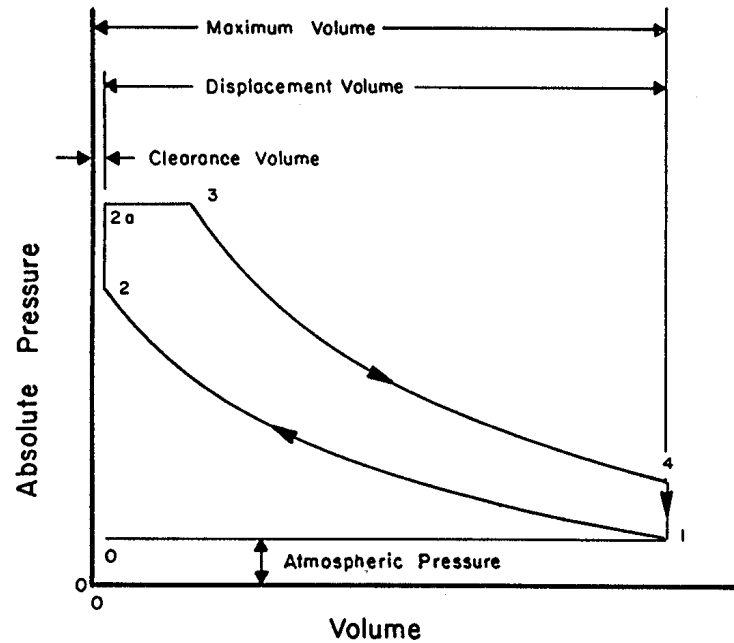**Figure 2.4 – Valve timing spiral showing typical valve timing.**

Figure 2.5 – The theoretical dual cycle.

When $\gamma = 0$, the dual cycle becomes the Otto cycle with points 2a and 3 becoming coincident (Figure 2.5). When $\gamma = 1$, the dual cycle becomes the original Diesel cycle with points 2 and 2a becoming coincident.

In the dual cycle, 0-1 is the intake process, followed by compression, 1-2. Process 2-2a is energy input to the cycle at constant volume and 2a-3 is constant-pressure energy input. Work is extracted from the cycle between points 2a and 3, followed by heat rejection, 4-1. Process 1-0 is exhaust, at which point the cycle starts over. The cylinder volume at CDC, V_1, is the *maximum gas volume*. The cylinder volume at HDC, V_2, is called the *clearance volume*. The *displacement* of a single cylinder is:

$$V_c = V_1 - V_2 \tag{2.7}$$

The displacement, V_e, of a multi-cylinder engine is simply V_c times the number of cylinders. The compression ratio of the engine is:

$$r = \frac{V_1}{V_2} \tag{2.8}$$

The *cycle mean effective pressure* is the net area within the p-v diagram of Figure 2.5 divided by V_c. Multiplying the cycle mean effective pressure by the piston area and stroke length gives the actual work performed by each power stroke. The cycle mean effective pressure can be calculated from:

$$\frac{p_{cme}}{p_1} = \frac{r - r^k + \Theta_r[r - r^{2-k}r_{co}^{k-1} + r\,r_{co}^{-1}(k-1)(r_{co}-1)]}{(k-1)(r-1)} \tag{2.9}$$

where p_{cme} = cycle mean effective pressure, kPa

$\quad$ p_1 = absolute pressure at beginning of compression, kPa

$\quad$ $\Theta_r = \Theta_3/\Theta_1$

$\quad$ $\lambda = k(\gamma^{-1} - 1)$

$\quad$ $r_{co} = (\lambda + 1)/(\lambda + (\Theta_3/\Theta_1)r^{k-1})$ = fuel cutoff ratio

$\quad$ $k = 1.4$ for air standard cycle

The pressure, p_1, is very nearly equal to the atmospheric pressure unless the engine is turbocharged. The fuel cutoff ratio is defined as the proportion of the power stroke during which energy is being released into the cycle from the burning fuel. The *cycle efficiency* is defined as:

$$\eta_{cy} = \frac{q_v + q_p - q_{out}}{q_v + q_p}$$

where each heat transfer quantity is calculated from the mass (M) in the combustion chamber, multiplied by the appropriate specific heat and temperature difference, i.e.:

$$q_v = Mc_v(T_{2a} - T_2)$$

$$q_p = Mc_p(T_{2a} - T_3)$$

$$q_{out} = Mc_v(T_4 - T_1)$$

where c_v = specific heat at constant volume, J/kg °K

$\quad$ c_p = specific heat at constant pressure, J/kg °K

$\quad$ $k = c_p/c_v$

The temperatures are those at the corresponding points in the cycle of Figure 2.5. Note that the mass (M) cancels out in the efficiency equation. Through use of the definition of k, the specific heats also cancel out of the efficiency equation. Then, in a lengthy derivation making use of the ideal gas law, the temperatures can be reduced to volume ratios (r or r_{co}) and the inlet pressure, p_1. The result is the following equation for cycle efficiency:

$$\eta_{cy} = 1 - \frac{\gamma(r_{co}^k - 1) + k(r_{co} - 1)(1 - \gamma)r^{1-k}}{k(r_{co} - 1)} \tag{2.10}$$

The theoretical values, p_{cme} and η_{cy}, cannot be achieved in practice, but are thermodynamic upper limits and targets against which practical designs can be compared.

Example Problem 2.2

Assume that the compression ratio of a NA (naturally aspirated, i.e., not turbocharged) diesel engine is r = 14.5. For typical conditions, estimate the cycle mean effective pressure and the cycle efficiency if $\gamma = 0.2$.

Solution

An estimate is needed for the ratio, Θ_3 / Θ_1. If the ambient temperature is 27°C, then $\Theta_1 = 300°K$. It is common practice to estimate Θ_3 as being equal to the equilibrium flame temperature for hydrocarbon fuels, i.e., $\Theta_3 = 2700°K$. Thus, for a NA diesel engine, a good estimate is $\Theta_3 / \Theta_1 = 9$. Then, using Equations 2.9, 2.10, and the supplementary equations that support them:

$\Theta_r = 8.078$
$r_{co} = 1.114$
$p_{cme}/p_1 = 11.36$
$\eta_{cy} = 0.655$

Theoretically, the specified cycle can convert 65.5% of the input energy to useful work. For a NA diesel engine, p_1 is approximately equal to barometric pressure or, approximately, $p_1 = 100$ kPa. Then $p_{cme} = 1136$ kPa. Because of friction and other losses, the theoretical efficiency and mean effective pressure cannot be achieved in practice, but it is possible to achieve at least 75% of the theoretical values.

2.4 HEAT LOSSES AND POWER AT THE PISTONS

Energy is liberated from the fuel when Combustion Reaction 2.3 occurs. The released energy causes a sharp rise in cylinder pressure but the pressure diminishes as the piston moves toward CDC. Through proper instrumentation, it is possible to obtain a plot similar to Figure 2.5, except that actual (not theoretical) cylinder pressure is plotted versus volume. Historically, cylinder pressures were plotted on indicator diagrams and thus the net area within the actual p-v diagram, divided by V_c, is called the indicated mean effective pressure, p_{ime}. Multiplying p_{ime} by the top area of the piston gives the average force exerted on the piston during the power stroke. Multiplying force by the stroke length gives the work per stroke and multiplying by the number of strokes per unit time gives the indicated power for a single-cylinder engine. Finally, multiplying by the number of cylinders gives the indicated power for the entire engine. Note, however, that the product of piston area times stroke times number of cylinders gives the engine displacement, V_e. Thus, the *indicated power* (power generated at the head of the pistons) for an engine can be calculated from:

$$P_i = \frac{p_{ime} V_e n_e}{2(60,000)} \tag{2.11}$$

where P_i = indicated power, kW

   p_{ime} = indicated mean effective pressure, kPa

   V_e = engine displacement, L

   n_e = engine speed, rev/min

The factor 2 is in the denominator of Equation 2.11 because 2 revolutions of the crankshaft are required for each power stroke in a four-stroke cycle engine. The factor 60,000 is simply a units constant. Equation 2.11 brings out the important point that only three ways are available to increase engine power. They are (1) increase the size (V_e) of the engine, (2) increase its speed (n_e), or (3) increase the pressure levels (p_{ime}) in the engine.

The indicated power is always less than the fuel equivalent power. The *indicated thermal efficiency* of an engine is defined as:

$$\eta_{it} = \frac{P_i}{P_{fe}} \tag{2.12}$$

The fraction $(1 - \eta_{it})$ of P_{fe} is not converted into work but is rejected as heat (Figure 2.1). Some of the rejected heat can be recovered using heat exchangers if there is a need for heat in the vicinity of the engine; otherwise the heat is lost. The cycle efficiency, η_{cy}, is an upper limit for η_{it} and a target against which achieved values of η_{it} can be compared.

2.5 MECHANICAL LOSSES AND POWER AT THE FLYWHEEL

After combustion and mechanical losses are subtracted, the remaining power reaching the flywheel is called *flywheel power*. The earliest devices used to measure engine power were called prony brakes, and thus flywheel power is more commonly called *brake power*. With modern technology, a device called a dynamometer is used to measure the torque and speed of the power shaft connected to the engine flywheel. If T_b is the torque in a shaft, the work accomplished per revolution of the shaft is equal to $2\pi T_b$. Then, since the engine speed gives the revolutions per unit of time, the brake power can be calculated from the following equation:

$$P_b = \frac{2\pi T_b n_e}{60,000} \tag{2.13}$$

where P_b = brake power, kW

   T_b = engine brake torque, N·m

The factor 60,000 is a units conversion factor.

The *mechanical efficiency*, η_m, is the fraction of P_i that is converted to brake power (Figure 2.1), i.e.:

$$\eta_m = \frac{P_b}{P_i} \tag{2.14}$$

By definition, all of the indicated power not converted to brake power is called *friction power*, i.e.:

$$P_f = P_i - P_b \tag{2.15}$$

What is included in friction power? All the friction of moving parts in the engine is included, as the name implies, but power to operate the fan, oil pump, alternator, and other engine accessories is also included.

Engine users are interested in the overall efficiency of the engine in converting fuel equivalent power to brake power. The overall efficiency is called the *brake thermal efficiency*, i.e.:

$$\eta_{bt} = \frac{P_b}{P_{fe}} \tag{2.16a}$$

It is easy to show that the following equation is true:

$$\eta_{bt} = \eta_{it}\, \eta_m \tag{2.16b}$$

Thus, for good overall efficiency, engine designers must design an efficient combustion process (high η_{it}) and a high percentage of the resulting power must be transmitted to the flywheel (high η_m).

Equation 2.11 shows that, for a given engine running at a given speed, P_i is proportional to p_{ime}. Engine designers have broadened that concept in defining *brake mean effective pressure*, p_{bme}, as:

$$p_{bme} = \frac{2(60{,}000)P_b}{V_e n_e} \tag{2.17}$$

and in defining friction mean effective pressure, p_{fme}, as:

$$p_{fme} = \frac{2(60{,}000)P_f}{V_e n_e} \tag{2.18}$$

In a diesel engine, p_{fme} is almost entirely a function of speed, i.e.:

$$p_{fme} = C_0 + C_1 n_e + C_2 n_e^2 \tag{2.19}$$

where C_0, C_1 and C_2 are constants that vary from engine to engine. The following approximate values were presented by SAE for the purpose of estimating the mechanical efficiency of a diesel engine:

$C_0 = 139.3$ kPa

$C_1 = -0.0259$ kPa·min/rev

$C_2 = 22.97 \times 10^{-6}$ kPa/(rev/min)^2

More accurate values can be obtained for a specific engine by fitting a curve to friction mean effective pressure values at various engine speeds. An important practical

consequence of Equation 2.19 is that engine friction power can be reduced and engine efficiency can be increased by running engines at reduced speeds.

The reader is encouraged to derive a relationship between the several mean effective pressures and to express η_m in terms of mean effective pressures.

2.6 ENGINE TORQUE AND EFFICIENT ENGINE LOADING

Combining Equations 2.12, 2.13, 2.15, and 2.19 provides an equation which gives insights into how an engine produces torque, i.e.:

$$T_b = \frac{H_g \eta_{it}}{4\pi} \left[\frac{C_f \dot{m}_f}{n_e} \right] - \frac{V_e}{4\pi} p_{fme} \tag{2.20}$$

where $C_f = 2(1000/60)$ = units conversion factor

$(C_f m_f / n_e)$ = grams of fuel injected per engine cycle

In Equation 2.20, the term between the equal sign and the minus sign is called indicated torque, while the last term in the equation is *friction torque*. Thus, the net or brake torque is the indicated torque minus the friction torque. Since H_g (the heating value of the fuel) is constant and η_{it} varies only a little with changes in torque and speed, the indicated torque varies nearly proportionally with the quantity of fuel injected into each engine cycle. As explained in Section 2.2.7, the quantity of fuel injected into each cycle is controlled by an *engine governor*.

Combining Equations 2.14, 2.15 and 2.16a gives the following alternate equation for brake thermal efficiency:

$$\eta_{bt} = \eta_{it} P_b / (P_b + P_f) \tag{2.16c}$$

Figure 2.6 is a plot of Equation 2.16c and illustrates the relationship of engine efficiency to load. All engines are most efficient at full load and are especially inefficient as the engine load approaches zero.

Engine designers have developed the term *SFC (Specific Fuel Consumption)* to indicate how much fuel is burned by an engine to accomplish a given amount of work. It is defined as:

$$SFC = \frac{\dot{m}_f}{power} \tag{2.21}$$

Because of losses in the transmission of power, it is important to use an adjective with SFC to indicate the point of power measurement. The two most common SFC terms in the literature are BSFC (for Brake SFC, i.e., when the denominator of Equation 2.21 is brake power) and ISFC (for Indicated SFC). Like η_{bt}, BSFC is an indicator of overall engine efficiency, except that BSFC is lowest when the engine is most efficient.
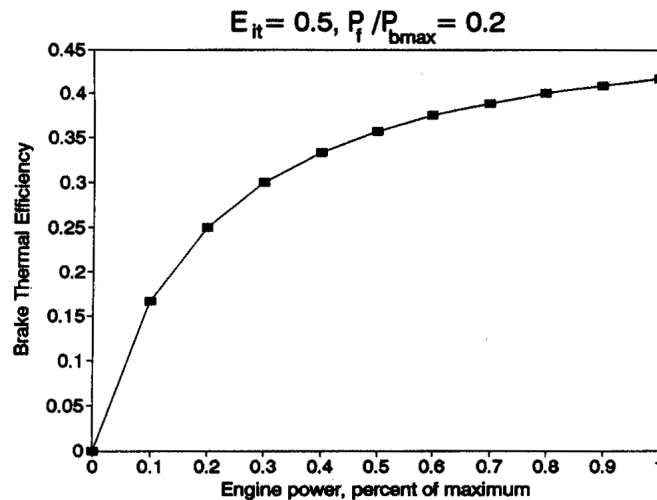
Figure 2.6 – Variation of brake thermal efficiency with engine load.

2.7 CONTROL OF ENGINE SPEED

It is desirable to perform many agricultural operations at nearly constant speed. Governors control speed by reducing fuel delivery to the engine when the speed is too high and increasing fuel delivery when the speed is too low. A *flyweight governor* is illustrated in Figure 2.7. The flyweights are hinge-connected to the governor shaft, which typically rotates at one-half of crankshaft speed. In the unit shown in Figure 2.7a, centrifugal force from increasing engine speed causes the weights to swing outward and the flyweight linkage forces the thrust bearing downward. The governor linkage rotates counterclockwise, stretching the spring and reducing fuel delivery. Conversely, reductions in engine speed allow the spring to contract, forcing the flyweights inward and increasing fuel delivery.

The force induced on the thrust bearing by centrifugal force on the flyweights varies proportionally with the radius of the path of the flyweights and with the square of the engine speed. Figure 2.7b shows curves for the limiting cases when the path radius is smallest (weights in) and largest (weights out). The governor can only operate between these two limiting curves.

If an ungoverned engine was receiving fuel at even a moderate rate and was running without load, the speed would quickly become excessive and destroy the engine. In a governed engine, however, the flyweights would swing out to their limit and fuel delivery would fall to a level sufficient to provide only the friction power of the engine. The engine would operate at point A on Figures 2.7b and 2.7c, which is called the *High Idle point* because the speed is high and the engine is idling (not doing any work). As an increasing torque load is applied to the engine, the flyweights move
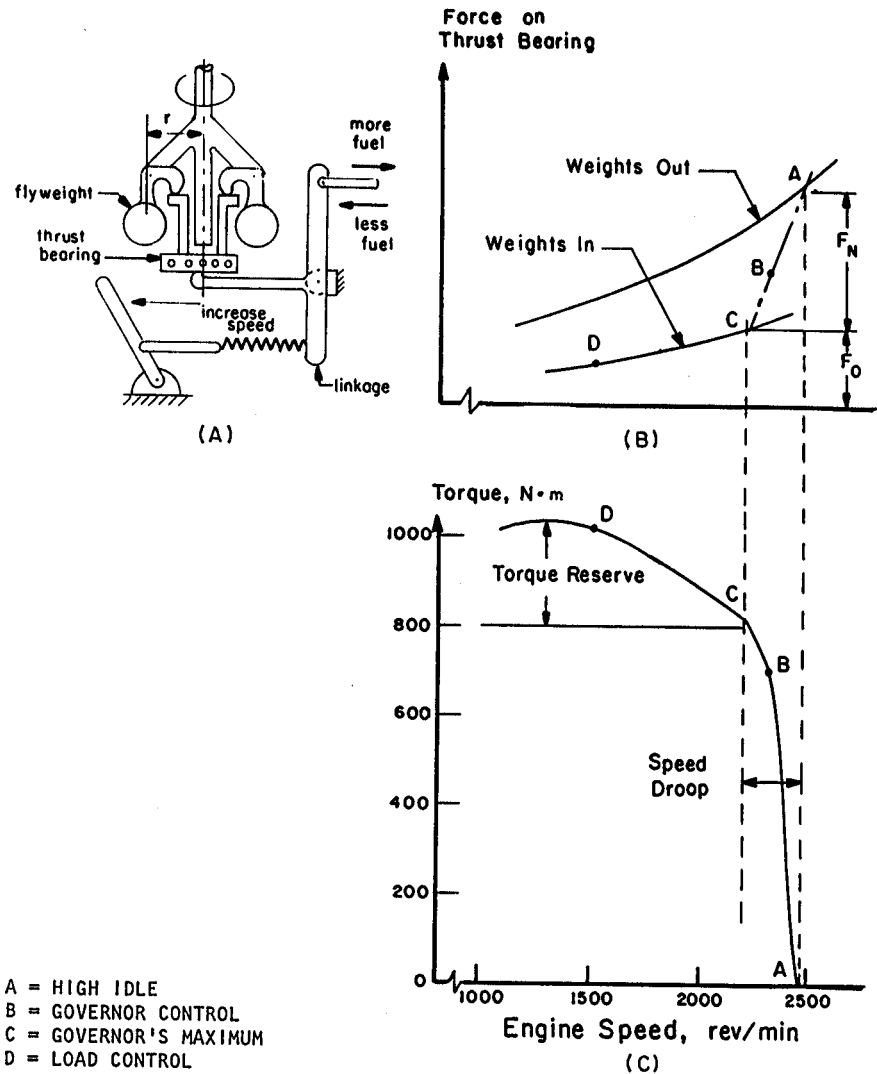
Figure 2.7 – Action of an engine governor.

inward to increase the stroke of the fuel injector pump and supply the fuel needed to provide that torque (see Equation 2.20). At point C in Figure 2.7, the flyweights are at their innermost position and cannot move the governor linkage or increase the injector pump stroke any further; thus Point C is called *Governor's Maximum*. With further increases in torque, the speed begins to fall rapidly because the governor cannot increase the fuel delivery per cycle. At points to the left of point C in Figure 2.7c, speed is controlled only by the torque load on the engine. Thus, the engine is under

governor control at points between A and C and under load control at points to the left of point C. Torque increases are possible in the *load-controlled range* because friction torque declines with speed (see Equation 2.20) and because injector pumps gain somewhat in pumping efficiency as speed decreases.

Governors cannot maintain perfectly uniform speed, even in the governor-controlled range. The *governor regulation*, as calculated in Equation 2.22, is a measure of how closely the governor controls the engine speed.

$$\mathrm{Reg}_g = \frac{200(n_{HI} - n_{GM})}{(n_{HI} + n_{GM})} \tag{2.22}$$

where Reg_g = governor regulation, %

n_{HI} = engine speed at high idle, rev/min

n_{GM} = engine speed at governor's maximum, rev/min.

The curves in Figures 2.7b and 2.7c show the governor controlling the engine at one speed setting. By moving the hand lever to the right, the operator can decrease the initial tension in the governor spring and thereby decrease the speed required to move the flyweights outward. The effect is to move curve ABC to the left, where it meets the load-control curve at some higher value of torque (see Figure 2.8a). Conversely, if the linkage stop will permit it, the operator can increase the speed setting of the engine by moving the speed control lever to the left. Manufacturers typically rate their engines at the governor's maximum speed that corresponds to the fastest setting of the governor. In Figure 2.8, for example, the highest governor's maximum speed is at 2200 rev/min and that would be the rated speed of the engine.

As shown in Figure 2.7c, *torque reserve* is defined as the difference between the peak torque of the engine and the torque at *rated speed*. Large torque reserve is desirable to prevent the engine from stalling during momentary overloads. Torque reserve is expressed as a percentage of rated torque. In Figure 2.7c, for example, the peak torque is 1020 N·m and the rated torque is 820 N·m, so the torque reserve would be 24.4%. It is also desirable for the torque peak to be well to the left of governor's maximum. In Figure 2.7c, the torque peak is at 1300 rev/min while rated speed is 2200 rev/min. Therefore, the torque peak appears at 59% of rated speed.

Figure 2.8b shows a power versus speed curve that results from the torque versus speed curve of Figure 2.8a. From Equation 2.13, the power rises nearly linearly with torque in the governor-controlled range because the speed varies little. Torque varies only modestly in the load-controlled range, so power falls in nearly direct proportion to the fall in speed. Some engine manufacturers market "constant power" engines; these are engines with sufficient torque rise to offset the falling speed in the load-controlled range, so that the power doesn't begin to fall until operation has moved some distance into the load-controlled range.
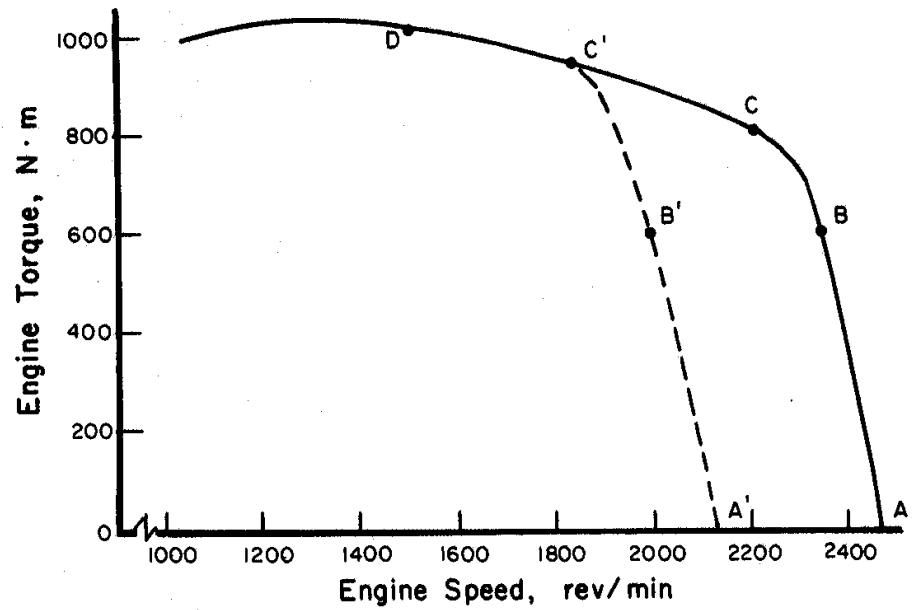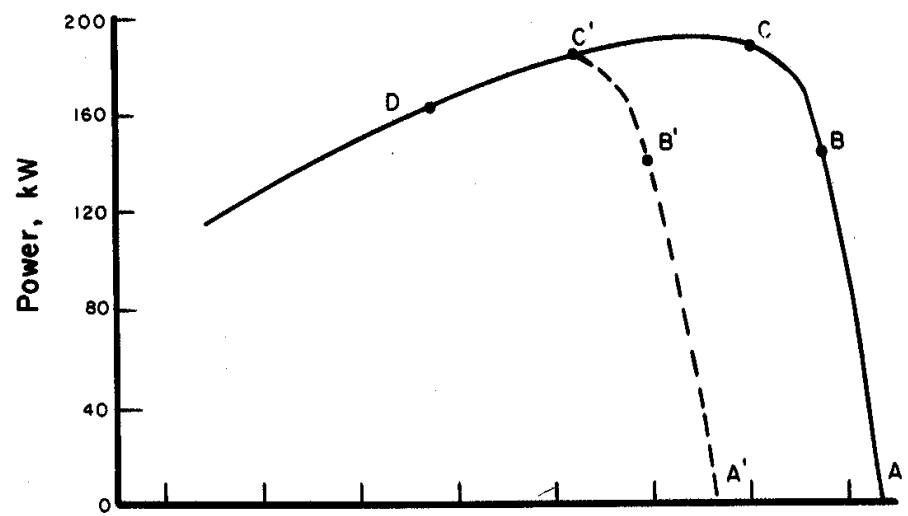
Figure 2.8 – Torque-speed and power-speed curves for a governed engine.

2.8 ENGINE PERFORMANCE SIMULATOR

A computer-based engine simulator (in the CD included with this book) was developed by the authors to allow the user to explore the operation of a compression-ignition engine. The simulator incorporates the same controls that would be found when performing a dynamometer test on an engine. The simulator user input data to specify the engine operating limits. Given these limits, the simulator computes operating variables under user-specified speed and load settings using equations from this chapter.

The simulator includes two screens. The first, Figure 2.9, is used to define the operating properties of an engine and the fuel. The second, Figure 2.10, is the engine control/display console. The model assumes that governor control is along a straight line between the high idle and governor's maximum points, while load control is on another straight line between the governor's maximum and peak torque points. The first five inputs in the specifications page fix the high idle, governor's maximum, and peak torque points on the engine map. The simulated torque is set by the position of the engine load slider on the console (Figure 2.10), and engine speed is calculated to maintain operation on the torque-speed lines described above. The remaining engine

Figure 2.9 – Engine and fuel specifications panel.

specifications are the engine displacement, volumetric efficiency under naturally aspirated (NA) conditions, and whether the engine is fitted with a turbocharger or not. The volumetric efficiency is used with the engine displacement and speed to calculate the air consumption at each simulated point selected by the user. Also at each point, the program calculates the brake power and estimates the brake thermal efficiency, then uses these data and the heating value of the fuel to calculate the fuel consumption needed to produce the brake power. Values of engine speed, torque, power and fuel consumption are displayed on the lower left quadrant of the control panel (Figure 2.10).

The volumetric efficiency of a naturally-aspirated engine is held at 85%. For a turbocharged engine, the volumetric efficiency is assumed to be 85% until load is applied to the engine. At each simulated engine load, the program estimates the turbocharger boost, then uses pressure and temperature ratios to estimate the volumetric efficiency. The program uses the calculated airflow and fuel consumption to calculate the fuel-air ratio of the combustion and the equivalence ratio.

The engine control and display console (Figure 2.10) allows the user to interact directly with the engine to observe its responses on an instantaneous basis. The display console has four quadrants. The top quadrants have user controls. Sliders allow adjustment of the governor setting and the engine load. Engine operating states are reported. Lights indicate when the engine is operating under governor control or load
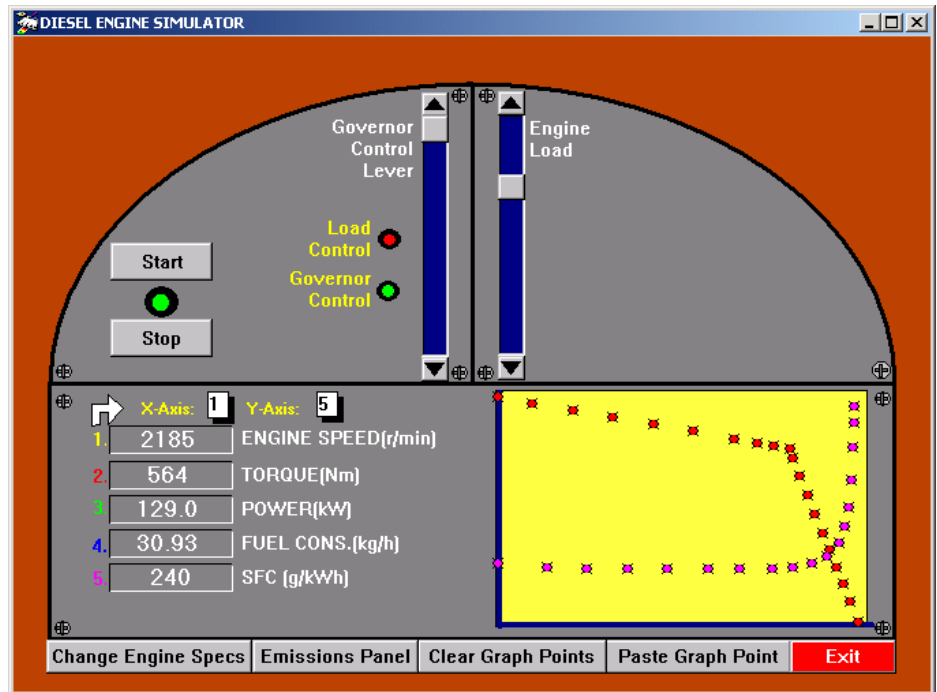

Figure 2.10 – Engine control and display console.

control and whether the engine is turbocharged. Clicking on the start button "starts" the engine and the red light below this button changes to green. Then the user adjusts the two sliders to control the governor setting and load. If the engine reaches stall, for instance when the engine is overloaded, a stall message appears and it is necessary to restart the engine. An emissions panel is displayed in the top right quadrant when activated by a button at the bottom of the console.

The bottom left quadrant of the simulator reports the current speed, torque, power, fuel consumption, and specific fuel consumption (SFC). The operator can also select these variables as axes for the graphical portion of the simulator in the lower right quadrant. The graphical window allows the user to visualize the operating characteristics of the simulator as load or the governor control sliders are adjusted. The current state of the engine is represented as a red dot. Buttons at the bottom of the console are used to paste points onto the graph and also to clear them. The different variables are color-coded so that they can be identified on the graph. As the governor setting or engine load are changed, the point on the graph moves.

As with any simulation, the user to must provide realistic inputs. For example, specifying a rated torque that is too high for the specified engine displacement and high idle speed will result in a too-rich fuel-air mixture (as indicated by the equivalence ratio) when the engine is fully loaded. As discussed earlier, the equivalence ratio of a compression-ignition engine should not go much above 0.7 to avoid engine overheating and damage.

2.9 TURBOCHARGING AND INTERCOOLING ENGINES

Power generation in an engine increases in proportion to the fueling rate, as indicated by Equation 2.1. To keep the equivalence ratio below 0.7, the air delivery rate must be much larger than the fuel delivery rate; thus it is air handling capacity that truly limits the power producing capacity of an engine. The *air handling capacity* can be calculated using the following equation:

$$\dot{m}_a = C_a V_e n_e \rho_a \eta_v \tag{2.23}$$

where $\dot{m}_a$ = air handling capacity, kg/hr

$C_a = 0.03$ = constant to convert units
V_e = engine displacement, L
n_e = engine speed, rev/min
ρ_a = density of the air entering the engine, kg/m3
η_v = *air delivery ratio* of the engine, a decimal

The air delivery ratio, or *volumetric efficiency* as it is sometimes called, is a measure of the air-pumping efficiency of an engine. It is equal to the ratio of the actual air handling capacity divided by the theoretical capacity that could be obtained at the same engine speed if each cylinder filled entirely with atmospheric air during each intake stroke. If the engine has no turbocharger, pressure drops in the intake system cause the air delivery ratio to be less than one. Conversely, a turbocharger delivers

pressurized air for intake and the air delivery ratio can be greater than one. The following equation, which was derived from the *ideal gas law*, can be used to calculate ρ_a if the barometric pressure and the ambient temperature are known:

$$\rho_a = \frac{29p_a}{8.314\Theta_a} \tag{2.24}$$

where p_a = air pressure, i.e., barometric pressure, kPa

$\quad\quad$ Θ_a = ambient air temperature, °K

Under most atmospheric conditions, ρ_a will be between 1.1 and 1.2 kg/m^3.

$\quad$ The air delivery ratio of a typical *naturally-aspirated (NA)* diesel engine is approximately 0.85; the air-handling capacity of a NA diesel engine can only be increased by increasing the displacement or the engine speed. However, the air delivery ratio and air handling capacity can be greatly increased by adding a turbocharger to the engine.

2.9.1   Operation of turbochargers

A *turbocharge*r consists of a *compressor* directly coupled to an exhaust-driven *turbine* as illustrated conceptually in Figure 2.11. Ambient air enters the compressor at point 1 and is compressed before entering the intake manifold at point 2. Hot exhaust gases in the exhaust manifold at point 3 drive the turbine before exiting at point 4. Thus, the turbocharger uses energy extracted from the engine exhaust to pressurize the air entering the combustion chamber. The *boost* is the increase in pressure provided by the compressor, i.e.:
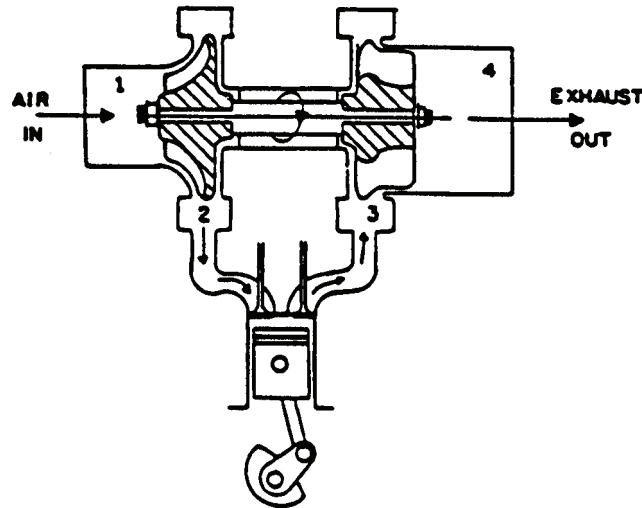

Figure 2.11 – The concept of a turbocharger.

$$\text{boost} = p_2 - p_1 \tag{2.25}$$

where p_1 and p_2 are the absolute pressures at points 1 and 2, respectively. The pressure ratio across the compressor, p_{rc}, is also important and is defined as:

$$p_{rc} = \frac{p_2}{p_1} \tag{2.26}$$

The temperature ratio across the compressor, Θ_{rc}, can be calculated from the following equation:

$$\Theta_{rc} = 1 + \frac{p_{rc}^{0.286} - 1}{\eta_c} \tag{2.27}$$

where η_c = compressor efficiency.

A turbocharger is ineffective when the engine is idling. The turbocharger becomes increasingly effective as load is put on the engine, because the fraction $(1-\eta_{it})$ of the increased fuel supplied is available to drive the turbine; the turbocharger reaches maximum effectiveness near governor's maximum. When the engine is well loaded, the air delivery ratio of the engine can be estimated with acceptable accuracy using the following equation:

$$\eta_v = p_{rc} / \Theta_{rc} \tag{2.28a}$$

Equation 2.28a fails when the engine is idling, but then η_v is close to 0.85. Example Problem 2.3 illustrates the use of Equations 2.23 through 2.28a.

Example Problem 2.3

A turbocharger is to be fitted to a 6.5 liter engine. A boost pressure of 110 kPa is desired when the engine is running under full load at 2200 rev/min. The map of the turbocharger compressor is shown in Figure 2.12. Ambient conditions are 27°C and 100 kPa. Determine the compressor (a) airflow, (b) efficiency, and (c) speed.

Solution
From Equation 2.24, the ambient air density is:

$$\rho_a = 29 \times 100 / (8.314 \times 273 + 27) = 1.16 \text{ kg/m}^3$$

From Equations 2.25 and 2.26, the desired pressure ratio across the compressor is:

$$p_{rc} = (p_1 + \text{boost}) / p_1 = (100 + 110)/100 = 2.1$$

The remainder of the problem must be solved by iteration, because the compressor efficiency, engine volumetric efficiency, and engine airflow are all unknown and
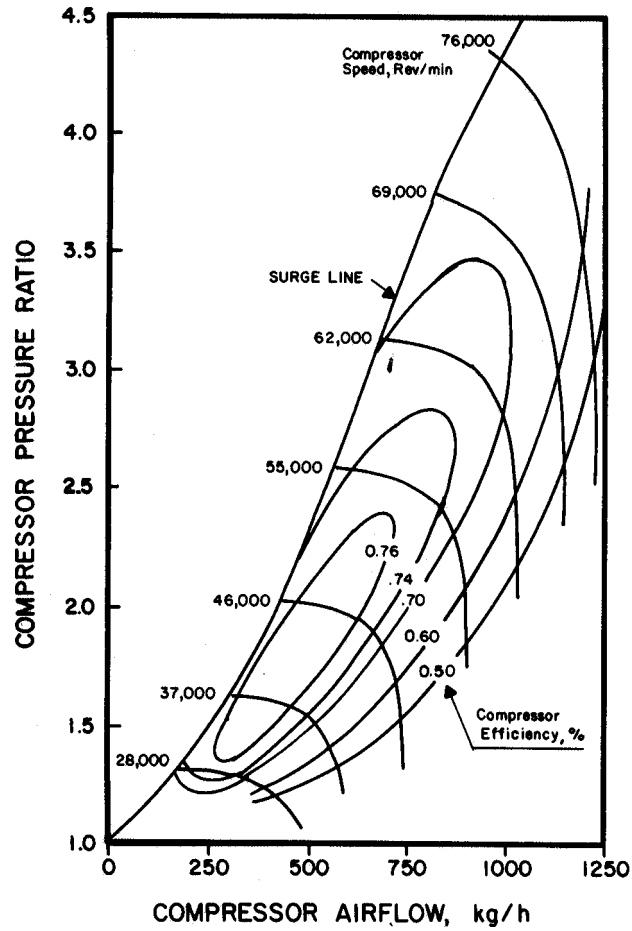
Figure 2.12 – A turbocharger compressor map.

interdependent. Begin by assuming a compressor efficiency of 70%. Then, from Equation 2.27, the initial estimate of the temperature ratio is:

$$\Theta_{rc} = 1 + (2.1^{0.286} - 1)/0.7 = 1.338$$

The estimated volumetric efficiency is, from Equation 2.28a:

$$\eta_v = 2.1/1.338 = 1.57$$

Finally, from Equation 2.23, the initial estimate of airflow into the engine is:

$$\dot{m}_a = 0.03 \times 6.5 \times 2200 \times 1.16 \times 1.57 = 781 \text{ kg/h}$$

Now we can check on the accuracy of the initial choice of compressor efficiency. From Figure 2.12, when the pressure ratio is 2.1 and the airflow is 781 kg/h, the

corresponding compressor efficiency is 72%. Using the new value for compressor efficiency, the new estimate of temperature ratio is 1.328, the new volumetric efficiency is 1.58, and the new airflow is 787 kg/h. From Figure 2.12, the compressor efficiency corresponding to pressure ratio of 2.1 and airflow of 787 kg/h is very close to 72%, so no further iteration is needed. Thus (a) the airflow into the turbocharged engine would be 787 kg/h, (b) the compressor efficiency would be 72%, and (c), interpolating between the adjacent speed curves on Figure 2.12, the compressor speed would be approximately 51,000 rev/min. It should be noted that pressure ratio-airflow combinations to the left of the surge curve in Figure 2.12 produce unstable, surging airflow and are therefore unacceptable. The solution to Example Problem 2.3 is to the right of the surge curve and is therefore acceptable.

Selection of the compressor operating point does not complete the problem of fitting a turbocharger to an engine; it is also necessary to select a compatible operating point for the turbine. The turbine must rotate at the same speed as the compressor while supplying the power necessary to drive the compressor. In addition, the flow rate through the compressor is $\dot{m}_a$ (1+FA), where FA is the fuel-air ratio of the turbocharged engine, that is, the mass airflow rate divided by the mass fuel flow rate. A turbine map (not shown in this book) is used to insure that the values selected for turbine flow rate, pressure ratio, speed, and efficiency are mutually compatible.

2.9.2 Intercoolers

Equation 2.27 can be used to show that the temperature of the air leaving the compressor can be very hot, i.e., well above the boiling point of water. An *intercooler* (sometimes called an *aftercooler*) may be used to reduce the temperature of the compressed air. An intercooler is a heat exchanger through which the compressed air is passed in giving up heat energy to a secondary fluid. The engine coolant is the most common secondary fluid used, but ambient air is used in some intercoolers. Intercooling is a constant-pressure process. When an intercooler is used, the volumetric efficiency of the turbocharged, intercooled engine can be estimated using the following equation:

$$\eta_v = \frac{p_{rc}}{\Theta_{rc}} \frac{\Theta_2}{\Theta_{2i}} \tag{2.28b}$$

where Θ_2 = temperature of air leaving compressor, °K

Θ_{2i} = temperature of air leaving intercooler, °K

2.9.3 Turbocharging and intercooling for versatility

In recent years, engine manufacturers have used turbocharging and intercooling to reduce the costs of manufacturing a *family of engines* and of maintaining an inventory of replacement parts for the engines. The procedure is illustrated in Example Problem 2.4.

MECHANICAL
POWER
TRANSMISSION

4

INTRODUCTION

In Chapter 1 we introduced the concept of support and process systems of an agricultural machine. In Chapters 2 and 3 we presented the main sources of power for agricultural machines, i.e., the diesel engine for self-propelled machines and the electrical motor for many stationary machines used on the farmstead. Pull-type machines must receive propulsion and rotary power from the tractor. Power is transmitted from the tractor to the machine by means of traction, power-take-off drives (PTO), and/or by fluid power. Rotary power is also transmitted by means of belts and chains. Topics related to rotary power transmission are presented here. Fluid power transmission is presented in Chapter 5

4.1   V-BELT DRIVES

V-belts are employed extensively in agricultural machinery applications in which it is not necessary to maintain exact speed ratios. V-belts tend to cushion shock loads, do not require lubrication, and are less likely to become misaligned than are other types of drives. They can be operated at speeds as high as 33 m/s, although speeds in agricultural machinery applications seldom exceed 15 m/s. V-belts are not suitable for high torque at low speeds.

V-belts may be used singly or in matched sets, although single belts are the most common on agricultural machines. Banded, multiple V-belts are sometimes employed on drives having high power requirements, pulsating loads, and inherent instability problems. A banded belt consists of a matched set of two or more conventional V-belts with a thin tie band connecting their tops. Tying the strands together minimizes lateral belt whip and improves the load distribution among the belts.

Because a V-belt wedges into the sheave grooves, it can transmit a given amount of power with less overall shaft pull than a flat-belt drive. V-belts can be operated with relatively small arcs of contact, as in close-center shaft arrangements with large shaft-speed ratios. A single belt on an implement often drives several components in an arrangement known as a serpentine drive. V-belts permit considerable latitude in possible orientation and arrangement of the shafts involved in a drive.
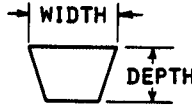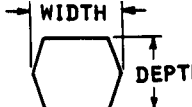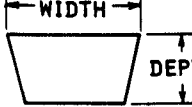
V-belts are adaptable to clutching arrangements. A close-fitting guard may be needed to maintain proper belt orientation and move the belt away from the driver when the tension is released. Under certain conditions it is convenient or economically desirable to drive a relatively large flat pulley with V-belts from a smaller, grooved sheave. This is known as a V-flat drive.

4.1.1   V-belt types and standardization

Three types of V-belts specially designed for agricultural machines are known as agricultural V-belts, agricultural double V-belts, and adjustable-speed belts. These are illustrated in Table 4.1. Banded belts made from agricultural V-belts are also available. Agricultural V-belts and double V-belts are distinguished from the corresponding cross-sectional sizes of industrial V-belts by the prefix H.

The cross-sectional dimensions of agricultural V-belts are identical with those of industrial belts but the construction is different because of the different type of use. Agricultural V-belts are more likely to be subjected to excessive shock loads, heavy pulsating loads, and other adverse conditions. Whereas V-belts in industrial drives are expected to last for several years of continuous operation, a life expectancy of 1000 to 2000 h is adequate for most farm machinery applications. Hence, agricultural V-belt loadings can be higher than in industrial applications.

Table 4.1. Agricultural V-belt cross-sectional dimensions, sheave groove angles, and differences between sheave effective outside diameters and pitch diameters.[*]

Type	Belt Cross Section	Nominal Belt Width (mm)	Nominal Belt Width (in.)	Nominal Belt Depth (mm)	Nominal Belt Depth (in.)	Sheave Groove Angle (deg.)[†]	Effective OD Minus PD for Std-Groove Sheave (mm)	Effective OD Minus PD for Std-Groove Sheave (in.)
Conventional V-belts								
	HA	12.7	0.50	7.9	0.31	30-38	6.35	0.250
	HB	16.7	0.66	10.3	0.41	30-38	8.89	0.350
	HC	22.2	0.88	13.5	0.53	30-38	10.16	0.400
	HD	31.8	1.25	19.0	0.75	30-38	15.24	0.600
	HE	38.1	1.50	23.0	0.91	32-38	20.32	0.800
Double V-belts								
	HAA	12.7	0.50	10.3	0.41	30-38	6.35	0.250
	HBB	16.7	0.66	13.5	0.53	30-38	8.89	0.350
	HCC	22.2	0.88	17.5	0.69	30-38	10.16	0.400
	HDD	31.8	1.25	25.4	1.00	30-38	15.24	0.600
Adjustable-speed V-belts								
	HI	25.4	1.00	12.7	0.50	26	7.6	0.30
	HJ	31.8	1.25	15.0	0.59	26	9.4	0.37
	HK	38.1	1.50	17.5	0.69	26	11.4	0.45
	HL	44.4	1.75	19.8	0.78	26	13.2	0.52
	HM	50.8	2.00	22.2	0.88	26	15.2	0.60

*   ASAE Standard S211.3.
†   For V-belts and double V-belts, sheave groove angle increases as diameter is increased.

Table 4.2 Diameters of ASAE standard adjustable-speed sheaves.[a]

Belt Cross Section	Recommended Minimum OD, mm (in)	Maximum PD with Minimum OD, mm (in)	Maximum Belt Diameter Change, mm (in)
HI	177.8 (7.00)	170.2 (6.70)	72.1 (2.84)
HJ	222.2 (8.75)	2112.8 (8.38)	94.7 (3.73)
HK	266.7 (10.5)	255.3 (10.05)	117.3 (4.62)
HL	311.2 (12.25)	298.0 (11.73)	140.2 (5.52)
HM	355.6 (14.0)	340.4 (13.40)	162.8 (6.41)

[a] ASAE Standard S211.3.

Double V-belts are employed in *serpentine drives* where the direction of rotation of one or more shafts is reversed, thus requiring that power be transmitted to grooved sheaves from both the inside and outside of the belt. Adjustable-speed belts are discussed later in the chapter.

The American Society of Agricultural Engineers (ASAE; now called ASABE, the American Society of Agricultural and Biological Engineers) has established a standard for agricultural V-belts. This standard covers cross-sectional dimensions (Table 4.1), belt lengths generally available, groove specifications, minimum diameters for idlers, procedures and examples for calculating required belt lengths, installation and take-up allowances, twisted-belt drives, and belt-measuring specifications. Table 4.2 includes diameters of ASAE standard adjustable-speed sheaves.

The ASAE standard is similar in many respects to the standard established by the Rubber Manufacturers Association (RMA) for industrial V-belts. There are minor differences in groove dimensions and in available belt lengths. The RMA standard specifies pitch lengths for belts, whereas the ASAE standard specifies effective outside lengths. The RMA standard is intended primarily for two-sheave drives and includes formulas and charts for power ratings. The ASAE standard covers a broad range of drive configurations and does not include power ratings. In designing an agricultural drive, the allowable load is related to the expected number of hours of actual operation for a specific drive.

4.1.2 V-belt drive geometry

Belts are generally used to connect parallel shafts so that the sheaves rotate in the same direction or in the opposite direction as shown in Figure 4.1. The angle of wrap is defined as the angle of belt contact around the sheave. For the open belt drive, the angles of wrap (rad) are

$$\theta_2 = \pi - 2\sin^{-1}\frac{D_3 - D_2}{2C} \tag{4.1}$$

and

$$\theta_3 = \pi + 2\sin^{-1}\frac{D_3 - D_2}{2C} \tag{4.2}$$

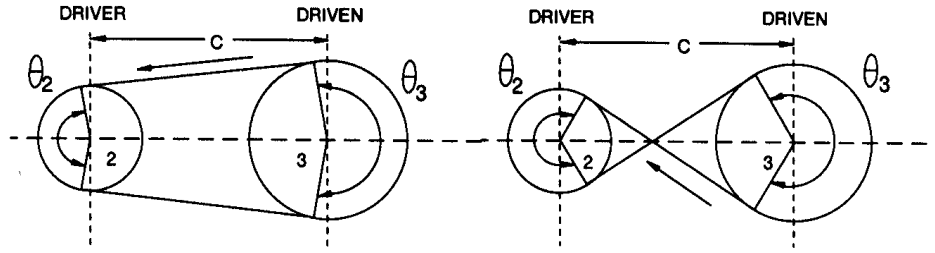where D_2 and D_3 are the outside sheave diameters.

Figure 4.1 – Geometry of V-belt drives.

The angles of wrap for the crossed-belt drive are equal and are given by:

$$\theta_2 = \theta_3 = \pi + 2\sin^{-1}\frac{D_3 - D_2}{2C} \tag{4.3}$$

The belt length for an open drive is approximated by:

$$L = 2C + \frac{\pi}{2}(D_3 + D_2) + \frac{(D_3 - D_2)^2}{4C} \tag{4.4}$$

and for the crossed belt drive the length is:

$$L = 2C + \frac{\pi}{2}(D_3 + D_2) + \frac{(D_3 + D_2)^2}{4C} \tag{4.5}$$

4.1.3   Kinematics of V-belt drives

As a belt bends to conform to the sheave curvature, the outer section stretches and the inner section is compressed. The location of the neutral axis, which establishes the pitch diameter of the sheave, is determined by the position of the load-carrying cords within the belt cross-section. Differences between sheave effective outside diameters and pitch diameters are included in Table 4.1. Pitch diameters, rather than outside diameters, should always be used in calculating speed ratios and belt speeds.

The belt speed (m/s) is calculated as:

$$v = \pi n_2 D_{p2} = \pi n_3 D_{p3} \tag{4.6}$$

where n_2, n_3 = angular speeds of rotation of sheaves 2 and 3, respectively, in rev/s

D_{p2}, D_{p3} = pitch diameters of sheaves 2 and 3, respectively, m

From the above equation we get the following relationship:
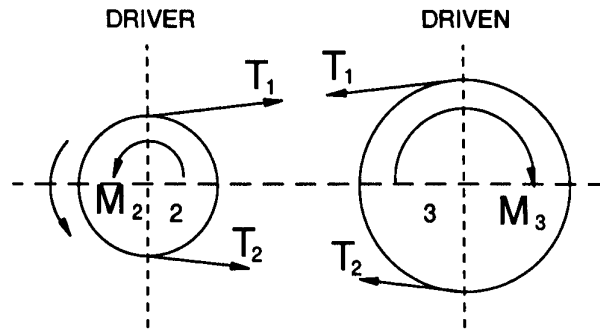
$$\frac{n_2}{n_3} = \frac{D_{p3}}{D_{p2}} \tag{4.7}$$

Figure 4.2 – Belt tensions and moments on the sheaves.
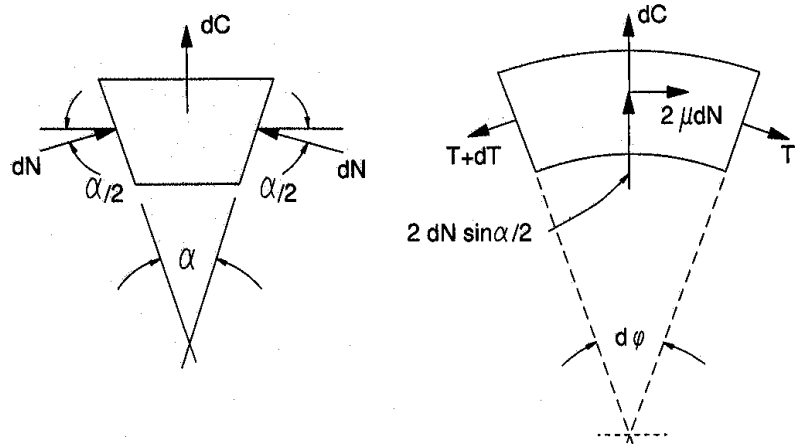

Figure 4.3 – Forces acting on an element of V-belt.

4.1.4 Mechanics of V-belt drives

A V-belt transmits power by virtue of the difference in belt tensions between the point at which it enters a sheave and the point at which it leaves (Figure. 4.2). This difference in tension is developed through friction between the belt sidewalls and the sides of the sheave groove. The wedging effect as the belt is pulled into the groove because of belt tension greatly increases the potential driving force.

Figure 4.3 shows the forces acting on a segment of the belt as it wraps around the sheave. In a belt drive there is a tight side and a slack side of the belt. In the free body diagram as shown in Figure 4.3, T + dT represents the tight side tension, T represents the slack side tension, dC is the centrifugal force, dN is the normal sheave reaction force, and μdN is the frictional force.

The centrifugal force (dC) is given by:

$$dC = \frac{dm\ v^2}{R} \tag{4.8}$$

where dm = mass of the belt element, kg
      R = pitch radius, m
      v = belt speed, m/s

Elemental belt mass (dm) can be obtained by multiplying the density of the belt material by its volume as follows:

$$dm = \rho_b a\ R\ d\phi \tag{4.9}$$

where ρ_b = density of the belt material, kg/m^3
      a = belt cross-section area, m^2
      $d\phi$ = elemental wrap angle, rad

Substituting Equation 4.9 into Equation 4.8 we obtain:

$$dC = \rho_b a\ v^2 d\phi \tag{4.10}$$

Summing forces in the radial direction we get:

$$dC + 2dN \sin(\alpha/2) - T \sin(d\phi/2) - (T + dT) \sin(d\phi/2) = 0 \tag{4.11}$$

Let $dN = p_N R\ d\phi$, where p_N is the normal reaction force per unit belt length. Substituting the expressions for dC and dN in Equation 4.11 and taking the limit we get:

$$\rho_b\ a\ v^2 + 2p_N R \sin(\alpha/2) - T = 0 \tag{4.12}$$

If the belt is not transmitting any power, the tension in the belt would only be due to the centrifugal force, i.e., $T_c = \rho_b a v^2$. Substituting T_c in Equation 4.12 and solving for p_N we get:

$$p_N = \frac{T - T_c}{2R \sin(\alpha/2)} \tag{4.13}$$

Summing forces in the tangential direction we get:

$$(T + dT) \cos(d\phi/2) - T \cos(d\phi/2) - 2\mu\ p_N R d\phi = 0 \tag{4.14}$$

which in the limit becomes:

$$dT - 2\mu\ p_N R d\phi = 0 \tag{4.15}$$

Substituting for p_N, letting $k = \mu/\sin(\alpha/2)$, and rearranging we get:

$$\frac{dT}{T - T_c} = \frac{\mu}{\sin(\alpha/2)} d\phi \tag{4.16}$$

Integrating we get:

$$\int_{T_2}^{T_1} \frac{dT}{T - T_c} = k \int_0^\theta d\phi \tag{4.17}$$

Carrying out the integration, applying the limits, and rearranging we get:

$$\frac{T_1 - T_c}{T_2 - T_c} = e^{k\theta} \tag{4.18}$$

If the belt speed is low, T_c may be eliminated in the above equation. The k is sometimes referred to as the effective coefficient of friction.

Power transmitted by a V-belt drive is determined by the effective pull and the belt speed as given by the following equation:

$$P = \frac{(T_1 - T_2)v}{1000} \tag{4.19}$$

where T_1 = tight-side tension, N
T_2 = slack-side tension, N
P = power transmitted, kW
v = belt speed, m/s
$T_1 - T_2$ = effective pull, N

It is customary to calculate tensions on the basis of a design power load that is somewhat greater than the average load to be transmitted, thus allowing for the effects of overloads or fluctuating loads. The design power for each driven wheel in a drive system is determined by multiplying the actual power by an appropriate service factor. Recommended values for service factors in agricultural machinery applications are included in Table 4.3 and range mostly from 1.2 to 1.5.

**Table 4.3. Service factor and service life for some
agricultural maachines (Gates rubber company).**

Machine or Operating Unit	Service Factor	Service Life, h
Combine cylinder	1.5	1000-2000
Sickle bar	1.5	1000-2000
Straw walker	1.0	1000-2000
Cleaning shoe	1.0	1000-2000
Stalk shredder	1.5	400-1000
Hay rake	1.2	600-1200
Ensilage cutter	1.5	500-1000
Ensilage blower	1.5	500-1000
Hay conditioner	1.5	800-2000
Delivery auger	1.3	400-1000
Tree shaker harvester	1.5	400-1000
Peanut digger	1.3	800-1600
Orchard sprayer	1.3	800-2000

If the ratio between the tight-side and slack-side tensions is too great, belt slippage will be excessive. Slippage in a properly designed drive should not exceed l% to 2%. If the ratio is smaller than it needs to be, unnecessarily high tensions will be needed for a given effective pull, thereby reducing belt life. The maximum allowable tension ratio is:

$$R_{a\theta} = \frac{T_1}{T_2} = e^{k\theta} \tag{4.20}$$

In designing a drive with a V-belt in a V-sheave, a tension ratio of $R_{aB} = 5$ (allowable tension ratio for 180° arc of contact) is commonly assumed. This gives a value of $k = 0.512$. A somewhat higher tension ratio is permissible if automatic tensioning is provided. For a V-belt running on a flat pulley, a value of $R_{aB} = 2.5$ is satisfactory ($k = 0.292$).

When the arc of contact is less than 180°, the allowable tension ratio is less, as indicated by Equation 4.20, thus requiring higher values of T_1 and T_2 for a given effective pull and power. For example, if an effective pull of 360 N is required for the design power, values of T_1 and T_2 would be 450 N and 90 N, respectively, if the arc of contact on a grooved sheave is 180° ($R_{aB} = 5$). But if the arc of contact is only 120°, the maximum allowable tension ratio is 2.9, requiring tensions of 549 and 189 N. Flat, backside idlers are often employed to effect tensioning and, at the same time, increase the arcs of contact on the loaded sheaves.

In a two-sheave drive without an idler, the smaller sheave is the critical one in regard to tension ratio (slippage) because it has the smaller arc of contact. In a V-flat, two-wheel drive without an idler, the sheave and the flat pulley have equal maximum allowable tension ratios when the arc of contact is about 130° on the sheave and 230° on the flat pulley. When a drive has more than one driven sheave or pulley, tensions must be determined in a cumulative manner. All tensions in the system must be adjusted so that no wheel has a tension ratio greater than its allowable value. In a multiwheel drive, the driver is usually the one most likely to slip.

4.1.5 Stresses and service life

Stresses in a V-belt drive arise from the effective pull needed for the power load, slack-side tension needed to prevent slippage, bending around each wheel, and centrifugal forces acting on the belt. The bending tension, T_b, in the outer fibers of a belt with a given cross section is inversely proportional to the wheel diameter. The tension due to centrifugal force may be expressed as:

$$T_c = wv^2 \tag{4.21}$$

where T_c = centrifugal tension, N

w = belt mass, kg/meter of belt length

The tensions in a three-sheave drive are illustrated in Figure 4.4. The slack-side tension is T_3 and the differences, $T_2 - T_3$, $T_1 - T_2$, and $T_1 - T_3$, represent the effective pulls needed to transmit the power. Note that there is one peak tension at each wheel. It has been determined experimentally that a V-belt usually fails from fatigue caused by repetition of peak tensions and that the average fatigue life of a belt is predictable if loads are accurately known or can be estimated.
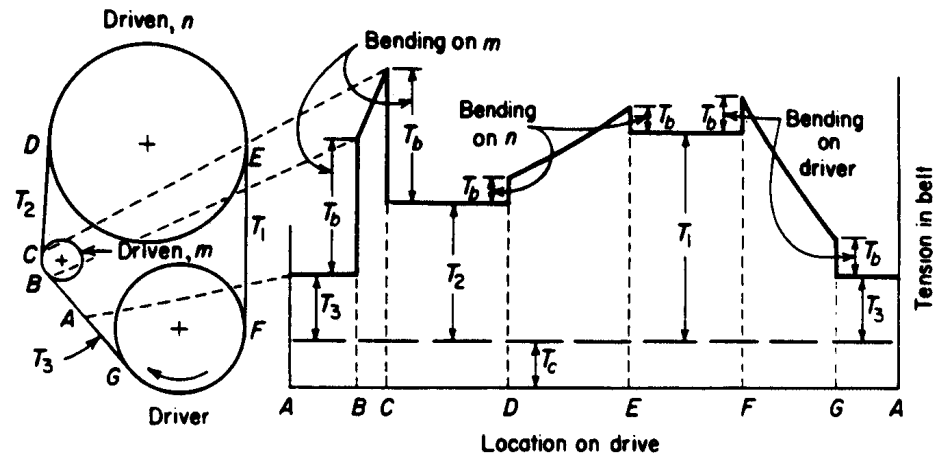
**Figure 4.4 – Belt tensions in relation to position on a three-sheave drive
(Gates Rubber Co.; reprinted from Kepner et al., 1978).**

The Gates Rubber Co. has developed a design method for predicting the service life of a V-belt that includes the effects of the following factors:

- The number of wheels on the drive.
- The design power for each wheel (including an appropriate service factor for each driven wheel).
- The belt speed.
- The arc of contact for each wheel.
- The sequence of loaded wheels and idlers on the drive.
- The pitch diameter of each wheel.
- The stress-fatigue characteristics and cross-sectional dimensions of the particular type and cross-section of belt being considered.
- The belt length.

The Gates system is based on the determination (from an empirical equation or nomographs) of a "fatigue rate" corresponding to the peak tension for each wheel at a given belt speed. The units of the fatigue rate are millimeters of belt length per 100 h of life. The fatigue rates for the individual wheels are added together to obtain the total fatigue rate for the particular size and type of belt being considered for the drive. The calculated average service life of the belt at a given speed is:

$$\text{Belt Service Life (h)} = \frac{\text{Belt length(mm)} \times 100}{\text{Total Fatigue Rate}} \qquad (4.22)$$

For a given tight-side tension and wheel pitch diameter, increasing the belt speed increases the fatigue rate, primarily because of the greater frequency of stress cycles but also because of increased centrifugal tension at high speeds. (The transmitted power would be increased also.)
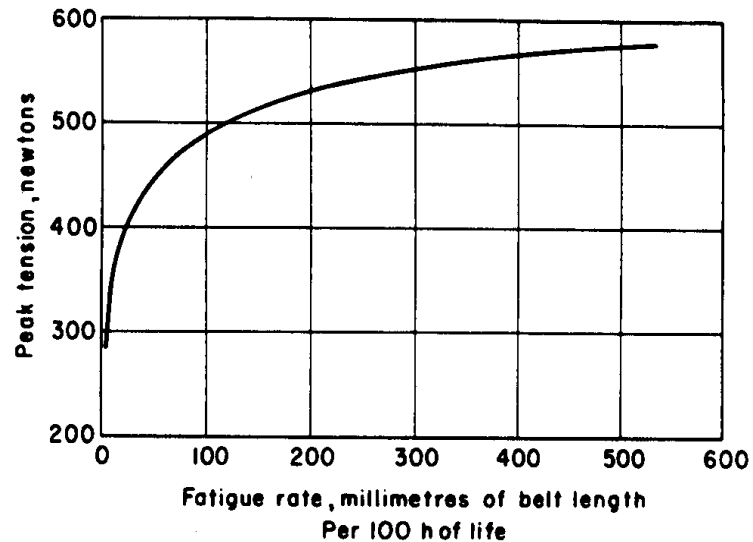
Figure 4.5 – Typical relation between tension and fatigue rate for one V-belt cross section and one speed (Gates Rubber Co.; reprinted from Kepner et al., 1978).

The relation of fatigue rate to tension and speed for each type or quality of belt and each cross section is determined experimentally by means of durability tests in the laboratory, from which constants in a generalized equation are evaluated. A typical curve for one speed is shown in Figure 4.5. Essentially, a tension-fatigue-rate curve is the inverse of the usual S-N curve (stress vs. fatigue cycles).

In designing a drive, the sequence of the driven sheaves or pulleys affects the magnitudes of the peak tensions and hence the service life. If a multiple sheave drive can be arranged so the belt leaving the driver comes to the driven sheaves in order of increasing power requirements, the magnitudes of tension peaks for the low-power sheaves will be minimized. Exceptionally small-diameter sheaves should be in belt spans of lesser tension to avoid the combination of a high tight-side tension and a high bending tension. An idler, if used, should be in the span with the least tension.

Increasing the sheave diameters on a particular drive, if feasible, reduces both the bending stresses and the required effective pull and may even permit the use of a smaller belt cross section. Centrifugal tension is seldom a limiting factor at speeds encountered in agricultural machinery drives.

4.1.6   Variable-speed V-belt drives

An adjustable-pitch V-belt sheave has provision for moving one face axially with respect to the other, thus changing the radius at which the belt operates. Some adjustable-pitch sheaves can be changed only when stopped, but others can be changed while in motion (Figure. 4.6). In this textbook, the term "variable-speed drive" implies the ability to change the speed ratio over the entire range of control while the drive is in operation and under load.
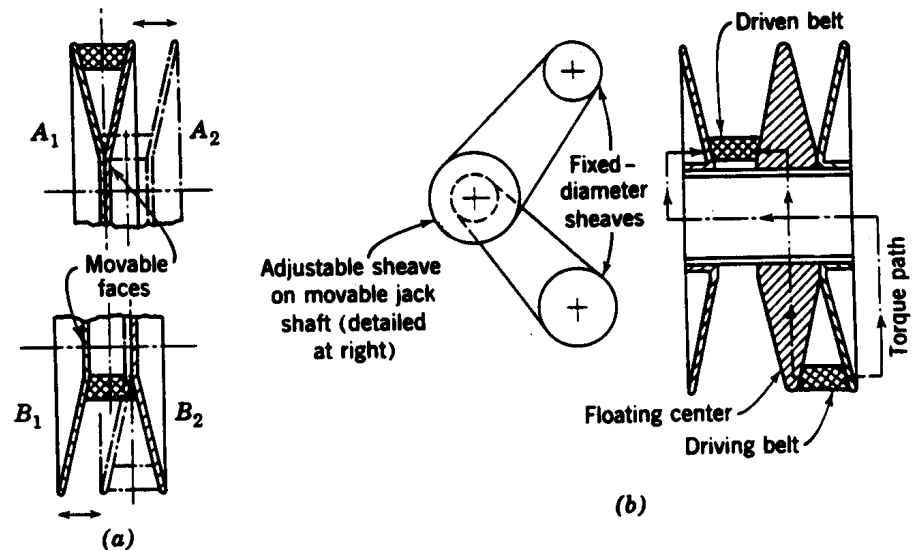
**Figure 4.6 – (a) Arrangement with two adjustable-pitch sheaves on fixed centers.
(b) Double adjustable-pitch sheave with floating center
(reprinted from Kepner et al., 1978).**

Belts designed specifically for variable-speed drives are wider than conventional V-belts in relation to their thickness. The extra width is necessary to obtain reasonable ranges of speed ratio as well as increased load capacities. Relatively thin belts are needed because minimum operating diameters are generally small in this type of drive.

With adjustable-speed sheaves and V-belts as shown in Tables 4.1 and 4.2, maximum speed-range ratios ranging from 1.75 for HI belts to 1.9 for HM belts are obtainable when one adjustable pitch sheave of the minimum allowable diameter is used in conjunction with a fixed-diameter sheave. The range for a given belt size varies inversely with the sheave diameter, since the maximum change in pitch diameter is fixed by the 26° groove angle and the belt top width (Figure. 4.6a).

The speed range for a combination of two adjustable-pitch sheaves is the product of the two individual ranges. When both sheaves have the minimum recommended diameter, the maximum speed ratio varies from 3.0 for HI belts to 3.7 for HM belts. The most common arrangement is with the two sheaves on fixed centers, as shown in Figure 4.6a. If the faces A_1 and B_2 are fixed axially while A_2 and B_1 are moved simultaneously, proper belt alignment is maintained at all speed ratios because the entire belt moves axially.

A third arrangement has two adjustable-speed belts in tandem and a double adjustable-pitch sheave with floating center section, as shown in Figure 4.6b. The speed ratio is changed by moving the adjustable-pitch sheave along a path that keeps the sum of the required belt lengths constant as the floating center changes its lateral position. This system is subject to belt misalignment as discussed above for arrangements employing a single adjustable pitch sheave.

4.1.7   V-belt drive design

The Gates design procedure is summarized below:

1. Determine the design power of the drive by multiplying the actual power demand by the service factors. Table 4.3 shows examples of service factors as recommended by the Gates Rubber Co.
2. Determine the belt type and cross section based on the design power. The selection of belt type and cross-section is based on the pitch diameter of the driver and the drive sheaves and their speeds. Graphs used to select appropriate belt sections based on the speed of faster shaft and the design power are given by Gates Rubber Co. (1976). As the design power increases for a constant shaft speed larger belt sections are required. Also, if the shaft speed decreases, bigger belts would be necessary to transmit the same power.
3. Layout the drive and determine pitch diameters of the driver and all driven sheaves, and calculate approximate belt length. Also, find arc of contact for each sheave.
4. The next step is to determine belt tension ratios, effective pull, and span tensions. These are computed using the equations given above.
5. Determine total fatigue rate and service life by peak tension at a given belt speed. The nomograms to determine the fatigue rate are given in the Gates manual.
6. The estimated belt life should be compared with the recommended values as given in Table 4.3. If the calculated belt life is not acceptable then make one or more of the following changes:
   - Increase the number of belts.
   - Increase the smallest diameter.
   - Change the belt cross section.
   - Increase the belt length or reduce speed.
   - Reduce the torque.

4.2   CHAIN DRIVES

Perhaps the first use of a chain drive was made in a reaper by Cyrus McCormick in 1837. Today chain drives play an important part in many agricultural machines such as hay balers, corn pickers, combines, cotton pickers, and beet harvesters. As opposed to V-belt drives, chain drives are used where it is important to maintain an exact speed ratio. Another benefit is that chain drives are capable of transmitting a large amount of power at slower speeds. However, chain drives require better shaft alignment and more maintenance than V-belt drives.

4.2.1   Types of chains and standardization

Roller chains are of two types, either standard-pitch or double-pitch. Other types of chains include detatchable-link chains, cast roller chains, and pintle chains.

Standard-pitch roller chain, double-pitch roller chain (the pitch of a chain is the effective length of one link), and detachable-link chain (Figure. 4.7) are commonly used in agricultural machines. All roller chains are so constructed that the rollers rotate when contacting the teeth of the sprocket. Roller chains may be used in a single or

multiple strand arrangement. Standardized dimensions for each of these types have been adopted by the American Standards Association (ASA). The standard dimensions of roller chains are given in Table 4.4.

Standard-pitch roller chain drives are satisfactory at linear speeds from less than 0.5 m/s up to 20 m/s and are well suited for heavy loads requiring a compact drive. The maximum permissible speed decreases as the pitch is increased. Multiple-width chains of short pitch can be used for extremely compact drives at high speeds. Roller chains are precision-built and under favorable conditions may have efficiencies as high as 98% to 99%.

Sprockets may be driven from either the inside or the outside of a roller chain. Although oil-bath lubrication is recommended for high-speed drives, this system often is not practical on agricultural machines. Standard-pitch roller chain is several times as expensive as steel detachable-link chain.

Double-pitch roller chain employs the same pins, bushings, and rollers as standard-pitch roller chain, but the side plates have twice the pitch. Thus, double-pitch chains have the same strength and precision as corresponding standard-pitch chains but less mass. They are less expensive than standard-pitch roller chains, but considerably more expensive than steel detachable-link chain. Double-pitch chains are suitable for slow and moderate-speed drives. Because the roller diameter is only $^5/_{16}$ of the pitch, there is ample space for sprocket teeth, and precision, cast-tooth sprockets are satisfactory (and more economical than machine-cut teeth).
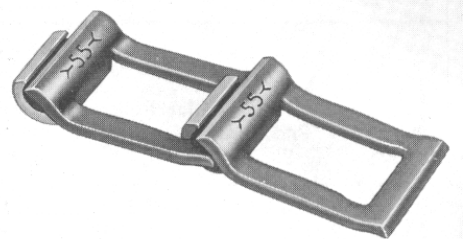
Standard-pitch roller chain
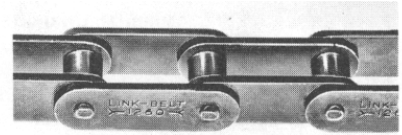
Double-pitch roller chain
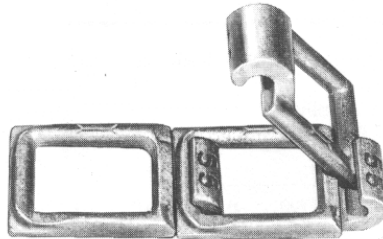
**Malleable-cast-iron, detachable-link chain**

Pressed-steel, detachable-link chain

Figure 4.7 – Four types of drive chain common on farm machines (reprinted from Kepner et al., 1978).

During the 1950s several companies developed chains that are physically inter-changeable with standard-pitch and double-pitch roller chains but which are self-lubricating. Self-lubricating chain has oil-impregnated, sintered-steel bushings at the joints, replacing the bushings and rollers of conventional roller chain. It was designed for applications where external lubrication is impossible or impractical. Many farm machinery applications fall into this category. However, because this chain does not have rollers, it is not recommended for high speeds or extremely heavy loads.

The cost of standard-pitch or double-pitch self-lubricating chain is the same as that of the corresponding size of conventional roller chain. Ultimate strengths are perhaps 5% to 20% lower. Laboratory tests and field experience have indicated that, for a given load and a given allowable percentage elongation due to wear, the service life of a self-lubricating chain is several times as great as that of non-lubricated conventional roller chain. But, where a conventional chain can be adequately lubricated, it will out-perform the self-lubricating chain.

Table 4.4. General chain dimensions, in mm (inches). (Reproduced from *Identification, installation, lubrication and maintenance of power transmission roller chains in ANSI B29.1 and ANSI B29.3,* **by permission of the American Chain Association, Rockville, MD.)**
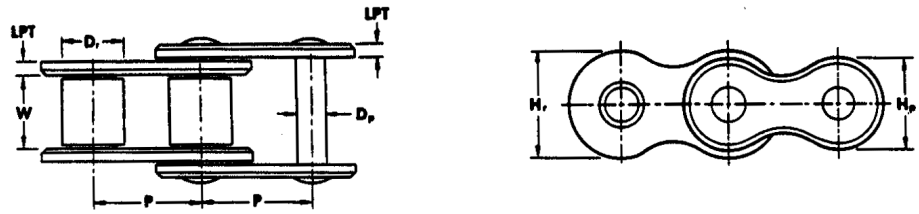
Standard Chain No.	Pitch P	Max. Roller Diam. D_r	Nominal Width W	Nominal Pin Diam. D_p	Link Plate Thickness LPT	
					Standard Series	Heavy Series
25	6.35 (0.250)	3.30 (0.130)*	3.18 (0.125)	2.30 (0.090)	0.76 (0.030)	– –
35	9.52 (0.375)	5.08 (0.200)*	4.78 (0.188)	3.58 (0.141)	1.27 (0.050)	– –
41	12.70 (0.500)	7.77 (0.306)	6.35 (0.250)	3.58 (0.141)	1.27 (0.050)	– –
40	12.70 (0.500)	7.92 (0.312)	7.92 (0.312)	3.96 (0.156)	1.52 (0.060)	– –
50	15.88 (0.625)	10.16 (0.400)	9.52 (0.375)	5.08 (0.200)	2.03 (0.080)	– –
60	19.05 (0.750)	11.91 (0.469)	12.70 (0.500)	5.94 (0.234)	2.39 (0.094)	3.18 (0.125)
80	25.40 (1.000)	15.87 (0.625)	15.87 (0.625)	7.92 (0.312)	3.18 (0.125)	3.96 (0.156)
100	31.75 (1.250)	19.05 (0.750)	19.05 (0.750)	9.52 (0.375)	3.96 (0.156)	4.75 (0.187)
120	38.10 (1.500)	22.22 (0.875)	25.40 (1.000)	11.10 (0.437	4.75 (0.187)	5.56 (0.219)
140	44.45 (1.750)	25.40 (1.000)	25.40 (1.000)	12.70 (0.500)	5.56 (0.219)	6.35 (0.250)
160	50.80 (2.000)	28.57 (1.125)	31.75 (1.250)	14.27 (0.562)	6.35 (0.250)	7.14 (0.281)
180	57.15 (2.250)	35.71 (1.406)	35.71 (1.406)	17.45 (0.687)	7.14 (0.281)	7.92 (0.312)
200	63.50 (2.500)	39.67 (1.562)	38.10 (1.500)	19.84 (0.781)	7.92 (0.312)	9.52 (0.375)
240	76.20 (3.000)	47.62 (1.875)	47.62 (1.875)	23.80 (0.937)	9.52 (0.375)	12.70 (0.500)

*Bushing diameter, these chains have no rollers.

An agricultural double-pitch roller chain has been developed that is dimensionally the same as the regular double-pitch chain but has a lower cost because of different materials and because the joints have more clearance, thus permitting greater manufacturing tolerances. Performance is said to be somewhat inferior to that of regular double-pitch chain.

Steel detachable-link chains are used extensively on agricultural implements, both for transmitting power and in conveyors and elevators. This is the least expensive type of chain and it is well suited for moderate loads at speeds not exceeding 2 to 2.5 m/s. Under dirty conditions, detachable-link chains are subject to greater wear than roller chains because of the loose-fitting, open hooks. Detachable-link chains usually are not lubricated, because the lubricant would tend to retain grit particles in the joint.

An improved type of "high-fatigue" steel detachable-link chain, developed in the early 1950s, is said to have one-third more tensile strength than conventional steel detachable-link chain, and more than twice the fatigue strength. The hook is rolled up from material in front of the link rather than from the material punched out from the center. It is more expensive than the conventional type.

Pintle chain is composed of identical links with hollow cored cylinders cast or forged integrally with two offset side bars. The links are jointed by pins inserted in holes in the ends of the side bars in through the cored cylinders.

4.2.2 Geometry of chain drives

The pitch diameter is a function of the chain pitch and the number of teeth in the sprocket. Referring to Figure 4.8, the pitch diameter is given by:

$$PD = \frac{P}{\sin(180/N)} \tag{4.23}$$

where P = the chain pitch

N = the number of teeth in the sprocket

The length (L) is determined in pitches and is approximated by the following formula:

$$\frac{L}{P} = \frac{2C}{P} + \frac{N_1 + N_2}{2P} + \frac{(N_2 - N_1)^2}{4\pi^2(C/P)} \tag{4.24}$$

where C is the center distance between the sprockets and N_1 and N_2 are the number of teeth on the two sprockets.

4.2.3 Kinematics of chain drives

Since a sprocket is essentially a polygon with as many sides as there are teeth or pitches, either the chain speed or the angular velocity of the sprocket must vary as the chain engages or leaves the sprocket due to the chordal action as shown in Figure 4.9.
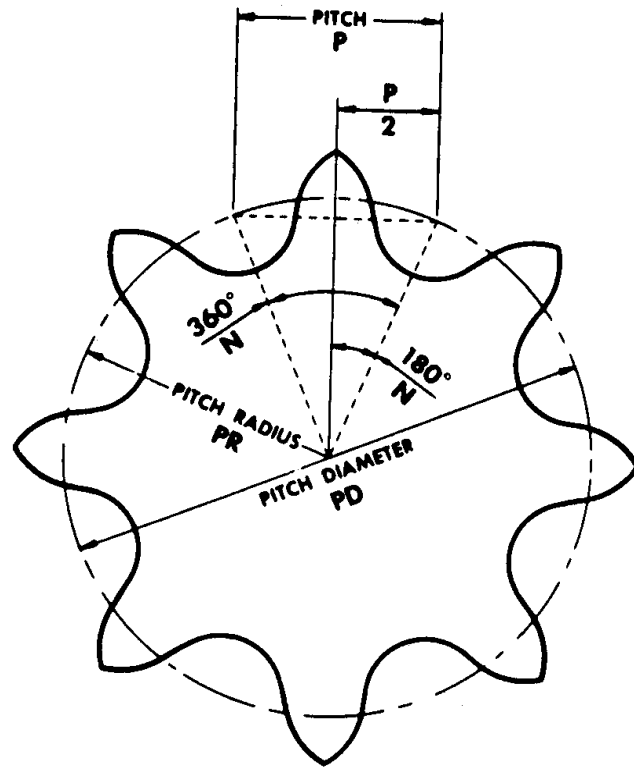
Figure 4.8 – Computation of sprocket pitch diameter
(reproduced from *Chains for Power Transmission and Material Handling*,
by permission of the American Chain Association, Rockville, MD).

The fewer teeth there are on the sprocket, the greater is the speed variation. Theoretically, a 10-tooth sprocket would give a variation of about 5%. Practically, however, small speed variations as well as sudden load shocks tend to be absorbed or cushioned by the natural elasticity of the chain and the catenary effect of the driving side. Although sprockets with as few as six teeth are available, sizes with less than 17 or 18 teeth are not recommended for high-speed drives. The chordal speed variation is given by:

$$\frac{\Delta v}{v} = \frac{\pi}{N}\left(\frac{1}{\sin(180/N)} - \frac{1}{\tan(180/N)}\right) \tag{4.25}$$

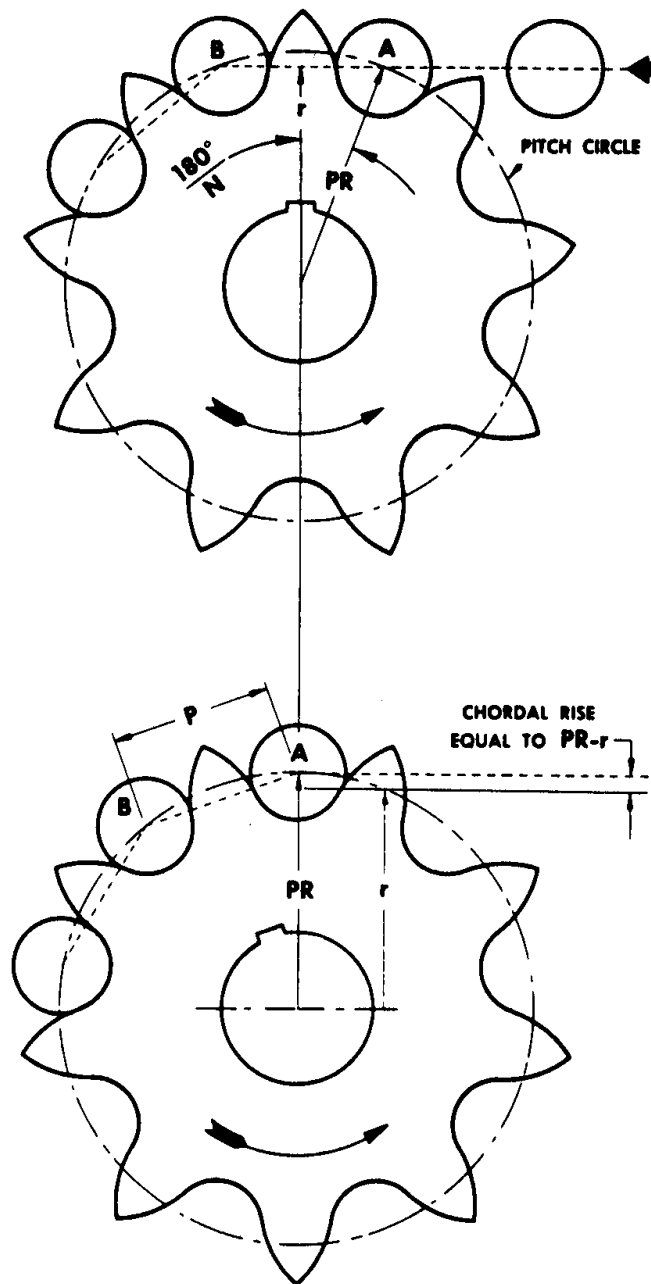where the chain velocity is $v = NPn$ and n = angular speed in rev/s.

Figure 4.9 – Chordal action of chain
(reproduced from *Chains for Power Transmission and Material Handling*,
by permission of the American Chain Association, Rockville, MD).

4.2.4   Design of chain drives

In general, the load capacity of a chain is based upon the rate of wear rather than on the ultimate strength. Because wear is mainly due to the hinge action as the chain engages or leaves a sprocket, the rate of wear is greater with small sprockets than with large ones. The rate of wear is also directly related to chain speed and inversely related to chain length. As a chain wears, the pitch length increases and the chain rides farther out on the sprocket teeth. The more teeth a sprocket has, the sooner the chain will ride out too far and have to be replaced. For this reason, speed ratios should not exceed 10:1 for standard-pitch roller chain or 6:1 for other chains.

Power ratings published in chain catalogs are for the relatively long life expected in industrial applications. As in designing V-belt drives, actual power requirements are multiplied by appropriate service factors to obtain design power. Because of the shorter life requirements on agricultural machines in comparison with industrial applications, somewhat greater loadings are often acceptable. However, unfavorable environmental conditions may tend to shorten the life.

Chain selection for extremely slow drives is sometimes based on ultimate strength rather than wear rate. With roller chains, the recommended maximum ratios of working load to ultimate strength range from 0.2 at 0.13 m/s to 0.1 at 1.3 m/s. Conventional steel detachable-link chain has inherent stress concentration points that promote early fatigue failures if the chain is loaded to more than 10% of its ultimate strength. The pull required for a given power and speed can be determined from Equation 4.19. T_2 is assumed to be zero, since a chain should run with essentially no slack-side tension. Chain speed in meter per second = (chain pitch, mm/1000) × (number of teeth on sprocket) × (sprocket r/min ÷ 60).

The chain drive design procedure, in general, includes the following steps:

1. *Design power.* A service factor based on the type of power source and the nature of load is selected to determine the design power. Table 4.5 gives the recommended values for service factors. Design power is determined by multiplying transmitted power by the service factor.

2. *Tentative chain selection.* Once the design power is determined chain pitch is selected based on Figure 4.10.

3. *Selection of small sprocket.* The sprocket selected must be large enough to accommodate the shaft. For a given chain speed and power the effect of increasing the number of teeth on the sprocket is to increase the linear speed of chain and to decrease the pull and to decrease the chordal action. This results in a quieter drive with less impact.

4. *Selection of large sprocket.* After selecting the small sprocket the desired speed ratio is used to determine the number of teeth on the large sprocket. It is recommended that the speed ratios greater than 10:1 should not be attempted in a single drive.

5. *Determine chain length and center distance.* The chain length is a function of number of teeth on both sprockets and the center distance. It is preferred that the chain consist of an even number of pitches in order to avoid an offset link. The center distance is based on the physical requirements of the application. The chain length is calculated by using Equation 4.24.

Table 4.5. Service factors of roller chains (reproduced from
*Chains for Power Transmission and Material Handling***,**
by permission of the American Chain Association, Rockville, MD).

	Type of Input Power		
Type of Driven Load	Internal Combustion Engine with Hydraulic Drive	Electric Motor or Turbine	Internal Combustion Engine with Mechanical Drive
Smooth	1.0	1.0	1.2
Moderate shock	1.2	1.3	1.4
Heavy shock	1.4	1.5	1.7

6.
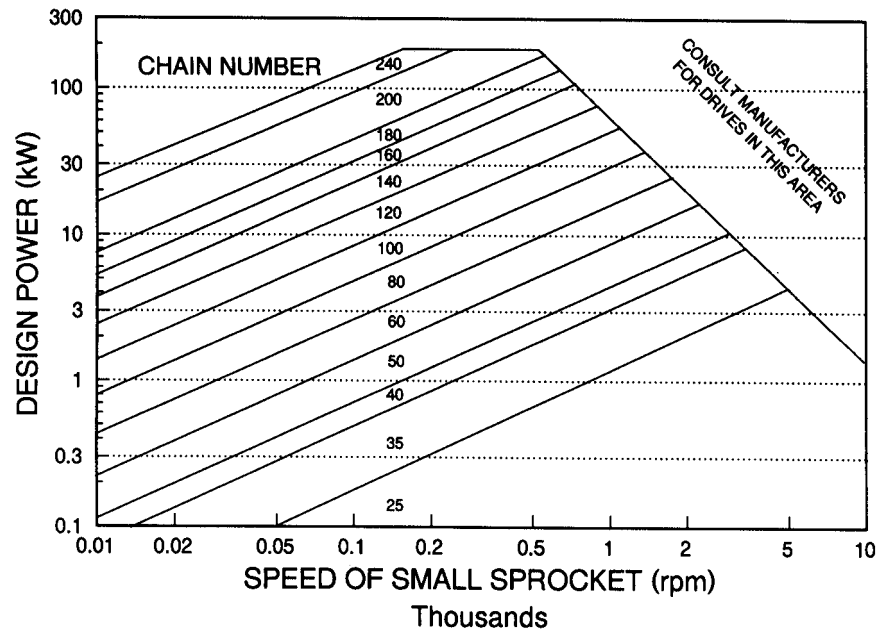
Figure 4.10 – Roller chain pitch selection chart (redrawn from *Chains for Power Transmission and Material Handling*, by permission of the American Chain Association, Rockville, MD).

4.3 POWER-TAKE-OFF DRIVES

A power-take-off (PTO) drive provides a means for transmitting rotary power to machines that are coupled to a tractor. The most common location for the PTO shaft is at the rear of the tractor (see Figure. 4.11), but some tractors have auxiliary PTO shafts at other locations. The direction of rotation, rotational speed, approximate location, and exact dimensions of the PTO shaft were standardized by the ASAE in 1926 so that equipment of different manufacturers could be interchanged. With growth in tractor
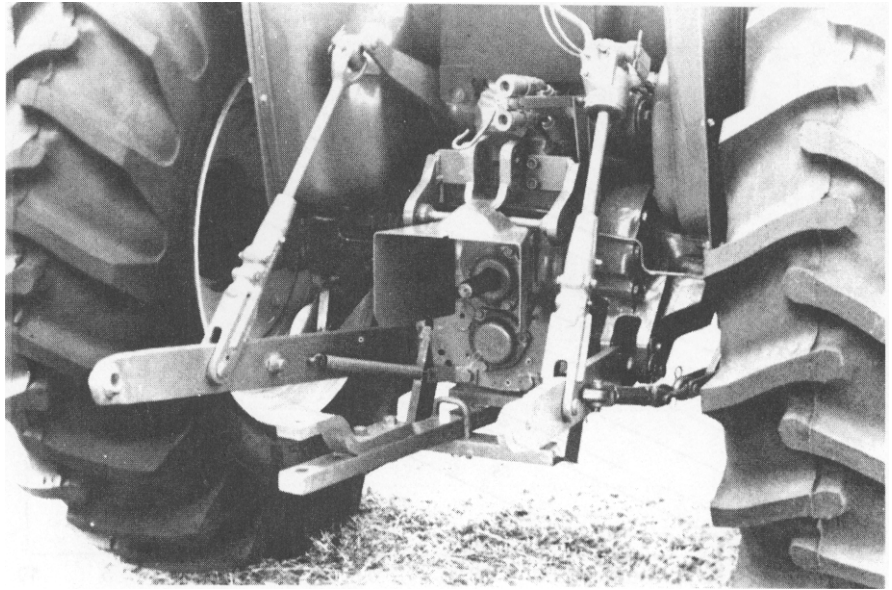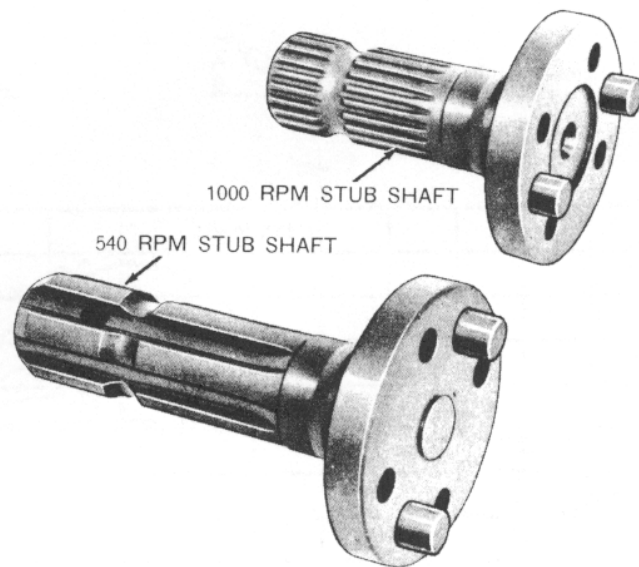
Figure 4.11 – A tractor PTO drive.

**Figure 4.12 – Splines for 540 and 1000 rev/min PTO shafts
(courtesy of Deere and Co.).**

size, it became necessary to develop faster and larger PTO shafts to transmit the increased available power. There are now three standard PTO shafts. Illustrated in Figure 4.12 are the 35 mm (diameter) shafts with standard rotation speeds of 540 rev/min and 1000 rev/min. The shaft with a standard speed of 540 rev/min is used on tractors with up to 65 kW PTO power. The 35 mm shaft with a standard speed of 1000 rev/min is used on tractors with 45 to 120 kW of PTO power. Note the power overlap, i.e., tractors in the 45 to 65 kW power range could be equipped with either of the shafts in Figure 4.12. The 45 mm shaft with a standard speed of 1000 rev/min is not shown in Figure 4.12; it is similar in appearance to the other 1000 rev/min shaft, except that it is larger in diameter and has 20 splines instead of 21. It is used on tractors of 110 to 190 kW of PTO power. Some large, four-wheel-drive tractors, used primarily for traction, do not have PTO drives.

Early PTO drives were driven from the tractor transmission and stopped rotating whenever the traction clutch was disengaged. Present standard practice is to provide an independent PTO which is controlled by its own separate clutch. Figure 4.13 illustrates the most common type of universal joint drive that is used for transmitting power from the PTO shaft to an implement. Two Cardan universal joints are included and the connecting shaft is telescoping to accommodate changes in angularity and distance between the implement and tractor. An integral shield surrounds the shaft and partially surrounds each joint. The shield normally rotates with the shaft but can stop if it contacts a person or other object. A single Cardan joint creates fluctuations in drive line rotation when operating at an angle, as shown in Figure 4.14. The curves in Figure 4.14 are based on the following equation:

$$\tan (\phi_{jo}) = \cos (\alpha) \tan (\phi_{ji}) \tag{4.26}$$

where ϕ_{jo} = angular displacement of joint output shaft, radians
$\quad \alpha$ = joint angle (see Figure. 4.14)
$\quad \phi_{ji}$ = angular displacement of joint input shaft, radians
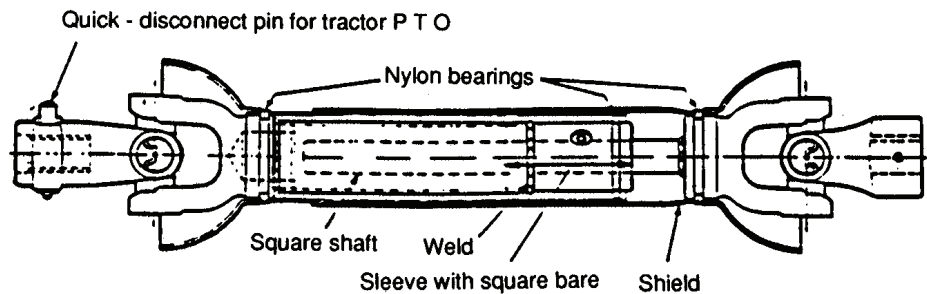

Figure 4.13 – A telescoping PTO shaft with integral safety shield (courtesy of Neapco Products, Inc.).

The relationship between shaft velocities is:

$$\frac{n_{jo}}{n_{ji}} = \frac{\cos(\alpha)}{1 - \sin^2(\alpha)\sin^2(\phi_{ji})} \tag{4.27}$$

where n_{ji}, n_{jo} = speeds of joint input and output shafts, respectively, in rev/min. When two Cardan joints are connected in series, as in Figure 4.13, the velocity fluctuations will cancel if the two joint angles are equal and the joints are 90° out of phase. Proper phasing is accomplished when the yokes connected to the two ends of the intermediate shaft are in line with each other. Then the velocity fluctuations are canceled in the output shaft but not in the intermediate shaft. Constant speed universal joints, such as the Bendix-Weiss joint, can transmit power through an angle without introducing the speed fluctuations of the Cardan joint. Although the Bendix-Weiss joints transmit torque more smoothly, they are not well suited for the high torque levels often encountered in agricultural equipment.

Experimental tests have shown that peak torques in a PTO driveline far exceed average torques. Thus, drive lines are designed on the basis of fatigue stresses imposed by repeated peak torques. One technique for reducing fatigue stresses is to limit the joint angles encountered during normal operations when the tractor and implement are not in a turn.
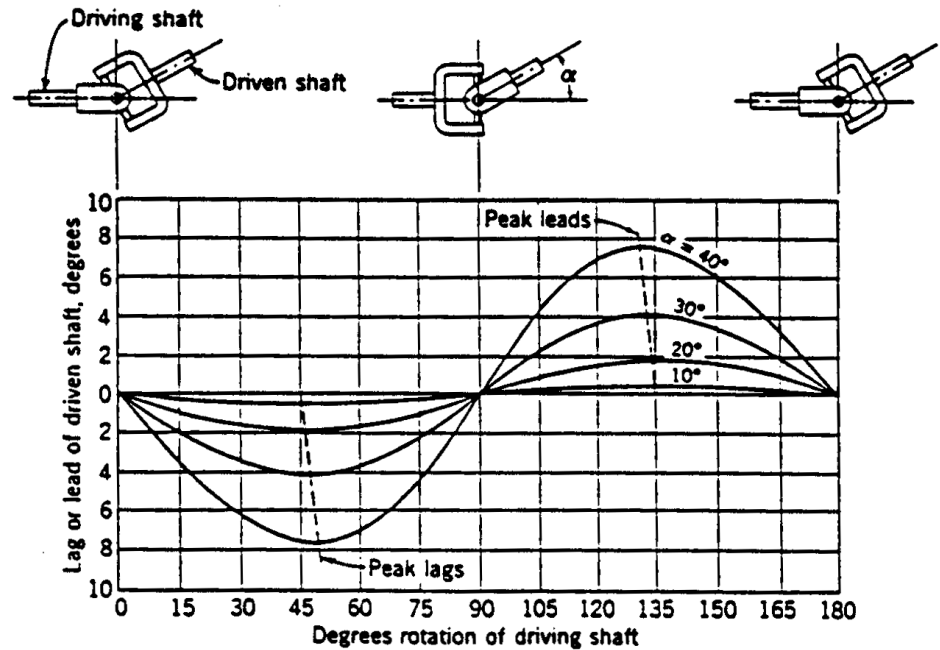

Figure 4.14 – Lead or lag of shaft driven by a Cardan-type universal joint, in relation to rotational position of the driving shaft (reprinted from Kepner et al., 1978).

4.4 OVERLOAD SAFETY DEVICES

In many types of farm machinery, a single power source drives various components that have widely differing power requirements and are subject to varying degrees of possible overload. In such a system some overload protection is almost mandatory, especially for the lower-powered components. Three general types of safety devices commonly used in rotary drives are:

- Those that depend upon shearing of a replaceable connecting member in the drive.
- Units in which spring force holds two corrugated members together, utilizing the principle of the inclined plane. These devices are also called jump clutches.
- Devices depending entirely upon friction.

4.4.1 Shear devices

Shear devices are simple and relatively inexpensive, but the sheared element must be replaced after each overload. Thus, they are most suitable where overloads are rather infrequent. Shear devices can be designed for almost any desired load rating, although pin or key sizes become rather small for low torque ratings unless a material with low shear strength is selected. Typical arrangements for shear devices are:

- Shear key between the shaft and hub (usually a brass key, with a tapered shaft and bore).
- Diametral shear pin through the hub and shaft (gives double shear).
- Flange-mounted shear pin parallel to the shaft, as illustrated in Figure 4.15.
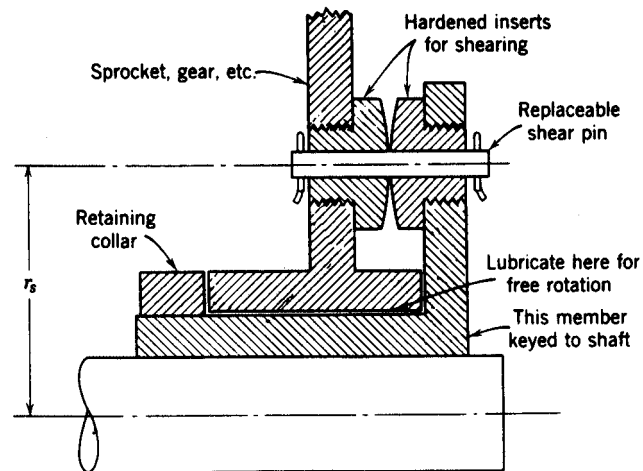

Figure 4.15 – An arrangement with a flange-mounted shear pin. The hardened shearing inserts could be omitted, particularly if overloads are expected only infrequently or if necked-down shear pins are used (reprinted from Kepner et al., 1978).

Regardless of the arrangement, the driving and driven members must rotate freely with respect to each other after the shear element has failed. With either of the first two types, the shaft or bore is likely to be scored by the sheared element. Removal of the hub from the shaft may be necessary in the first type to replace a sheared key.

The flange-mounted shear pin is the most easily replaced, but the unit is more costly than a diametral pin and not as well adapted to low torques because of the greater radius to the shear section. For experimental testing, interchangeable pins necked down to different diameters can be used to vary the load at which failure occurs. In production units, a full-sized pin of an ordinary material (such as hot-rolled steel) is desirable for convenience of replacement by the operator.

The torque at which a flange-mounted shear pin will fail, and the power, are given by the following equations:

$$T = r_s \left(\frac{\pi}{4} d_1^2 S_s \right) 10^{-3} \tag{4.28}$$

and
$$kW = \frac{2\pi NT}{60,000} = 8.225 N r_s d_1^2 S_s 10^{-8} \tag{4.29}$$

where N = shaft speed, rev/min
      T = torque, N · m
      r_s = distance between shaft center and shear pin center (Figure. 4.15), mm
      d_1 = diameter of shear pin at shear section, mm
      S_s = ultimate shear strength of shear pin, MPa
    Similarly, a diametral shear pin (double shear) will fail when:

$$kW = 8.225 N D d_1^2 S_s 10^{-8} \tag{4.30}$$

where D = shaft diameter (diameter at which shear occurs), mm.

4.4.2 Jump clutch devices

A jump clutch has rounded, mating jaws or corrugations that are held together by an adjustable spring. In Figure 4.16, part A is keyed to the shaft and part B, the driving member, is free to rotate on the shaft when an overload occurs. The overload torque required to rotate B with respect to A and cause jumping is a function of the slope of the inclined corrugation faces, the coefficient of friction between the faces, the effective radius from the shaft centerline to the contact area, and the force required to compress the spring and permit axial movement of B with respect to A.

The spring must have sufficient deflection available so it is not compressed solid before the relative displacement of the two corrugated faces is sufficient to permit jumping. Although friction between the corrugated faces influences the magnitude of the torque required for jumping, the unit would function (at a lower torque) even if the coefficient of friction were zero.

Because of its automatic resetting feature, the jump clutch is more suitable than shear devices where overloads may occur rather frequently. There is no slippage until
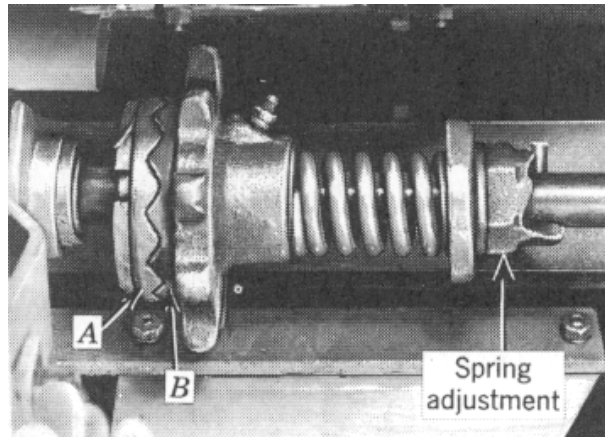
**Figure 4.16 – Typical arrangement of a jump clutch
(reprinted from Kepner et al., 1978).**

the load exceeds the setting of the unit, and then the operator is warned audibly that an overload has occurred. Jump clutches are more expensive than shear devices and are not well suited to large loads because of the excessive physical size required. When they are jumping, they impose high shock loads upon the drive system.

The magnitude and variability of the friction force required to slide the movable member axially can have an important effect upon the torque required to cause jumping. To minimize the axial friction force, the torque should be transmitted to or from the movable member at a relatively large radius, as with a sprocket or sheave, rather than through splines or a key in the shaft.

4.4.3 Friction devices

A properly designed belt drive can serve as a friction safety device, although its performance is affected by variations in belt tension and by the increase in coefficient of friction as the percentage of belt slip increases. The performance is more consistent with a spring-loaded idler than with a fixed adjustment.

Single-plate clutches with two friction surfaces, similar to tractor or automotive clutches, are often used for overload protection. The spring pressure is adjusted to drive normal loads but slip under abnormal loads. In comparison with jump clutches, friction safety clutches have the advantages of more consistent breakaway torque and no damaging peaks during slippage. However, tests have shown that the momentary dynamic torque capacity under sudden load application may be two to three times the static value.

Friction clutches are very effective in protecting a drive from frequent peak torques. But under some conditions it is possible to have a friction clutch slipping sufficiently to become overheated without the operator being aware of the overload.

FLUID POWER, MECHATRONICS, AND CONTROL

5

INTRODUCTION

When fluid power systems gained widespread use on agricultural equipment in the 1940s, physical strength was no longer a necessary qualification for equipment operators. Fluid power permits the raising and lowering of heavy implements with a minimum of physical effort. Also, fluid power can be transmitted to remote locations much more conveniently than mechanical power. In this chapter, you will learn the basic principles and be introduced to the elements of fluid power systems.

5.1 BASIC PRINCIPLES AND ELEMENTS OF FLUID POWER

There are five principles that are important to an understanding of fluid power circuits. They are: (a) liquids have no shape of their own but will flow to acquire the shape of their container, (b) liquids can be considered incompressible at the pressures used in fluid power systems, (c) liquids transmit pressure equally in all directions, (d) the rate of flow from a positive displacement pump varies proportionally with pump speed but is virtually independent of system pressure, and (e) any flow of liquid through a pipe or orifice is accompanied by a reduction in liquid pressure.

Fluid power systems include, at a minimum, a reservoir, one or more pumps to convert mechanical power into fluid power, one or more control valves, one or more actuators to convert the fluid power back into mechanical power, lines to join the various components, and filters to remove contaminants from the hydraulic fluid. Each of these components will be discussed, as well as the types of circuits in which the components can be used.

Making physical drawings of the many components in fluid power systems would be very time consuming and such drawings would not necessarily convey the system logic. Thus, a joint industry conference of the fluid power industry was convened to devise symbols for fluid power components. The resulting symbols were initially called JIC symbols. Later, they were standardized by the International Standards Organization and by the National Fluid Power Association and are now called NFPA symbols. The NFPA symbols are summarized in Appendix B. The NFPA symbols are

analogous to electrical symbols and they simplify the drawing of fluid power circuits in the same way that electrical symbols simplify the drawing of electrical circuits. The shape of every NFPA symbol was chosen to be as self explanatory as possible and you should be able to recognize and use the symbols very quickly. Physical drawings may be used to explain some fluid power components in this chapter, but the corresponding NFPA symbols will also be shown.

5.2 PUMPS

A pump is the heart of any fluid power system; it converts mechanical power into fluid power. Only positive displacement pumps are used in fluid power systems, thus the pump delivery is nearly independent of the pressure at the outlet port of the pump. The three basic types of pumps used in fluid power systems include *gear pumps*, *vane pumps*, and *piston pumps*.

Diagrams of gear and vane pumps are shown in Figure 5.1. The displacement of these pumps is the theoretical amount of liquid that would be moved from the inlet port to the outlet port in one revolution of the pump shaft. Liquid is carried in the tooth spaces of the gear pump but meshing of the gears prevents oil from making a full circle; thus the oil is forced out of the outlet port. Likewise, oil is carried in the spaces between the sliding vanes in the vane pump. Both the gear pump and the vane pump have fixed displacement, i.e., the displacement cannot be changed after the pump is manufactured.

Both axial-piston pumps (Figure 5.2) and radial-piston pumps (Figure 5.3) are available. The former have pistons parallel to the pump shaft, while the latter have pistons arranged radially to the shaft. The piston pumps in Figures 5.2 and 5.3 both have variable displacement, but piston pumps can also be designed with fixed displacement.
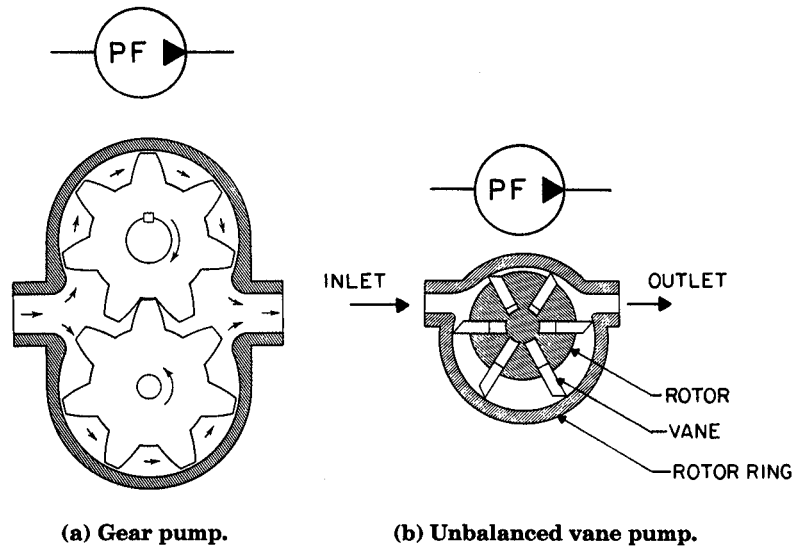

(a) Gear pump.   (b) Unbalanced vane pump.
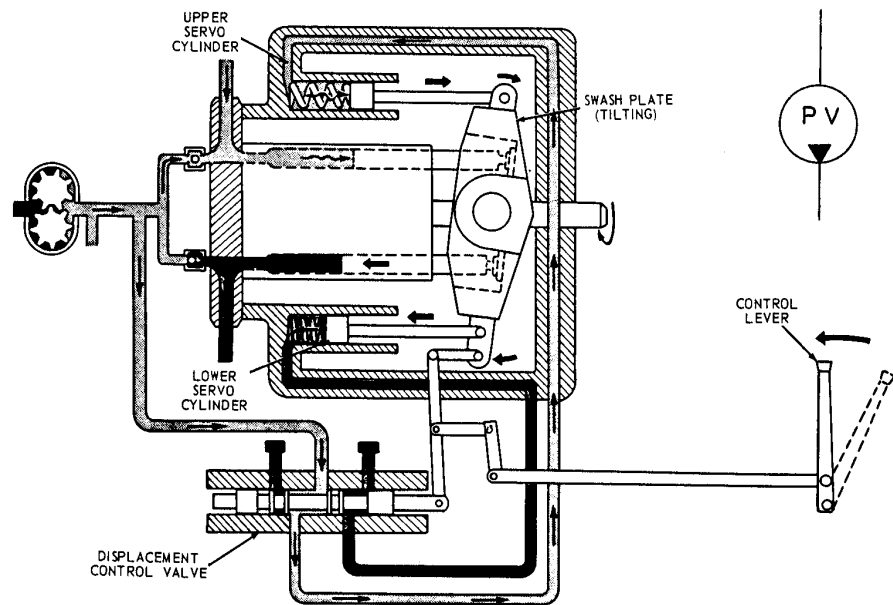
Figure 5.1 – Fixed-displacement pumps.

Figure 5.2 – Variable-displacement, axial piston pump (courtesy of Deere and Co.).
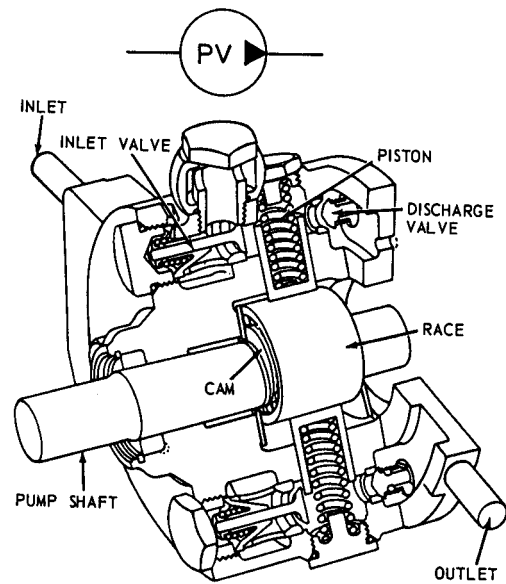

Figure 5.3 – Radial-piston pump (courtesy of Deere and Co.).

The delivery of oil from a pump can be calculated using Equation 5.1:

$$Q_p = \frac{V_p n_p \eta_{vp}}{1000} \tag{5.1}$$

where Q_p = pump delivery, L/min
  V_p = pump displacement, cm^3/rev
  n_p = pump speed, rev/min
  η_{vp} = volumetric efficiency of the pump, decimal

Because of internal leakage within a pump, the volumetric efficiency is always less than one, i.e., the pump always delivers less than its theoretical delivery. Generally, internal leakage in a hydraulic component is directly proportional to the area of the leakage path and the pressure drop across the leakage path and inversely proportional to viscosity. The leakage flow is given by the following equation:

$$Q_L = \frac{(6 \times 10^7)C_L A \Delta p}{\mu} \tag{5.2}$$

where Q_L = leakage flow, L/min
  C_L = leakage length constant, cm
  A = cross-sectional area of the leakage path, cm^2
  μ = dynamic viscosity of the fluid, mPa·s
  Δp = pressure drop, MPa

Therefore, the volumetric efficiency can be calculated as:

$$\eta_{vp} = \frac{Q_{tp} - Q_L}{Q_{tp}} = 1 - \frac{Q_L}{Q_{tp}} \tag{5.3}$$

where Q_{tp} is the theoretical pump delivery and can be calculated from Equation 5.1 by equating $\eta_{vp} = 1$.

The torque requirement of a pump can be calculated from Equation 5.4:

$$T_p = \frac{\Delta p V_p}{2\pi \eta_{tp}} \tag{5.4}$$

where T_p = torque required to drive the pump, N·m
  Δp = pressure rise across the pump, MPa
  η_{tp} = torque efficiency of the pump, decimal

Because of friction within the pump, the torque efficiency is always less than one and more than the theoretical amount of torque required to drive the pump. The frictional torque (T_{fp}) is the amount of torque require to overcome friction within the pump. The frictional torque is given by:

$$T_{fp} = \frac{2\pi C_f \mu n_p}{6 \times 10^{10}} \tag{5.5}$$

where C_f = constant (cm^3). The friction torque is called the damping torque since it is proportional to the shaft speed. There is an additional frictional torque due to shaft seals. The torque efficiency can be calculated as:

$$\eta_{tp} = \frac{T_{tp}}{T_{tp} + T_{fp}} = \left(1 + \frac{T_{fp}}{T_{tp}}\right)^{-1}$$
(5.6)

where T_{tp} is the theoretical torque and it can be calculated from Equation 5.4 by letting $\eta_{tp} = 1$.

The fluid power produced by a pump can be calculated using Equation 5.7:

$$P_{fl} = \frac{Q_p \Delta p}{60}$$
(5.7)

where P_{fl} = fluid power, kW. The shaft power required to drive a pump can be calculated from Equation 5.8:

$$P_{sp} = \frac{P_{fl}}{\eta_{pp}}$$
(5.8)

where P_{sp} = shaft power required to drive the pump, kW

$\eta_{pp} = \eta_{vp} \times \eta_{tp}$ = power efficiency of the pump

Since both η_{vp} and η_{tp} are less than one, η_{pp} is also less than one and more than the theoretical amount of power is required to drive the pump.

The efficiencies of a pump vary with operating conditions, as illustrated in Figure 5.4. The internal leakage in a pump increases with Δ_p; as pump speed approaches zero, the entire theoretical delivery can leak back to the inlet and η_{vp} goes to zero. As pump speed increases, however, the internal leakage becomes small relative to the
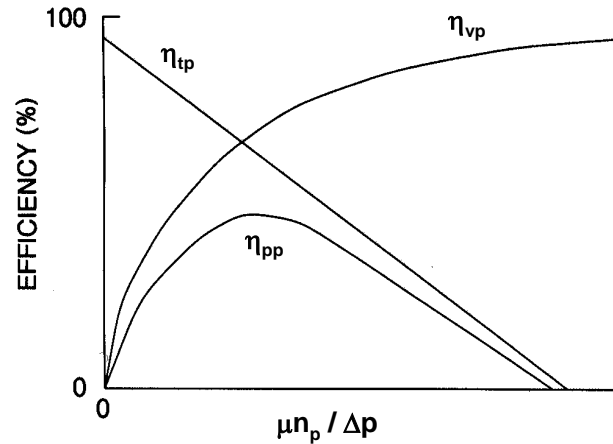

Figure 5.4 – Torque, volumetric, and power efficiencies.

theoretical delivery and η_{vp} approaches its maximum. Some shaft torque is used to overcome the friction which is always present in a pump; at high Δp, that friction torque is relatively small compared to the theoretical torque required and η_{tp} is at a maximum. Conversely, at low Δp, the friction torque is dominant and η_{tp} reaches zero. Since η_{pp} is the product of η_{vp} and η_{tp}, the shape of its curve on Figure 5.4 is defined by the shape of the torque and volumetric efficiency curves. Figure 5.4 implies that a pump must be operated within proper limits of speed and pressure or its power efficiency will drop to unacceptable levels.

5.3   VALVES

Valves are used in fluid power systems to control pressure, volume, and direction of flow. Valves are classified, accordingly, as *pressure control valves* (PCV), *volume control valves* (VCV), and *directional control valves* (DCV).

5.3.1   Pressure control valves

Liquid passes through orifices in control valves, resulting in pressure drops. Equation 5.9 relates the pressure drop across an orifice to the flow through it:

$$Q = 60C_oA_o\sqrt{\frac{2\Delta p}{\rho_f}} \tag{5.9}$$

where Q = flow through orifice, L/min
$\quad\quad$ C_o = orifice coefficient, dimensionless
$\quad\quad$ A_o = orifice area, mm^2
$\quad\quad$ Δp = pressure drop across the orifice, MPa
$\quad\quad$ ρ_f = mass density of the fluid, kg/m^3

In the usual case where A_o is much smaller than the upstream channel and flow is turbulent, C_o= 0.60 for a sharp-edged orifice, but can rise to more than 0.80 if the orifice edges are rounded. The orifice shape has little effect, i.e., C_o will be nearly the same for a long narrow orifice as for a circular one. For typical, petroleum-based fluids used in fluid power systems, ρ_f = 850 to 950 kg/m^3.

The most common PCV is the relief valve. Relief valves are closed during normal operation, but open at a set pressure to discharge liquid to the reservoir. Thus, relief valves are intended to limit the pressure in a circuit to a safe level. Because direct-acting relief valves (Figure 5.5) have a large pressure override (Figure 5.6), pilot-operated relief valves are sometimes used (Figure 5.7). Pilot-operated relief valves have a light spring which allows a pilot relief valve (see numbers 3 and 4 in Figure 5.7) to open at the desired cracking pressure. The resulting flow passing through an orifice in the valve piston causes a pressure drop (see Equation 5.9) which raises the piston, thus opening the main relief valve. The pressure override, which is the full-flow pressure minus the cracking pressure, is thus much smaller in a pilot-operated relief valve than in a direct-acting relief valve. Note that the direct-acting relief valve is classified as a two-way valve, meaning that it has two ports for connection to the fluid power circuits. The pilot-operated relief valve would be classified as a three-way valve unless the drain was internally connected to the discharge port.
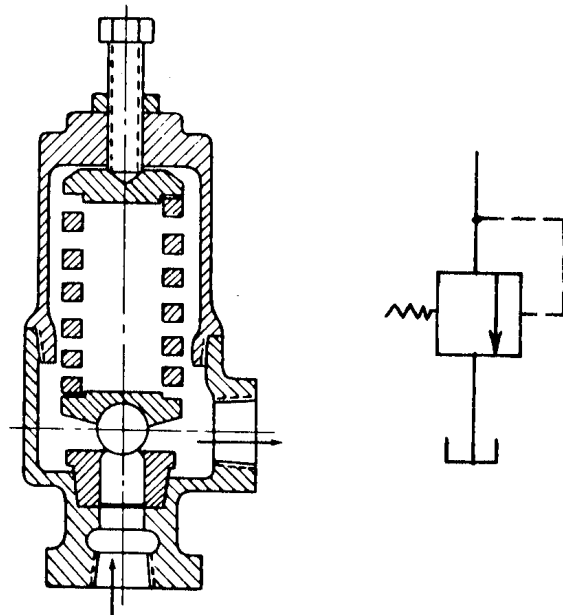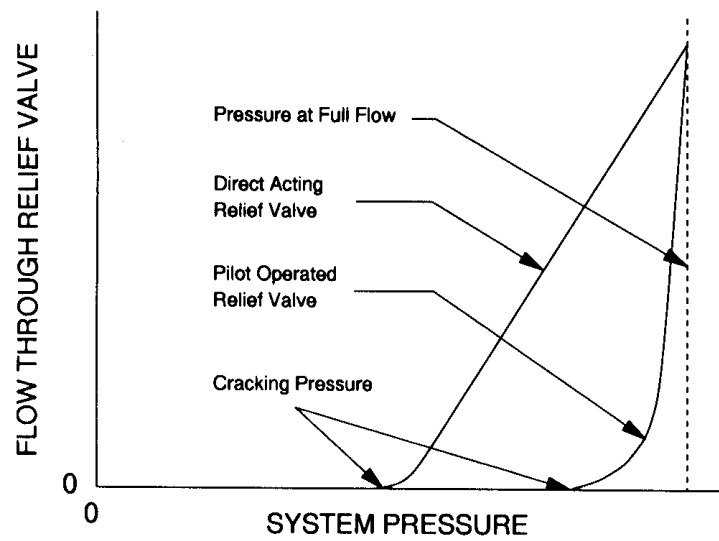
Figure 5.5 – A direct-acting relief valve.

Pressure at Full Flow

Direct Acting
Relief Valve

Pilot Operated
Relief Valve

Cracking Pressure

FLOW THROUGH RELIEF VALVE

0

0

SYSTEM PRESSURE

Figure 5.6 – Pressure override in a relief valve.
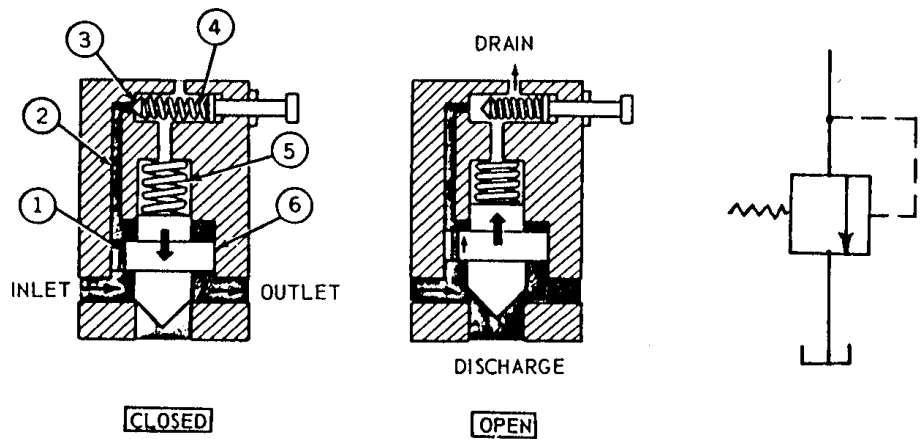
Figure 5.7 – A pilot-operated relief valve.

5.3.2   Volume control valves

The two most common VCVs are the throttling valve (Figure 5.8) and the flow-divider valve (Figure 5.9). The purpose of both valves is to regulate the flow to the outlet port regardless of downstream pressure. Both valves have a spring-loaded spool valve whose purpose is to maintain a constant pressure across an orifice and thus, in accordance with Equation 5.9, maintain constant flow to the outlet port. If the flow through the orifice increases, the pressure drop across the orifice will also increase in accordance with Equation 5.9 and the pressure within the spool will fall. The resulting pressure imbalance across the head of the spool will move the spool to the right to partially block the outlet port, thus reducing the flow to the outlet port. Conversely, if the flow through the orifice declines, the spool will move to the left to create a larger opening to the outlet port. Both the throttling valve and the flow-divider valve are pressure compensated, because they automatically compensate for changes in down-
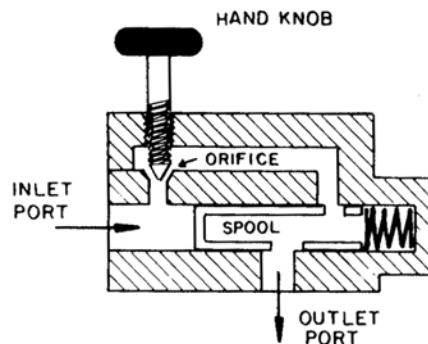

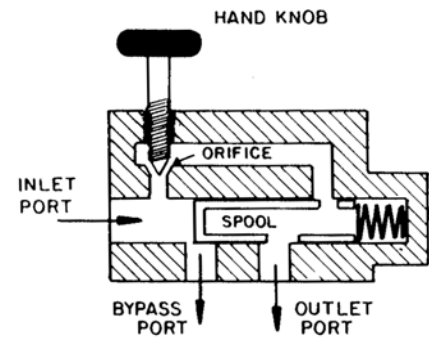**Figure 5.8 – A pressure-compensated throttling valve.**

Figure 5.9 – A bypass-type flow-divider valve.

stream pressure. Both of the valves that are illustrated have adjustable flow rates, i.e., the operator can use the hand knob to set the desired flow level. Nonadjustable valves are also available.

The primary difference between the throttling valve and the flow-divider valve is that the latter has a third port for bypass flow. The throttling valve can only be used in systems in which the pump flow reduces automatically when the flow is throttled. In systems with fixed-displacement pumps, any surplus flow must be bypassed and thus only the flow-divider valve is suitable. The flow-divider valve can also be used as a priority valve, i.e., circuits with top priority (for example, steering circuits) are connected to the outlet port. Any excess flow passes to through the bypass port to circuits with lower priority.

5.3.3   Directional control valves

A directional control valve (DCV) is illustrated in Figure 5.10. It has four ports and is thus classified as a four-way valve. It is also classified as a three-position valve because the valve spool has three possible positions: right, centered, or left. In Figure 5.10a, the spool is to the right to connect port P (for pump) to B and port T (for tank, or reservoir) to A. These connections are reversed when the spool is to the left as in Figure 5.10c. An actuator can be connected to ports A and B and, by moving the DCV spool left or right, the direction of movement of the actuator can be reversed. With the spool centered, as in Figure 5.10b, all ports are blocked and thus the valve is also classified as a closed-center valve, in circuits in which pump flow changes automatically to meet demand. In drawings of fluid power circuits, DCVs are always shown with the spool centered for simplicity and it is left to the reader to imagine the other spool positions.

The valve illustrated in Figure 5.11 is a four-way, three-position, open-centered DCV. It could be used with a fixed-displacement pump because, with the spool centered, pump flow can pass through the DCV to the reservoir. Note, however, that any actuator connected to the DCV would be free to move when the spool was centered. If the actuator was a hydraulic cylinder used to raise an implement, for example, the implement would lower as soon as the spool was centered. For that reason, open-centered DCVs are seldom used on agricultural equipment. Instead, if the fluid power system
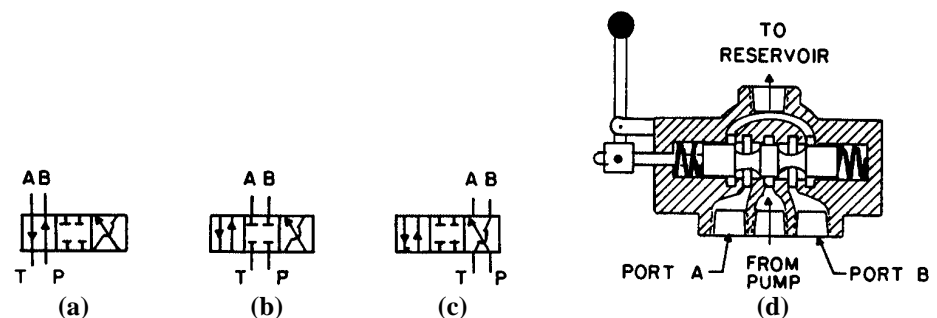

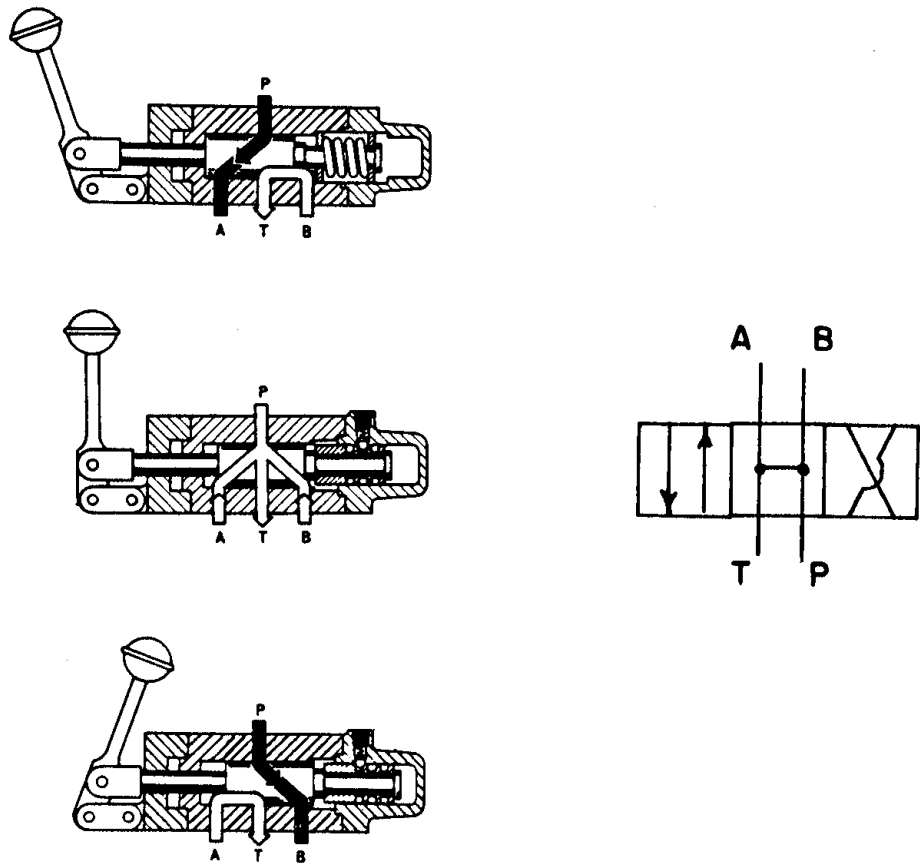**Figure 5.10 – A closed-center directional control valve.**

Figure 5.11 – An open-center directional control valve.

has a fixed-displacement pump, a tandem-centered DCV is used. A dual tandem-centered DCV is illustrated in Figure 5.12. With both spools centered, all actuator ports are blocked but the pump port is connected to the reservoir port. Moving either spool left or right blocks the pump connection to the reservoir and oil is forced to flow to an actuator.

Although the NFPA symbols do not reveal it, all DCVs also provide some degree of flow control. By partial movement of the spool to either the left or right, the orifice within the valve can be partially opened and, in accordance with Equation 5.9, can provide partial flow delivery to the actuator.
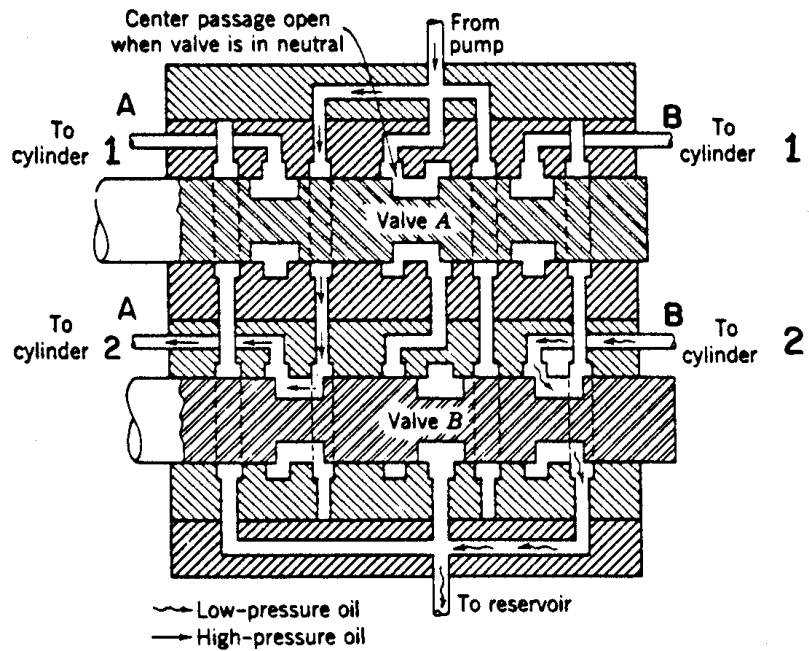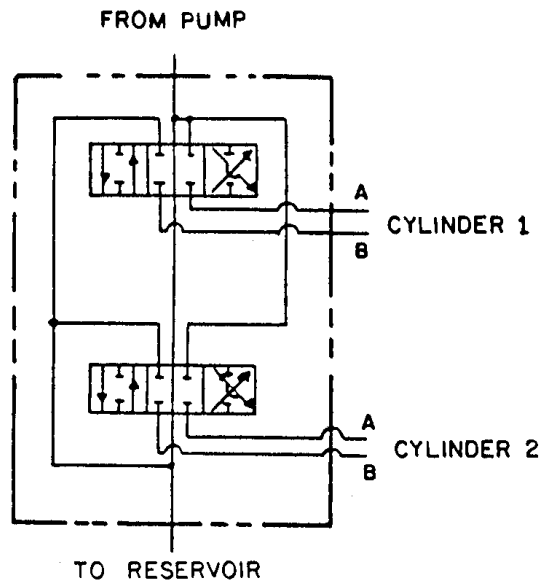
Figure 5.12 – A dual tandem-center directional control valve
(reprinted from Kepner et al., 1978).

5.4   ACTUATORS

Actuators include hydraulic motors to provide rotary mechanical power and hydraulic cylinders to provide linear mechanical power.

5.4.1   Hydraulic motors

Motors are similar to pumps and, with suitable precautions, the pumps shown in Figure 5.1 could also be used as motors. To prevent seal damage, the shaft seals of most pumps and motors are internally vented to the low pressure port. Low pressure exits at the inlet of a pump but at the outlet of a motor and thus, to use a gear or vane pump as a motor, the direction of rotation must be reversed. Axial-piston motors of either fixed or variable displacement are also available.

Equations 5.10 to 5.12 are for the speed, torque, and power output, respectively, of a hydraulic motor:

$$n_m = \frac{1000 Q \eta_{vm}}{V_m} \tag{5.10}$$

and

$$T_m = \frac{\Delta p \, V_m \eta_{tm}}{2\pi} \tag{5.11}$$

and

$$P_{sm} = \frac{Q \Delta p \eta_{pm}}{60} \tag{5.12}$$

where n_m = motor speed, rev/min

η_{vm} = volumetric efficiency of motor

V_m = motor displacement, cm^3/rev

T_m = motor torque, N·m

η_{tm} = torque efficiency of motor

P_{sm} = motor shaft power, kW

$\eta_{pm} = \eta_{vm} \times \eta_{tm}$ = power efficiency of motor

Q = fluid flow through motor, L/min

Δp = pressure drop across motor, MPa

The volumetric, torque, and power efficiencies for a motor are analogous to those for a pump and vary as illustrated in Figure 5.4.

5.4.2   Hydraulic cylinders

Both single-acting and double-acting hydraulic cylinders are available. A cutaway of a double-acting cylinder is shown in Figure 5.13. Oil is forced into the port on the left to extend the cylinder and the piston movement forces oil out of the port on the right. Conversely, by reversing the port connections, the cylinder can be made to retract. The double-acting cylinder of Figure 5.13 could be converted into a single-acting cylinder by emptying the oil to the right of the piston and installing an air breather in the port to the right. A single-acting cylinder is used in those situations where an external load is available to make the cylinder retract. Dimensions for hydraulic cylinders to control implements have been specified in ASAE Standard S201.4.
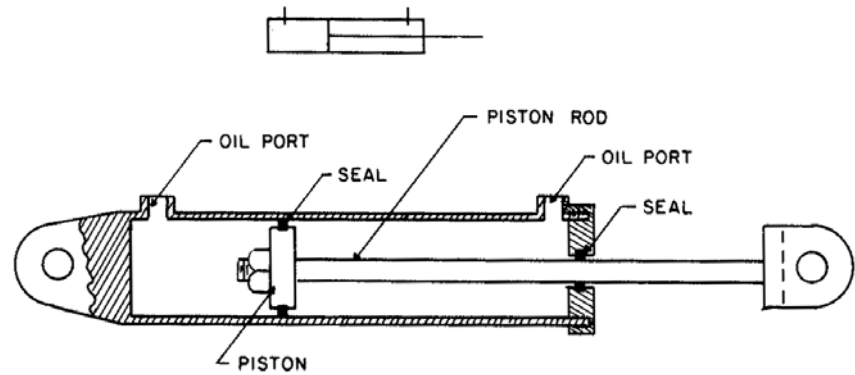
Figure 5.13 – A double-acting hydraulic cylinder.

The load capacity of a cylinder can be calculated using Equation 5.13:

$$F = \frac{p_1 A_1 - p_2 A_2}{10}$$ (5.13)

where F = force capacity of the cylinder, kN
A_1 = area of piston, cm^2
A_2 = area of piston minus area of piston rod, cm^2
p_1 = pressure (gage) acting on area A_1, MPa
p_2 = pressure (gage) acting on area A_2, MPa

The factor of 10 is simply a units conversion factor. A negative answer indicates the cylinder is retracting. In many situations, one of the ports will be connected to the reservoir and the corresponding pressure will be zero gage pressure.

The speed at which a cylinder extends or retracts can be calculated using Equation 5.14:

$$v = \frac{Q}{6A_i}$$ (5.14)

where v = speed of movement of rod, m/s
Q = flow into cylinder, L/min
$A_i = A_1$ if cylinder is extending or A_2 if retracting

Note that, for a given Q, the cylinder extends slower than it retracts, since $A_1 > A_2$. The return flow from a double-acting cylinder is calculated from the following equation:

$$Q_{cr} = 6A_j \, v$$ (5.15)

where Q_{cr} = cylinder return flow, L/min
$A_j = A_2$ if cylinder is extending or A_1 if retracting

Equations 5.14 and 5.15 will show that a cylinder returns less oil than it receives while extending and more oil than it receives while retracting. The reservoir must supply the flow deficit or absorb the excess flow.

5.5   RESERVOIRS, FLUIDS, FLILTERS, AND LINES

A reservoir supplies oil to the pump and provides a place for oil to return from the circuit. The reservoir must be large enough to allow the oil to cool, i.e., a larger reservoir allows more resident time for the oil to cool in the reservoir. If the reservoir cannot provide sufficient cooling, an oil cooler can be used to provide supplementary cooling. A properly designed reservoir has internal baffles to reduce oil splashing and has its inlet and outlet ports arranged to prevent oil returning from the hydraulic circuit from immediately re-entering the pump. The return port should be below the oil surface to reduce air entrainment and foaming as the oil returns to the reservoir. Finally, the reservoir must be vented to the atmosphere to accommodate changing oil levels and the vent should have a filter to prevent dust entry. As the oil passes through lines, valves, and other devices that do no mechanical work, any pressure drops result in conversion of fluid power to heat. The power loss and heat generation rate can be calculated from Equation 5.16:

$$P_L = \frac{\Delta p Q}{60} \tag{5.16}$$

where P_L = power loss in a nonworking device, kW
  Δp = pressure drop across the device, MPa
  Q = flow through the device, L/min
The number 60 is a units constant

Viscosity is the most important property of a hydraulic fluid. Manufacturers generally recommend fluid viscosities between 12 and 49 mPa·s at the operating temperature of the pump. Fluid viscosities fall markedly with increased temperatures, but the viscosity dependence on temperature is less if the fluid has a high viscosity index. A high viscosity index is thus highly desirable for hydraulic fluids, since the fluid is subject to wide variations in temperature and pumps and motors become very inefficient when the viscosity is either too low or too high (see Figure 5.4). Petroleum-based hydraulic fluids are subject to oxidation. The oxidation rate doubles for every 10°C increase in temperature but is very low when the temperature is below 60°C. Additives are used in the fluid to reduce oxidation, foaming, and wear. A rust inhibitor is also generally used. The transmission case on tractors and self-propelled machinery is often used as the reservoir for the hydraulic system. Then the same fluid that serves as the hydraulic fluid must also lubricate the gears in the transmission.

Metal particles and other solid contaminants can be very damaging to hydraulic components. Clearances between mating parts are 10 µm or less in some hydraulic components and, if particles of that size pass between the mating parts, rapid failure can result. Thus filters are used to remove contaminants in fluid power systems. Three possible alternatives for locating a filter in a fluid power circuit include (a) between the reservoir and the pump inlet port, (b) immediately after the pump outlet port, and (c) just before the return inlet to the reservoir. Location (a) is seldom used because the pressure drop across the filter can cause subatmospheric pressures to be generated

within the pump, leading to cavitation and pump damage. Location (b) is seldom used because the filter would have to withstand very high pressures in that location. Thus, location (c) is usually chosen for filters that can remove particles as small as 10 μm. In addition, a strainer or porous filter may be used in location (a) to prevent the largest particles (typically larger than 150 μm) from reaching the pump.

Lines consist of hydraulic tubing and/or hydraulic hoses to convey fluid between the various devices in a fluid power circuit. Both the tubing and the hoses are treated as smooth conduits for which the correct diameter must be selected to avoid excessive pressure drops in the lines. The Reynolds number is used to determine whether flow in the lines is laminar or turbulent. Reynolds number is defined as:

$$N_{Re} = \frac{4C\rho_f Q}{\pi \mu \, d} \tag{5.17}$$

where N_{Re} = Reynolds number, dimensionless
  $C = 16.67$ = units constant
  ρ_f = fluid density, kg/m^3
  Q = flow through conduit, L/min
  μ = dynamic viscosity of oil, mPa·s
  d = inside diameter of conduit, mm

Flow is laminar for Reynolds numbers less than 2000 and fully turbulent for Reynolds numbers above 4000. Between these limits, flow is in a transition region. The Hagen-
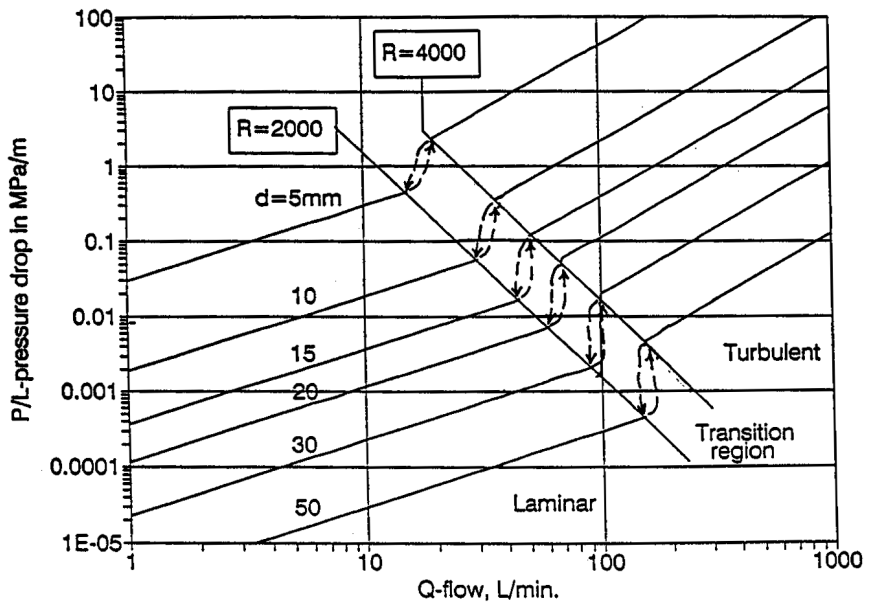

Figure 5.14 – Pressure drop in hydraulic conduits for $\rho_f = 850$ kg/m^3 and $\mu = 27.6$ mPa·s.

Poiseuille law is used to compute pressure losses for laminar flow in conduits, i.e.:

$$\frac{\Delta p}{L} = \frac{2.13 \mu \, Q}{\pi \, d^4} \qquad (5.18)$$

where Δp = pressure drop, MPa.

  L = length of conduit over which pressure drop occurs (m)

  For fully turbulent flow, the pressure drop can be calculated from the following equation:

$$\frac{\Delta p}{L} = \frac{0.0333 \mu^{0.25} \rho^{0.75} Q^{1.75}}{d^{4.25}} \qquad (5.19)$$

where terms are defined as in Equation 5.18. For convenience, Equations 5.18 and 5.19 have been plotted in Figure 5.14.
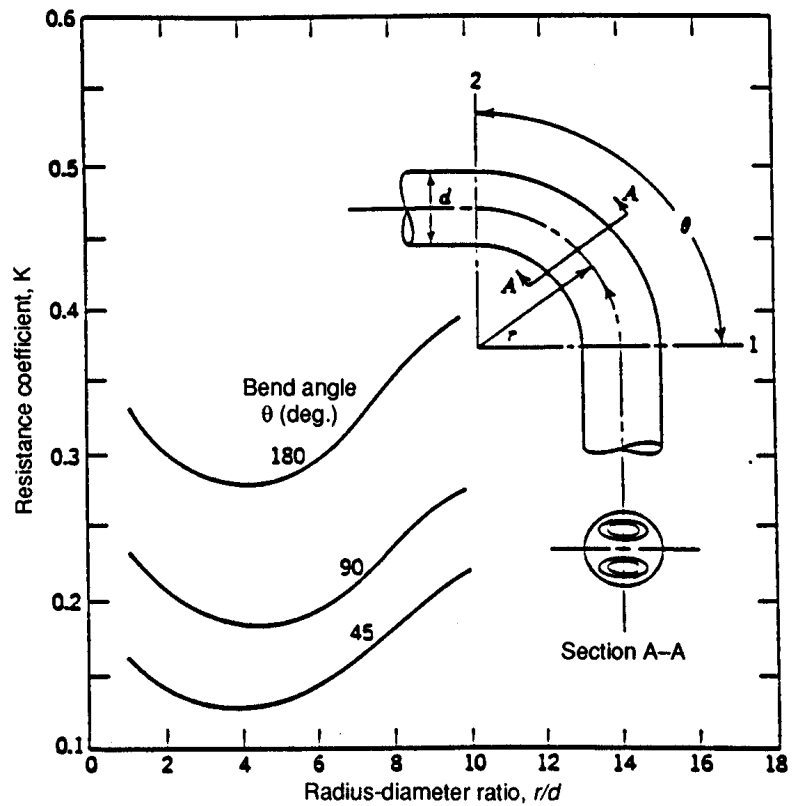

Figure 5.15 – Resistance coefficients of pipe bends (reprinted from J. J. Taborek, "Fundamentals of Line Flow," *Machine Design Magazine*, 16 April 1959).

The term *minor losses* refers to pressure drops that result from fittings, bends, and sudden changes in cross section. The pressure drop associated with bends can be calculated from the following equation:

$$\Delta p = (1.39 \times 10^{-4}) K \rho_f \frac{Q^2}{A^2} \tag{5.20}$$

where Δp = pressure drop, MPa

$\quad$ K = dimensionless factor taken from Figure 5.15

$\quad$ ρ_f = fluid density, kg/m^3

$\quad$ Q = flow in conduit, L/min

$\quad$ A = cross-sectional area of the conduit, mm^2

The numerical constants in Equations 5.18 through 5.20 are unit conversion factors. The pressure drop calculated from Equation 5.20 is added to the pressure drop that would be calculated for a straight conduit of equal length. Pressure drops occur in the various elbows, valves, and other fittings that are used in connecting fluid power circuits. Data on these pressure drops can be obtained from component manufacturers or by measurement.

5.6 TYPES OF FLUID POWER SYSTEMS

On most modern agricultural equipment, the hydraulic pump is driven directly by the engine so that fluid power will be available whenever the engine is running. The fluid power system is said to be in standby when the pump is running but no fluid power is needed. Any power delivered to the pump during standby is converted into heat, so it is necessary to minimize shaft power to the pump during standby. As Equations 5.7 and 5.8 show, there are three ways to minimize standby power. They are to minimize (a) pump pressure, (b) pump delivery, or (c) pump delivery and pressure. These approaches have led, respectively, to the *open-center* (OC), *pressure-compensated* (PC), and *load-sensing* (LS) fluid power systems that are now available for use on agricultural equipment.

5.6.1 Open-center systems

An open-center fluid power system (Figure 5.16) was the first system used on agricultural equipment and is still used on some smaller tractors. It includes a fixed-displacement gear pump, a relief valve, a tandem-center DCV with one or more spools, and one or more actuators. A pressure-flow diagram for an OC system is shown in Figure 5.17. During standby, the system operates at full flow but very low pressure because the pump can discharge freely to the reservoir through the tandem-center DCV. When a DCV spool is displaced to send oil to an actuator, pressure rises only enough to move the load; flow declines slightly as η_{vp} falls with increasing pressure (see Figure 5.4). If the actuator load is too large, the relief valve cracks open and flow to the actuator declines as oil is diverted to the reservoir through the relief valve.
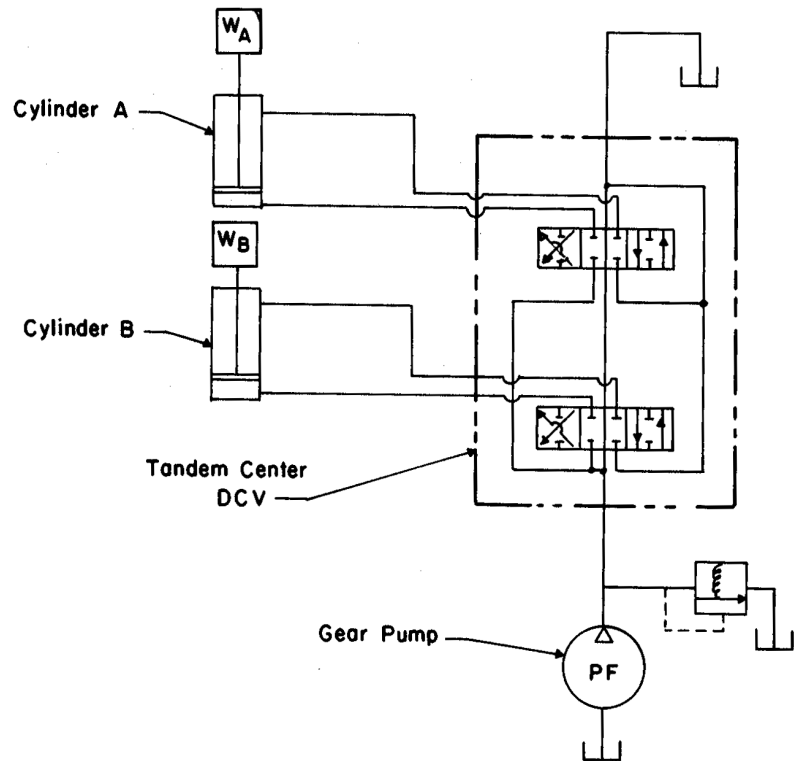
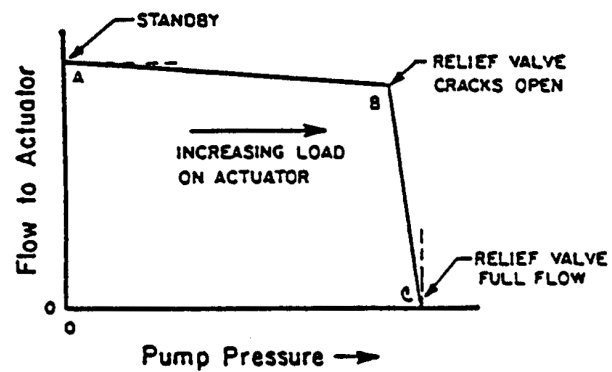**Figure 5.16 – An open-center hydraulic system.**

Figure 5.17 – A pressure-flow diagram of an open-center hydraulic system.

Maximum fluid power is produced just to the left of point B in Figure 5.17, i.e., just before the relief valve opens. When two or more spools in the DCV are displaced at the same time, oil flows to the actuator that requires the least pressure; the remaining actuators are stalled until the pressure can rise. If cylinder load WA in Figure 5.16 was larger than cylinder load WB, for example, cylinder B would move first and cylinder A would be stalled until cylinder B reached the end of its stroke. Such action is called sequencing and is a major disadvantage of OC systems.

5.6.2   Pressure-compensated systems

The pressure-compensated system (Figure 5.18) was developed to overcome some of the limitations of the OC system. The heart of the system is a pressure-compensated pump (see Figure 5.3) that automatically adjusts its delivery to meet demand. When no flow is needed, the stroke control valve opens to admit oil to the pump crankcase, holds the radial pistons away from the cam, and causes delivery to cease. If pressure falls, for example, when a DCV spool is displaced, the pressure in the crankcase drops and the pump again begins delivering oil. The stroke-control valve eliminates the need for a relief valve. Notice that the PC system includes a closed-center DCV, thus the pump flow is zero at standby, as shown in Figure 5.19. Any number of actuators can be connected simultaneously; since the pump automatically adjusts its stroke to maintain full pressure, no sequencing will occur unless the pump reaches full stroke. If oil demand is more than the pump can supply at full stroke, the system moves to the left of point B in Figure 5.19 and behaves like the OC system of Figure 5.17. Thus, sequencing can occur in the PC system if one of the connected actuators has a high flow demand and a low pressure demand.

5.6.3   Load-sensing systems

The most recent innovation in fluid power systems is the load-sensing (LS) system illustrated in Figure 5.20, alternatively called a pressure-flow-compensated system. It includes a closed-center DCV, so that flow is near zero at standby. Unlike the PC system, however, pressure is also low at standby and rises only high enough to meet the highest pressure demand in the system. Thus, sequencing is eliminated. The heart of the LS system is a pressure-compensated, axial-piston pump whose stroke is controlled by a differential-pressure compensating valve (DPCV). With port B of the DPCV blocked, the system would behave like a PC system with very low standby pressure, since a weak spring is used in the DPCV. Thus, standby pressure is low, typically about 1.4 MPa. When a DCV spool is displaced, the pressure demand of the load is transmitted to port B of the DPCV via a sensing line, thus assisting the spring and allowing the pump outlet pressure to rise to 1.4 MPa above the actuator demand. The same differential pressure of 1.4 MPA appears across the throttling valve (see Figure 5.8) which regulates flow to the actuator. When two or more actuators with differing pressure demands are engaged simultaneously, the highest pressure is transmitted to port B of the DPCV. A pressure drop larger than 1.4 MPa appears across those throttling valves controlling the actuators with smaller pressure demands. Each throttling valve has a manual adjustment to allow the operator to control the speed of the associated actuator. The pressure-flow diagram for the LS system is similar to that
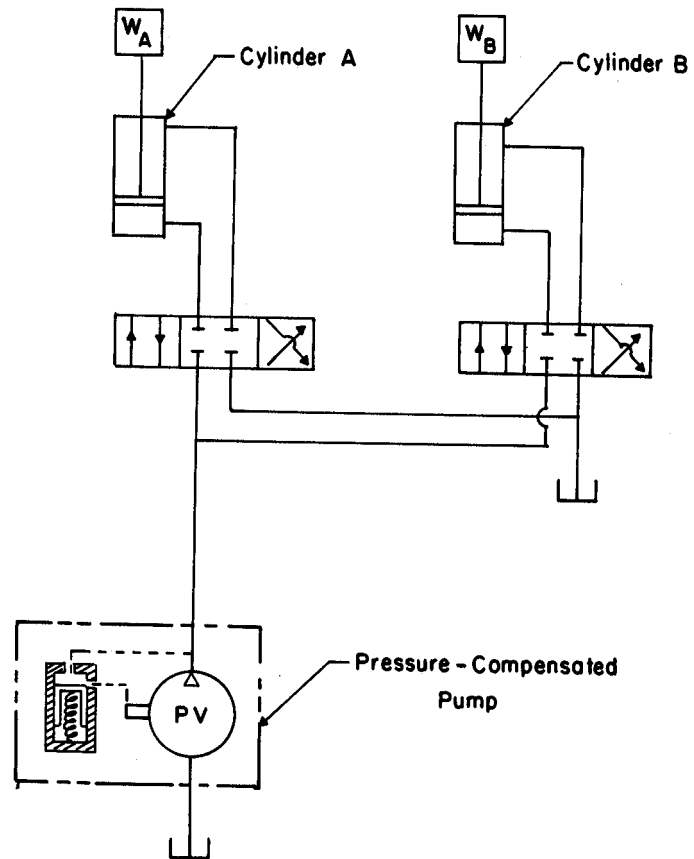
Figure 5.18 – A pressure-compensated hydraulic system.
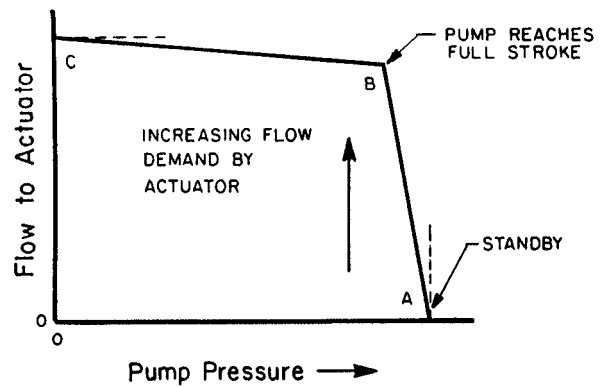
Figure 5.19 – A pressure-flow diagram of a pressure-compensated hydraulic system.

Figure 5.20 – A load-sensing hydraulic system.

of Figure 5.19, except that the system can operate at any point under the curves. Pressure is controlled by actuator demand and flow is controlled by the throttling valves. Standby for the LS system is near the origin in Figure 5.19, not at point A.

5.7 PRESSURE TRANSIENTS

The equations that have been presented up to this point are for the steady-state behavior of fluid power systems. They are generally sufficient for analyzing and designing manually controlled fluid power systems. Pressure transients must be considered in automatically controlled systems that incorporate feedback, or the systems may exhibit unstable behavior. The equations that describe transient behavior are beyond the scope of this textbook. However, software packages are available that enable the use of computers to simulate transient behavior of fluid power systems.

5.8 HYDROSTATIC TRANSMISSIONS

A hydrostatic transmission consists of a pump connected to a hydraulic motor, as illustrated in Figures 5.21 and 5.22. The output speed of the transmission can be calculated from:

$$n_m = \eta_{vp}\eta \frac{V_p}{V_m} n_p \tag{5.21}$$

Two equations are available for calculating output torque:

$$T_m = \eta_{tp}\eta_{tm} \frac{V_m}{V_p} T_p \tag{5.22}$$

or

$$T_m = \frac{V_m \eta_{tm}}{2\pi} \Delta p \tag{5.23}$$

Variables in Equation 5.21 through 5.23 are as defined previously.

Equation 5.22 calculates the output torque, subject to the maximum pressure limit expressed by Equation 5.23. To provide a variable speed ratio, the pump or the motor or both must have variable displacement. Equations 5.21 and 5.23 show that a transmission with a variable V_p and fixed V_m is a constant-torque transmission; decreasing V_p reduces the output speed but the output torque is limited by the pressure rating of the transmission and cannot be increased. Thus, power capability declines with decreasing output speed. Constant-torque hydrostatic transmissions are used in some lighter-duty vehicles which require only limited output torque.

A transmission with constant V_p and variable V_m is a constant-power transmission because, as V_m is increased to reduce the output speed, the output torque is automatically increased with no increase in system pressure. All gear-type transmissions have the constant-power feature, which is desirable in a transmission. However, the constant-power hydrostatic transmission is seldom used because of its limited range; V_m cannot reach the infinite value that would be needed to bring the output speed to zero. Also, V_m cannot reach zero without blocking the pump flow, so the tilt of the motor swash plate (see Figure 5.22) cannot be reversed and the transmission cannot reverse the direction of travel of the vehicle.
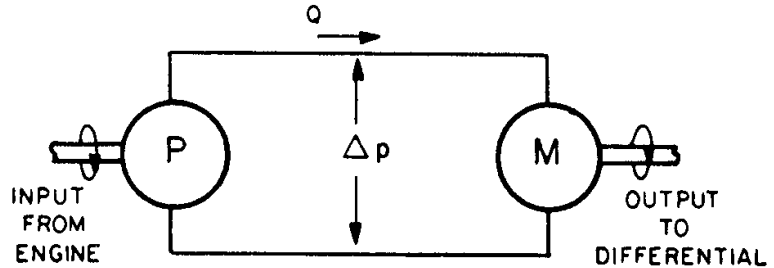

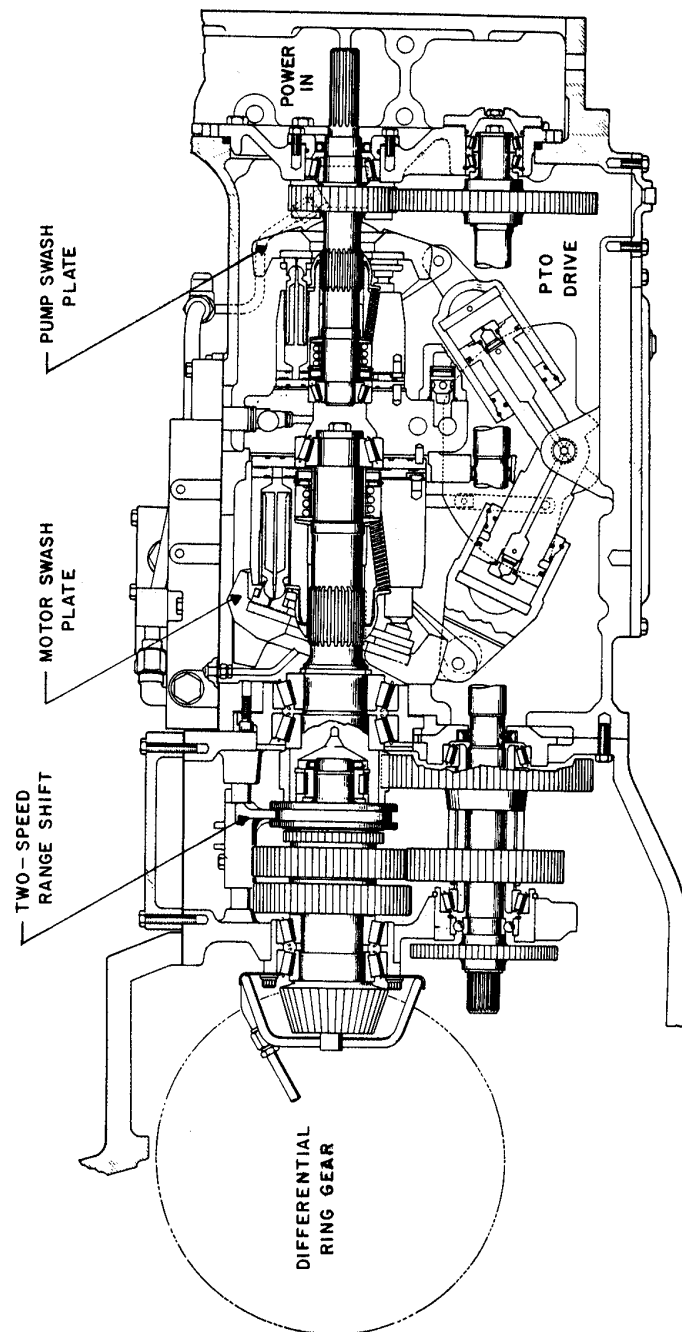**Figure 5.21 – A hydrostatic drive.**

Figure 5.22 – A heavy-duty hydrostatic transmission in series with a manual shift transmission (courtesy of CNH).

As Figure 5.22 illustrates, hydrostatic transmissions for heavy-duty tractors include a variable-displacement pump and a variable-displacement motor. The variable V_p allows linear control of output speed and full reversing capability. The variable V_m allows some increase in output torque as the output speed declines. Theoretically the hydrostatic transmission can provide full-range speed control but, as Figure 5.4 illustrates, the transmission efficiency would be very low at either low or high speed ratios. To improve efficiency, a mechanical transmission is often used in series with the hydrostatic transmission, as shown in Figure 5.22. The mechanical transmission allows the hydrostatic transmission to work over a much narrower speed range and thus better maintain its efficiency.

5.9 MECHATRONICS AND SYSTEM CONTROL

Many functions accomplished by hydraulics were previously accomplished by mechanical devices in earlier machines. However, the great flexibility of hydraulic systems has allowed them to replace mechanical systems in many cases. Hydraulic systems and especially mechatronic systems allow much more precise and flexible control than mechanical systems.

5.9.1 An introduction to mechatronics

Electrohydraulic valves have been used in hydraulic circuits for many years to allow control of the valves at locations remote from the valves. Microprocessors are becoming ever more widely used in the control of off-road vehicles. Microprocessor control of electrohydraulic valves is one example of the emerging field of *mechatronics*. The microprocessors in mechatronic devices allow such devices to have unique capabilities and great flexibility. Figure 5.23 is an example of a prototype mechatronic valve.
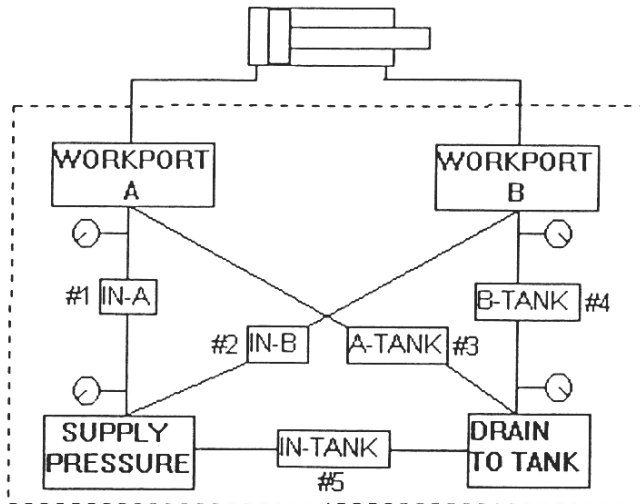

**Figure 5.23 – A mechatronic directional control valve
(from Book and Goering, 1999).**

Through microprocessor control, the valve in Figure 5.23 can perform many functions in a hydraulic circuit. The valve has four ports, as in an ordinary, single-spool DCV. Five proportional cartridge valves can block or open any of the possible passages between the four ports. A pressure transducer in each port allows the microprocessor to determine the pressure in each port. Cartridge valve 5 is normally open but can be closed on signal from the microprocessor. The other four cartridge valves are normally closed but can be opened on signal from the microprocessor. Although the mechatronics valve of Figure 5.23 can perform many functions, only a few will be discussed.

The mechatronics valve removes the distinction between open-center and closed-center DCVs. The computer keeps cartridge valve 5 closed to simulate a closed-center valve. For the mechatronics valve to function in an open-center circuit, the computer keeps cartridge valve 5 open until actuator action is needed; to extend a hydraulic cylinder, for example, the computer might open cartridge valves 1 and 4, then smoothly close cartridge valve 5 to cause a smooth start to cylinder extension. When the pressure in work port A indicated the cylinder had reached the end of its stroke, the computer would close cartridge valves 1 and 4 while opening cartridge valve 5. The reader can deduce which cartridge valves the computer would need to control to cause the cylinder to retract.

The mechatronic valve of Figure 5.23 has built-in pressure relief. If the pressure in the supply pressure port became too high, for example, the computer could cause cartridge valve 5 to open to provide a flow path to the tank. Compared to ordinary relief valves, the mechatronics relief valve could have near zero pressure override (see Figure 5.6).

In addition to providing relief against excessively high pressures, the mechatronics valve can provide protection against sub-atmospheric pressures and cavitation. Consider the situation if a hydraulic motor was powering a high-inertia load at high speed when the controlling DCV was closed to stop the motor. Momentarily, the external load would drive the motor, causing it to function as a pump to remove fluid from the motor supply line and pump fluid into the motor discharge line. With the DCV closed, there would be no inflow to the supply line or outflow from the discharge line. The pressure in the supply line would fall below atmospheric pressure and could possibly cause collapse of the line. If the mechantronic valve was used in place of the DCV, the computer could sense the approach of sub-atmospheric pressure and open cartridge valve 3 to allow oil from the reservoir to relieve the vacuum. Note also that the mechatronics valve could also close cartridge valve 4 in a controlled way to stop the hydraulic motor without causing excessively high pressures in the motor discharge line.

5.9.2   System control

Many machine functions are powered and controlled by hydraulics and space does not permit a discussion of all of them. Instead, we will discuss only one control function, i.e., the control of the hitch used to link implements to tractors. Hitches are discussed more fully in Chapter 7. Many types of hitches have been used in the past, but the *three-point hitch* illustrated in Figure 7.2 has become the standard hitch. Figure 7.6 is an example of a mechanical system for controlling a three-point hitch. A single-

acting hydraulic cylinder rotates lift arms for raising the two lower links. The weight of the attached implement provides the force for lowering the hitch.

The earliest use of three-point hitches was for mounting a plow to a tractor. Undulating soil surfaces caused difficulties during plowing with a fully mounted plow. When the tractor front wheels encountered an incline or the tractor rear wheels encountered a swale, the plow depth could increase until the tractor engine approached stall. Operators found they could avoid shifting to a lower gear by raising the hitch to reduce the plowing depth somewhat, thus reducing the load on the tractor. The operator would lower the hitch when the soil surface became level again. Tractor designers automated this practice by adding a load control lever and linkage. In Figure 7.6, the lower link points are attached to arms on a torsionally rigid torque tube. One end of a torsion bar is attached to the torque tube, while the other end of the torsion bar is anchored to the vehicle frame. With increasing pull on the lower links, the torsion bar allows increasing rotation of the torque tube. An arm near the center of the torque tube moves to control the DCV actuating linkage as the torque tube rotates. An increasing load signals the DCV to raise the hitch while a decreasing load signals the DCV to lower the hitch. The operator uses the load control handle to set the desired load on the hitch. Note that the system of Figure 7.6 has two control levers, one for load control and one for position control. The two controls together control the hitch. Pulling the load control lever to the rear increases the hitch sensitivity to implement draft, which can result in erratic plowing depth in variable soils. Conversely, moving the draft control lever forward decreases hitch sensitivity to draft and provides for more constant plowing depth on level ground. The three-point hitch enhances weight transfer from the front to the rear wheels of the tractor, thus improving traction and reducing the need for tractor ballast.

While mechanical linkages were able to control three-point hitches successfully, the complex linkages were expensive to manufacture and were subject to wear. Thus, such linkages are being replaced by mechatronic devices. In the mechatronic equivalent of the hitch shown in Figure 7.6, each control handle is replaced by a very small handle that sets the position of a potentiometer. Another potentiometer senses the rotation of the shaft that rotates the lower-link lift arms. The lower hitch links are linked to the tractor by special pins that produce an electric signal proportional to the shear in the pins. The mechanically controlled DCV is replaced by an electrically controlled DCV. For position control, the microprocessor senses the setting of the position-control handle, compares it with the current hitch position, and signals the DCV to raise or lower the hitch as needed. For load control, the microprocessor senses the setting of the load-control lever, compares it with the load as measured by the lower link pins, and raises or lowers the hitch as needed. In addition to having fewer moving parts subject to wear, the mechatronic system offers enhanced control of the hitch. For example, while controlling load, the microprocessor might restrict the raising and lowering of the hitch to programmed limits to avoid excessive variation in tillage depth.

TRACTOR HITCHING, TRACTION, AND TESTING

7

INTRODUCTION

Tractors frequently serve as the power source for field machines. A hitch connects the implement to the tractor. The tractor provides the tractive force to move the implement through the field. Thus, this chapter deals with tractor hitching and traction. Standard testing procedures have been developed for tractors and tractor testing is also discussed in this chapter.

7.1　HITCHING SYSTEMS

7.1.1　Principles of hitching

Most agricultural operations involve hitching some type of implement to a tractor. The forces transmitted through a hitch can affect the performance of both the tractor and the implement. Modern hitches include feedback for automatic control of pull and/or depth of tillage implements. In addition to transmitting forces, the hitch may also be required to carry the implement for transport.

7.1.2　Types of hitches

Early tractors included only a *drawbar* hitch, which permitted pulling but not carrying an attached implement. The three-point hitch has now become standard equipment on most tractors. The tractor of Figure 7.1 is equipped with both a drawbar and a *three-point hitch.* Terminology of a three-point hitch is illustrated in Figures 7.2 and 7.3. The points of attachment of the hitch links to the tractor are called link points, while the links are attached to the implement at the hitch points. Quick-attaching couplers (Figure 7.4) have been developed to allow faster attachment of three-point hitches to implements. Dimensions of three-point hitches have been standardized by ASAE (now ASABE) since 1959. Table 7.1 shows four of the hitch categories that have been standardized for different sized tractors; in addition, there is a category 0 hitch standard for garden tractors. The hitch dimensions that are standardized include
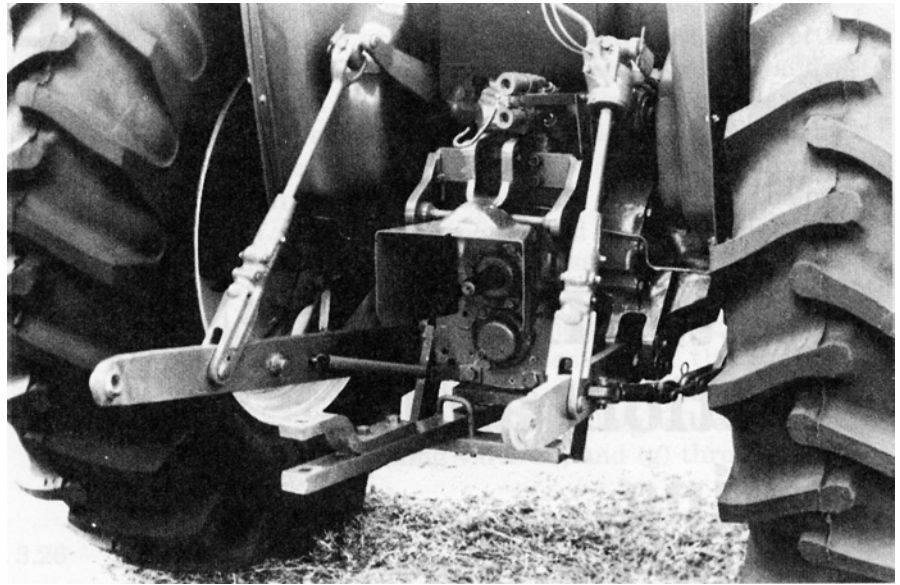
Figure 7.1 – A tractor with a drawbar and three-point hitch.
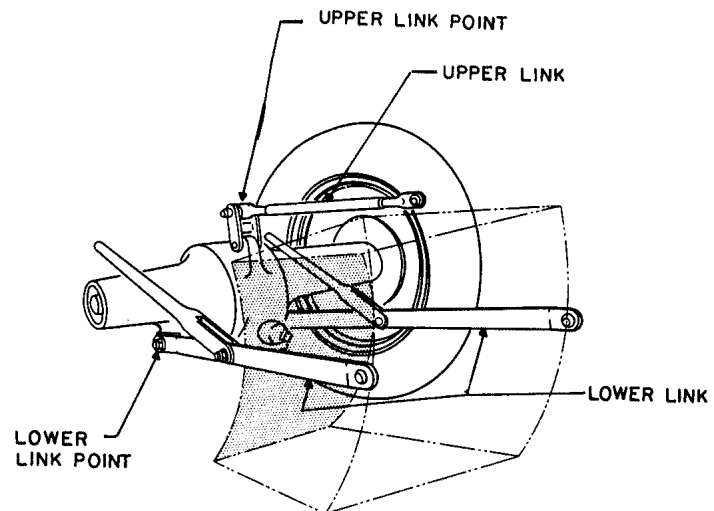

Figure 7.2 – A three-point hitch for a tractor (reprinted from ASAE Standard S217.10, Three-point, free-link attachment for hitching implements to agricultural wheeled tractors).
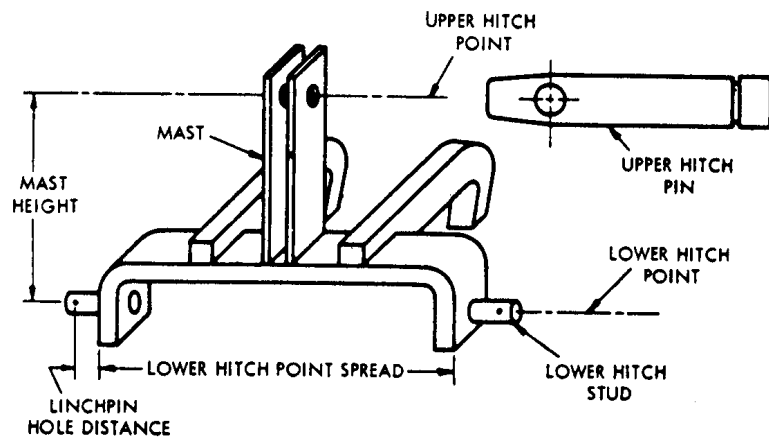
Figure 7.3 – Three-point hitch connections on an implement (reprinted from ASAE Standard S217.10, Three-point, free-link attachment for hitching implements to agricultural wheeled tractors).
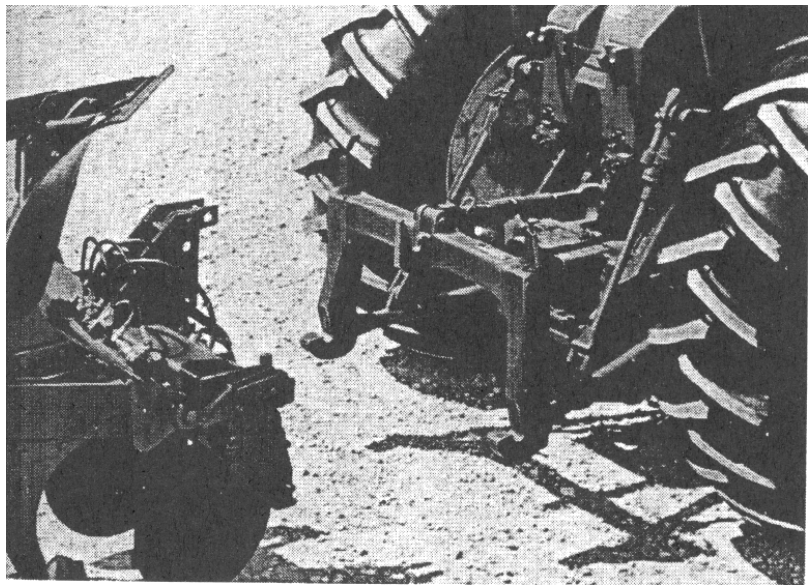

Figure 7.4 – Three-point hitch with quick-attaching coupler (courtesy of Deere and Co.).

Table 7.1. Three-point hitch categories (ASAE Standard S217.10).

Category	Maximum Drawbar Power, kW (hp)
I	15 - 35 (20 - 45)
II	30 - 75 (40 - 100)
III and III-N	60 - 168 (80 - 225)
IV and IV-N	135 - 300 (180 - 400)

hitch pin diameters, mast height, and lower hitch point spread. Exact dimensions can be found by referring to ASAE Standard S217. There are also ASAE standards relating to the drawbar; Standard S207 specifies minimum vertical loads that drawbars must withstand, while Standard S203 specifies the location of the drawbar hitch point relative to the *PTO shaft*.

An implement with a mast (Figure 7.3) can be carried entirely by the tractor and such implements are said to be *fully mounted*. *Semi-mounted* implements are attached to the tractor by only the two lower links and the ground must provide part of the implement support. Semi-mounted moldboard plows are the best known example of this type of hitch. Thus, the three types of hitching include *towed* (for implements hitched to the drawbar), semi-mounted, and fully mounted implements.

7.1.3   Hitching and weight transfer

Hitching affects both vertical and horizontal force relations between tractor and implement. Vertical effects on the tractor are of special interest because of their effect on the tractive performance of the tractor. The force imposed on the tractor by the implement (Figure 7.5) could be transmitted through a drawbar or through a semi-mounted or fully mounted hitch. The following equations can be obtained by taking moments about points C_2 and C_1, respectively:

$$R_r = \frac{m_t g(x_1 - x_2)}{x_1} + \frac{F_{hx} z}{x_1} + F_{hz} \qquad (7.1a)$$

and
$$R_f = \frac{m_t g x_2}{x_1} - \frac{F_{hx} z}{x_1} \qquad (7.2a)$$

where R_r = total vertical soil reaction on rear wheels, kN
   R_f = total vertical soil reaction on front wheels, kN
   m_t = tractor mass, Mg
   g = acceleration of gravity = 9.801 m/s^2
   F_{hz} = z-component of hitch force, kN
   F_{hx} = x-component of hitch force, kN
   x_1 = wheelbase of tractor, mm
   x_2 = distance from rear axle center to tractor center of gravity, mm
   z = distance from ground to intersection of R_r with line of pull, mm
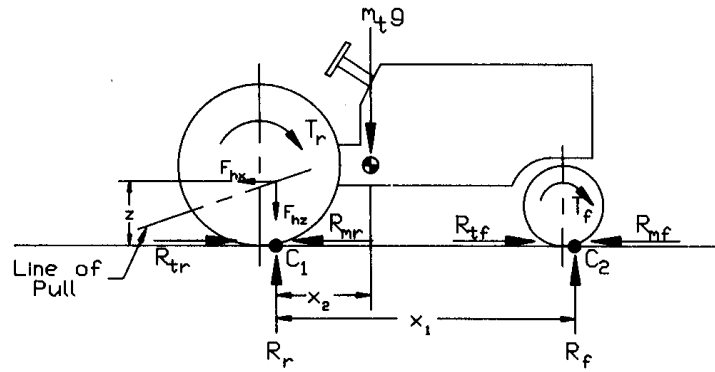
Figure 7.5 – Force and moment relations for a tractor when pulling an implement at a uniform velocity on level ground.

Points C_1 and C_2 are directly under the axle centers when a tractor is sitting on level ground with $F_{hx} = 0$, but move forward somewhat due to rolling resistance when the tractor is moving. The vertical wheel forces calculated from Equations 7.1a and 7.2a when $F_{hx} = F_{hz} = 0$ are called the static wheel reactions. The quantity, $(F_{hx}\ z/x_1)$, is called *weight transfer* because it is removed from the front wheel reaction and added to the rear wheel reaction due to the moment of the pull transmitted through the hitch. If the line of pull is inclined as shown in Figure 7.5, an additional term, F_{hz}, is also added to the rear wheel reaction. Some weight transfer is helpful on 2WD (two-wheel drive, typically rear-wheel drive) tractors because the tractive ability of the drive wheels is limited by the vertical soil reaction. However, too much weight transfer will bring R_f to zero, upon which the front wheels will raise off the ground. For 4WD (four-wheel drive) tractors, weight transfer is not helpful because tractive effort gained at the rear wheels is lost at the front wheels.

While Equations 7.1a and 7.2a give exact values for wheel reactions, they are difficult to use in practice. The distances x_2 and z are not easily measured and are constantly changing during agricultural operations. Thus, an approximate method has been developed for computing wheel reactions. The approximate equations are:

$$R_r = R_{ro} + C_{dw}\ F_{hx} \tag{7.1b}$$

$$R_f = R_{fo} - C_{dw}\ F_{hx} \tag{7.2b}$$

where $R_{ro} = m_t\ g(x_1 - x_2)/x_1$ = static rear wheel reaction, kN
$R_{fo} = m_t\ gx_2/x_1$ = static front wheel reaction, kN
C_{dw} = dynamic weight coefficient, dimensionless
Experimental studies have shown that the approximate values for C_{dw} are 0.20, 0.45, and 0.65 for towed, semimounted, and fully mounted hitching, respectively. The C_{dw} values were chosen to incorporate the effect of force F_{hz} on the rear wheels; thus Equation 7.2b somewhat overestimates the weight transfer from the front wheels.

7.1.4   Control of hitches

A single-acting hydraulic cylinder is usually provided to raise the lower links of a three-point hitch and lowering is accomplished by the weight of the attached implement. In the system illustrated in Figure 7.6, the cylinder rotates a rockshaft; arms attached to the ends of the rockshaft lift the lower links to raise the hitch. A feedback control system is provided as a standard feature of three-point hitches so that the hitch movement will mimic the movement of the hitch control lever. In the system shown in Figure 7.6, moving the position-control handle leftward pulls on the spool of the main control valve, initiating oil flow to the cylinder to raise the hitch. As the hitch raises, a cam on the rockshaft pushes on the spool of the main control valve so that hitch movement stops at a position corresponding to that of the position control handle. Conversely, when the position control handle is moved to the right, the hitch mimics that movement in lowering as the control valve releases oil from the cylinder.

With the first three-point hitches, when a tractor was pulling a heavy-duty tillage implement under varying field conditions, the operator would raise the hitch slightly when the pull became excessive in heavy soils and would again lower the hitch when the pull subsided in lighter soils. Engineers soon modified the three-point hitch controls to accomplish such raising and lowering automatically. In Figure 7.6, a torsion bar is used to sense force in the lower links; as the force increases, twisting of the torsion bar moves a linkage to pull out on the spool of the main control valve and causes the lower links to be lifted. Conversely, declining force in the lower links causes them to be lowered. Just as the position control handle is used to set the desired position of the lower links, the load (draft) control handle is used to set the desired amount of force in them. On some small tractors, *draft sensing* is accomplished by sensing compressive force in the top link. In recent larger tractors, the torsion bar and mechanical linkage are eliminated. Lower link sensing is accomplished by use of instrumented link pins that sense shear at the lower link points. Through circuitry that is provided, the voltage from the link pins is used to control an electrically actuated hydraulic valve which, in turn, controls raising and lowering of the hitch.

7.2   TIRES AND TRACTION

The power of a tractor engine may be transmitted through the PTO shaft, the hydraulic system, or through a hitch. The latter is the most common means of transmitting tractor power and the efficiency of transmission is limited by *tractive efficiency*. Thus, traction mechanics that support the design of efficient tractive devices is of great interest. Wheels are the tractive devices considered in this textbook. When a wheel works on soil, the soil must compress in order to acquire sufficient strength to provide a high tractive force to the wheel. The compression is provided by relative movement between the wheel and the soil. Consequently, some *wheel slip* must occur to provide traction, but excessive slip is inefficient. Traction mechanics provides a means for determining optimum wheel slip. The soil strength is an important factor in traction mechanics, and is represented by the *cone index*.
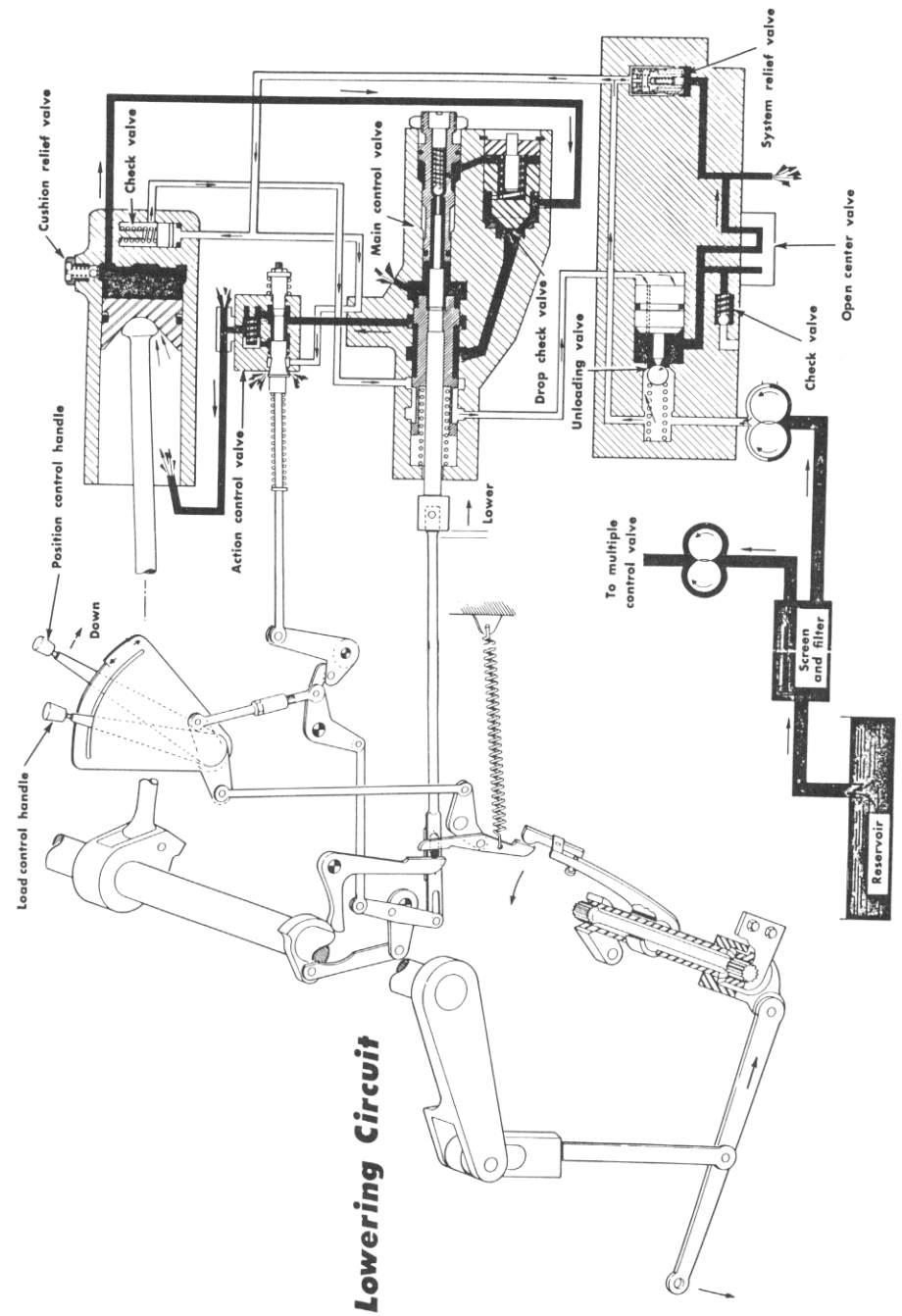
Figure 7.6 – A combination draft and position control system for a tractor hitch (courtesy of CNH).

7.2.1   Basic tire design

Dimensions associated with tires are illustrated in Figure 7.7. The *aspect ratio* of a tire is the *section height* divided by the *section width*. Typical aspect ratios range from 0.75 or less for low-profile tires to 1.0 or higher for high molded tires. Agricultural tires typically deflect about 19% of their section height at rated inflation pressure when the rated vertical load is applied, and thus the *loaded radius* (Figure 7.7) is less than half of the outside diameter of the tire. As the tire deforms under load, the section height decreases and the width increases. The dimensions for the loaded tire in Figure 7.7 are for a motionless tire. The stress distribution in a moving tire causes a slight lifting action and thus the rolling radius is slightly larger than the static loaded radius.

Agricultural tractors have not yet been converted to metric sizes. Thus, the tire size gives dimensions in inches. Consider the following tire, for example:

<p style="text-align:center">20.8-32, 8</p>

The first number is the section width in inches, the second number is the rim diameter in inches, and the third number is the ply rating. The tire in the above example has a section width of 20.8 inches, a rim diameter of 32 inches, and it is an 8-ply tire.

Tire manufacturers specify the *load-carrying capacity* of their tires. The load-carrying capacity increases with tire size, *ply rating*, and inflation pressure. Travel speed affects the load rating and thus manufacturers of agricultural tires publish two
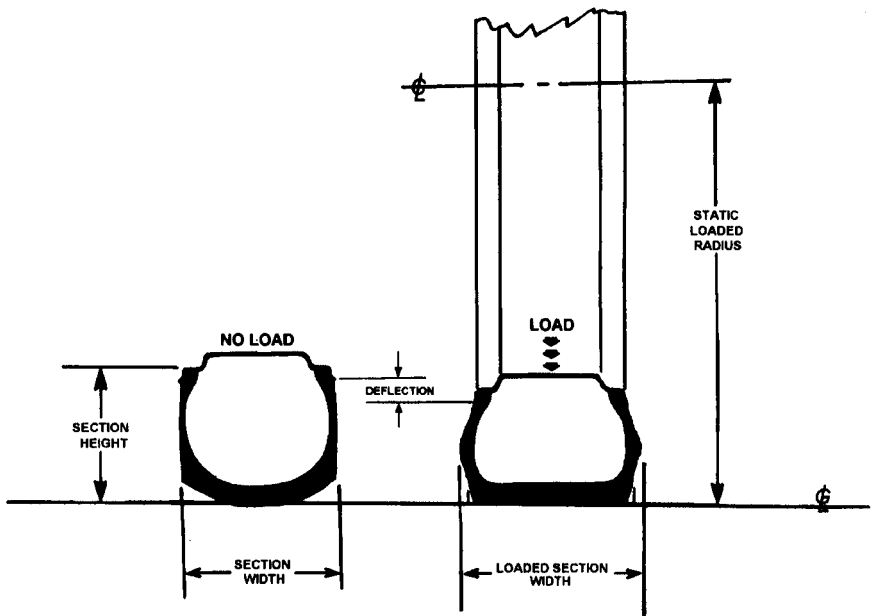

Figure 7.7 – Tire and rim dimensions.

sets of load rating tables. One table is for speeds up to 32 km/h and the other for speeds below 8 km/h. Considerably higher loading is permitted for the slower speeds. Lugged tires are used to convert axle torque to pull and, on such tires, the maximum tangential pull on the tire must be kept within allowable limits. Thus, the drawbar power must be limited to keep the tire bead from slipping on the rim and/or the tire sidewall from buckling. Figure 7.8 illustrates the use of dual tires to increase the tangential-pull-limited drawbar power. The figure is for bias-ply tires on a 2WD tractor. For example, if 20.8-34, 8 ply tires are on the rear axle, the maximum allowable drawbar power is 55 kW when the tractor is pulling at 4 km/h with a single tire on each rear axle. Pulling with duals (two 20.8-34, 8 ply tires on each rear axle) at 4 km/h would increase the allowable drawbar power to 96 kW. Notice that, at a given speed, the allowable power with duals is not double the power with singles; tire manufacturers de-rate the tangential pull on each tire by 12% when used in the dual configuration and by 18% when triples are used. Allowable drawbar power can also be increased by increasing the travel speed. When 20.8-34, 8-ply singles are used, for example, Figure 7.8 shows that the allowable drawbar power increases from 55 kW to 110 kW when the travel speed is increased from 4 to 8 km/h.

The previous discussion has been on agricultural tires with *bias-ply* construction, but *radial tires* are also available. Figure 7.9 illustrates differences between these two types of construction. With bias-ply construction, the reinforcing cords in the tire are
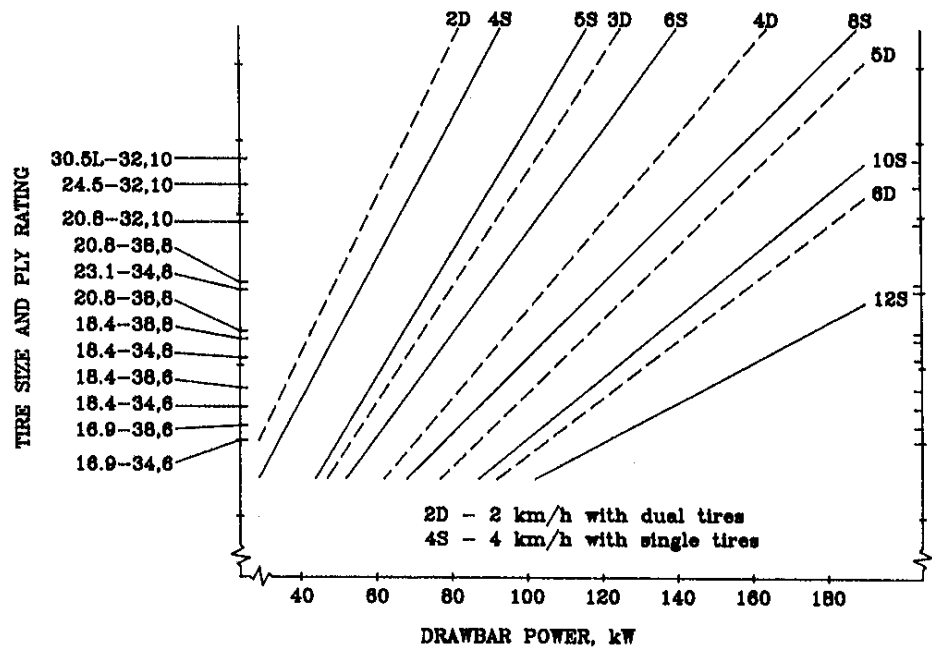

Figure 7.8 – Tangential-pull limited drawbar power.
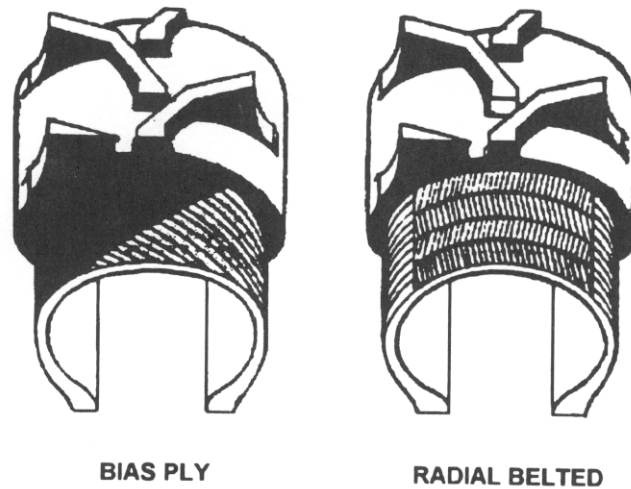
BIAS PLY   **RADIAL BELTED**

Figure 7.9 – Bias and radial-ply agricultural tires.

arranged diagonally across the tire from bead to bead. With radial construction, the cords are arranged perpendicular to the tire beads. An inextensible belt is positioned between the plies and the tread to restrict the flexing action of the radial tire. Radial construction permits increased radial deflection and increased bulging of the sidewall compared to bias-ply tires. Radial tires thus have a larger footprint, resulting in approximately 10% higher pull for a given slip or 15% to 25% reduced slip at a given pull compared to bias-ply tires.

The tires in Figure 7.9 have rubber lugs on the outer tread to provide better traction on soft soil. Agricultural tires without lugs are available for implements and for unpowered tractor wheels. The tire industry has established the codes listed in Table 7.2 to indicate the various types of tires. Only those with prefix R have lugs or knobs, to indicate that they are the *rear* tires on a 2WD tractor. R-type tires are also used on the front wheels of 4WD tractors. The terms *lugged* and *nonlugged* would be more descriptive of the tires, but the R-designation is still used by the tire industry to indicate lugged tires. R-2 tires have much taller lugs than R-1 tires to provide traction in the wet conditions encountered in rice production. The letter F in Table 7.2 is used to indicate *front* tires, that is, tires which are used on the front wheels of 2WD tractors. *Implement tires* have the prefix I and off-road *industrial tires* have the prefix E.

In selecting tires for a tractor or implement that is being designed, only a rough estimate of the tire loading may be available initially. It is good practice to base the tire selection on the lowest ply rating available when selecting a tire that can fit within available space and carry the estimated load. Also, the tires must provide a large enough contact area to carry the vertical load without excessive sinkage into soft soils. Tires on driving wheels must be able to transmit the required amount of power without exceeding the tangential pull limits. Thus many factors influence the initial tire selection. If refinement of the design shows increased tire loading, a larger ply rating can be selected to provide increased load-carrying capacity without increasing the tire size.

Table 7.2. Standard industry codes for tire types.[a]

Type of Tire	Code
Front Tractor	
Rice tread	F-1
Single rib tread	F-2
Dual rib tread	F-2D
Triple rib tread	F-2T
Industrial tread	F-3
Drive Wheel Tractor (Rear)	
Rear wheel, regular tread	R-1
Cane and rice, deep tread	R-2[b]
Shallow, non-directional tread	R-3
Industrial, intermediate tread	R-4
Implement	
Rib tread	I-1
Traction tread	I-3
Plow tail wheel	I-4
Smooth tread	I-6
Off-The-Road Tires (Industrial)	
Rib	E-1
Traction	E-2
Rock	E-3
Rock deep tread	E-4
Rock intermediate	E-5
Rock maximum	E-6
Flotation	E-7

[a] Source: Reprinted with permission © 1970 Deere and Co., *Fundamentals of Service - Tires and Tracks,* 4.

[b] Also includes similar treads for "G," "L," and "ML" series codes.

7.2.2 Traction models

The equations that govern traction were developed by grouping all of the relevant traction variables into dimensionless quantities (as discussed in Chapter 1). Then individual wheels were tested in a soil bin while forces, speed, and slip were measured. Using the dimensionless quantities, two basic equations were then developed to fit the soil bin data. One was for a *gross traction ratio* and another was for a *motion resistance ratio*. The equations are thus for single wheels, but the same equations can be assembled into a traction model for an entire vehicle. The gross traction ratio relates torques and forces on a wheel (see Figure 7.5) to wheel and soil parameters, i.e.:

$$\frac{T_i}{r_{Li} R_i} = C_{gi} = 0.88(1 - e^{-0.1 B_{ni}})(1 - e^{-k_1 s}) + k_2 \qquad (7.3)$$

where T_i = traction-limited torque on wheel i, N·m

i = f for a front wheel or r for a rear wheel

r_{Li} = static loaded radius of wheel i, mm
R_i = dynamic vertical load on wheel i, kN
C_{gi} = gross traction ratio for wheel i, dimensionless
B_{ni} = wheel numeric (See Equation 7.4)
k_1 = constant = 7.5 for bias-ply tires or 8.5 to 10.5 for radial tires
k_2 = constant = 0.04 for bias-ply tires or 0.03 to 0.035 for radial tires
S = wheel slip, decimal

The torque calculated using Equation 7.3 is the maximum torque that can be supported by traction. If the engine and power train attempts to deliver higher torque, wheel torque will increase somewhat until maximum wheel slip is reached but will not increase further. Note that, for a given C_{gi}, the maximum torque increases in direct proportion with the dynamic load on the wheel. Also, C_{gi} increases with wheel slip and with B_{ni}. The *wheel numeric*, B_{ni}, is defined as:

$$B_{ni} = \frac{CI_i b_i d_i}{1000R_i} \cdot \frac{1+5\delta_i / h_i}{1+3/r_A} \qquad (7.4)$$

where B_{ni} = dimensionless wheel numeric for *i*th wheel
CI_i = effective cone index for *i*th wheel, N/mm^2
b_i = section width of *i*th wheel, mm
d_i = outside diameter of *i*th wheel, mm
δ_i = deflection of *i*th tire due to vertical loading, mm
h_i = section height of *i*th wheel, mm
r_A = aspect ratio = section height over section width

The wheel numeric is the product of two dimensionless terms. The numerator of the first term is a measure of the load carrying capacity of the soil, while the denominator gives the actual loading. The second dimensionless term is a correction term to account for deformation of the tire under load. As Equation 7.4 indicates, B_{ni} increases with soil strength, wheel diameter, tire width, and tire deflection. The quantities, b_i, d_i, and r_{Li}, can be found in ASAE Standard S220 for specific tires. If the standard is not available or for tires not listed in the standard, d_i and r_{Li} can be calculated from the tire size specifications by using the following equations:

$$d_i = 25.4(d_{nri} + 2r_A b_{nri}) \qquad (7.5)$$

and
$$r_{Li} = 25.4\left(\frac{d_{nri}}{2} + 0.81r_A b_{nri}\right) \qquad (7.6)$$

where d_{nri} = *nominal rim diameter* for the *i*th wheel, inches
b_{nri} = *nominal section width* for the *i*th wheel, inches
r_A = aspect ratio = section height over section width

Note the inclusion of a factor, 25.4, in the above equations to convert to mm from the tire size specifications in inches. Equation 7.6 is based on an assumed tire deflection of 19% of the section height. The following aspect ratios should be used in Equations 7.5 and 7.6:

- For low-profile, R-1 and R-2 type tires (indicated by an L in the tire size designation), use 0.70.
- For other R-1 and R-2 type tires, use an aspect ratio of 0.85.
- For low-profile F- or I-code tires (indicated by an L after the width in the size specification), use an aspect ratio of 0.78.
- For other F- or I-code tires, use an aspect ratio of 1.01.

These choices for aspect ratio and tire deflection generally allow calculation of d_i and r_{Li} with less than 10% error.

Two other tire parameters can be calculated using the following equations:

$$\delta_i = \frac{d_i}{2} - r_{Li} \tag{7.7}$$

and
$$h_i = \frac{d_i - 25.4d_{nri}}{2} \tag{7.8}$$

The motion resistance ratio, ρ_i, is defined as follows:

$$\frac{R_{mi}}{R_i} = \rho_i = k_2 + \frac{k_3}{B_{ni}} + 0.5SB_{ni}^{-0.5} \tag{7.9}$$

where R_{mi} = motion resistance force on ith wheel, kN (see Figure 7.5)
$\qquad$ k_3 = constant = 1.0 for bias-ply tires or 0.9 for radial tires
$\qquad$ ρ_i = motion resistance ratio for ith wheel, dimensionless
$\qquad$ S = slip of powered wheels or zero for unpowered wheels

The motion resistance ratio is subtracted from the gross traction ratio to obtain the *net traction ratio* (C_{ni}) for the ith wheel, i.e.:

$$C_{ni} = C_{gi} - \rho_i \tag{7.10}$$

Wheel slip, S, is defined as:

$$S = 1 - \frac{V_A}{V_{ti}} \tag{7.11}$$

where V_a = actual travel speed of vehicle, m/s
$\qquad$ V_{ti} = theoretical travel speed of ith wheel, m/s

The theoretical travel speed can be calculated from the engine speed, tire radius and drive train speed ratio, i.e.:

$$V_{ti} = \frac{\pi n_e r_{Li}}{30000N_{pti}} \tag{7.12}$$

where n_e = engine speed, rev/min
$\qquad$ N_{pti} = power train speed ratio for ith wheel

The tractive efficiency, η_{ti}, is the ratio of the tractive power out of the ith wheel divided by the rotational power in, i.e.:

$$\frac{(R_{ti} - R_{mi})V_i}{T_i \omega_i} = \eta_{ti} = \frac{(1 - S_i)C_{ni}}{C_{gi}} \qquad (7.13)$$

where $R_{ti} - R_{mi}$ = net tractive force on ith wheel, kN (see Figure 7.5)

η_{ti} = tractive efficiency of ith wheel, dimensionless

ω_i = rotational speed of ith wheel, rad/s

The preceding equations can be used to calculate the tractive performance of an entire vehicle. By summing forces in the x-direction of Figure 7.5:

$$F_{hx} = C_{nr}R_r + C_{nf}R_f \qquad (7.14)$$

In applying Equation 7.14, R_r is the combined dynamic load on all wheels on the rear axle, while R_f is the combined load on all front wheels. The value for b_i in Equation 7.4 must be the combined width of all tires on axle i. Equation 7.14 is valid for vehicles with two- or four-wheel drive. For two-wheel drive, $C_{gi} = 0$ for all nondriving wheels while V_{ti} is calculated only for the driving wheels.

Note that, for a specified s, F_{hx} must be calculated iteratively because B_{ni} for each axle depends on the dynamic weight on that axle, the dynamic weight depends on the weight transfer, and the weight transfer depends on F_{hx}. A suitable procedure is to assume zero weight transfer in the first iteration, which allows calculation of an initial value of F_{hx}. That value can be used in Equations 7.1b and 7.2b to find new dynamic weights, after which a new value of F_{hx} can be calculated. After a few iterations, the value of F_{hx} will converge to some constant. If the dynamic reaction on the front axle reaches zero during the iterations, the entire tractor weight is supported on the rear axle and no further iteration is necessary.

What value of slip should be used in the calculations? The form of Equation 7.3 is such that C_{gi} and, consequently, F_{hx} increase with slip. The draft of most soil-engaging implements increases with speed but, since slip reduces forward speed, greater slip reduces implement draft. Thus, when an equation for implement draft (see ASAE Data D497 for such equations) is added to the traction model presented above and the model is solved iteratively, the solution for the tractor-implement combination will converge to some equilibrium slip, S_e. The calculated S_e may not produce maximum tractive efficiency, so it may be desirable to change it until maximum η_t is achieved. The S_e can be increased by removing ballast to reduce the vertical loads on the powered wheels or by increasing implement draft, i.e., by use of a larger implement. The S_e can be reduced by the converse measures. The goal of traction is to transmit drawbar power, which can be calculated using Equation 7.15:

$$P_{db} = V_a F_{hx} \qquad (7.15)$$

where P_{db}=drawbar power in kW. Increasing V_a reduces the F_{hx} and thus the ballast needed to transmit a given amount of drawbar power. To prevent overloading the tractor and excessively compacting the soil, it is recommended that V_a be at least 2 m/s or 7.2 km/hr.

The effective cone index is measured by pushing a cone penetrometer into the soil. Dimensions of the standard *penetrometer* and directions for using it are given in ASAE Standard S313. The cone index varies with depth but, by averaging the cone

index values over the first 150 mm of depth, an effective cone index is obtained for use in Equation 7.4 for wheels that run in undisturbed soil. Typically, effective cone indexes range from 0.33 N/mm^2 for soft soil to 1.75 N/mm^2 for firm soil. If the rear wheels run in the track of the front wheels, the effective cone index for the rear wheels is increased due to the compaction provided by the front wheels. The following equation can then be used to estimate the effective cone index for the rear wheels:

$$\frac{CI_a}{CI_b} = 1 + 1.8e^{-0.11B_{ni}} \qquad (7.16)$$

where CI_a = effective cone index after wheel passage, N/mm^2
CI_b = effective cone index before wheel passage, N/mm^2

7.2.3 Traction predictor spreadsheet

Frank Zoz developed a spreadsheet, "Predicting Tractor Field Performance," that uses the above traction theory to predict the tractive performance of tractors. The spreadsheet, in EXCEL format, is in the CD-ROM that is included with this textbook. Instructions for using the spreadsheet are given in the spreadsheet itself. There are 11 pages in the spreadsheet. The calculations are done in customary units and displayed on page one. Page two shows the results of the page one calculations in SI units. Instead of entering tractor parameters directly, the user can select one of the tractors listed on page three of the spreadsheet and the parameters for that tractor are entered automatically. Page five has a list of "help" instructions. Page six is provided to enter parameters of the user's "own" tractors. The remaining pages include an introductory page and various performance charts.

Soil strength is indicated in the spreadsheet by entering a soil cone index (CI) value. In practice, the soil cone index is measured by pushing a standardized soil penetrometer into the soil to measure the penetration resistance. ASAE Standard S313.2 gives dimensions of the standardized penetrometer. Soft soil CI values could range from 0 to 700 kN/m^2 (102 psi). Tilled soil values could range from 350 to 1200 kN/m^2 (51 to 174 psi). Firm soil would have a CI value of 1750 kN/m^2 (254 psi). For comparison with the theory above, 1 N/mm^2 = 1000 kN/m^2.

The parameters for the tractor selected for analysis are those that were present when the tractor received an official OECD/Nebraska tractor test. The spreadsheet user can change any of these parameters to study their effect. For example, a menu is provided to allow the user to change the size of tires used on the tractor and to specify whether singles, duals, or triples are used on each axle. The user can also change the type of hitch by which an implement is attached, i.e., the user can specify whether the implement is towed, semi-mounted, or integrally-mounted.

Two calculation modes are provided in the spreadsheet, i.e., a performance mode and a weight mode. In the performance mode, slip is increased until the calculated pull is sufficient to use all of the available engine torque. In the weight mode, the spreadsheet calculates the amount of tractor weight needed to achieve the calculated pull at a slip level selected by the user.

In the performance mode, after a tractor make and model are selected, the following parameter values appear automatically on the spreadsheet: static weight on front

axle, front power efficiency (if front wheels are driven), static weight on rear axle, rear power efficiency, wheel base, hitch point height, hitch point distance behind rear axle, pull angle below the horizontal, no-slip travel speed, maximum PTO power from the OECD/Nebraska test, and a load factor to de-rate the maximum power. Reducing the load factor reduces the pull proportionally. Outputs in performance mode include weight transfers to the rear axle from the front axle and from the implement, the resulting dynamic loads on the front and rear axles, drawbar pull, actual travel speed, slip, drawbar power, power delivery efficiency (drawbar power/PTO power), and pull-weight ratio (drawbar pull/tractor weight).

In weight mode, after a tractor make and model are selected, the parameters that automatically appear on the spreadsheet are the same as in performance mode with two exceptions. First, the static axle loads on the front and rear axles do not appear as parameters; instead, they are calculated as outputs. Also, in weight mode, the user must enter the percentage of the total dynamic weight that is to be carried on the front axle and the desired slip. Outputs are the same as in performance mode. Note that, by subtracting the front and rear static axle loads of the base tractor from the corresponding static axle loads calculated in the weight mode, the user can determine the amount of ballast needed on the front and rear axles.

Simulation problems at the end of this chapter provide an opportunity for the reader to experiment with the traction prediction spreadsheet.

7.3   SOIL COMPACTION

The passage of wheels over agricultural soils results in soil compaction, that is, an increase in soil cone index as indicated by Equation 7.16 and an accompanying increase in soil density. The cone index is a composite measure of soil strength that is a function of soil texture, density, and moisture. A proven relationship for field soils is not yet available, but Ayers and Perumpheral (1982) developed an equation to relate soil density to cone index and soil moisture for several artificial soils. The artificial soils consisted of mixtures of zircon sand, fire clay, and water. The following equation is equivalent to the one presented by Ayers and Perumpheral:

$$\frac{\rho_d}{\rho_{do}} = \left\{\frac{CI}{CI_o}\left[1 + C_o\left(\frac{m_s}{m_{so}} - 1\right)^2\right]\right\}^n \tag{7.17}$$

where ρ_d = dry density of soil, Mg/m^3

ρ_{do} = reference density of soil (a constant), Mg/m^3

CI = soil cone index, kPa

CI_o = reference cone index (a constant), kPa

m_s = soil moisture content, percent, dry basis

m_{so} = reference moisture content (a constant), percent

C_o, n = dimensionless constants

The five constants in Equation 7.17 depend upon soil type. Although values are not yet available for field soils, one of the homework problems provides data for illustrating the use of the equation with artificial soils.

Compaction results in an increase in soil density, but the effect of soil density on crop growth and yield is complex. In a relatively dry growing season, increased soil density may help to keep plant roots in contact with moisture and provide increased crop yields. Conversely, in a wet season, internal drainage is retarded by dense soil and crop yields may be reduced. Even within a given growing season, there is an optimum soil density for maximum crop production. Vomicil (1955) proposed a relationship between crop yield and soil density which can be expressed as follows:

$$\frac{Y}{Y_i} = 1 - C_y \left(\frac{\rho_d}{\rho_{di}} - 1 \right)^2 \qquad (7.18)$$

where Y = actual crop yield

Y_i = crop yield with ideal soil density

C_y = a soil-crop-climate constant

ρ_d = actual dry density of soil, Mg/m^3

ρ_{di} = ideal dry density of soil, Mg/m^3

Notice from Equation 7.18 that $Y = Y_i$ when $\rho_d = \rho_{di}$, and that the yield decreases with either smaller or larger values of ρ_d. Limited amounts of data are provided with one of the homework problems for illustrating the use of Equation 7.18.

SOIL TILLAGE

8

8.2   MECHANICS OF TILLAGE TOOLS

8.2.1   Soil texture

One aspect of the physical properties of soil, its *texture*, is described by the percent of particles in various size classes (Table 8.1). Particle size is the defining difference between sand, silt, and clay, but of course the size of the particle has much to do with its other properties. Natural soils are nearly always mixtures of sand, silt, and clay particles, as well as organic matter and stones. One convenient method of naming soils is the soil texture triangle (Figure 8.22). The sides of the triangle are axes, each representing the percentages of sand, silt, and clay that constitute the soil. Special names are assigned to various combinations as designated by the areas within the triangle. Thus, if a soil is composed of 40% sand, 35% silt, and 25% clay, it is called a loam. This is noted by the * in the figure. Note that because of the importance of the surface area-to-volume ratio, soils with as little as 20% clay still are called clay soils.

There are various laboratory methods of measuring the relative amounts of sand, silt, and clay, but a field key such as Figure 8.23 gives useful results.
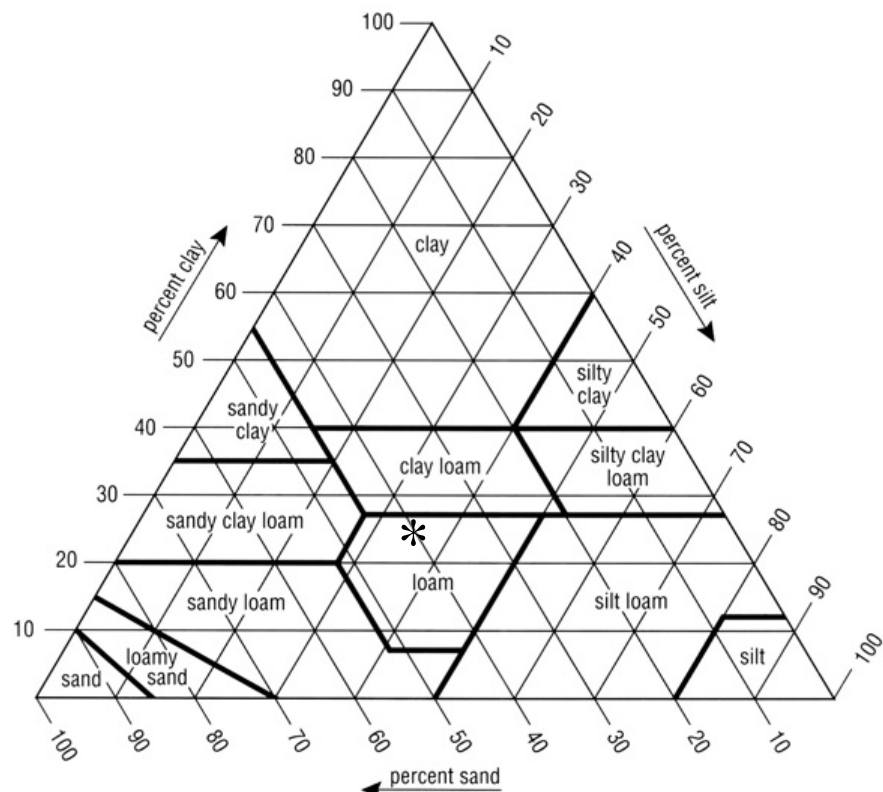

Figure 8.22 – USDA soil texture triangle showing the percentages of sand, silt, and clay in various soils. Note that these percentages are after sieving out particles > 2.0 mm (gravel and stones) and removing the organic matter.

Table 8.1. USDA soil particle size definitions.

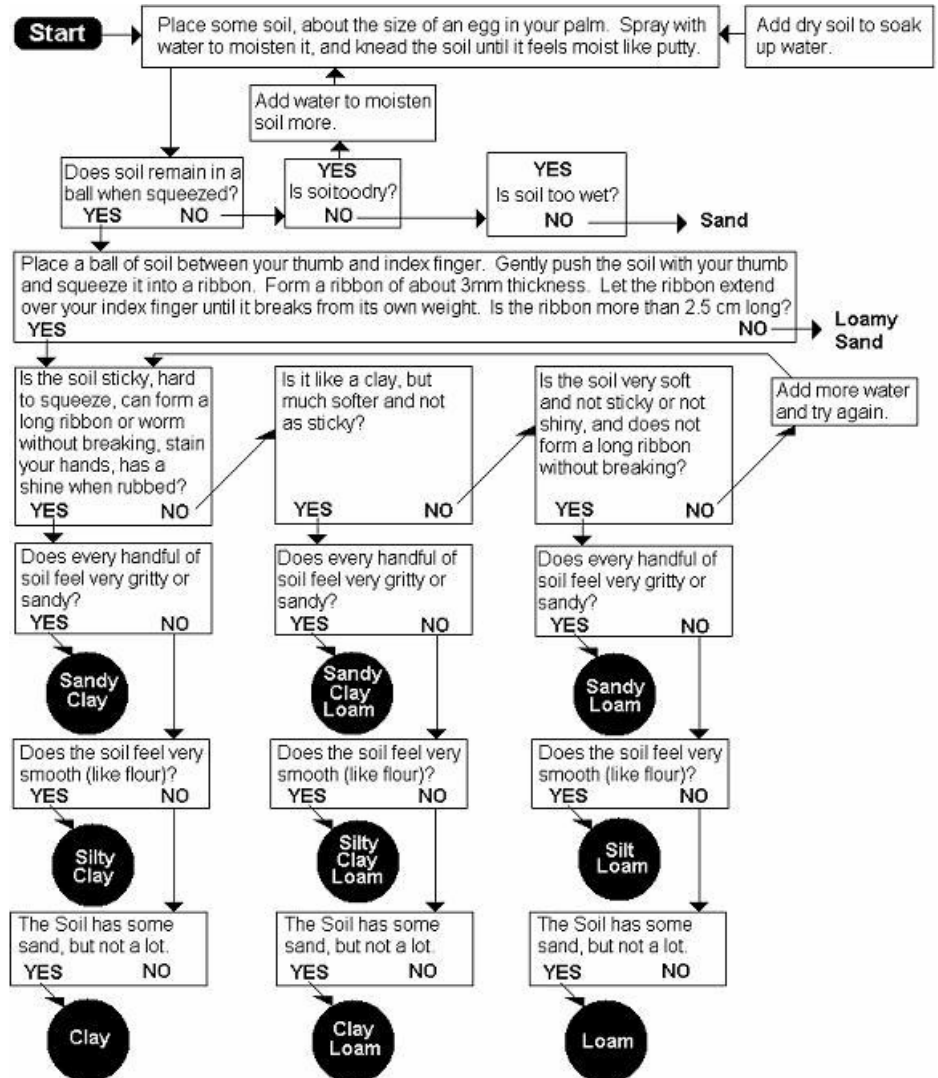| Particle class	Size (diameter)
clay	less than .002 mm
silt	.002-.05 mm
sand	.05-2.0 mm
gravel, stone	larger

Figure 8.23 – Guide to soil texture by feel (from USDA-NRCS, http://soils.usda.gov/education/resources/k_12/lessons/texture/).

8.2.2   Physical properties of soils

Porosity, n, is a measure of the relative amount of voids in the soil. It is the ratio of the void volume, V_v, to the total volume, V, of the soil sample (Figure 8.24), or:

$$n = \frac{V_v}{V} \tag{8.1}$$

The *void ratio,* e, is the ratio of the void volume to the volume of the solids in a soil sample, or:

$$e = \frac{V_v}{V_s} \tag{8.2}$$

where V_s = volume of solids.

The *water content* of the soil, w, is the ratio of the weight of water, W_w, to that of the solids, W_s, expressed as a percentage, or:

$$w = \frac{100\ W_w}{W_s} \tag{8.3}$$

The *degree of saturation,* S_r, is the percentage of void space that is occupied by water, or:

$$S_r = \frac{100\ V_w}{V_v} \tag{8.4}$$

where V_w = volume of water.

The *unit weight* or *density,* γ, is defined as the weight divided by the volume. For soils:

$$\gamma = \frac{W}{V} = \frac{W_s + W_w}{V_s + V_w + V_a} \tag{8.5}$$
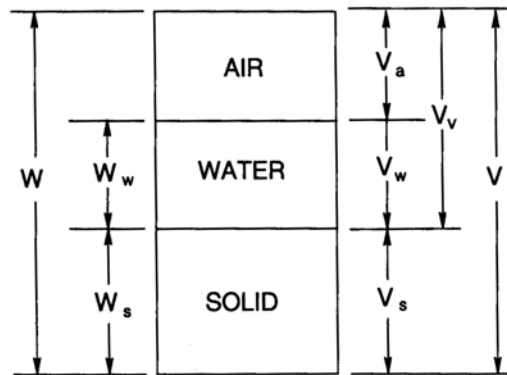

Figure 8.24 – Soil weight and volume fractions.

The *dry density,* γ_d, is the weight of solids divided by the total volume, or:

$$\gamma_d = \frac{W_s}{V} \tag{8.6}$$

Finally, the density of the solid particles in the soil, γ_s, is expressed as follows:

$$\gamma_s = \frac{W_s}{V_s} \tag{8.7}$$

The density of the solids in soils is found to be somewhat constant. It generally remains between 2.6 and 2.8 g/cm^3. The average value is 2.65 g/cm^3 for sand and silt and 2.75 g/cm^3 for clay.

Example 8.1

A 100 cm^3 soil sample weighs 165 g and its water content was found to be 49%. If the specific gravity of the solids is assumed to be 2.6, find the void ratio, porosity, degree of saturation, and dry density.

Solution
First, find the weights and volumes of all fractions of the soil specimen.

$w = W_w/W_s = 0.49$

$W_w = 0.49\ W_s$

$W_s + W_w = 165$ g

$W_s + 0.49\ W_s = 165$ g

$W_s = 165/1.49 = 110.74$ g

$W_w = 165 - 110.74 = 54.26$ g

$V_s = W_s/\gamma_s = 110.7/2.6 = 42.59$ cm^3

$V_w = W_w/\gamma_w = 54.26/1.0 = 54.26$ cm^3

$V_a = V - V_s - V_w = 100 - 42.59 - 54.26 = 3.15$ cm^3

Now find the required ratios from the weight and volume values as computed above.

Void ratio, $e = V_v/V_s = (V_w - V_a)/V_s$

$\qquad = (54.26 - 3.15)/42.59 = 1.35$

Porosity, $\eta = V_v/V = (54.26 + 3.15)/100 = 0.57$

Degree of saturation, $S_r = 100\ V_w/V_v$

$\qquad = 100\ (54.26)/5741 = 0.95\%$

Dry density, $\gamma_d = W_s/V = 100.74/100 = 1.107$ g/cm^3

8.2.3   Mechanical properties of soils

8.2.3.1 Shear strength

   If a soil specimen is subjected to shear stress the shear stress-strain diagram may look like one of the curves in Figure 8.25, depending upon the soil conditions. A highly cemented soil will result in a well defined failure point as shown by curve A. Loose soil may not show any definite failure point and the stress may increase exponentially with strain reaching some maximum value as shown by curve B. Curve C is for a soil that is well compacted but not cemented.

   The soil strength refers to the value of the shear stress on a plane within the soil sample where soil failure has taken place either by rupture or breakage. For curves A and C this point is clearly defined but for curve B soil failure is not distinct. In the case of curve C the failure is considered to have taken place by yielding or plastic flow and the asymptotic value of shear stress is taken as the shear strength for this case. The shear stress-strain curves shown in Figure 8.25 are for a given normal stress on the sample. If the normal stress is changed the shear stress-strain diagram will change and consequently the value of the maximum shear stress will also change. An increase in the normal stress would cause an increase in maximum shear. Therefore, the shear strength is a function of the normal stress on the failure plane.

   Mohr-Coulomb failure theory states that failure in a material occurs if the shear stress on any plane equals the shear strength of the material. Furthermore, the shear strength (s) along any plane is a function of the normal stress (σ) on the plane, as shown below:

$$s = f(\sigma) \tag{8.8}$$

   Coulomb, in 1776, conducted experiments to determine the maximum shear stress that could be applied on a plane within a sample of soil at varying levels of normal stress. He plotted the maximum shear stress values at failure against the corresponding normal stress on the failure plane and suggested the following linear relationship:
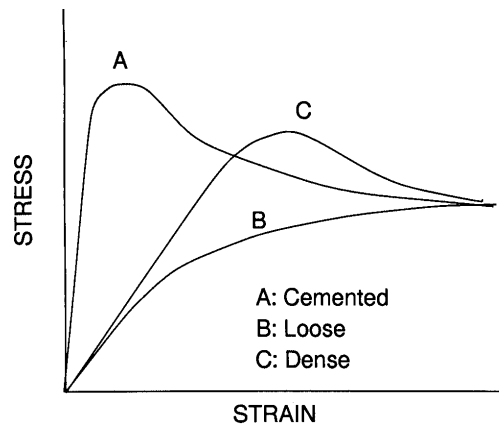
$$s = c + \sigma \tan(\phi) \tag{8.9}$$

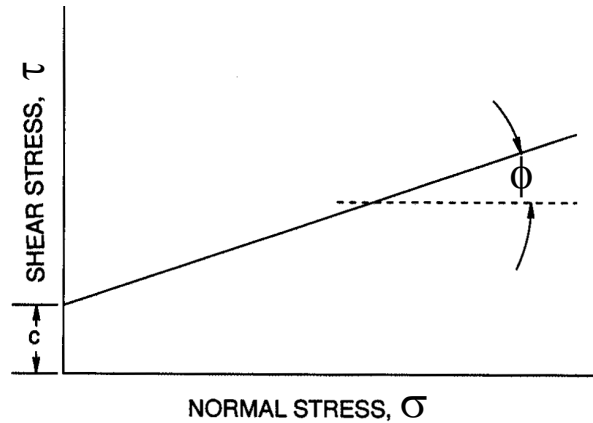**Figure 8.25 – Typical shear stress-strain diagrams for soils in three conditions.**

Figure 8.26 – Soil failure envelopes.

The Coulomb criterion is shown as a straight line in Figure 8.26, with an intercept on the shear stress (τ) axis equal to c and a slope equal to tan ϕ. The quantities c and ϕ are material properties frequently called cohesion and angle of internal friction, respectively. The shear strength as defined by Equation 8.9 represents the maximum shear stress that may be sustained on any plane in a given material. The strength function is called the failure envelope since it defines the limiting stress.

8.2.3.2 *Determination of shear strength*

Direct shear test and the *triaxial test* are the two most widely used methods for determining soil shear strength. The purpose of these tests is to determine the value of c and ϕ needed in Equation 8.9 to define the soil shear failure envelope.

The direct shear test. The direct shear test is performed using an apparatus as illustrated in Figure 8.27. The box consisting of an upper and a lower half contains the
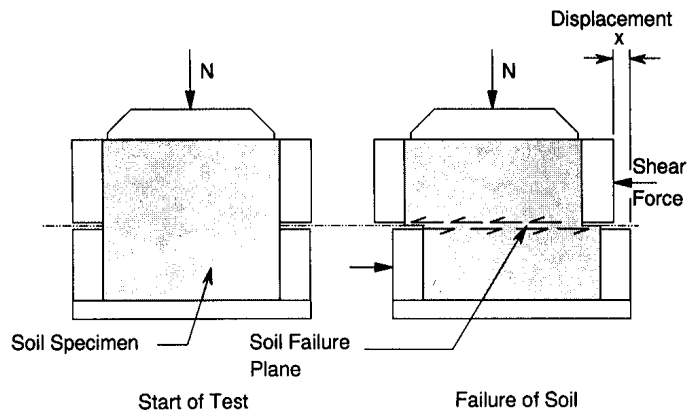

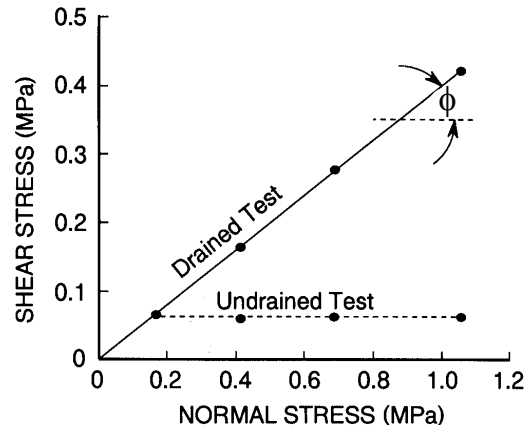**Figure 8.27 – Direct shear test apparatus.**

Figure 8.28 – Typical result of direct shear test.

soil sample to be tested. Drainage of water from the specimen is permitted using a porous stone at the bottom. The soil sample fails at the interface of the two halves. A normal stress is applied through a loading head, and the shear stress is increased until the specimen fails. A stress-strain curve is obtained by plotting the shear stress against the shear displacement.

To obtain the failure envelope, several tests utilizing different normal stresses are performed on specimens of the same soil. The specimens are then sheared at a slow rate to allow time for volume changes. If the shear strength is plotted against the normal stress, we obtain the solid line in Figure 8.28. The linear relationship between s and ϕ is the failure envelope.

The triaxial test. Consider a cylindrical soil sample subjected to a hydrostatic stress σ_3 as shown in Figure 8.29a and then an additional normal stress called the deviator stress (σ') as shown in Figure 8.29b. The deviator stress is increased until the soil fails. Figure 8.30a shows a two dimensional representation of stresses on the soil specimen. The soil failure plane orientation is shown by an angle (θ) from the horizontal. Figure 8.30b shows the shear and the normal stresses on the failure plane. Since the specimen failed the shear stress on this plane is equal to the shear strength. We now have to determine the values of the shear stress (τ) and the normal stress (σ) on this plane. These stresses can be determined by means of Mohr's circles as shown in Figure 8.31. Point A on the circle represents the failure plane. It should be noted that the angle or orientation of the failure plane is doubled in the Mohr's diagram. The coordinates of this point are the shear and the normal stresses on the failure plane. Using this diagram the following relationships can be written for these stresses:

$$\sigma = \frac{\sigma_1 + \sigma_3}{2} + \frac{\sigma_1 - \sigma_3}{2} \cos 2\theta \qquad (8.10)$$

and
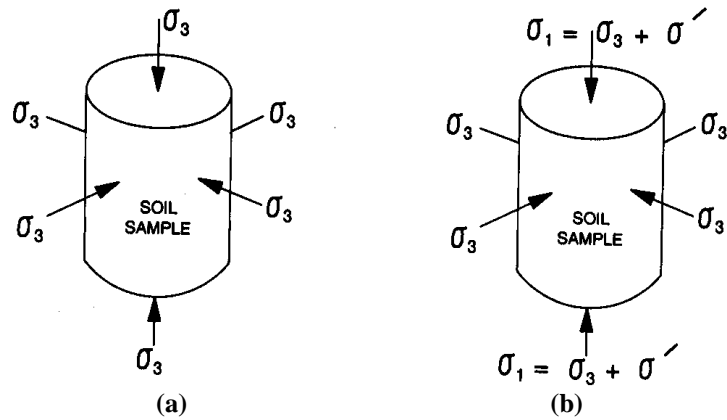$$\tau = \frac{\sigma_1 - \sigma_3}{2} \sin 2\theta \qquad (8.11)$$

Figure 8.29 – (a) Application of hydrostatic stresses during consolidation, (b) application of the normal deviatoric stress to cause shear failure.
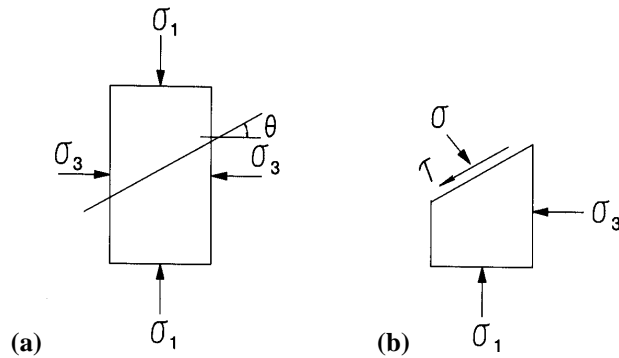

Figure 8.30 – (a) Two-dimensional representation of the stresses on a soil sample during the tri-axial shear test, showing (b) the shear and normal stress on the failure plane.
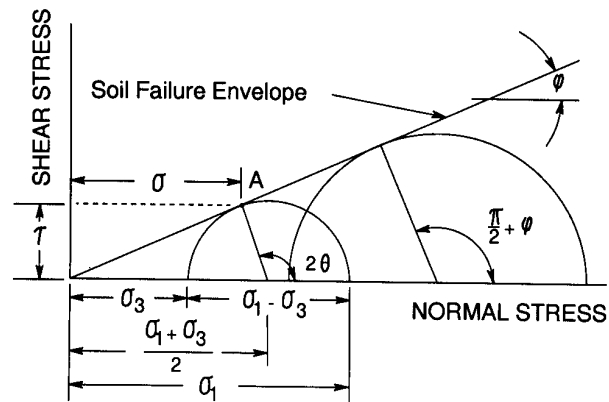

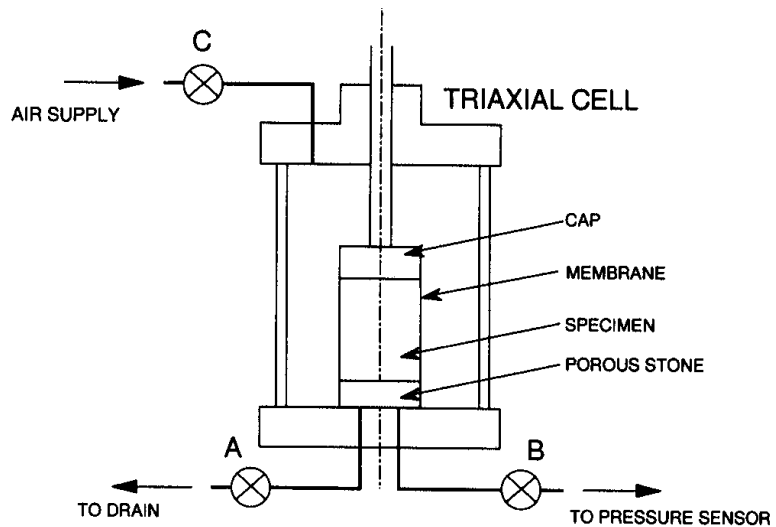**Figure 8.31 – Mohr's circle representation of principal stresses.**

Figure 8.32 – A tri-axial shear test apparatus.

Figure 8.32 is a schematic diagram describing the triaxial apparatus and the application of stresses. The cylindrical soil specimen is enclosed within a thin rubber membrane and is placed inside a triaxial cell. The cell is then filled with a fluid. The specimen is subjected to a hydrostatic compressive stress (σ_3) by pressurizing the cell. This causes the soil sample to consolidate. An additional vertical stress (σ') is applied through the piston as shown in the figure. This deviator stress is steadily increased until failure of the specimen occurs. The specimen fails under a set of principal stresses $\sigma_3 + \sigma'$ and σ_3.

Drainage of water from the specimen is measured by a burette, and valve A can be closed to prevent drainage from the specimen. Another line from the base leads to a pressure sensor to measure pore water pressure.

To obtain the failure envelope, several triaxial tests are performed on specimens of the same soil at different values of cell pressure (σ_3). A Mohr's circle is drawn for the principal stresses at failure for each specimen. These are shown in Figure 8.31 and the line tangent to these circles constitutes the failure envelope. The stress on the failure surface is represented by the point of tangency. From the geometry of Mohr's circle this plane makes an angle of $(\pi/2 + \phi)/2$ with the major principal stress plane.

The triaxial test may be performed as a drained (d), consolidated-undrained (c-u), or undrained test (u). In the drained test, water is allowed to seep out of the sample during the application of the hydrostatic and deviator stresses, and the pore water pressure is equal to zero. During the c-u test drainage is permitted during the application of the hydrostatic stress and the corresponding pore water pressure $u_a = 0$. When the deviator stress is applied, drainage is not permitted and the pore water pressure $u_b > 0$. In an undrained test, no drainage is permitted and the total pore water pressure is equal to u. The effective stress $\overline{\sigma}$ for the three drainage conditions may be calculated using the following equations:

Drained:	$\bar{\sigma}_1 = \sigma_1$	$\bar{\sigma}_3 = \sigma_3$	(8.12)
Consolidated-Undrained	$\bar{\sigma}_1 = \sigma_1 - u_b$	$\bar{\sigma}_3 = \sigma_3 - u_b$	(8.13)
Undrained	$\bar{\sigma}_1 = \sigma_1 - u$	$\bar{\sigma}_3 = \sigma_3 - u$	(8.14)

Figure 8.33 illustrates typical Mohr's envelopes obtained from undrained, drained, and consolidated-undrained triaxial tests; the envelopes are constructed from the principal stresses at failure. The failure envelope corresponding to the drained test, called the effective failure envelope, may be determined from Equations 8.13 and 8.14 depending on the drainage condition of the test. Regardless of the type of the test performed, there exists an effective failure envelope unique to the soil being tested.

The effective-stress failure envelope is written as:

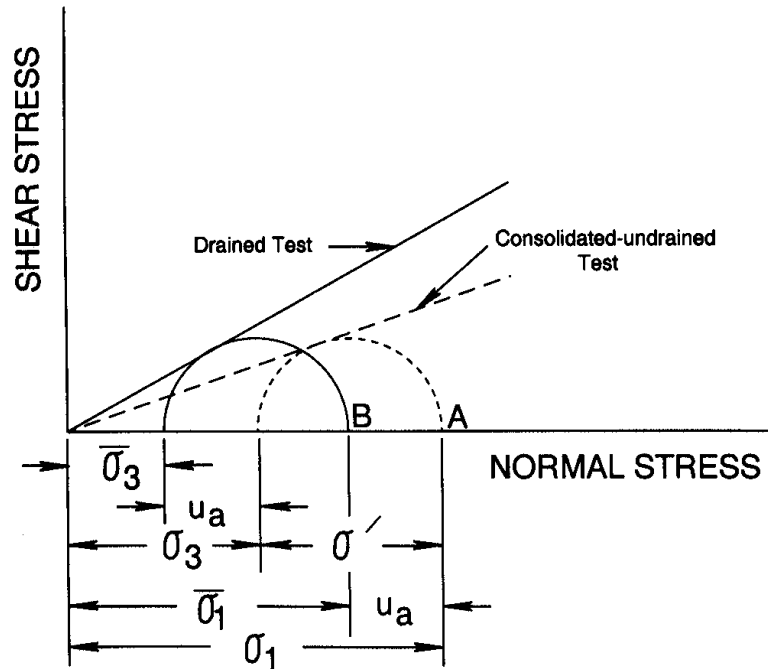$$s = \bar{c} + \bar{\sigma} \tan \phi \qquad (8.15)$$

Figure 8.33 – Effective-stress and total-stress envelopes.

CROP PLANTING

INTRODUCTION

The growth of a new crop begins with the planting of seed or transplanting of seedlings. After planting, seeds must survive on energy stored within the seed until germination occurs and a seedling emerges through the soil surface. Usually not all of the seeds are able to survive through *germination* and *emergence*; thus the number of seeds planted per unit area must be greater than the final desired *plant population*. The most important factors affecting germination and emergence include seed viability (percent germination under controlled laboratory conditions), soil temperature, availability of moisture and air to the seeds, and soil strength and resistance to seedling emergence. An ideal seed environment is one in which the seed depth and soil firmness provide adequate moisture, oxygen, and temperature to the seed but without excessive soil firmness that retards root development and seedling emergence. While transplanted seedlings are already emerged, their survival and initial rate of growth are also dependent upon soil moisture and temperature. A planter can exert a strong influence on the rate of germination and emergence of seeds through control of planting depth and firming of soil around the seeds or roots of seedlings. In addition, the planter must meter seeds at the proper rate and, in some cases, must control the horizontal placement of seeds in a desired pattern.

9.1   METHODS AND EQUIPMENT

Three different planting methods can be distinguished by the horizontal pattern of seed placement. *Broadcasting* refers to random scattering of seeds on the soil surface. *Drilling* is the random placement of seeds in furrows that are then covered; the seeds thus emerge in rows. In *precision planting*, the seeds are planted in rows and the spacing of seeds within the rows is uniform. A fourth method of planting is the *transplanting* of plant seedlings into a field. Mechanisms and machines have been developed to permit each of these planting methods.

9.1.1   Broadcast seeding

A *centrifugal broadcast seeder* is shown in Figure 9.1. The seed is metered from a hopper through a *variable orifice*. An *agitator* is provided above the orifice to prevent bridging of the seed over the gate and to assure continuous feeding. Sometimes a fluted wheel is used to meter the seed. The metered seed drops onto a *spinning disk*

Figure 9.1 – A centrifugal broadcast seeder (courtesy of Vicon Corporation).

that accelerates and throws it, usually horizontally. The width of coverage depends upon the size, shape, and density of the seeds. Two counter-rotating spinning disks may be used to increase the width of coverage. The seeding rate is controlled by the size of the gate opening, the speed of travel, and the width of coverage. Centrifugal broadcasters are flexible in that they can be used for broadcasting seed, dry fertilizer or pesticides, or other granular materials. After broadcast seeding, a secondary tillage operation may be performed to cover the seeds with soil.

9.1.2   Drilling

A *drill seeder* is illustrated in Figure 9.2. Typically, for each row, the seeds are metered from a *hopper* by a ground-driven *fluted wheel* past an *adjustable gate* that controls the seeding rate. The seeds then enter a tube and fall by gravity to a furrow that has been opened by a disk. Typical row spacings range from 150 to 400 mm. A common method of covering the seeds is to pull a small *drag chain* behind each *furrow opener*. Figure 9.2 is an example of a *wheel drill*, in which the weight of the machine is carried on transport wheels. In the *press drill* illustrated in Figure 9.3, much of the

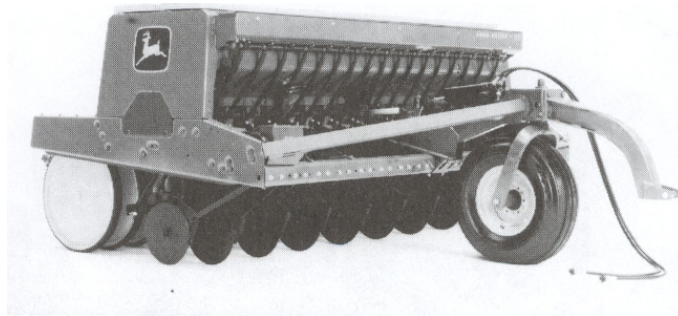**Figure 9.2 – A drill seeder (courtesy of Deere and Co.).**

Figure 9.3 – A press drill (courtesy of Deere and Co.).

weight of the drill is carried on press wheels that follow each row. Press drills thus provided firmer soil around the seeds compared to wheel drills. The term *fluid drilling* has been used to describe a planting technique in which germinated seeds are sown using a protective gel. The gel and seed mixture can be pumped through a hose for transport to the furrow if seed spacing is not critical. For more uniform seed placement, Shaw (1985) was issued a patent for a device to singulate and meter seeds from a liquid gel or suspension.

9.1.3   Precision planting

Precision planters provide accurate placement of single seeds at equal intervals within rows; the rows are usually spaced widely enough to allow cultivation (Figure 9.4). Precision planters are available in many variations, but four functions are always included. These are: opening a furrow of controlled depth, metering seeds into the furrow at uniform intervals, covering the furrow, and firming the soil against the seeds. On some planters, a pair of inclined wheels accomplish both the covering and the soil firming. Until the mid-1960s, most precision planters included *seed plates* for metering seeds. Pockets along the periphery of the plates were sized to match the seed dimensions, so that only one seed could fit in each pocket. As each pocket passed the
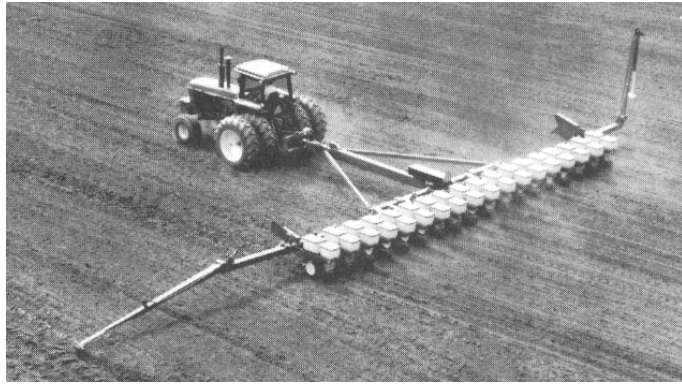
Figure 9.4 – A precision planter (courtesy of Deere and Co.).

seed tube, a spring-loaded knockout device would push the seed into the tube. Plates were easily replaceable, and farmers kept sets of plates to match each size of seed that was to be planted. *"Plateless" planters* were developed in the late 1960s and now there are a wide variety of mechanisms available for metering seed. The term *punch planting* is used to describe planting in *dibbles* created by a spaded wheel rather than planting in furrows. When vegetable crops are to be grown in soil covered by a plastic sheet, punch planting is especially useful in planting through the plastic cover.

9.1.4   Transplanting

A number of crops, including cabbage, lettuce, rice, strawberries, sweet potatoes, tobacco, and tomatoes, may be grown from seed in special beds and then transplanted into fields. Trees grown for commercial purposes are nearly always transplanted. The transplanting operation has not been fully mechanized, but a *transplanter* machine (Figure 9.5) can greatly increase the rate at which workers can do the transplanting.

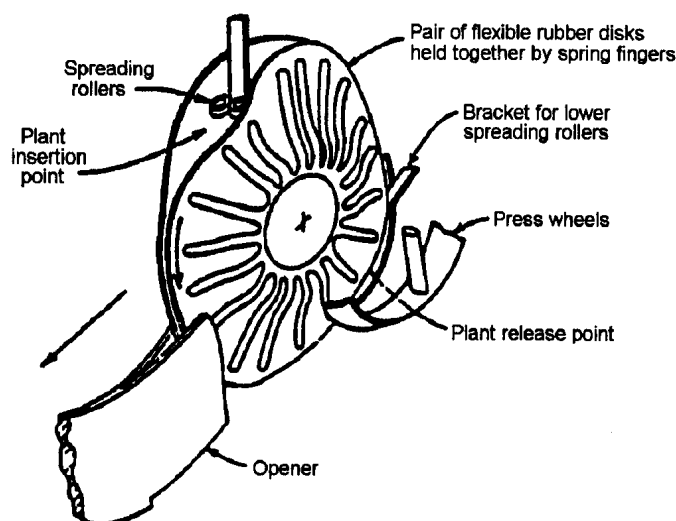**Figure 9.5 – A seedling transplanter (courtesy of Deere and Co.).**

Figure 9.6 – Key elements of a seedling transplanter (courtesy of Deere and Co.).

One or more seats are included on transplanters to position the workers conveniently for doing the transplanting. The transplanter also includes a hopper for the seedlings, provision for opening a furrow, means for accepting seedlings from a worker (see Figure 9.6) and placing them in the furrow, and means for closing the furrow and firming the soil around the seedlings. Runner-type furrow openers are usually employed, while a pair of press wheels tilted outward at the top accomplish furrow closing and soil firming. A water supply tank and suitable plumbing is often included to water the newly planted seedlings, and some signaling device may be provided to help the workers achieve correct spacing of the seedlings along the furrow.

9.2   FUNCTIONAL PROCESSES

9.2.1   Seed metering

Seed metering has two aspects. The first, *metering rate*, refers to the number of seeds that are released from the hopper per unit of time. Metering rate is important in any planter to insure that the desired final plant population will be achieved. In addition, seeds must be *singulated* in precision planters to allow placement of seeds at uniform spacing in each row.

9.2.1.1   Seed metering mechanisms

The oldest principle for metering seeds is the *variable orifice* and its simple principle is still in use. The volumetric flow rate of seeds is regulated by changing the orifice size. An agitator is used above the orifice to prevent bridging of the seeds (Figure 9.7).
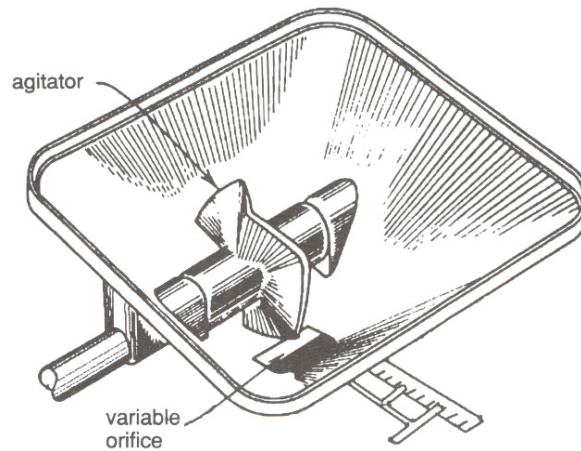
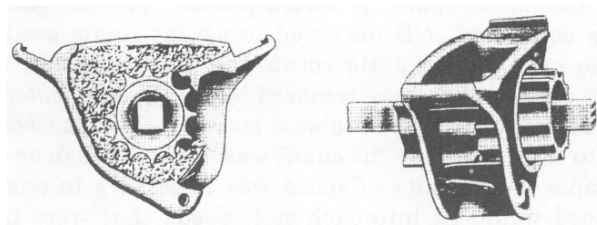**Figure 9.7 – Metering seeds with a variable orifice.**

Figure 9.8 – Metering seeds with a fluted wheel.

The most popular system for seed metering in a drill is the *fluted wheel* (Figure 9.8). The fluted wheel assemblies are positioned at the bottom of the seed hopper so that seed can flow into the openings by gravity. The fluted wheel provides quasi-positive-displacement metering, i.e., seeds in the flute openings are carried toward an adjustable gate as the fluted wheel rotates. The gate opening is set to match the seed size. The fluted wheel can be moved endwise to control the volumetric flow rate of seeds. Maximum flow rate occurs when the fluted wheel covers the entire width of the gate, while zero flow rate occurs when the non-rotating cutoff covers the full gate width. The flow rate also varies with the rotational speed of the fluted wheel.

The *internal double-run seed metering* mechanism is used on some drills (Figure 9.9). As with the fluted wheel, the internal run is a quasi-positive-displacement metering device but the seed spaces are formed by fins on the inside of the wheel. It is called a double run because two wheels are positioned back to back. One has much smaller seed spaces and is used for small seeds, while the side with large spaces is used for large seeds. The internal double-run units are positioned at the bottom of the seed hopper so that seeds can flow in by gravity. Only one side of the internal double-run is used at a time; a removable feed cover is used to block off the side that is not being used. An adjustable feed gate is provided for each side of the unit. The distance between the gate edge and the internal fins can be regulated to control the feed rate.
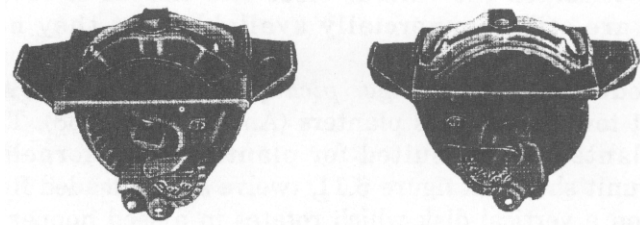
Figure 9.9 – Internal double-run metering.

Mechanisms previously mentioned in this section have metered seeds by volume. The remaining mechanisms to be discussed all meter individual seeds for precision planting.

Until the mid-1960s, the horizontal *seed plate planter* (Figure 9.10) was by far the most popular precision planter. The periphery of the seed plates contained cells designed to accept single seeds. Seeds entered the cells as the plate rotated in the bottom of the seed hopper. Any excess seeds were removed by a stationary *cutoff* and, as each cell passed over the seed tube, a spring-loaded *knockout* forced the seed into the drop tube. The cutoff was either a brush or a spring-loaded scraper. Uniformity of seeds was necessary to ensure that only one seed would fit into each cell. Seeds that were naturally non-uniform, such as corn kernels, had to be graded into uniform lots prior to planting. A wide variety of replaceable seed plates were available to match the various sizes and shapes of seeds. Plate planters are still commercially available, but they no longer dominate the market.

Introduction of the *finger pickup planter* in 1968 started a movement toward plate-less planters (*Agricultural Engineering*, 1968). The finger pickup planter is best suited for planting corn kernels. In the metering unit shown in Figure 9.11, twelve spring-loaded fingers are mounted on a vertical disk that rotates in a seed hopper. As they travel on their circular path, the fingers ride on a stationary disk that is concentric with
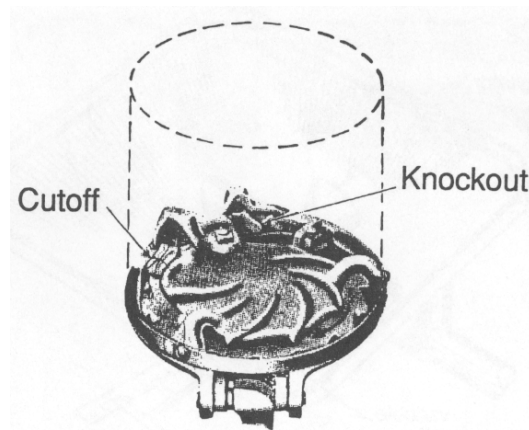

Figure 9.10 – Metering with gravity-fed seed plates.
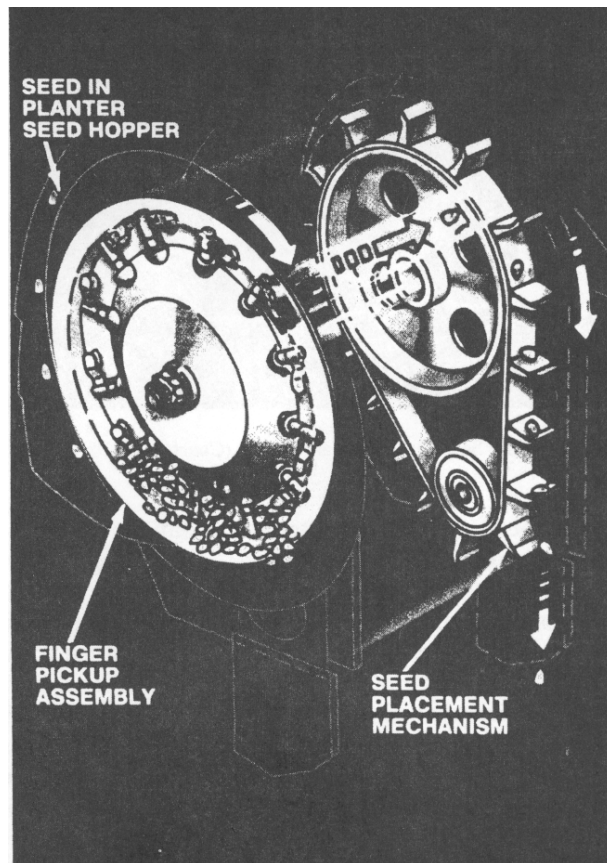
Figure 9.11 – Seed metering by finger pickup (courtesy of Deere and Co.).
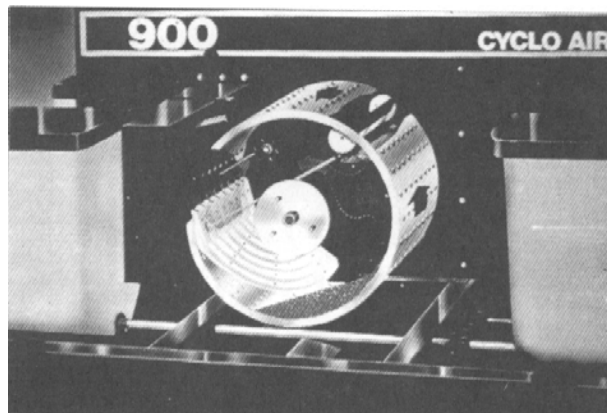
Figure 9.12 – Seed drum in an air planter (courtesy of CNH).

the rotating disk. As each finger passes through the bottom of the hopper, it picks up one or more seeds. With continued movement, the finger passes over an indentation in the stationary disk, causing it to grip one seed while any others fall back into the seed hopper. With further movement, the finger passes across an opening in the stationary disk and the seed is ejected into the seed placement belt for transport to the seed tube. The entire seed metering unit is ground driven to provide controlled spacing of the seeds along the rows.

The next innovation in plateless planting was the *air planter* (*Agricultural Engineering*, 1971). A ground-driven *seed drum* (Figure 9.12) is pressurized to about 4 kPa by a PTO-driven fan. Maximum practical drum speed is approximately 35 rev/min. Seeds flow by gravity from a central hopper to maintain a shallow reservoir of seed in the bottom of the drum. Each drum can be designed to serve 4, 6, or 8 rows, depending upon the number of rows of perforated holes that are provided. The drum shown in Figure 9.12 has eight rows of holes and thus meters seeds to eight rows in the field. Each hole terminates in a seed pocket at the inner face of the drum. As the drum rotates, air escapes through the holes and, when seeds enter the seed pockets, differential

**Figure 9.13 – Pressure-disk metering of seeds
(courtesy of White Farm Equipment Co.).**

pressure holds each seed in its pocket until drum rotation brings the seed close to a seed tube. A row of external wheels near the seed tubes blocks the holes momentarily, thus removing the differential pressure and allowing the seeds to fall into the seed tubes. Air escaping through the seed tubes carries the seeds to the planting units and deposits them in the rows. Crops that can be planted with the air planter include beans, corn, delinted cotton seed, and sorghum. The seed drums are easily replaceable and are changed to suit the seed being planted. A key advantage of the air planter is that it has only one seed hopper to be refilled, thus permitting faster refilling.

The *pressure-disk planter* (Figure 9.13) is similar to the air planter in that positive pressure in the seed reservoir is used to hold seeds in the pockets of the rotating seed plate. Unlike the air planter, however, the pressure-disk planter has a separate seed reservoir and plate for each row. Gravity moves the seeds from the hopper to the metering unit, where differential pressure holds a seed in each cell. As each cell nears the drop tube, a soft brush cuts off the air supply to the cell and the seed falls into the seed tube by gravity. Unlike the air planter, the seed tubes are not a conduit for escaping air. As with all precision metering units, the seed plate must be ground driven. Seed disks are replaceable and disks are available for corn, soybeans, edible beans, delinted cotton seed, pelleted or segmented sugar beet seeds, sunflowers, and sorghum.
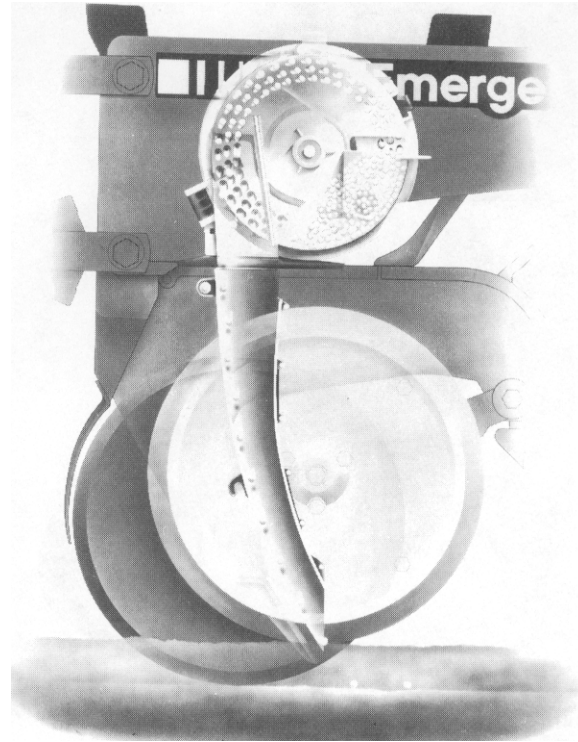

Figure 9.14 – Vacuum-disk metering of seeds (courtesy of Deere and Co.).

Vacuum-disk metering (Figure 9.14) is similar to pressure-disk metering, except that the pressure differential is supplied by creating a vacuum on the side of the seed disk opposite the seeds. Seed from the hopper enters the seed reservoir, where vacuum created by a pump holds the seeds in the seed cells on the rotating seed disk. The vacuum is blocked as the cells reach a point above the seed tube and the seeds fall into the tube by gravity. A vacuum of 15 kPa was used for holding seeds in a vacuum-disk planter designed by Giannini et al. (1967). In commercially available vacuum-disk planters, seed disks are available for metering edible beans, soybeans, corn, delinted cotton seed, edible peas, peanuts, sorghum, sugar beets, and sunflowers.

9.2.1.2 Seed metering theory

The two classes of seed metering mechanisms are those that meter by volume and those that meter individual seeds. When planting with metering by volume, the application rate can be expressed in number of seeds per hectare or in kilograms of seed planted per hectare. The application rate can be calculated by using the following equation:

$$R_s = \frac{10,000\,Q\rho_b}{w\,v} \tag{9.1}$$

where R_s = seeding rate, kg/ha or seeds/ha

Q = flow rate of seeds from the metering unit, L/s

ρ_b = seed bulk density, kg/L or number of seeds/L

w = width of coverage of the planter, m

v = travel speed of planter, m/s

It is impractical to count the number of very small seeds per unit volume and seeding rates are thus given in kg/ha. For larger seeds, the seeding rate can be given either in kg/ha or in seeds/ha. If the planter plants in rows and has a separate metering device for each row, Q is the flow rate from one device and W is the row spacing. The method of controlling Q varies with type of metering device.

The variable orifice is the simplest and oldest method for volume metering of seeds. In studying the flow of grain through orifices, Moysey et al. (1988) reported that the flow rate is independent of the depth of grain above an orifice in the bottom of a hopper. The following equation was adapted from their data:

$$Q = -0.0342 + 770A_n\sqrt{gD_e} \tag{9.2}$$

where Q = volume flow rate, L/s

A_n = net effective area of orifice, m^2

g = acceleration of gravity = 9.801 m/s^2

D_e = hydraulic diameter of orifice, m

The equation is valid for circular or rectangular orifices that are centered at the bottom of the hopper. The volume flow rate is about 15% greater for a given orifice when the orifice is at the edge of the hopper. Both the effective diameter and the effective net area are smaller than the physical opening because seeds overhanging the edge reduce the effective opening size. To account for this effect, each linear dimension of

the orifice should be reduced by k times the seed size. For a circular orifice of diameter D, the hydraulic diameter is $D_e = D - k\,d$, where d = seed effective diameter and k is a constant. For a rectangular orifice with physical length a and width b, the effective opening is $a' = a - kd$ and $b' = b - k\,d$. The area is $A_n = 0.25\,\pi\,D_e^2$ for the circular orifice or $A_n = a'\,b'$ for the rectangular orifice. The hydraulic diameter for a rectangular orifice is $D_e = (0.5\,a'\,b')/(a' + b')$. Moysey et al. (1988) reported kd values of common seeds as 7.5 mm for barley, 5 mm for wheat. 3.3 mm for flax, and 1.8 mm for rapeseed, where k = 1.4 for all seeds. The flow through the orifice became irregular when D_e was less than 6d and was independent of grain size when D_e was more than 20d. The hopper shape had little effect on flow rate when D_e was greater than 12d. Equation 9.2 was developed for stationary hoppers without agitation. In a seeder, an agitator is used to prevent bridging and the vibration of the hopper due to rough terrain could influence the flow rate. Thus, Equation 9.2 only provides a starting point for design and accurate flow rates must be determined through calibration of a prototype. Example Problem 9.1 illustrates the use of Equation 9.2.

Example Problem 9.1

Calculate the flow rate of sweet clover seed from a seed hopper on a centrifugal spreader. The rectangular orifice with dimensions of 30 mm by 80 mm is located at the edge of the hopper. (Seed properties are given in Table 9.1, in the Problems section at the end of this chapter.)

Solution
The seed properties table indicates the diameter of sweet clover seeds is 1.41 mm. The effective orifice dimensions are:

$$a' = a - k\,d = 0.03 - 1.4(0.00141) = 0.0280 \text{ m}$$

$$b' = b - k\,d = 0.08 - 1.4(0.00141) = 0.0780 \text{ m}$$

$$A_n = a'\,b' = (0.0280)(0.0780) = 0.00218 \text{ m}^2$$

$$D_e = 0.5a'\,b'/(a' + b') = 0.5(0.028)\,(0.078)/(0.028 + 0.078) = 0.0103 \text{ m}$$

Then, from Equation 9.2, the flow rate for a centered orifice would be:

$$Q = -0.0342 + 770\,(0.0218)(9.801 \times 0.0103)^{0.5} = 0.499 \text{ L/s}$$

The flow rate for an orifice on the edge is 15% greater, that is:

$$Q = 0.499(1.15) = 0.574 \text{ L/s}$$

Both the fluted wheel and the internal run metering mechanisms are quasi-positive-displacement devices. For such devices, the following equation is useful for estimating the volume flow rate of seeds:

$$Q = \frac{V_c \lambda_c n}{60 \times 10^6} \tag{9.3}$$

where Q = volumetric flow rate, L/s
V_c = cell volume = volume of each cell, mm^3
λ_c = number of cells on periphery of fluted wheel or internal run
n = rotational speed of fluted wheel or internal run, rev/min

The flow rate is controlled by changing of the speed ratio between the ground drive wheels and the metering device and/or by changing V_c. As noted in Section 9.2.1.1, V_c is changed by sliding the fluted section endwise (Figure 9.8) or by changing the gate setting on a double internal run device (Figure 9.9). The term *quasi-positive* was used to describe the displacement of the fluted wheel or the internal double run because the void space between seeds results in not all of the cell volume being occupied by seeds. Also, some seeds will typically project beyond the edge of the cells. Thus, the volume of seeds delivered each time a cell passes the seed tube is not precisely equal to the cell volume. Equation 9.3 can be used for design purposes, but accurate determination of the flow rate for any given type of seed requires calibration using a prototype machine.

For any of the planters that meter individual seeds, the theoretical seeding rate can be calculated by using the following equation:

$$R_{st} = \frac{10,000}{w \, x_s} \tag{9.4}$$

where R_{st} = theoretical seeding rate, seeds/ha
w = row width, m
x_s = seed spacing along the row, m

The seed spacing along the row can be calculated by using the following equation:

$$x_s = \frac{60v}{\lambda_c n} \tag{9.5}$$

where λ_c = number of seeds delivered per revolution of the metering device
n = rotational speed of metering device, rev/min
v = travel speed of planter, m/s

Note that, for a given row spacing, the theoretical seeding rate can be changed only by changing the seed spacing in the rows. The seed spacing is changed by changing the speed ratio between the ground drive wheels and the metering device.

9.2.1.3 *Performance of seed metering mechanisms*

Of the various types of planters discussed in this chapter, the broadcast seeder is least accurate in holding to a desired rate for three reasons. The first is that the variable orifice is not a positive-displacement metering device. The second is that, since the

metering unit does not have positive displacement, the metering rate is not linked to the travel speed of the seeder; rather, operator skill is required to coordinate the travel speed with the metering rate. Finally, the swath width of the broadcast seeder is not as precisely determined as the swath width of the other seeders mentioned in the chapter. Thus, the broadcast seeder is best suited to situations in which precise control of the seeding rate is not important. Broadcast seeders are capable of fast application, with spreading widths up to 15 m and travel speeds of 5m/s or more.

Drilling provides more precise control of seeding rates because the swath width can be controlled precisely and the metering rate is automatically linked to the travel speed. Through calibration, the volumetric flow rate of any given seed from the metering device can be determined with good accuracy. Seed spacing within the row is not uniform because the seeds are delivered to the seed tube in cells. Seeds began to trickle into the seed tube as a cell approaches the tube and, after the cell empties into the tube, seeds again began to trickle in as the next cell approaches the tube. Thus, although the average seeding rate may be accurate, the seed tends to be deposited in bunches along the row. Field slope may affect the flow rate from fluted wheel metering. The tendency is for flow rates to increase as the drill travels down slope; in one case, flow rate increased 44% on a 15% down slope. Since the metering device is ground driven, the inflation pressure of the ground drive wheels can affect seeding rate; if the tires are under-inflated, the wheel radius will be reduced, thereby causing more rotations of the wheels per distance traveled and increasing the seeding rate. Slippage of the drive wheels reduces the seeding rate, so wheel slippage must be considered in calculating the seeding rate. Typical travel speeds for drills are in the range from 1 to 3 m/s. Power requirements for pulling a drill are typically in the range from 1.0 to 1.4 kW per row.

Planters that meter individual seeds provide the most precise control of seeding rates. The actual seeding rate will equal the theoretical rate if and only if every finger pickup or seed cell carries exactly one seed. Some cells may fail to fill for various reasons, and then the actual seeding rate will be less than the theoretical rate. Conversely, if some cells contain more than one seed due to a poor fit between seed size and cell size, the actual rate can be higher than the theoretical rate. The metering device on precision planters is ground driven and, as with drills, drive wheel slippage and/or inflation pressure therefore affect the seeding rate. Electronic seed monitors have been developed for precision planters. A sensor in each seed tube senses the passage of seeds. Some monitors can be programmed to sound an alarm if the seed passage rate is too high or too low. Travel speeds for precision planters are typically in the range from 1 to 3 m/s. Power requirements for pulling a row-crop planter are typically in the range from 1 to 2.4 kW per row.

9.2.1.4 Monitoring and control of seed metering

For crops that require metering of individual seeds, malfunctioning of the metering system can cause unacceptable planting performance. Monitors have been developed to warn the operator when the metering system is malfunctioning. Early monitors included mechanical switches that were tripped by passage of seeds in the seed delivery tubes, but the mechanical devices disrupted the natural trajectory of the seeds. Current monitoring devices are non-contacting. For example, seeds can be made to interrupt

the light transmission path between a light source and a photocell, resulting in an electrical pulse each time a seed passes. Simple monitors use each electrical pulse to flash a light on the operator console (there is a separate light for each row) each time a seed passes. Operation is satisfactory as long as the light for each row continues to flash. In more advanced systems, the amount of forward travel between the electrical pulses is measured. The seeding rate (in seeds/ha) is computed and displayed for the operator. Feedback control permits automatic control of metering rates. With feedback control systems, the operator sets the desired seeding rate. The seeding rate detected by the counters is compared with the desired rate and, if the desired and actual rates differ, an actuator is signaled to readjust the variable-speed drive of the metering device to correct the seeding rate.

9.2.1.5   *Variable rate seeding*

As discussed in Chapter 6, fields are not uniform but vary in natural productivity. Variable rate seeding involves increasing the plant density for higher-yielding areas of a field and reducing it for lower-yielding areas. Some initial research has shown that, if a producer has full information about the yield response to seeding rate for every part of a field and has access to a variable rate seeder, variable rate seeding can be profitable in that field. The difficulty is that few producers have such detailed information about their fields.

Variable rate corn planters are available for those producers who choose to use variable rate seeding of corn. The seed metering system on conventional planters is ground driven; thus the seed flow rate, Q, varies directly with v, the planter travel speed (see Equation 9.1). One variable rate planter on the market uses a hydraulic motor to drive the seed metering unit for each row. While a speed sensor inputs planter travel speed, an on-board computer consults a field map giving the desired seeding rate for each row, then computes the hydraulic motor speeds needed to obtain the desired seeding rate at each row. The resolution (see Section 6.4.3) of such a planter is thus one row width.

9.2.2   Seed transport

9.2.2.1   *Seed transport mechanisms*

After the seeds are metered, they must be transported to the soil surface or into a furrow. Most transport systems rely primarily on gravity for vertical movement of seeds. Horizontal movement, if it is needed, must be generated by the transport device. Friction is always present in seed transport and may have an effect on the path traveled by the seeds. Some seeders use pneumatic conveying to transport seeds.

9.2.2.2   *Seed transport theory*

For broadcast seeders, typically one or more spinning disks (Figure 9.15) are used to transport the seed. Seeds traveling down through a central seed tube enter the spinner through gates. Only one gate is shown on Figure 9.15. The following equations governing seed movement on the disk assume that the seeds slide along the disk and vane surfaces rather than rolling (Cunningham, 1963). The analysis below is for a cone-shaped spinner with radial blades, i.e., with $\delta = 0$. The angle (θ) through which
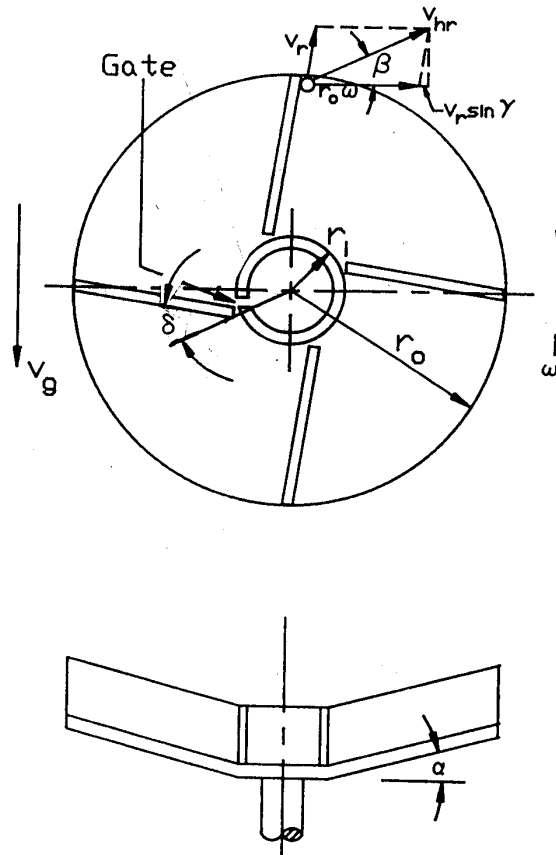
Figure 9.15 – A centrifugal spreader.

the disk turns while a seed is in contract with a vane can be calculated by solving the following equation:

$$\frac{(C_1+f)e^{C_2(C_1-f)\theta} + (C_1-f)e^{-C_2(C_1+f)\theta}}{2C_1} = \frac{r_o - \dfrac{C_3 g}{C_4 \omega^2}}{r_i - \dfrac{C_3 g}{C_4 \omega^2}} \tag{9.6}$$

After θ is calculated, the following equation can be used to calculate the velocity of seeds relative to a blade:

$$v_r = \frac{C_4 \omega}{C_2} \left(\frac{r_1 - \dfrac{C_3 g}{C_4 \varpi^2}}{2C_1} \right) \left(e^{C_2(C_1-f)\theta} - e^{-C_2(C_1+f)\theta} \right) \tag{9.7}$$

where v_r = velocity of seeds relative to a blade, m/s

  f = coefficient of friction between spinner and seeds

  g = acceleration of gravity = 9.801 m/s^2

  $C_1 = (f^2 + C_4/C_2)^{0.5}$

  $C_2 = \cos \alpha$

  $C_3 = \sin \alpha + f \cos \alpha$

  $C_4 = \cos \alpha - f \sin \alpha$

  r_i = radius to inner ends of blades, m

  r_o = outer radius of disk, m

  ω = rotational speed of disk, rad/s

  Angles θ, δ and α are all in radians.

Angles α and δ are shown on Figure 9.15. The spinning disk is a flat disk when $\alpha = 0$ and a cone-shaped disk when $\alpha > 0$. The cone-shaped disk increases the range of the seed trajectory by giving the seeds an upward component of velocity, $v_v = v_r \sin \alpha$. Angle δ is positive when the blades are forward pitched as shown in Figure 9.15, zero when the blades are radial, and negative when the blades have backward pitch.

 Equation 9.6 cannot be solved explicitly for θ, so an iterative solution is required. As an alternative, Figure 9.16 has been prepared to solve Equation 9.6 graphically. The three variables on the left side of Equation 9.6 are f, α, and θ. In Figure 9.16, the value of the left side of Equation 9.6 has been plotted on the y-axis versus values of θ on the x-axis; curves are shown for three values of α. Although f = 0.33 was used in plotting the graph, the solution is only weakly dependent on f and would be useable for any $0.2 < f < 0.45$. The coefficient of sliding friction falls within that range for virtually all seeds sliding on steel. To use Figure 9.16, the value of the right side of Equation 9.6 is calculated for the specific situation and entered on the y-axis of Figure 9.16. A line is drawn to the right to the curve for the appropriate α, and then a vertical line is drawn to the x-axis to find the corresponding value of θ. Then, as previously mentioned, Equation 9.7 can be used to calculate the sliding velocity of the seed relative to the blade at the outer end of the blade.
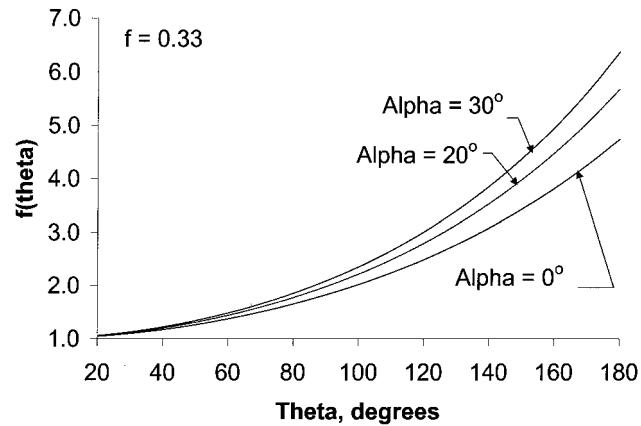

Figure 9.16 – Graphical solution of Equation 9.6.

The magnitude (v_{hr}) and direction (β) of the horizontal component of velocity as the seeds leave the disk can be calculated by using the following equations:

$$v_{hr} = \sqrt{(v_r \cos\alpha \cos\gamma)^2 + (r_o\omega + \cos\alpha \sin\gamma)^2} \tag{9.8}$$

and

$$\beta = \arctan\left(\frac{v_r \cos\alpha \cos\gamma}{r_o\omega + v_r \cos\alpha \cos\gamma}\right) \tag{9.9}$$

where $\gamma = \arctan(r_1 \tan\delta/(r_o - r_1))$. The velocity at which the spreader moves over the ground, v_g, is shown in Figure 9.15. By adjusting the parameters in Equation 9.6, the direction of the seed trajectory relative to the direction of travel can be adjusted. Usually, several gates must be provided in the central seed tube to generate good coverage of seeds over the swath. Example Problem 9.2 illustrates the calculations.

Example Problem 9.2

A centrifugal spreader is to be used to seed sweet clover seed. The following data are available:

Blade inner radius, $r_i = 0.05$ m

Blade outer radius, $r_o = 0.20$ m

Dish angle, $\alpha = 10^o$

Blade direction angle, $\delta = 0^o$

Rotational speed, $\omega = 78.5$ rad/s (750 rev/min)

Coefficient of friction, $f = 0.28$

Determine (a) the angle θ through which the spinner turns while the seed is in contact with the blade, (b) the velocity of each seed relative to the blade at the outer end of the blade, (c) the magnitude and direction of the horizontal component of velocity as the seeds leave the spinner, and (d) the vertical component of velocity as the seeds leave the spinner.

Solution

The first step is to calculate values for constants in Equation 9.6.

$C_2 = \cos(10°) = 0.985$

$C_3 = \sin(10°) + (0.28)\cos(10°) = 0.449$

$C_4 = \cos(10°) - (0.28)\sin(10°) = 0.936$

$C_1 = (0.28^2 + 0.936/0.985)^{0.5} = 1.014$

$C_3\, g\,/(C_4\, \omega^2) = (0.449 \times 9.801)/(0.936 \times 78.5^2) = 0.0007627$

(a) The value of θ can now be determined. The value of the left side of Equation 9.6, $f(\theta)$, is:

$$f(\theta) = (0.20 - 0.0007627)/(0.05 - 0.0007627) = 4.046$$

By consulting Figure 9.16, a value of $f(\theta)$ corresponds to $\theta = 146.1°$ or 2.549 radians when $\alpha = 10°$.

(b) Next, Equation 9.7 can be used to calculate v_r. The lengthy equation will not be rewritten, but when the values are inserted the result is:

$$v_r = 11.38 \text{ m/s}$$

(c) Next, angle γ must be calculated for use in Equations 9.8 and 9.9:

$$\gamma = \arctan[(0.05 \tan(0°)/(0.20 - 0.05)] = 0° \text{ or 0 radians}$$

Then, from Equation 9.8, the seeds leave the disk with a horizontal velocity of:

$$v_{hr} = [(11.38 \cos(10°) \cos(0°))^2 + (0.20 \times 78.5 + 11.38 \cos(10°) \sin(0°))^2]^{0.5}$$

$$= 19.3 \text{ m/s}$$

From Equation 9.9, the departure angle is:

$$\beta = \arctan[11.38 \cos(10°) \cos(0°)/(0.2 \times 78.5 + 11.38 \cos(10°) \cos(0°))]$$

$$= 22.6°$$

(d) Finally, the vertical component of velocity of the seeds is:

$$v_v = 11.38 \sin(10°) = 1.97 \text{ m/s (upward)}$$

Upon leaving the spinner, the seeds enter ballistic trajectories with absolute velocity v_v and velocity v_{hr} relative to the moving spreader. While the absolute horizontal velocity is the vector sum of v_{hr} and v_g, the contribution of v_g is usually negligible and v_{hr} can be used as the absolute initial horizontal velocity of the seeds. The following equations can be used to calculate the trajectory of a particle in still air (Goering et al., 1972; Pitt et al., 1982):

$$\ddot{h} = -C_6 \dot{h}\left[\dot{h}^2 + \dot{z}^2\right]^{0.5} \tag{9.10}$$

and

$$\ddot{z} = g - C_6 \dot{z}\left[\dot{h}^2 + \dot{z}^2\right]^{0.5} \tag{9.11}$$

where h = horizontal direction, m
z = vertical direction, m, positive downward
g = acceleration of gravity, m/s^2
$C_6 = 0.5 C_D \rho_a A_p/m$
where A_p = projected frontal area of particle, m
m = mass of particle, kg
ρ_a = mass density of air, kg/m^3 = $29 p_b/(8.314 \Theta_a)$
where p_b = barometric pressure, kPa
Θ_a = ambient air temperature, °K = °C + 273

The single dot over h or z indicates the first derivative with respect to time (velocity) while two dots represents the second derivative (acceleration). The drag coefficient,

C_D, varies with the Reynolds number. The following equations give a good approximation to drag coefficients first measured by Eisner (1930):

$$C_D = \frac{24}{N_{Re}} \quad \text{for} \quad N_{Re} \leq 1 \tag{9.12}$$

or $$C_D = \left(26.38 N_{Re}^{-0.845} + 0.49\right) \quad \text{for} \quad N_{Re} \geq 1 \tag{9.13}$$

where the Reynolds number is given by the following equation:

$$N_{Re} = \frac{\rho_a v_p d_p}{\mu_a} \tag{9.14}$$

where N_{Re} = dimensionless Reynolds number
v_p = velocity of particle, $\text{m/s} = \left(\dot{h}^2 + \dot{z}^2\right)^{0.5}$
d_p = effective diameter of particle, m
μ_a = dynamic viscosity of air, N·s /m^2

Over a wide range of barometric pressures, the air viscosity is a function only of air temperature, i.e.:

$$\mu_a = 4.79 \times 10^{-6} e^{0.678 + 0.00227\theta_a} \tag{9.15}$$

Equations 9.10 through 9.15 do not have a general closed solution but, by use of a computer, they can be solved iteratively to calculate the trajectory of a seed. The required parameters are the seed mass, effective diameter and frontal area, the air temperature and barometric pressure, and the initial velocity of the seed as it leaves the spinner. For a cone-shaped disk, the initial velocity in the z-direction is $-v_v$. The initial velocity in the z-direction is v_{hr}. The trajectory equations are based on the assumption of wind-still conditions.

Pitt et al. (1982) made further simplifying assumptions to enable calculation of trajectories without iteration. The first assumption is that the particle is launched horizontally, that is, the initial vertical velocity is zero. Also, the vertical velocity was set equal to zero in Equation 9.10 while the horizontal velocity was set equal to zero in Equation 9.11. Finally, the drag coefficient was assumed to be constant. Under those simplifying assumptions, the time required for the particle to fall distance z can be calculated by using the following equation:

$$t = \frac{\ln\left[\text{Arg} + \left(\text{Arg}^2 - 1\right)\right]}{2C_6 C_7} \tag{9.16}$$

where $\text{Arg} = 2e^{2C_6 z} - 1$
$C_7 = (g/C_6)^{0.5}$

The horizontal distance traveled during that fall time can be calculated from:

$$h = \frac{\ln\left(C_6 \dot{h}_o t + 1\right)}{C_6} \qquad (9.17)$$

where t = time for particle to fall distance z

h_o = initial velocity in h-direction, m/s

Equations 9.6 through 9.17 provide a means for evaluating the various transport factors that influence the uniformity of the pattern created by a broadcast seeder. Example Problem 9.3 illustrates the use of Equations 9.16 and 9.17 to calculate the end point of a seed trajectory.

Example Problem 9.3

Alfalfa seeds leave a centrifugal spreader horizontally with an initial velocity of 20 m/s. If the spreader disk is 2 m above the land surface, calculate the horizontal distance traveled by each seed before it reaches the ground. The barometric pressure is 100 kPa and the air temperature is 20°C.

Solution
Before Equation 9.16 can be used, values must be calculated for constants C_6 and C_7. For a spherical particle, it can be shown that:

$$C_6 = 0.75 C_D \rho_a / (\rho_p d_p)$$

where ρ_p is the particle density in kg/m^3. From Table 9.1 in the Problems section at the end of the chapter, d = 0.00153 m and ρ_p = 1184 kg/m^3. The Reynolds number must be calculated for use in calculating a drag coefficient. The air density is:

$$\rho_a = 29 \times 100 / (8.314 \times 20 + 273) = 1.19 \text{ kg/m}^3$$

From Equation 6.15, at 20°C, the air viscosity is 1.835×10^{-5} N·s/m^2. Although the particle velocity changes throughout the trajectory, we will use the initial velocity of 20 m/s in computing the Reynolds number, that is:

$$N_{Re} = 1.19 \times 20 \times 0.00153 / (1.835 \times 10^{-5}) = 1984$$

Then, from Equation 9.13, the drag coefficient is:

$$C_D = 26.38 \times 1984^{-0.845} + 0.49 = 0.533$$

Now, values for C_6 and C_7 can be calculated, that is:

$$C_6 = 0.75 \times 0.533 \times 1.19 / (1184 \times 0.00153) = 0.263$$

$$C_7 = (9.801 / 0.263)^{0.5} = 6.10$$

For a seed fall distance of 2 m, the value for Arg is 4.727 and, from Equation 9.16, the fall time is 0.697 s. Finally, from Equation 9.17, the horizontal distance traveled by the seed in 0.697 s is 5.86 m.

By comparison, a computer simulation of the trajectory of Example Problem 9.3 using Equations 9.10 through 9.15 indicated that the time for a 2 m fall would be 0.82 s and the horizontal travel in that time would be 6.05 m. Thus, the simplified approach using Equation 9.16 under-predicted the fall time by 15% but Equation 9.17 under-predicted the horizontal distance by only 3%. A plot of the entire trajectory showed that the seed was moving almost vertically near the end of the trajectory and thus the under-prediction of fall time had only a small effect on horizontal distance traveled. Using typical parameters for broadcasting of seeds, Equations 9.16 and 9.17 can generally predict the horizontal distance within 10% of the value calculated by Equations 9.10 through 9.15. If Equations 9.16 and 9.17 are used to calculate and plot a complete trajectory, inserting a factor in Equation 9.16 to increase each fall time by approximately 10% would improve the accuracy of the calculated trajectory.

Drills and precision planters include drop tubes for transporting seed from the metering device to the furrow. The drop tubes are nearly vertical and, if friction between the seed and the tube walls is neglected, Equation 9.11 can be used to calculate the time required for the seed to pass through the drop tube and the vertical velocity at the exit point. Since the tube is nearly vertical, at least at the seed entry point, the velocity in the x-direction can be set equal to zero in Equation 9.11. If C_D is variable, as in Equations 9.12 and 9.13, a computer is required to solve Equation 9.11. If C_D is assumed to be constant, the approximate transit time in the seed tube can be calculated using Equation 9.16 with z equal to the length of the tube. Also, by solving Equation 9.16 for z and differentiating with respect to time, the following equation can be obtained for seed velocity in the drop tube:

$$\dot{z} = \frac{C_7 \sin h(2C_6 C_7 t)}{1 + \cos h(2C_6 C_7 t)} \tag{9.18}$$

When t is taken as the transit time in the drop tube, then Equation 9.18 gives the z-direction velocity at the exit. Often the tube is curved toward the rear near the exit (see Figure 9.14) to give the seed a rearward velocity component near the exit. If the exit velocity is at an angle θ_e from the vertical, then the x-component of velocity at the exit, relative to the planter, is:

$$\dot{x}_r = \dot{z} \tan \theta_e \tag{9.19}$$

Seed bounce in the furrow disrupts the spacing of uniformly metered seeds. Seed bounce can be minimized or eliminated if the x-component of seed velocity relative to the planter is equal to the forward velocity of the planter. Then the seed will drop with zero horizontal velocity relative to the ground.

In the air planter, seeds are pneumatically conveyed from the metering point to the furrow through flexible hoses. It can be shown that the seeds must quickly attain the velocity of the air flowing through the hoses. Thus, the transit time in a hose can be calculated if the length of hose and the air velocity in the hose are known. v_a is the velocity of the air in the hose and if the exit velocity is at an angle θ_e from the vertical, then the horizontal component of the exit velocity relative to the planter will be:

$$\dot{x}_r = v_a \sin \theta_e \tag{9.20}$$

Again, seed bounce can be eliminated by insuring that the horizontal component of exit velocity relative to the planter is equal to the forward speed of the planter. Example Problem 9.4 illustrates the calculation of velocities in drop tubes.

Example Problem 9.4

A precision planter is to plant soybean seeds. The seeds leave the metering device with zero velocity relative to the planter and fall through a vertical distance of 0.5 m through a drop tube to reach the furrow. The barometric pressure is 100 kPa and the air temperature is 20°C. Calculate (a) the vertical velocity of the seed at the exit and (b) the exit angle required if the seed is to have zero horizontal velocity relative to the furrow when the planter speed is 1.8 m/s.

Solution
(a) As in Example Problem 9.3, values are needed for C_6 and C_7 before the fall time can be calculated. The air density is 1.19 kg/m^3 and the air viscosity is 1.835 N·s /m^2, as in Example Problem 9.3. From the table of seed properties (Table 9.1 in the Problems section at the end of this chapter), the soybean seed diameter is 0.00676 m and the seed density is 1176 kg/m^3. However, values are needed for the Reynolds number and drag coefficient before C_6 can be calculated. The fall velocity increases from zero to some as yet unknown value. To permit a solution, we will use the terminal velocity of 13.11 m/s for soybeans (Table 9.1). Then the values for Reynolds number and drag coefficient are:

$$N_{re} = 1.19 \times 13.11 \times 0.00676 / (1.835 \times 10^{-5}) = 5747$$

$$C_D = 26.38 \times 5747^{-0.845} + 0.49 = 0.507$$

The resulting values for C_6 and C_7 are:

$$C_6 = 0.75 \times 0.507 \times 1.19 / (1176 \times 0.00676) = 0.057$$

$$C_7 = (9.801 / 0.057)^{0.5} = 13.11$$

The value for Arg is 1.117 and, from Equation 9.16, the calculated fall time is 0.321 s. Then, from Equation 9.18, the vertical velocity at the exit is 3.09 m/s.

For comparison, a computer simulation using Equations 9.10 through 9.15 gave an exit velocity of 3.0 m/s. Note that this exit velocity is much less than the 13.11 m/s terminal velocity that was used in calculating the Reynolds number. The solution could be repeated while using a velocity of 3.09 m/s to calculate the Reynolds number. At high Reynolds numbers, however, the drag coefficient is so weakly dependent on Reynolds number that a second iteration would change the drag coefficient very little.

(b) From Equation 9.19, the required exit angle to give the seed zero horizontal velocity relative to the furrow is:

$$\theta_e = \arctan(1.8/3.09) = 30° \text{ from vertical}$$

9.2.2.3   Air seeders

The time required to fill seed boxes on individual row units tends to degrade the field efficiency (see Chapter 15) of a planter. Fill time with air seeders is reduced by storing the seeds in a central bin and transporting them to the individual row units pneumatically. The reduction in fill times allows air seeders to have high field efficiency. Theory for doing calculations for pneumatic seed transport is given in Chapter 14.

9.2.2.4   Performance of seed transport mechanisms

Of the seed transport mechanisms discussed in the previous section, the spinning disk provides the least accurate control of seed transport. Since the seeds travel on ballistic paths, wind can disrupt the pattern of coverage. As can be seen from Equations 9.6 and 9.7, both the swath width and the uniformity of the pattern are affected by the rotational speed of the spinning disk. Pattern is affected because the disk speed influences the angle at which the seed departs from the spinner (Equation 9.6); swath width is affected because the disk speed controls the launch speed of the seeds. Spinner speeds typically are in the range from 500 to 600 rev/min. Some typical distribution patterns from centrifugal spreaders are shown in Figure 9.17. By proper overlapping of adjacent swaths, it is theoretically possible to achieve uniform distribution using either the pyramid or flat top patterns.

Seeds are transported through drop tubes when drilling or precision planting. Since drilling does not require precise placement of seeds, drop tubes have only to remain open for acceptable performance. In the usual case in which the furrow openers can move vertically relative to the seed hopper, the drop tubes must accommodate the vertical movement. In precision planting, precise metering is of little value unless the transport process also distributes the seeds uniformly in the rows. Horizontal bounce of the seeds can be eliminated if the seeds are released with zero horizontal velocity relative to the ground (Equations 9.19 and 9.20). Vertical bounce can be reduced by releasing the seeds close to the bottom of a narrow furrow. It is also important that each seed should have the same transit time in the drop tube. Thus, all seeds should have the same initial velocity upon entering the drop tube and random bouncing within
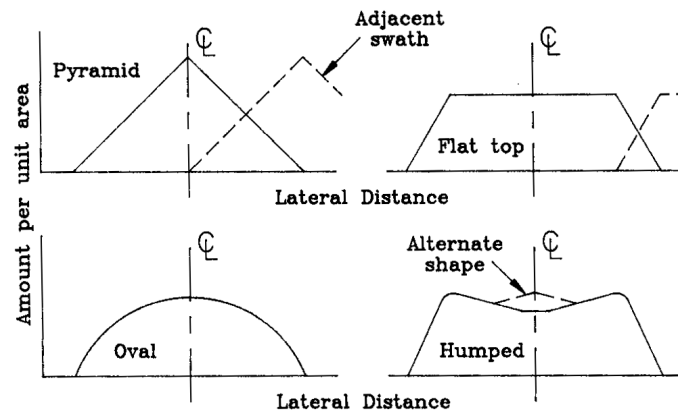

Figure 9.17 – Typical lateral distribution patterns from centrifugal spreaders.

the tube must be minimized. A tube with smooth interior will minimize seed-to-wall friction forces and a tube of small diameter will minimize bouncing within the tube.

9.2.3 Furrow opening and covering

9.2.3.1 Furrow opening and covering mechanisms

Hoes, runners, and single and double disks can be used to open furrows for planting seeds (Figure 9.18). Drills (Figures 9.2 and 9.3) normally employ the single-disk opener to open a furrow. Runner openers were widely used with plate-type planters and are still used on some precision planters. The double-disk opener is now used on many precision planters, either alone or in combination with a runner-type opener. For precision planting, the seeds must be placed at the proper spacing and also at the proper depth. Thus gage wheels (Figure 9.19) are located in close proximity to the furrow opener and seed release point to insure controlled, uniform planting depth. Use of a V-shaped tool to further shape the furrow provides a furrow cross section that minimizes seed bounce (Figure 9.20a and Figure 9.20b). After the seeds are deposited, covering disks (Figure 9.20c) or a scraper may be used to close the furrow. A press wheel (Figure 9.20d) may be used to firm the soil to assure good moisture transfer to the seeds. Alternatively, both covering and soil firming can be accomplished by a set of soil firming wheels (Figure 9.19) which move and firm the soil horizontally and without vertical pressure. A continuous furrow is not opened when the punch planter is used. Rather, spade-shaped wedges on the wheel (Figure 9.21) open holes or "dibbles" in the soil into which the seeds are dropped. Then the press wheel closes the soil over the seeds. The punch planter eliminates the non-uniform seed spacing that results from seed bouncing in a furrow. The spade wheel can roll over and punch through surface residue or other cover. It is the only type of planter that can plant through the plastic covers that are sometimes used in growing high value crops.

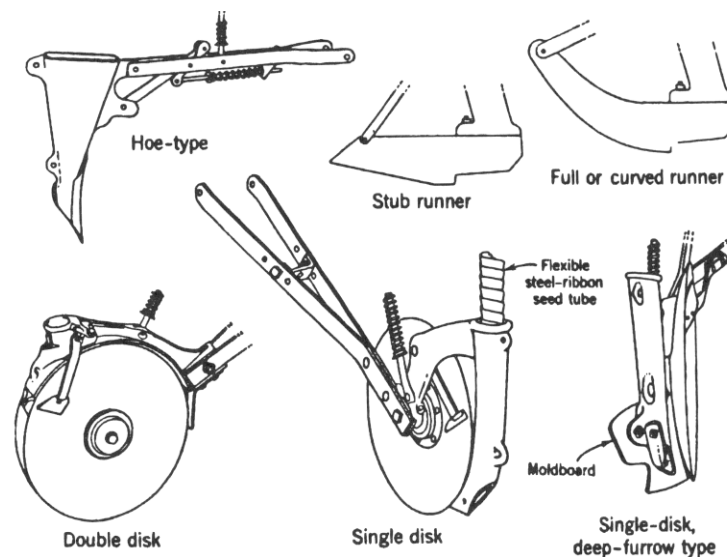**Figure 9.18 – Some common types of furrow openers.**

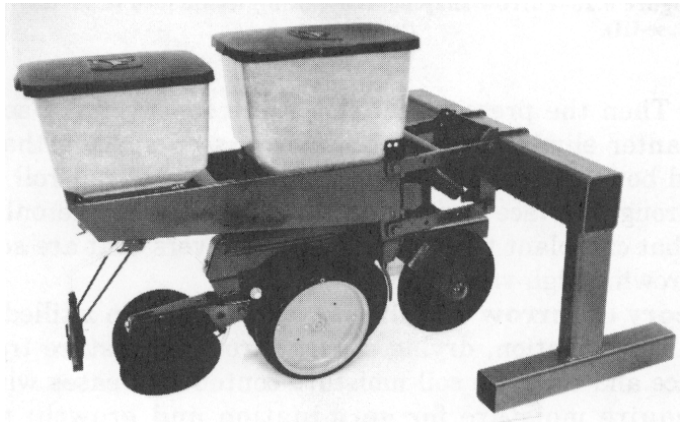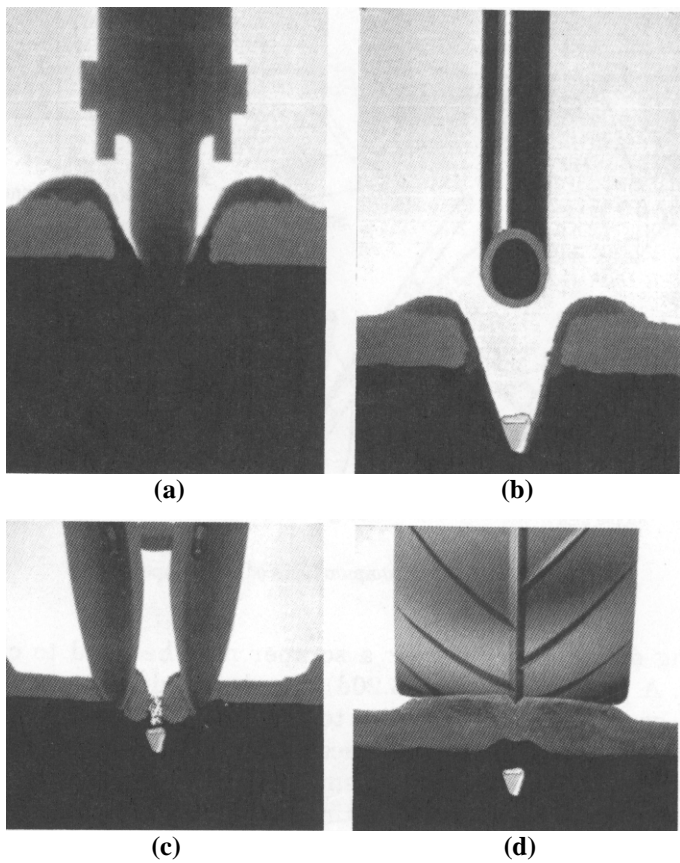**Figure 9.19 – A complete precision planter unit (courtesy of Deere and Co.).**

(a)   (b)

(c)   (d)

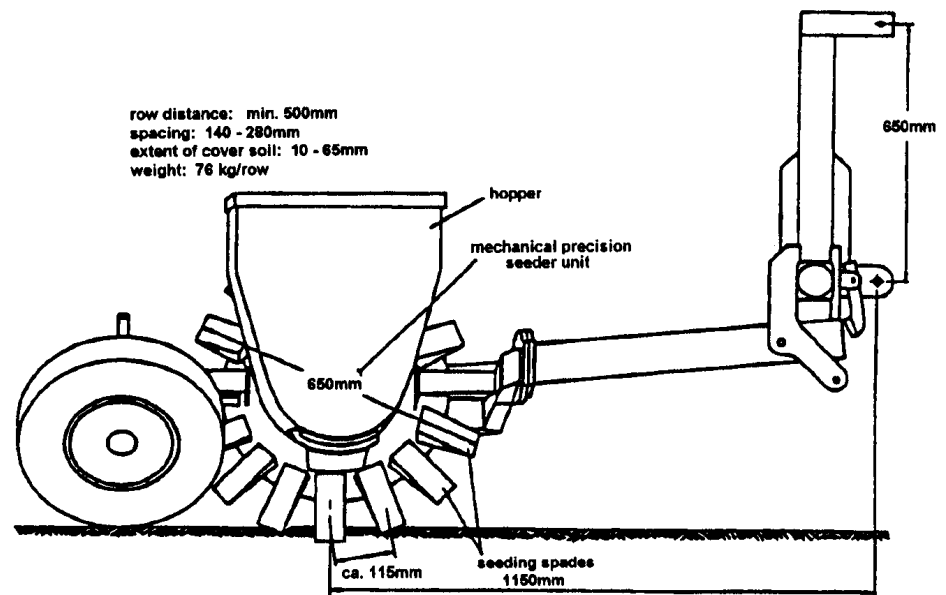**Figure 9.20 – Furrow-shaping and closing techniques (courtesy of CNH).**

Figure 9.21 – A punch planter
(courtesy of L.N. Shaw, University of Florida, Gainesville).

9.2.3.2 Theory of furrow opening and covering

In a tilled soil that is devoid of vegetation, drying occurs through moisture transfer to the surface and thus the soil moisture content increases with depth. Seeds require moisture for germination and growth; moisture transfer from soil to seed is promoted by placing the seeds in firm contact with moist soil. Increased depth of planting thus promotes better moisture transfer to the seeds. Choice of an optimum seed depth is a compromise, however, because two factors favor shallower planting. The first is that soil is normally warmer near the surface at planting time and warmer soil promotes seed germination. The second is that a seedling may not have sufficient strength to emerge if the seed is planted too deep in firm soil. Thus there is an optimum depth of planting which varies with type of crop and other factors (Morrison and Gerik, 1985). Typical planting depths, in mm, are: corn, 40-65; cotton, 25-50; grass seeds, 5-10; sorghum, 19-25; soybeans, 25-50; and wheat, 25-50. Theory relating to soil-seedling relationships is beyond the scope of this book, but the reader is referred to publications of a number of researchers who have investigated these relationships (Stapleton and Meyers, 1971; Vaughn and Bowen, 1977; Phene et al., 1978; and Goyal et al., 1980).

9.2.3.3 Performance of furrow opening and covering mechanisms

The most important criterion for judging the success of a furrow opening and covering mechanism is the percent emergence of the seeds that are planted in the furrow. Since percent emergence varies with soil and weather factors that vary from year to year, it is not possible to judge the effect of any given mechanism on emergence based

on data from only one season. However, there are other performance criteria which can be judged based on more limited testing. Many farmers are now using tillage techniques which leave crop residues on the soil surface in order to reduce soil erosion. The furrow openers must be able to cut through these crop residues. Disk-type openers are much better than runner-type openers (Figure 9.18) in cutting through surface residues. In addition, special notched disks may be attached ahead of the furrow opener to clear a path through the residue. The ability of the planter to maintain the desired, uniform depth of planting is an important criterion that may be evaluated using short-term tests.

CHEMICAL APPLICATION 10

INTRODUCTION

The purpose of applying agricultural chemicals is to provide nutrients for plant growth and to control weeds, insects and other crop pests, and plant diseases. Proper application of agricultural chemicals is crucial in successful modern agriculture. Agricultural chemicals, over the years, have become more sophisticated but also more expensive, so good methods avoid over-application. The major classifications of agricultural chemicals are fertilizers, pesticides (including insecticides, which kill insects), herbicides (which kill plants), fungicides (which kill fungi), growth regulatory hormones, and pheromones for biological control of insects. These chemicals may be either dry or liquid. The chemicals may be applied before planting during seed bed preparation, during planting, and/or after germination during the active growth period.

In this chapter we will discuss the chemical application methods and related equipment, their functional components and operating principles, equipment calibration, testing, and other related topics.

10.1 APPLICATION OF GRANULAR CHEMICALS

Dry chemicals in agricultural use are primarily fertilizers, herbicides, and insecticides. Technically many of these are powders; however, powders that are large in particle size and flow easily—as is the case with these agricultural chemicals—are referred to as granular material. That is the term used in this book. There are some agricultural chemicals that are non-granular powders of small size, such as insecticide powders applied by dusters. Because of drift and poor coverage these are of limited use in commercial farming. Better choices include liquid pesticides or granular pesticides that are liquid chemicals impregnated on inert granular carriers such as clay, sand, or corncobs.

Application of dry granules has certain advantages. It eliminates the need to haul water and the mixing required with liquid chemicals. Chemical drift, i.e., droplets that do not land on the intended target, is generally not as great a problem as it can be with liquids. The application equipment is less expensive and more trouble-free since no mixing, pumping, and agitation is involved. While practicing conservation tillage, better control is possible with granules than sprays since granules filter through the foliage onto the soil. Also, granules are generally safer to use than liquid formulations.

However, granular material is generally more expensive than the liquid chemicals. Granular material has poor metering characteristics and uniform distribution is a problem. The use of granules is limited to soil applications as they require moisture to become activated. Granular pesticides must be kept in a dry place and they are more bulky to store and transport.

Traditional granular pesticide rates have been 12 to 24 kg/ha (15 to 30 lb/acre) with 5% to 15% active ingredient. With the availability of granular pesticides that are 20% to 50% active ingredient there is a trend toward lower rates of application. Some new formulations have 75% to 90% active ingredient with a recommended application rate as low as 1.12 kg/ha (1 lb/acre). With increases in the concentration of active ingredients, there has been a shift toward smaller granular particles. Smaller particles tend to give better coverage by increasing the number of particles per unit area, but they are more prone to drift.

10.1.1 Methods for application of granular chemicals

Granular fertilizer may be spread uniformly over the entire field, in a *broadcast application,* or it may be applied in narrow rows, which is called a *banded application*. It may be applied before planting, during planting, or in established crops.

Pre-planting applications include applying the material either on the soil surface or placing it below the surface using an appropriate tillage attachment. Material applied on the surface may be incorporated into the soil using an appropriate tillage tool (generally a field cultivator or a disk harrow) as part of normal seed bed preparation. Fertilizers may be placed deep into the soil with a chisel type cultivator. A fertilizer distributor may be used as an attachment to a plow that places it in the furrows below the surface at plowing depth.

Application during planting is commonly done by fertilizer drills. Hoppers, tubes, and furrow openers are built in the drills to place the fertilizer below and to the side of the seed rows. Similarly, row-crop planters have attachments to place fertilizers in a narrow band on either side of the seed row. The furrow openers for fertilizer are separate from the seed furrow openers and they can be adjusted independently in the vertical and horizontal directions.

Application in established crops puts chemicals either on the surface or below the surface of the soil. The method of application depends upon the crop and the planting type. In solid-planted crops, fertilizers may be surface applied using either a drop-type or a rotary spreader. In row crops, granular chemicals may be banded between the rows or applied on either side of the rows as *side dressing*.

10.1.2 Equipment for application of granular chemicals

The equipment for applying granular material includes drop-type (gravity), rotary (centrifugal), and pneumatic (air) spreaders. Equipment may be drawn behind tractors or mounted on trucks or aircraft.

Drop-type spreaders may be either for broadcast application or for banded application. A truck-mounted drop-type spreader for broadcast application with a 15.24 m (50 ft) boom is shown in Figure 10.1. Tractor drawn units have 2.4 to 3.7 m (8 to 12 ft) long hoppers with narrowly spaced openings in the bottom. The openings are gener-

**Figure 10.1 – A drop-type fertilizer distributor
(courtesy of Ag-Chem Equipment Co.).**

ally 150 mm apart. A ground-wheel-driven shaft located inside the hopper near the bottom carries agitators to help flow the material. A slide gate is used to control the openings and to shut off flow during turnaround. A drop-type applicator for banded application is shown in Figure 10.2. This applicator utilizes several small hoppers as compared to one long one. The material is metered and dropped through a tube and is spread in a wide band by a diffuser. Some fertilizer distributors have furrow openers to place the material below the surface. This type of spreader is most commonly used as an attachment to planting equipment.
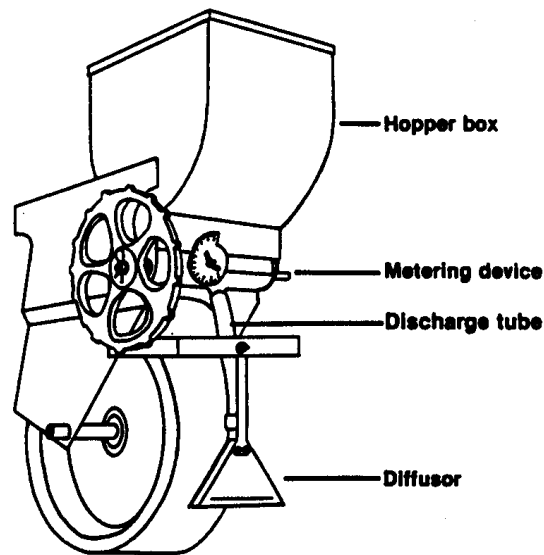
**Figure 10.2 – A drop-type applicator for banded application
(reprinted from Bode and Pearson, 1985).**

**Figure 10.3 – A truck-mounted commercial rotary applicator
(courtesy of Ag-Chem Equipment Co.).**

Rotary spreaders are used for broadcast application. These spreaders have one or two rotating disks with multiple vanes to impart energy to the granules. The material is metered onto the disks and is thrown wide due to the centrifugal force. Rotary spreaders are generally tractor mounted, but some of the larger commercial units are truck mounted with twin spinners as shown in Figure 10.3. The trucks used for chemical application use high flotation tires.

Pneumatic applicators can be used for either broadcast or banded application. They have a centrally located hopper from which granules are metered, delivered by air through tubes across the width of the machine, and spread by being impinged onto deflector plates. Pneumatic applicators allow central tank filling, easier installation on tillage implements, improved distribution, and easier transporting of trailer mounted applicators. A pneumatic applicator is shown in Figure 10.4.
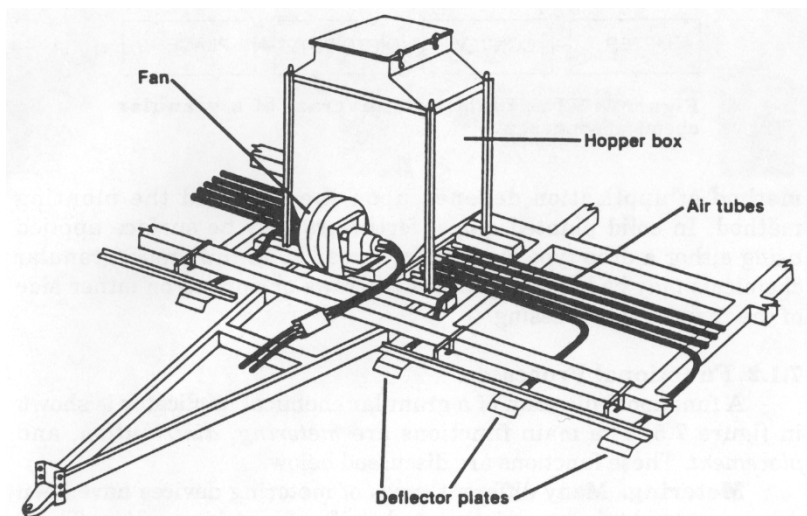

Figure 10.4 – A pneumatic applicator (reprinted from Bode and Pearson, 1985).

Aircraft are used to broadcast fertilizers in areas that are either too large or too difficult (rough terrain, flooded rice fields) for ground rigs. Airplanes carry a maximum payload of 500 to 1100 kg at working speeds of 130 to 190 km/h. The height of application usually varies from 9 to 15 m. *Ram-air spreaders* located underneath the fuselage consist of an air scoop, a venturi or restricted-throat section where the material is introduced, and a diverging section with dividers to give the proper lateral velocity components to the material being carried by the air streams. The air stream is generated by the propeller blast. Many ram-air spreaders give a trapezoidal distribution pattern that allows for a fairly uniform application with proper overlap at swath widths of 12 to 14 m. At application rates above 280 kg/ha (250 lb/acre) the particles are not accelerated properly and the distribution is not very uniform. The uniformity of application is also severely affected by crosswinds. Rotary spreaders are also used in aircraft applications. The spinners used in aerial applications rotate at a much faster speed as compared to the ground rigs in order to cover a much broader swath. Helicopters are used in areas where fixed-wing aircraft are not suitable, such as rugged, hilly terrain that is far away from a suitable landing site. The operating cost of helicopters is 2 to 3 times higher compared to fixed-wing aircraft.

10.1.3 Functional processes of granular chemical applications

A functional diagram of a granular chemical applicator is shown in Figure 10.5. The main functions are *metering, conveying, distribution*, and *placement*. These functions are discussed below.

$$\boxed{\text{METER}} \rightarrow \boxed{\text{CONVEY}} \rightarrow \boxed{\text{DISTRIBUTE}} \rightarrow \boxed{\text{PLACE}}$$

Figure 10.5 – The functional diagram of a granular chemical applicator.

10.1.3.1 *Metering*

Many different types of devices have been developed to obtain a consistent and uniform metering of granular chemicals. These devices are generally driven by a ground wheel that stops metering when the implement is stopped or lifted off the ground. Metering devices may be divided into *positive flow* and *gravity flow*. Positive flow metering devices provide for more accurate metering because a cavity is used to meter a certain volume of fertilizer (or other material). The rate of movement of the cavity determines the metering rate. Gravity flow devices rely on the orifice size to meter the flow rate. These differences are discussed in the following sections.

The *star-wheel feed* metering device (Figure 10.6) is used on some grain drills and a few row crop side-dressing attachments. Fertilizer, carried between the teeth of the feed wheel, falls into the delivery tube by gravity while material carried on top of the wheel is scraped off into the delivery opening. The discharge rate is controlled by raising or lowering a gate above the wheel.

Metering devices for some row-crop attachments have horizontal *rotating bottom plates* that fit up against the stationary bottom ring of the hopper base (Figure 10.7). The discharge rate is controlled by an adjustable gate over a side outlet. Sometimes there are two outlets permitting two bands from one hopper.
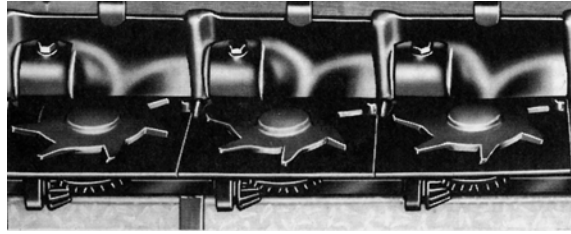
**Figure 10.6 – Star wheel metering mechanism of a grain drill
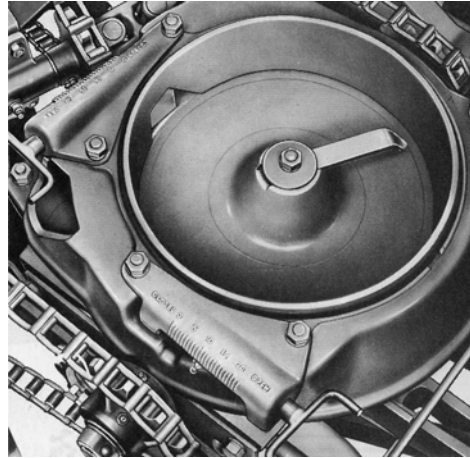(reprinted from Kepner et al., 1978).**

**Figure 10.7 – A rotating bottom metering device
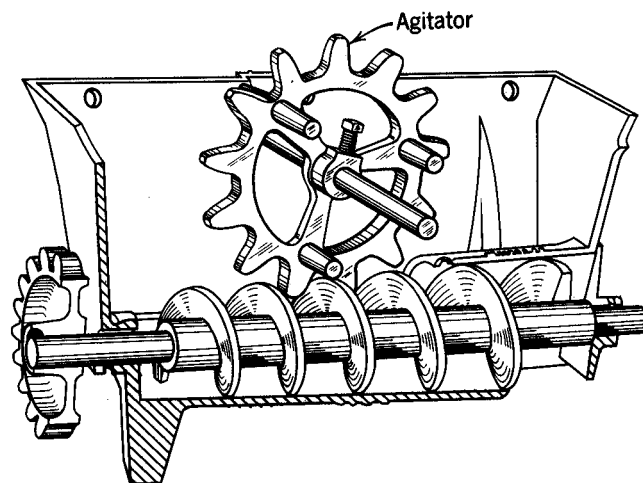(reprinted from Kepner et al., 1978).**

**Figure 10.8 – A metering device with close fitting auger
(reprinted from Kepner et al., 1978).**

Auger-type metering devices are illustrated in Figures 10.8 and 10.9. The type shown in Figure 10.8 has a close-fitting auger tube and the auger has relatively large displacement per revolution. The loose-fitting or floating-auger arrangement shown in Figure 10.9a is widely used on row-crop attachments. The inside diameter of the tube is about 12.5 mm greater than the auger diameter. Each of the two auger sections move the material toward one end of the hopper, where it is discharged from the end of the tube or dropped through an outlet opening. One hopper serves two rows. Augers are easily removed for cleaning.

Figure 10.9b shows a variation of the *loose-fitting auger* principle in which the material enters the auger tube from the top instead of from the end, is transported a short distance through the chute, and is then discharged from a bottom outlet. The tube assembly forms the bottom of the hopper and is removable. A series of openings along the tube provide multiple outlets for row crop use or for drop-type broadcasters. With any of the auger-type metering devices, the discharge rate is adjusted by changing the speed ratio between the auger and the ground wheel.
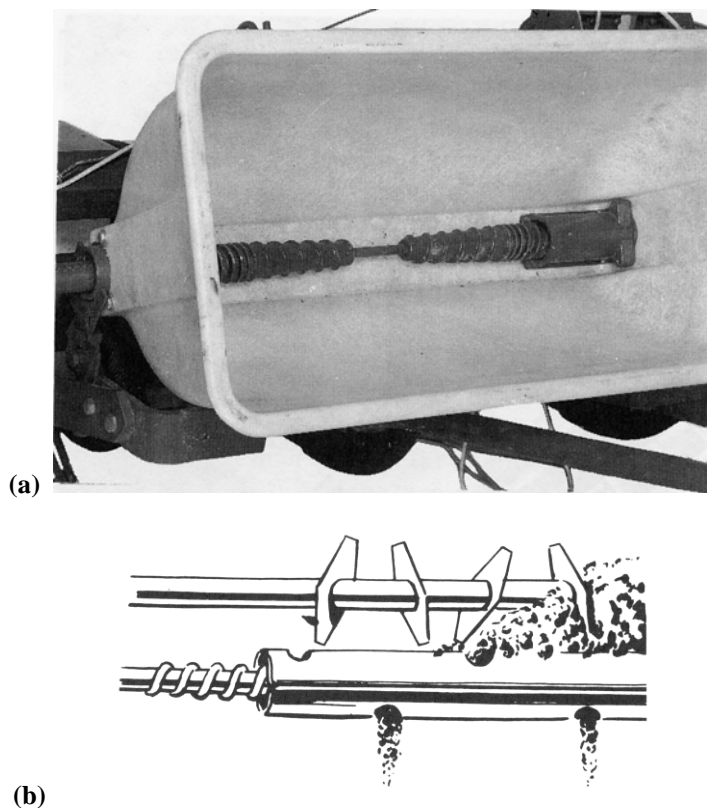

(a)

(b)

Figure 10.9 – Metering devices with loose-fitting auger (a) for row-crop attachments, (b) for row-crop attachment or drop-type broadcasters (reprinted from Kepner et al., 1978).
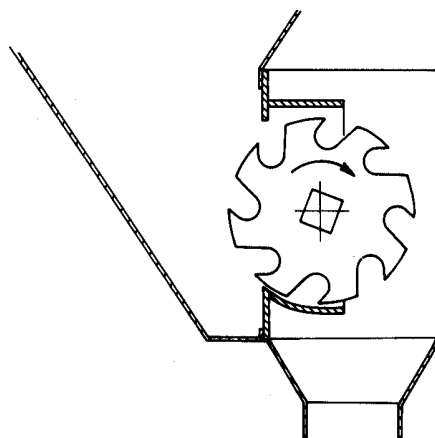
**Figure 10.10 – An edge-cell vertical rotor metering device
(reprinted from Kepner et al., 1978).**

An *edge-cell, positive-feed metering device* is shown in Figure 10.10. Metering wheel assemblies are spaced as required along the hopper and are driven by a common shaft. Rotor widths ranging from 6 mm to 32 mm are employed for different rate ranges. The discharge rate for a given rotor is controlled by changing the rotor speed.

Belt-type metering devices are sometimes employed where relatively large application rates are required, as on rotary broadcasters with large hoppers. Some units have a flat wire belt (usually stainless steel) that drags the material along the hopper bottom (Figure 10.11) and others employ rubberized fabric belts. The discharge rate is controlled by an adjustable gate above the belt. The discharge can be split into two or more streams if desired.

**Figure 10.11 – A wire-belt metering device on a centrifugal broadcaster
(reprinted from Kepner et al., 1978).**

**Figure 10.12 – A positive feed fluted roll type metering device
(reprinted from Bode and Pearson, 1985).**

Fluted metering devices are used for most granular-pesticide applicators. They consist of a ground-driven *vaned* or *fluted rotor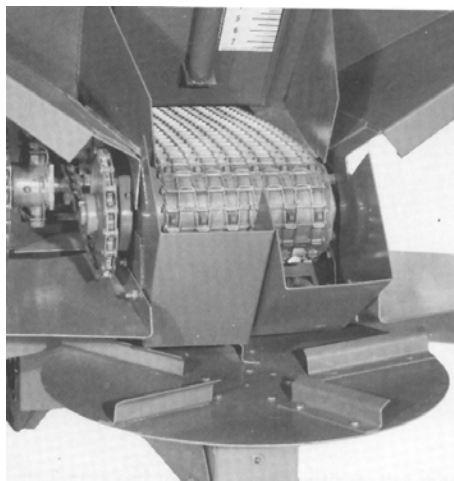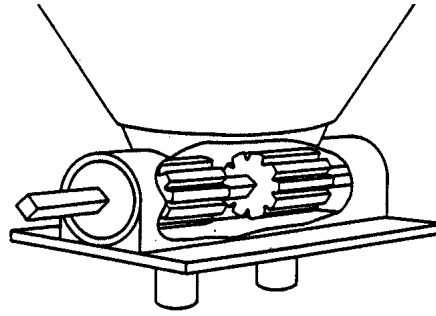* above an adjustable discharge opening (Figure 10.12). Hoppers for row crops sometimes have two or four openings whose outputs can be used separately or combined. Rotors fit closely in the hopper bottoms thus providing positive shut-off when the rotor is not turning.

Ideally, the discharge rate should be proportional to the rotor speed so that the application rate will not be affected by the forward speed. Tests have shown that this is not the case. Also, discharge rates are not proportional to the forward speed. This is due to incomplete filling of the inter-vane cavities, which is affected by the material flow characteristics. Fluted metering devices, like many other devices, produce a cycle variation in the uniformity of the application rate.

Gravity flow metering devices are common on drop-type broadcasters (Figure 10.13). In gravity flow devices, as opposed to the various positive flow metering devices discussed above, the metering rate is controlled by adjusting the size of the openings. A rotating agitator breaks up lumps and moves the material across the opening to assist in feeding. Rotating broadcasters have hoppers of a size that can be tapered down to a small bottom area and usually employ stationary-opening metering devices. Gravity metering devices are sensitive to ground speed.
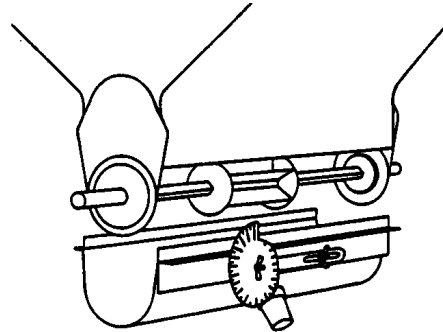

**Figure 10.13 – A gravity flow metering device
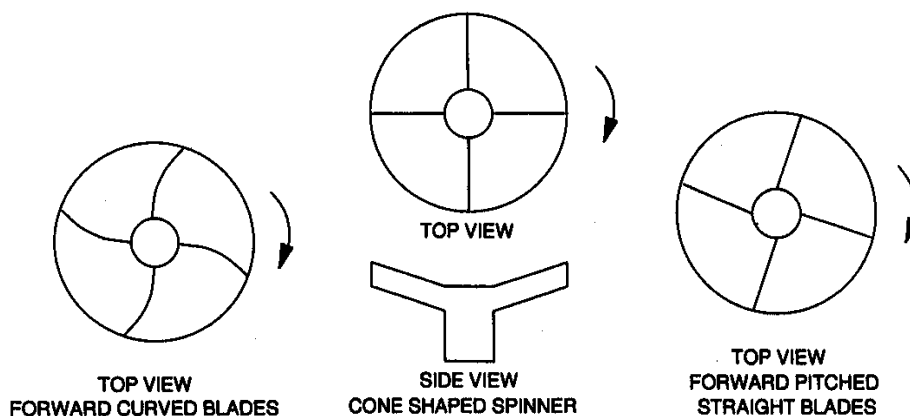(reprinted from Bode and Pearson, 1985).**

Figure 10.14 – Different types of spinners for rotary spreaders.

10.1.3.2 Distribution

Devices to distribute dry chemicals are of three main types: rotary, gravity, and ram-air spreaders.

Rotary spreaders usually consist of a single or a double counter-rotating horizontal spinner. The direction of rotation is such that the adjacent sides in the counter-rotating spinners move the material rearward. The spinners have blades that may be radial, forward pitched, or rearward pitched with respect to the radius. The blades may be either straight or curved. Forward-pitched blades give greater carrying distances for free-flowing materials, while rearward-pitched blades unload sticky material (e.g., moist lime) more readily. These spinners are shown in Figure 10.14. Rotary spreaders are used with broadcast types of applicators. A stream of granular material is dropped on the spinner and is thrown out by the action of centrifugal force. For a double spinner the stream is usually split in two by an inverted v-shaped splitter.

Gravity diffusers are made of an inverted v-shaped housing made of either plastic or sheet metal at the bottom of the drop tube. The housing has distributing vanes or other parts that take the stream of granular material and distribute it evenly into a wide band. Unlike rotary spreaders, the gravity type diffusers apply chemicals in more controlled manner and, therefore, they are more suitable as attachments to row-crop planters and cultivators. They are also available in open field fertilizer drills for full coverage of the field. Figure 10.15 shows various gravity type diffusers.

Ram-air spreaders are found in aircraft equipment. These are located in the propeller blast beneath the fuselage. A spreader of this type consists of an air scoop, a venturi or restricted-throat section where the material is introduced, and a diverging section with dividers to give the proper lateral velocity components to the material being carried by the air streams. Many different designs of the ram-air distributors have been developed. Most of those for spreading fertilizers or seeds are 910 to 1140 mm long, have a throat 610 to 760 mm wide and 150 to 200 mm high, and have a discharge area at least twice the throat area. The discharge angle for the outer sections is usually at least 45° from the line of travel.
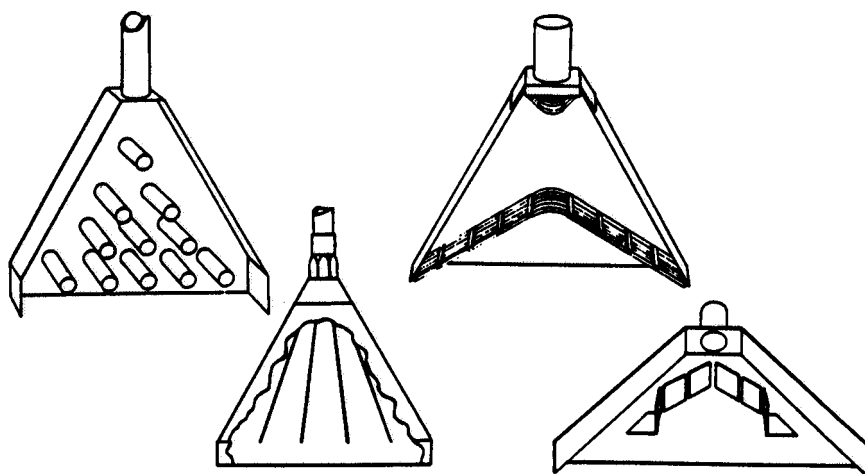
Figure 10.15 – Various types of diffusers used in drop-type applicators (reprinted from Bode and Pearson, 1985).

Many of the ram-air spreaders give a trapezoidal distribution pattern with a fairly flat top so that reasonably uniform distribution can be obtained with proper overlap at swath width of 12 to 14 m. However, as the material flow rate increases, the air velocity through the spreader is decreased and there is less energy available to accelerate the particles. Consequently, distribution patterns are poor for discharge rates greater than 900 kg/min. Another limitation of the ram-air distributors is the high aerodynamic drag and power requirement (Yates and Akesson, 1973).

Uniformity of coverage is one of the most important performance criteria. The horizontal distance through which the particles are thrown is affected by the particle size, density, and shape in addition to the spinner speed and geometric configuration. The components of a dry blend tend to separate as the larger particles of the same density travel farther. Wind also affects the carrying distance, and hence, the distribution pattern.

Uniformity of application is influenced by the shape of the pattern from the spreader and by the amount of overlap. Most patterns from rotary spreaders can be approximated by one of the shapes shown in Figure 9.17 (Chapter 9). Theoretically, pyramid, flat-top, and oval patterns give a uniform distribution if they are symmetrical, straight-sided, and overlapped as shown. The pyramid pattern allows more leeway for driving error. Humped patterns are undesirable from the standpoint of uniformity, but of the shapes shown would give reasonably uniform distribution, if the swath width were not over 40% of the overall pattern width, or if there were 60% overlap.

10.1.3.3 Placement

Placement devices may apply the chemical on the surface or below the surface. Surface applications are often incorporated into soil by a tillage tool if done before planting. On growing crops, especially solid-planted crops, a chemical is nearly always applied as top dressing and not incorporated into the soil. Fertilizer may be placed below the surface by a planter or a cultivator, or placed deep in the soil using chisel plows, or drilled into established pastures and other sods with special equipment.

Banded placement during row-crop planting is accomplished with applicators that are independent from the seed furrow opener. Double-disk, single-disk, and runner-type openers, similar to seed furrow openers, are often used.

Fertilizer grain drills often deliver the fertilizer through the seed tube, placing it in direct contact with the seeds in furrow. Separate disk openers are sometimes provided in front of the seed openers so that the seed row is not disturbed.

10.2 APPLICATION OF LIQUID CHEMICALS

Liquid chemicals include fertilizers, herbicides, pesticides, and growth-regulating hormones. These may be water emulsions, solutions, or suspensions of wettable powders. Liquid pesticides may be either *contact* or *systemic* type. Contact pesticides kill insects, fungi, etc., by coming in contact. To be effective, full coverage of the target, normally achieved by smaller droplets, is necessary. Systemic pesticides are taken in by the plant and they translocate within the plant. Full coverage of the plant is not required and larger droplets that are less prone to drift are acceptable.

10.2.1 Methods for application of liquid chemicals

Liquid chemical application methods vary depending on whether they are applied pre-planting**,** during planting, or post-planting. Pre-planting applications generally are fertilizers and herbicides and may include subsurface or surface application. Applications of aqua ammonia and anhydrous ammonia fertilizers are usually subsurface. Their application is accomplished by means of specially designed knives or chisel injectors. Liquid chemicals applied during planting generally include fertilizers and herbicides. Post-planting chemical applications may include fertilizers and all types of pesticides.

Liquid chemical application methods may be further divided based on the area covered. This may be *broadcast*, *banded*, and *directed spray*. In a broadcast application the chemical is applied uniformly on the ground or on the crop. In banded application the chemical is applied in narrow bands or strips. Several nozzles are used in directed spray for row-crop applications for a more complete coverage of the plants. Figure 10.16 shows the three methods of application.

10.2.2 Equipment for application of liquid chemicals

10.2.2.1 Sub-surface application

Sub-surface application is generally used for liquid chemical fertilizer in the form of anhydrous ammonia or aqua ammonia. These are called *pressure liquids* because they have a high vapor pressure that is used to create flow. *Anhydrous ammonia* contains 82% nitrogen and its boiling point is –28° F. When water is added to anhydrous ammonia to reduce the vapor pressure it is called *aqua ammonia*. It contains only 20% to 25% nitrogen, has a higher boiling point, and is termed *low pressure liquid fertilizer*.

With anhydrous ammonia, aqua ammonia (as well as other liquids with high vapor pressures), it is essential that the material be released in narrow furrows and
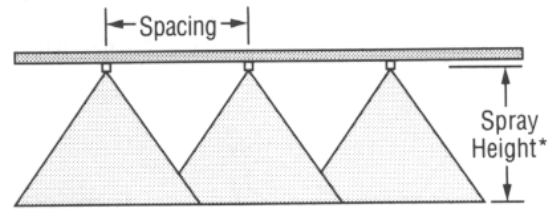
Broadcast
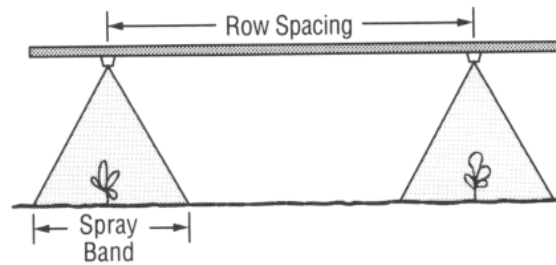
Banded
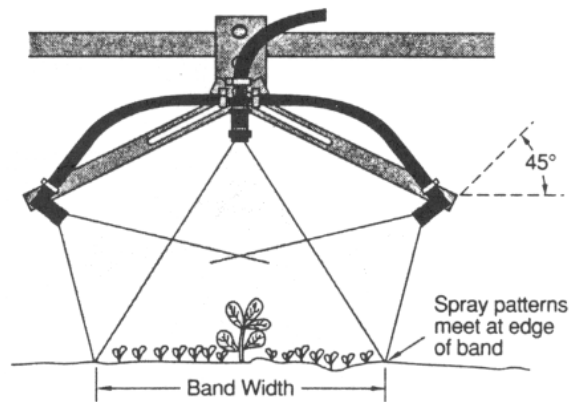
Directed

**Figure 10.16 – Methods of liquid chemical application
(courtesy of Spraying Systems Co., 1991).**

covered immediately to prevent escape. Anhydrous ammonia should be released at a depth of at least 10 to 15 cm. Aqua ammonia is applied about 5 cm below the surface since it is not as volatile. A loose, friable soil with adequate moisture is important for good sealing and for absorption of ammonia on the soil particles. Under some conditions press wheels or some other covering devices follow immediately behind the applicators.

Figure 10.17 shows a schematic of a trailing ammonia applicator. Note that there is no pump in the system, as the vapor pressure of the ammonia is used to pump the liquid. A regulator valve is needed to control the flow as the vapor pressure varies with the amount and concentration of ammonia in the tank and with temperature. For example, at 15.6° C the vapor pressure is 620 kPa (93 psi) but at 37.8° C the pressure rises to 1.3 MPa (197 psi). For subsurface application of aqua ammonia a pump is necessary because of its lower vapor pressure.

A typical narrow applicator blade for sub-surface applications is shown in Figure 10.18. The liquid is discharged from holes in the sides of the delivery tubes near the lower end. The spacing of the knives depends on the crop being grown.

Ground driven, variable stroke pumps are also employed to meter ammonia. Both mounted and pull-type implements are available for applying pressure liquids.
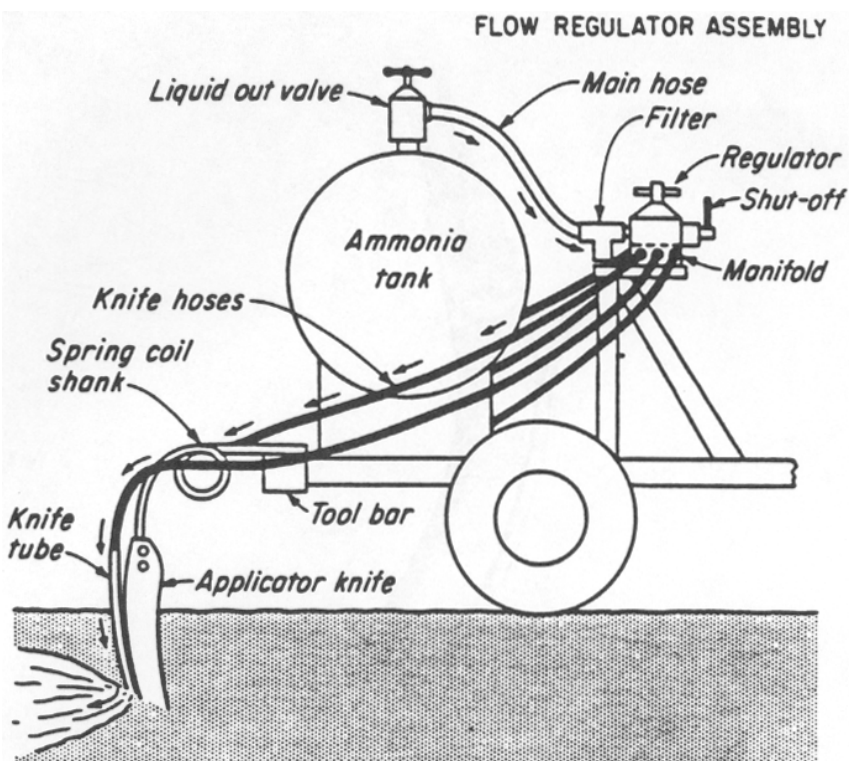
**Figure 10.17 – A schematic of a trailing ammonia applicator
(reproduced from Smith, 1964, by permission of McGraw-Hill Book Co.).**
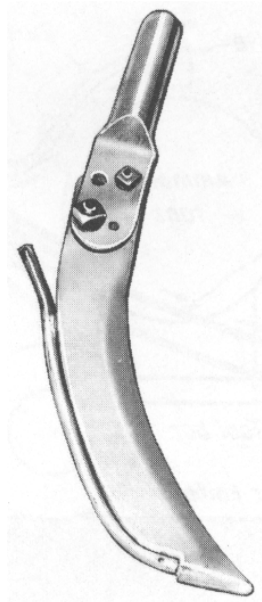
Figure 10.18 – An applicator blade for anhydrous ammonia (reprinted from Kepner et al., 1978).

10.2.2.2 Application of non-pressure liquids

In *non-pressure-liquid applicators*, the flow of liquid is due to gravity and the flow rate is controlled by fixed orifices. The attachments generally have a sediment bowl, a filter, one or two orifice disks with a range of orifice sizes, and a quick shut-off valve. Unless the tank elevation is large in relation to its depth, or bottom venting is employed, head changes will cause appreciable variations in flow rate. Bottom venting (inverted siphon) is obtained by having the tank sealed such that air can enter only through an open tube that runs from the top of the tank to a point inside the tank near the bottom. The height of the bottom end of the tube in relation to the orifice then establishes the liquid head. This tube may be attached to a sealing-type filler cap. With a given orifice size and head, the application rate per hectare is inversely proportional to the forward speed.

A simple squeeze pump as shown in Figure 10.19 has been developed for many non-pressure-liquid applicators. Units are available with as many as 20 tubes, each serving one applicator outlet. The positive-displacement, ground-wheel-driven pump produces flow rate proportional to ground speed. The application rate is adjusted by changing the speed ratio between the reel and the ground wheel.

Non-pressure liquids can be applied directly to the soil surface, as well as on pasture and other solid-planted crops. Banded application of non-pressure liquids are sometimes made during a row-crop planting operation or as later side dressing. Non-pressure liquid chemicals are available for many planters. Usually one tank is provided for each two rows. Liquid is discharged close to the furrow through small tubes.
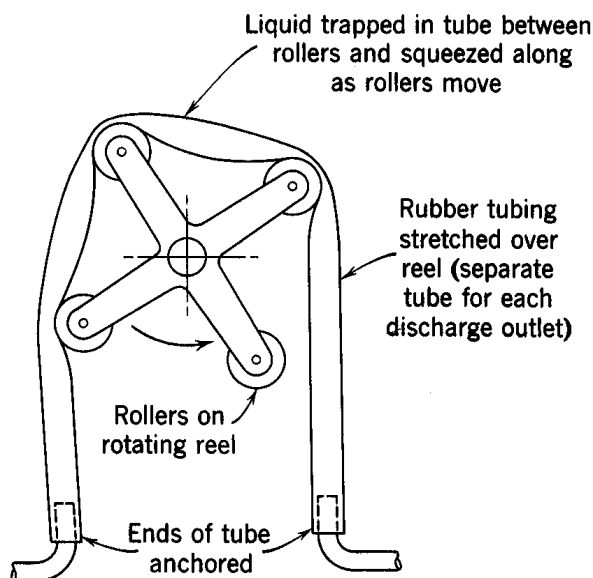
Figure 10.19 – A squeeze pump (reprinted from Kepner et al., 1978).

10.2.2.3 Low-pressure sprayers

Low-pressure sprayers are used to apply pre- and post- emergent chemicals to control weeds, insects, and diseases. Boom-type sprayers are used on tractors, trucks, or trailers; a tractor-mounted boom-type of field sprayer is shown in Figure 10.20. Low-pressure units usually operate in 150 to 350 kPa range and apply 50 to 200 L/ha. However, in some ultra low volume (ULV) applications, the rates may be as low as 10 L/ha to a few mL/ha. Tank-on-tractor mounted sprayers hold from 575 to 1000 L. For application in the standing row crop, high-clearance sprayers have been developed. They have a frame high enough to clear corn, cotton, and other tall crops. The spray boom may be raised or lowered depending upon the crop height. The sprayer may be mounted on a trailer or wheels and pulled through the field by a tractor. Tank capacity may be as high as 3750 L. The boom width may vary from 4 to12 m. Skid-mounted sprayers may be placed on a pickup truck or a flatbed truck. The tank size may be up to 10,000 L and the boom width up to 18 m. The trucks are fitted with flotation tires so they can operate in wet conditions.

Aircraft-mounted low-pressure sprayers have the advantage of rapid coverage and applying chemicals when conditions are otherwise unsuitable for ground rigs. Because of the limited weight carrying capacities, aircraft-mounted sprayers are most suited for low application rates of less than 50 L/ha. The aircraft speed varies between 50 to 125 km/h for helicopters and 175 to 250 km/h for airplanes as they fly about 1 to 8 m above the crop height.

Figure 10.20 – A boom-type field sprayer (reproduced by permission of Deere and Co., © 1991. All rights reserved).

10.2.2.4 High-pressure sprayers

High-pressure sprayers are similar to low-pressure sprayers except they operate under much higher pressure, up to 7000 kPa, and generally do not have a boom with multiple nozzles. High-pressure sprayers are used in orchards where it is necessary to spray to the top of the trees and to penetrate the thick tree canopy. High-pressure sprayers are more expensive because the parts are made to withstand higher pressures.

10.2.2.5 Air-carrier sprayers

Air-carrier sprayers are sometimes called *air-blast sprayers* or *mist blowers*. The liquid is atomized either by pressure nozzles or rotary atomizers in a high velocity air stream. The atomized liquid is then carried to the target by the air stream. The sprayers are capable of generating air flow rates in the range of 2.5 to 30 m³/s with air speeds ranging from 125 to 240 km/h. Since air is used to carry the pesticide to the target, concentrated pesticides can be used resulting in a substantial savings in the amount of water needed and the time required for refilling. Two different types of air-carrier sprayers are shown in Figures 10.21 and 10.22.
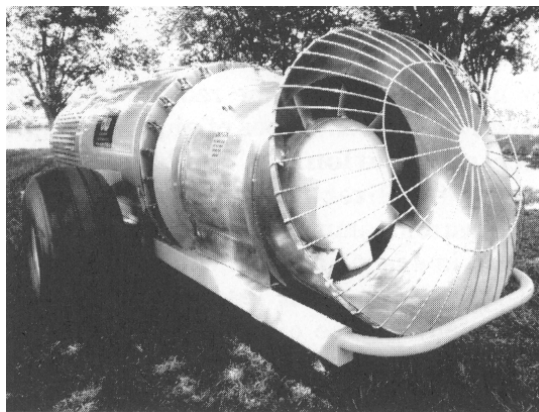
Figure 10.21 – An air-blast sprayer (courtesy of Durand-Wayland, Inc.).
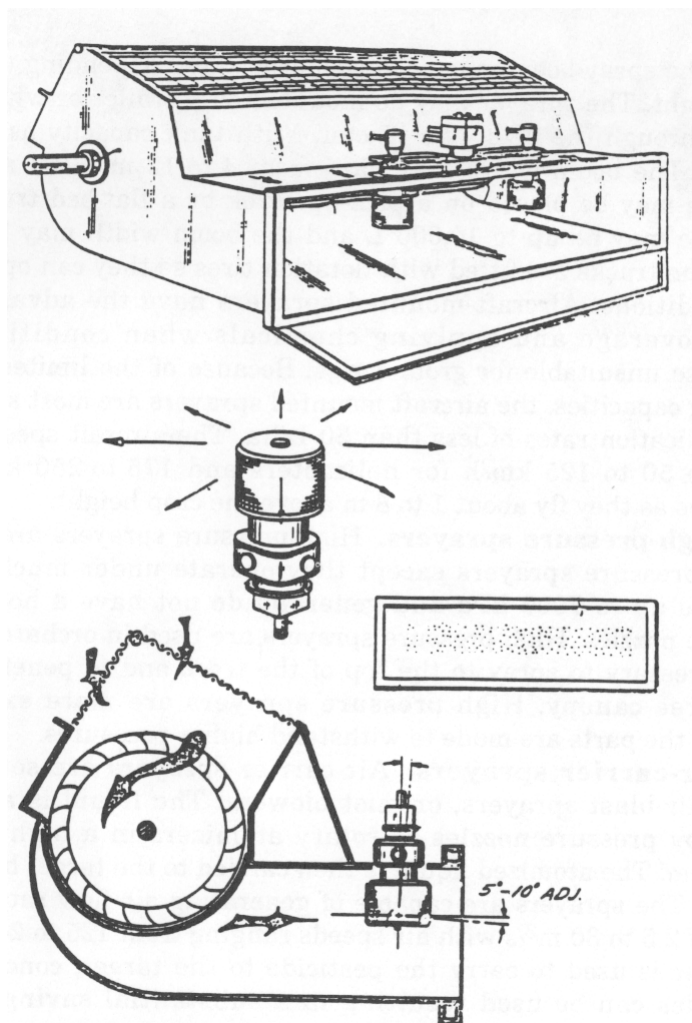
**Figure 10.22 – An air-curtain sprayer utilizing a cross-flow fan and a
rotary controlled droplet atomizer (Van Ee and Ledebuhr, 1987).**

10.2.3 Functional processes of applying liquid chemicals

Figure 10.23 shows two typical arrangements for a hydraulic sprayer. A hydraulic
sprayer consists of a tank to hold the liquid chemical, an agitation system to keep the
chemical well mixed and uniform, a pump to create flow, a pressure regulator valve to
control rate of flow, a series of nozzles to atomize the liquid, and miscellaneous com-
ponents such as boom, shut-off valves, fittings and strainers.

The main functional processes—pumping, agitation, and atomization—are dis-
cussed below.

(a)

(b)
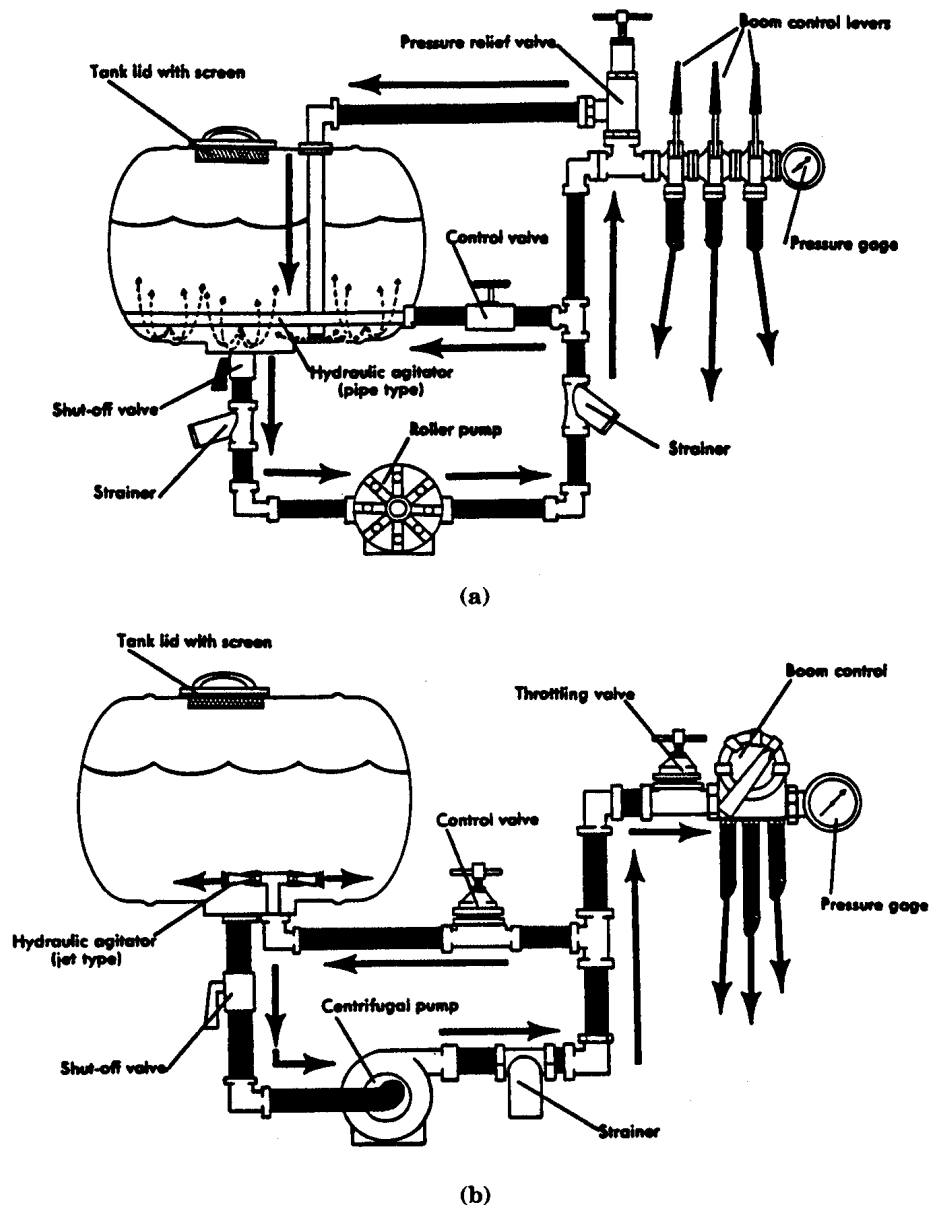
Figure 10.23 – Schematic diagrams of low-pressure hydraulic sprayers utilizing (a) a roller pump, (b) a centrifugal pump (reprinted from Bode and Butler, 1981).

10.2.3.1 Pumping

Positive-displacement pumps. With *positive-displacement pumps*, the output is not affected by the output pressure and the flow is created by positively displacing a volume by a mechanical means such as a piston or plunger. In contrast, with a *centrifugal pump*, flow is created by the action of centrifugal force. The output drops as the output pressure is increased.

Positive-displacement pumps found on sprayers include piston (plunger), rotary, and diaphragm types. These are self-priming, and they all require automatic (spring-loaded) bypass valves to control the pressure and to protect the equipment against mechanical damage if the flow is shut off.

Piston (plunger) pumps are a kind of positive-displacement pump that is well suited for high-pressure applications such as high-pressure orchard sprayers and multipurpose sprayers designed for both high- and low- pressure spraying. They are more expensive than other types, occupy more space, and are heavy, but they are durable and can be constructed so they will handle abrasive materials without excessive wear.

The volumetric efficiency of a piston pump in good condition is generally high (90% or more), and the discharge rate is essentially a direct function of crank speed and volumetric displacement. Crank speeds on the smaller piston sprayer pumps [38 L/min (10 gpm) and less] are mostly 400 to 600 rev/min. High-pressure piston sprayer pumps [4.1 to 5.5 MPa (600 to 800 psi)] are usually operated at 125 to 300 rev/min have capacities of 75 to 225 L/min (20 to 60 gpm). Mechanical efficiencies may range from 50% to 90%, depending on the size and condition of the pump.

*Rotary pumps,* another type of positive-displacement pump, are popular for low-pressure sprayers, the most common types being roller pumps (Figure 10.24a). Roller pumps have a slotted rotor that rotates in an eccentric housing. Rollers in each slot seal the space between the rotor and the wall of the case. The rollers are held against the case by centrifugal force during pump operation. As the rollers go past the inlet the space expands creating low pressure and causing the liquid to be drawn in toward the housing. The liquid trapped between the rollers is moved towards the outlet as the rotor turns. Now the cavity between the rollers contracts, expelling the liquid out through the outlet port. Pump output is determined by the length and diameter of the housing, its eccentricity, and the speed of rotation.

Teflon is a common material for the rollers, although rubber, steel, and carbon are also used. Rotary pumps of are compact and relatively inexpensive, and can be operated at speeds suitable for direct connection to the tractor PTO. Although they are classed as positive-displacement pumps, leakage past the rollers causes a moderate decrease in flow as the pressure is increased. Normal output of roller pumps ranges from 19 to 114 L/min (5 to 30 gpm) and maximum pressures range from 1 to 3 MPa (150 to 300 psi). However, pressures above 690 kPa (100 psi) are not generally recommended for rotary pumps when pumping non-lubricating liquids. Roller pumps wear rather rapidly under abrasive conditions, but the rollers can be replaced economically.

Diaphragm pumps are another type of positive-displacement pump. They are becoming more widely used and are available with flow rates up to 19 to 23 L/min (5to 6
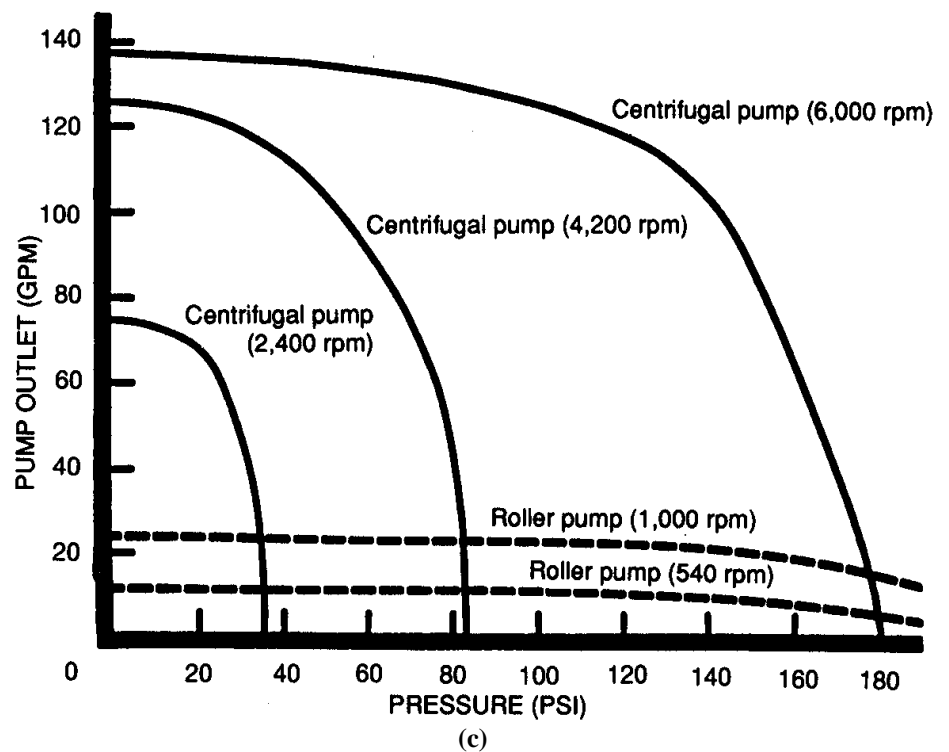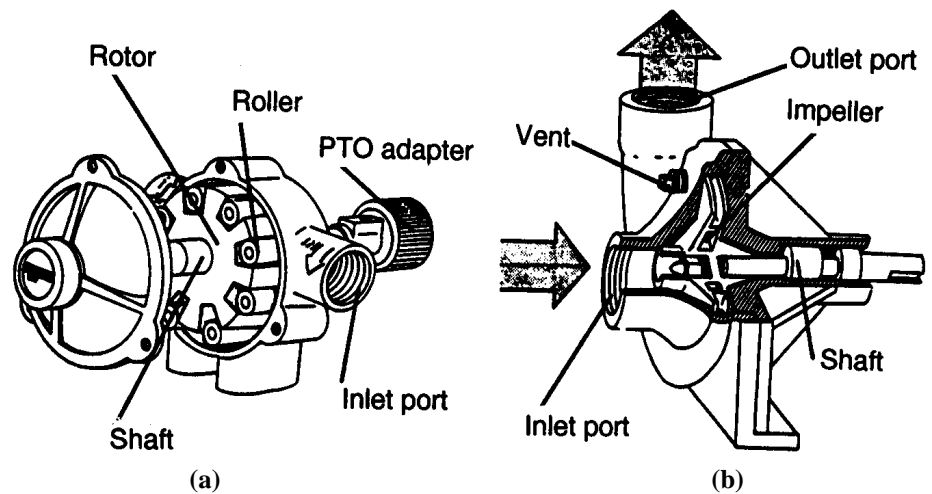
Figure 10.24 – (a) A typical roller pump, (b) a typical centrifugal pump,
and (c) performance curves of roller and centrifugal pumps
(reprinted from Bode and Butler, 1981).
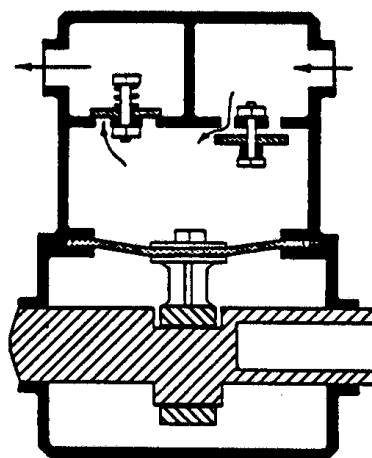
Figure 10.25 – A positive displacement diaphragm pump. (Reproduced by permission of Deere and Co. © 1991. All rights reserved.)

gpm) and pressures up to 3.4 MPa (500 psi). Since the valves and the diaphragm are the only moving parts in contact with the spray material, these pumps can readily handle abrasive materials (Figure 10.25).

Centrifugal pumps. *Centrifugal pumps* (Figure 10.24b) do not create flow by mechanically displacing a volume, as do positive-displacement pumps. Instead, they depend upon centrifugal force for their pumping action. They are essentially high-speed (3000 to 4500 rev/min), high-volume (70 to 130 gpm) devices not suitable for high-pressure applications because the pump output drops off rapidly when the outlet pressure is above 206 to 275 kPa (30 to 40 psi). The pressure or head developed by a given centrifugal pump at a particular speed is a function of the discharge rate, as indicated by the typical performance curves in Figure 10.24c. Note that the peak efficiency, which occurs at a relatively high flow rate, is well above 70% for this particular unit, whereas efficiencies at small flows are low.

For a given centrifugal pump and a given point on the efficiency curve, the discharge rate varies directly with the speed, the head varies as the square of the speed, and the power varies as the cube of the speed. If two or more stages are connected in series, the head and power at a given discharge rate are increased in proportion to the number of stages. Thus, multi-staging provides increased pressures without increasing the capacity range.

Centrifugal pumps are popular for certain types and sizes of sprayers because of their simplicity and their ability to handle abrasive materials satisfactorily. They are well suited to equipment such as air-blast sprayers and aircraft sprayers, for which high flow rates are needed and the required pressures are relatively low, and are used on many low-pressure field sprayers. The high capacities are advantageous for hydraulic agitation and for tank-filling arrangements. Speeds in these applications are generally in the range between 1000 and 4000 rev/min, depending upon the pressure required and the diameter of the impeller.

Since centrifugal pumps do not have positive displacement, they are not self-priming and do not require pressure relief valves for mechanical protection. Priming is usually accomplished by mounting the pump below the minimum liquid level of the tank or providing a built-in reservoir on the pump that always retains sufficient liquid for automatic priming.

Power requirements. Power requirements of pumps are determined by flow rate, operating pressure, and mechanical efficiency. The mechanical efficiency used for estimating the power requirements is 50% to 60%. The pump input power can be calculated using the following formula:

$$P = \frac{Qp}{60,000\eta_m} \tag{10.1}$$

where P = power, kW

Q = flow rate, L/min

p = pressure, kPa

η_m = mechanical efficiency, decimal

10.2.3.2 Agitation

Many spray materials are suspensions of insoluble powders or are emulsions. Consequently, most sprayers are equipped with agitating systems, either mechanical or hydraulic.

Mechanical agitation is commonly accomplished by flat blades or propellers on a shaft running lengthwise in the tank near the bottom and rotating at a speed of 100 to 200 rev/min (Figure 10.26). The following relations apply to round-bottom tanks with flat, I-shaped paddles sweeping close to the bottom of the tank. They are based on results originally reported by French (1942) as cited in Kepner (1978).
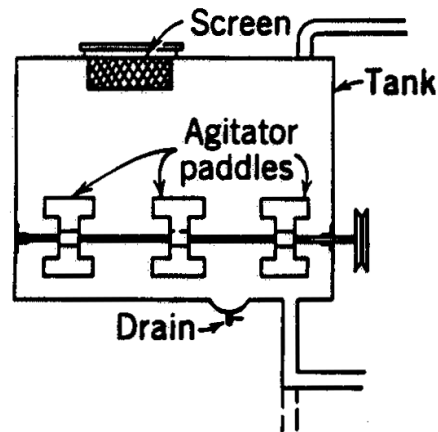
Figure 10.26 – Mechanical agitation (reprinted from Kepner et al., 1978).

$$s_m = 5.39A^{0.422}R^{-0.531}F_e^{0.293} \tag{10.2}$$

$$P_s = 3.26 \times 10^{-11} R^{0.582} s_m^{3.41} L \tag{10.3}$$

where s_m = minimum peripheral speed of paddles, m/min
    A = depth of liquid above agitator shaft center line, mm
    R = total combined width of all paddles divided by tank length
    F_e = agitation factor indicating relative difficulty of agitating a given
        oil-water emulsion, either hydraulically or mechanically
    P_s = shaft input power at any peripheral speed, s kW
    L = length of tank, mm

Values of F_e for various oil-in-water emulsions are shown in Table 10.1. These were established during tests with hydraulic agitation but are assumed to apply reasonably well for mechanical agitation. French's tests were conducted with an emulsion containing 1% to 2% oil. No data are available to indicate mechanical agitation requirements for suspensions of wettable powders.

Paddle tip speeds in excess of about 150 m/min may cause significant foaming of some mixtures. For mechanical agitation of emulsions in flat-bottom tanks with rounded corners, the minimum tip speed from Equation 10.2 must be multiplied by the factor 1.11. This increase in minimum speed causes the minimum power requirement to be approximately doubled (Equation 10.3).

For *hydraulic agitation*, a portion of the pump's output is discharged into the spray tank through a series of jet nozzles or orifices located in a pipe along the bottom of the tank. The energy and turbulence from the jets provide the mixing action. Figure 10.27a shows different hydraulic agitator nozzles. In tests with various sizes of cylindrical tanks, Yates and Akesson (1963) found that best results were obtained when the jet nozzles were mounted as shown in Figure 10.27b. The location shown for wettable powders was satisfactory for an emulsion containing 40% oil and 60% water only when a suitable emulsifier was included in the formulation. Nozzle spacings from 75 to 710 mm were satisfactory for oil-water emulsions but not to exceed 305 mm for wettable powders.

Table 10.1. Values of agitation factors (F_e) for oil-in-water emulsions (Kepner et al., 1978).

Oil, %	Water, %	Emulsifier, %	Jet Position (Figure 10.27b)	Agitation Factor, F_e
60	40	0	emulsion	0.83
50	50	0	emulsion	1.00
40	60	0	emulsion	1.00
10	90	0	emulsion	0.89
1 – 2	99 – 98	0	emulsion	0.50
40	59.9	0.1	emulsion	0.50
40	59.9	0.1	wettable powders	0.68

The minimum total recirculation rates for hydraulic agitation in a cylindrical or round-bottom tank, based on complete mixing of a full tank of material in 60 s, were found to be as follows:

$$Q_m = 3830 \frac{VF_e}{p^{0.56}}$$

For oil-water emulsions, (10.4)

For wettable powders, $$Q_m = 1380 \frac{VF_e}{p^{0.3}}$$ (10.5)
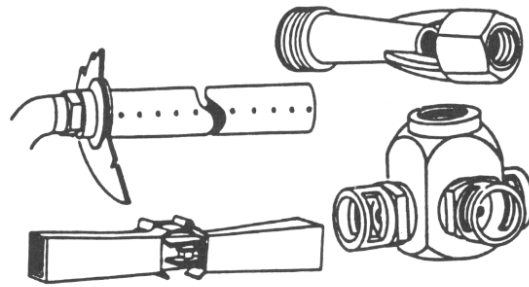
(a)
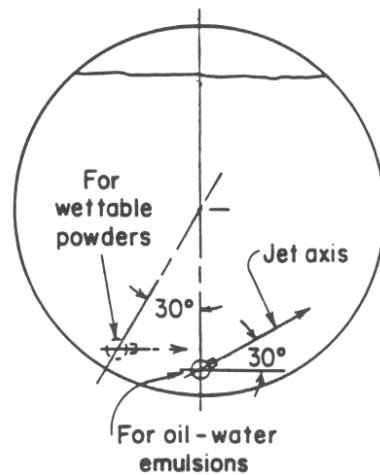
(b)

Figure 10.27 – (a) Various types of nozzles for hydraulic agitation (Bode and Butler 1981), and (b) locations of nozzles in the tank for agitation (reprinted from Kepner et al., 1978).

where Q_m = minimum total recirculation rate, L/min
$\qquad$ V = tank volume, m^3
$\qquad$ p = pressure at the agitation jet nozzle, kPa (ordinarily this will be essentially
$\qquad$ the same as the spray nozzle pressure)

The value of F_e was arbitrarily taken as 1.00 for a mixture of 120 g wettable sulfur per liter of water (1 lb/gal), since this is a difficult material to keep in suspension. Values of F_e for concentrations of 60, 12, and 6 g/L (0.5, 0.1, and 0.05 lb/gal) were found to be 0.87, 0.43, and 0.27, respectively. Table 10.1 indicates that adding an emulsifier to an oil-water mixture reduces the agitation requirements and also shows that F_e is greater when the jets are in the wettable powder optimum position (Figure 10.27b) instead of the emulsion position.

From basic hydraulic relations, the hydraulic useful power output required for any recirculation rate and pressure is:

$$P_h = \frac{Q_m p}{60,000} \qquad (10.6)$$

where P_h = hydraulic power, kW
$\qquad$ Q_m = total recirculation rate, L/min

The principal advantage of hydraulic agitation is its simplicity as compared with the mechanism and drive required for mechanical agitation. With hydraulic agitation, however, the spray pump must have additional capacity and the power requirements will be considerably greater than that for mechanical agitation, especially at high pressures. For high-pressure sprayers, mechanical agitation is definitely the more economical system.

Example 10.1

Determine the power requirements of a boom-type orchard sprayer if the spray gun pressure is 1.375 MPa and the flow rate is 15 L/min. The hose has an inside diameter of 2.54 cm, and it is 50 m long. The volume of the tank is 375 L and contains wettable powder. It is also recommended that a 20% over-capacity of flow should be designed to compensate for normal pump wear. The mechanical efficiency of the pump ranges from 50% to 60%. Assume the viscosity of the chemical is the same as that of water at 21° C or 0.98 MPa·s.

Solution

First we determine the pressure loss in the hose. Determine the flow regime by calculating the value of the Reynolds number as follows:

$$N_{Re} = \frac{4C\rho Q}{4\mu d} = \frac{4(16.67)1000(15)1.2}{\pi(0.98)25.4} = 15,348$$

Note that Q = 15 × 1.2 to account for 20% over-capacity as desired in the problem statement. The flow is fully developed turbulent flow since the Reynolds number is above 4000. To calculate the pressure drop, we use Equation 5.19:

$$\frac{\Delta p}{L} = \frac{0.0333\mu^{0.25}\rho^{0.75}Q^{1.75}}{d^{4.25}}$$

$$= \frac{0.0333(0.98)^{0.25}(1000)^{0.75}(15\times1.2)^{1.75}}{(25.4)^{4.25}}$$

$$= 0.922 \quad kPa/m$$

and Δp = 0.992(50) = 49.59 kPa. Thus, the total pressure required at the pump is:

$$p = 1375 + 49.59 = 1424.59 \text{ kPa}$$

Now, determine the flow rate required for hydraulic agitation using the following equation for wettable powder:

$$Q_m = 1380\frac{VF_e}{p^{0.35}} = \frac{1380(0.375)0.68}{(1425)^{0.35}} = 27.7 \quad L/min$$

Thus, the total flow that the pump must generate is:

$$Q = 15(1.2) + 27.2 = 45.2 \text{ L/min}$$

Pump output power is, from Equation 10.14:

$$P = 1.667 \times 10^{-5} QP = 1.667 \times 10^{-5} (45.2)(1424.59) = 1.07 \text{ kW}$$

Considering the lowest efficiency of 50%, the input power is:

$$P_{input} = 1.07/0.5 = 2.14 \text{ kW}$$

10.2.3.3 Atomization

The main objective of atomization is to increase the surface area of the liquid by breaking it into many small droplets for effective coverage of plant and soil surfaces. During atomization, energy is imparted to the liquid to break it into small droplets by overcoming surface tension, viscosity, and inertia.

Types of atomizers. Based on the form of energy applied to produce atomization, the atomizers may be categorized as *pressure, rotary,* or *pneumatic* atomizers. Pressure atomizers are the most common type used in agriculture; use of the pneumatic kind is virtually non-existent.

In *pressure atomizers,* pressure energy is used to breakup a liquid jet. Pressure atomizers (but not rotary atomizers), often referred to as *nozzles* (Figure 10.28), produce several different spray patterns (Figure 10.29), described below.
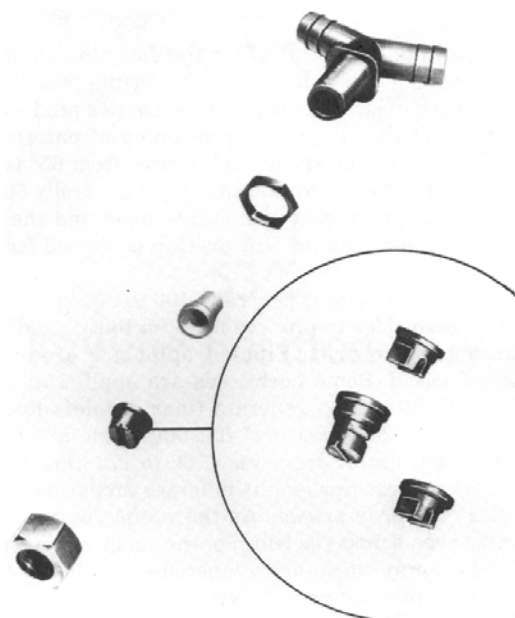
Figure 10.28 – A typical nozzle assembly. (Reproduced by permission of Deere and Co. © 1991. All rights reserved.)
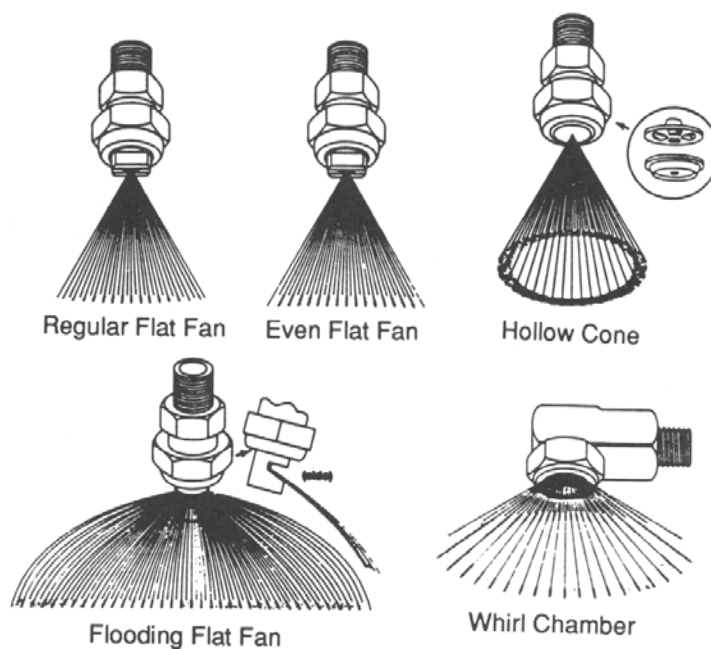

Regular Flat Fan   Even Flat Fan   Hollow Cone

Flooding Flat Fan   Whirl Chamber

Figure 10.29 – Various types of spray nozzles and spray patterns (reprinted from Bode and Butler, 1981).

Regular flat-fan nozzles are used for most solid applications of herbicides and for certain pesticides when it is not necessary to penetrate foliage. These nozzles produce a tapered-edge flat-fan spray that requires overlapping of pattern to obtain uniform coverage. The spray angle varies from 65° to 110° with 80° being the most common. Nozzle spacing is generally 50 cm on the boom. The boom height varies with spray angle and the amount of overlap desired. A minimum of 50% overlap is needed for uniform coverage.

The operating pressure is generally 100 to 200 kPa (15 to 30 psi) when applying herbicides to produce medium to coarse droplets that are not susceptible to drift. Finer droplets are produced as the pressure is increased. Some herbicides are applied at pressure of 275 to 413 (40 to 60 psi) to generate finer droplets for maximum coverage. The LP or "low pressure" flat-fan nozzle develops normal pattern at pressures of 69 to 172 kPa (10 to 25 psi). Operating at lower pressures results in larger drops and less drift.

Even flat-fan spray nozzles provide a spray density that is more even across the width of the spray, as compared to the standard flat-fan spray with its tapered spray distribution. Since overlapping would produce a very uneven spray pattern, these nozzles are only for band application over or inbetween rows. The band width is determined by adjusting the boom height. The common spray angles are 80° and 95° and the operating pressures range from 100 to 200 kPa (15 to 30 psi).

Flooding flat-fan nozzles produce a wider spray pattern than the other flat-fan nozzles. They are most suited for broadcast applications where uniform surface application is critical. Uniform spray application is obtained by 100% overlap of individual spray patterns. These nozzles produce large droplets and reduce drift, when operated at 55 to 170 kPa (8 to 25 psi) pressure. Pressure changes affect the uniformity of spray pattern more with flooding flat-fan nozzles than with regular flat-fan nozzles.

Hollow-cone spray nozzles (both disk and core types) utilize a two-piece, disk-core, hollow-cone spray tip. The core gives the fluid a swirling action before it is metered through the orifice disk, resulting in a circular, hollow-cone, spray pattern. These nozzles are most suited for directed spray in row-crop applications when drift is not a concern, as these nozzles are operated at 275 to 550 kPa (40 to 80 psi) pressures. Since the droplets are small, these nozzles are most suited for contact herbicides, insecticides, and fungicides where full coverage of plant foliage is essential.

Whirl-chamber hollow-cone nozzles have a whirl-chamber above a conical outlet that produces a hollow-cone pattern of cone angles up to 130°. These nozzles are best suited for broadcast surface applications of herbicides. For best results the nozzle is tilted towards the rear at a 45° angle. Since the droplets tend to be larger, these nozzles are most suited for systemic herbicides and where drift may be a problem. The operating pressure ranges from 35 to 138 kPa (5 to 20 psi).

In *rotary atomizers*, as opposed to the various pressure nozzles listed above, the energy to produce droplets comes from a rotating wheel, disk, or cup. As the speed increases, smaller droplets are produced. Rotary atomizers (Figure 10.30) are not as common in agricultural applications as are pressure nozzles. Rotary atomizers are also called *controlled droplet atomizers* (CDA) for their ability to produce droplets that are more uniform in size compared to other atomizers.
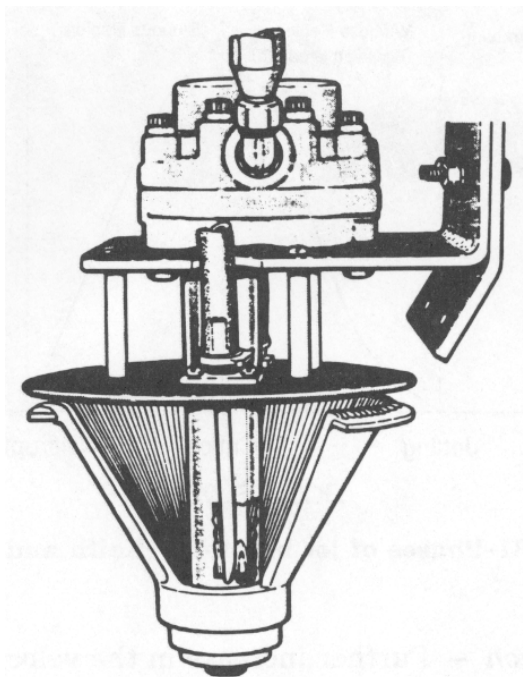
**Figure 10.30 – A rotary or controlled droplet atomizer
(courtesy of Farm Fans, Inc.).**

   Theory of pressure atomization. Atomization is a very complex process and depends highly upon the type of atomizer. To get a better understanding of the process we will discuss breakup of *liquid jets*, *liquid sheets*, and *liquid droplets*.

   Liquid jet breakup. As the liquid flow rate is increased through a horizontal nozzle, it goes through the following four phases based on the Reynolds number (Figure 10.31). Think of N_{Re} as an indicator of flow rate. With everything else being the same, as flow rate increases, N_{Re} also increases. There are generally two flow regimes: laminar and turbulent. Two very different flow behaviors exist in these regimes.

   1. *Drop formation.* At low flow rates drops form individually at the tip of the nozzle and grow in size until the weight overcomes the interfacial tension and the drop is released (Figure 10.32).

   2. *Varicose region.* As the jet velocity is increased, symmetrical bulges and contractions appear and the jet lengthens. The drops become smaller and less uniform.

   3. *Sinuous region.* Further increase in the velocity results in the transverse oscillations of the jet. The jet waves irregularly in an S-curve fashion. The jet becomes shorter and the drops become larger.

   4. *Atomization.* Finally, the jet breaks down into small droplets, usually within a distance of 15 times jet diameter of the orifice. The breakup is highly chaotic. The ligaments shed at the crest as the jet oscillates further break down into droplets. This occurs when a simple orifice is employed for atomization.
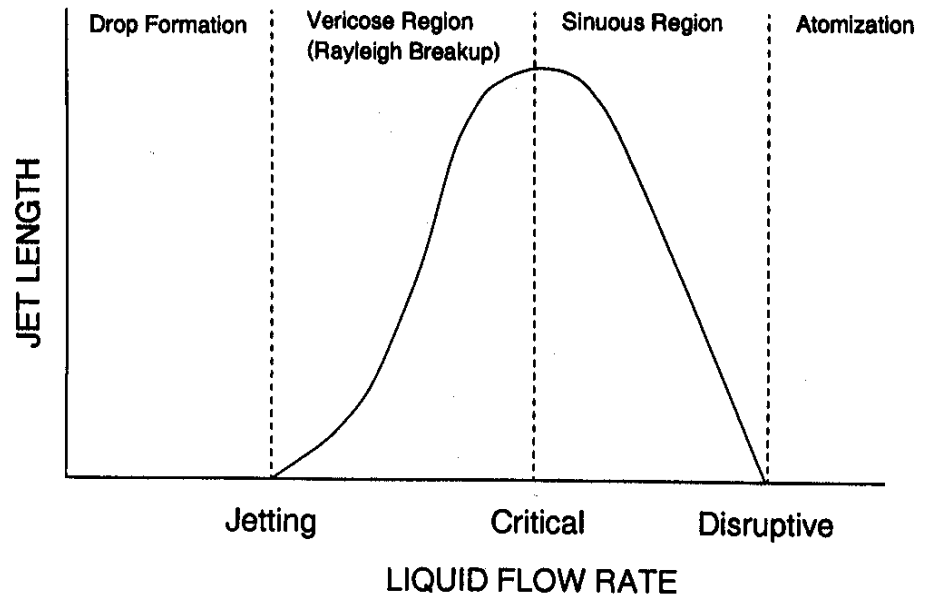
Figure 10.31 – Phases of jet breakup (Keith and Hixon, 1955).
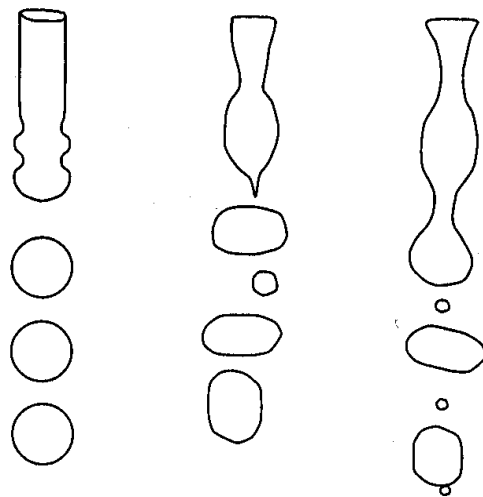
Figure 10.32 – Idealized and actual jet breakup (Marshall, 1954).

The jet is moving from the sinuous region to the atomization region when the following equation is true:

$$\left(\frac{d_j v_j \rho_1}{\mu_1}\right) \geq 280 \left[\frac{\mu_1}{(\sigma \rho_1 d_j)^{0.5}}\right]^{-0.82} \tag{10.7}$$

where d_j = jet diameter, m
$\quad$ v_j = jet velocity, m/s
$\quad$ ρ_1 = liquid density, kg/m^3
$\quad$ μ_1 = liquid viscosity, Pa·s
$\quad$ σ = surface tension (N/m)

The jet velocity can be computed as follows once flow through the nozzle is known:

$$v_j = C_v \left(2\frac{\Delta p}{\rho_1}\right)^n \tag{10.8}$$

where C_v = velocity coefficient, dimensionless
$\quad$ Δp = total pressure drop, Pa
$\quad$ n = 0.5 for turbulent flow

The discharge coefficient represents the ratio of the actual liquid discharge rate to that theoretically possible. The volumetric flow rate is determined by:

$$Q = v_j C_A A \tag{10.9}$$

where C_A = area coefficient, dimensionless
$\quad$ A = nozzle orifice area, m^2

C_A takes into account the vena contracta effects. Combining Equations 10.8 and 10.9 we obtain:

$$Q = C_v \left(\frac{2\Delta p}{\rho_1}\right)^{0.5} C_A A \tag{10.10}$$

Now, if we let discharge coefficient $C_D = C_v C_A$, the above equation becomes:

$$Q = C_D A \left(\frac{2\Delta p}{\rho_1}\right)^{0.5} \tag{10.11}$$

The average jet velocity may be computed from the above equation as follows:

$$v_j = \frac{Q}{C_D A} \tag{10.12}$$

The discharge coefficient (C_D) varies depending upon the size of the orifice and the nozzle design. For a given nozzle, if we plot flow rate against the square root of the pressure drop, the slope of the line will be $C_D A \sqrt{2/\rho_1}$ from which the discharge coefficient (C_D) may be computed.

Example 10.2

A spray nozzle manufacturer has provided the following pressure-flow rate data for a hollow-cone nozzle spraying water.

Nozzle flow rates at various pressures for an orifice diameter of 2.39 mm.

Pressure, kPa	207	276	345	414	552	689	862	1034	1379	2068
Flow, L/min	1.17	1.63	1.82	2.00	2.31	2.57	2.95	3.14	3.71	4.54

For the above nozzle determine the flow required to produce atomization phase of a jet of water issuing from the nozzle.

Solution

Equation 10.7 is to be used to determine the jet velocity required to produce atomization. This equation can be rewritten as:

$$v_j \geq 280 \frac{\sigma^{0.42} \mu_l^{0.18}}{\rho_l^{0.59} d_j^{0.59}}$$

For water, $\sigma = 0.0728 \text{ N/m}$
                $\mu_l = 1 \text{ mPa·s}$
                $\rho_l = 1000 \text{ kg/m}^3$
                $d_j = 2.39 \text{ mm}$

Using the above values, $v_j > 16.06 \text{ m/s}$.

Equation 10.12 may be used to calculate the flow corresponding to the minimum jet velocity of 16.06 m/s as:

$$Q = C_D \, A \, v_j$$

However, the discharge coefficient (C_D) is to be determined from the data given by the manufacturer. If we plot the nozzle flow against the square root of the nozzle pressure as shown on the next page, we find the slope as:

$$0.104 \frac{\text{L/min}}{\text{kPa}} \qquad \text{or} \qquad 10^{-6} \frac{\text{m}^3/\text{s}}{\sqrt{\text{kPa}}}$$

Using Equation 10.11 we get:

$$\frac{C_D A \sqrt{2}}{\sqrt{\rho_l}} = 5.48 \times 10^{-8} \frac{\text{m}^3/\text{s}}{\sqrt{\text{Pa}}} \qquad \text{(note conversion from kPa to Pa)}$$

or $$C_D = \frac{\sqrt{\rho_l}}{A\sqrt{2}} \times 1.735 \times 10^{-6}$$
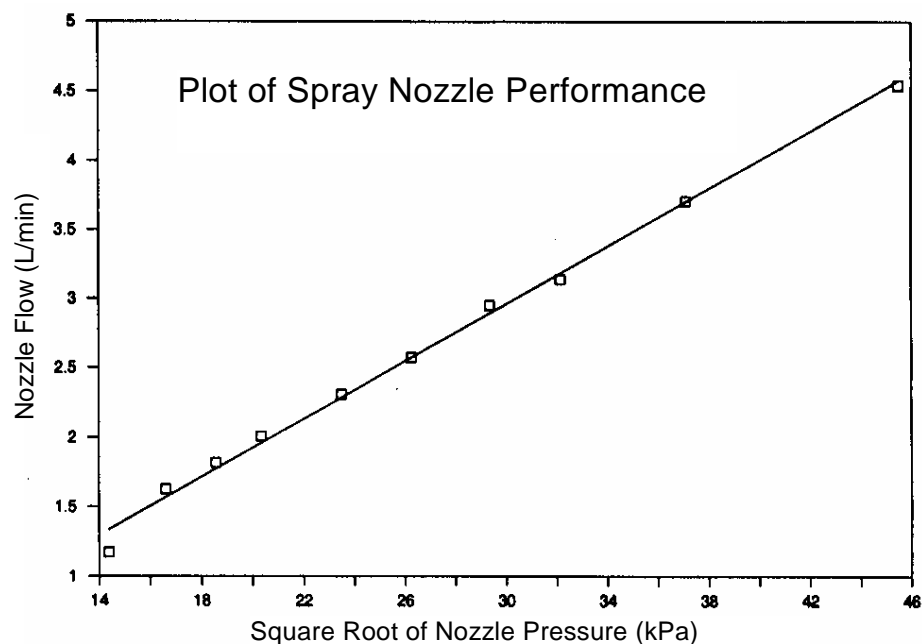
Substituting the values of ρ_l and A, C_D is found to be 0.274. Note that this value is considerably less than 0.611 normally used for turbulent orifice flow. This is due to the inserts and screens used in a working nozzle.

Once C_D is known, the flow is calculated as:

$$Q = 0.274 \left[\frac{\pi}{4} (2.39 \times 10^{-3})^2 \right] \times 16.06$$

$$= 19.7 \times 10^{-6} \, \text{m}^3 / \text{s}$$

$$= 1.18 \ \text{L} / \text{min}$$

It should be noted that this value corresponds to a pressure drop of 207 kPa. If the nozzle is operated at pressure less than 207 kPa, complete atomization will not occur. It should also be noted that this value corresponds to the minimum value of pressure given by the manufacturer. If lesser flow is desired, a smaller orifice should be used.

Growth of waves on sheet | **Fragmentation and formation of ligaments** | **Breakdown of ligaments into drops**
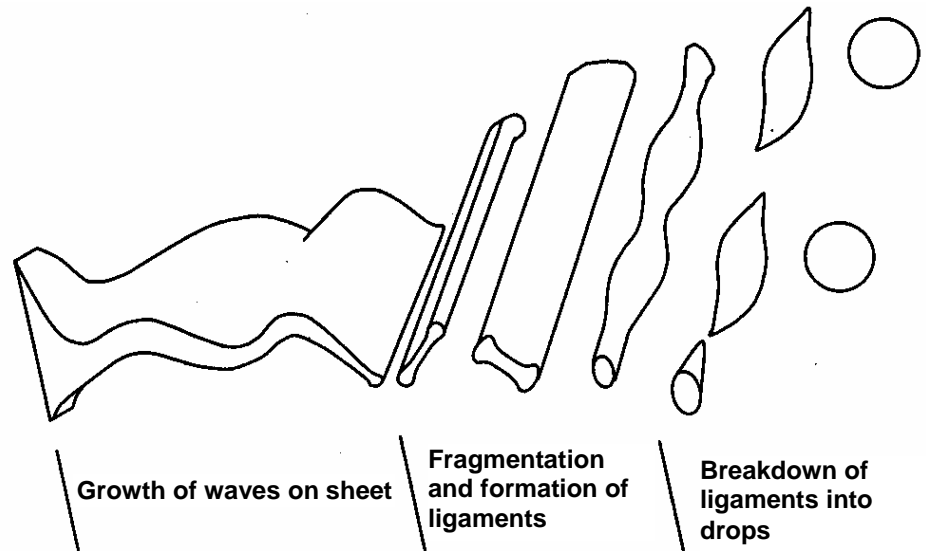
Figure 10.33 – Breakup of a liquid sheet (after Dombrowski and Johns, 1963).

SPRAY NOZZLE   **DROPLET BREAKDOWN**   **AIR RESISTANCE**
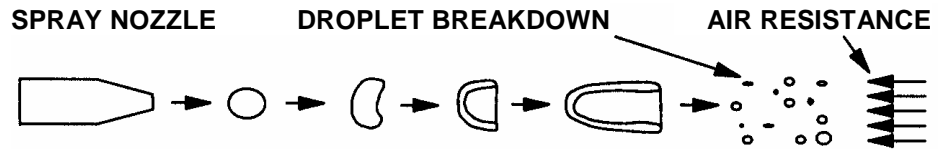
Figure 10.34 – Breakup of a droplet.

Liquid sheet breakup. When the liquid is pumped through a pressure nozzle, either a flat-fan (fanjet) nozzle or a whirl-chamber (swirl) nozzle, a sheet of liquid is formed. The liquid sheet breaks up into droplets of many sizes. The mechanism of sheet breakup is complex and depends upon many factors. However, four main mechanisms have been observed (Figure 10.33):

1. *Rim disintegration.* The free edge of the sheet contract into a cylinder, that then breaks from the surface as large drops followed by their liquid fingers.

2. *Sheet perforations.* Perforations appear in the sheet that expand under the influence of surface tension until ligaments remain.

3. *Unstable waves* are formed in the sheet at a right angle to the direction of flow of liquid. The amplitude increases until the sheet breaks up.

4. *Thick sheet breakup.* The crests of sheet are shed as ligaments.

Liquid droplet breakup. Droplets further break down in an air stream if the aerodynamic forces exceed the surface tension force. This may occur in air carrier sprayers. A sequence of droplet breakup is shown in Figure 10.34.

Droplet size and size distribution. When liquid is atomized, droplets of various sizes are formed. The spray droplets are classified by their diameters, typically measured in microns (μ).[1] The performance and effectiveness of an atomizer depends upon the droplet size and size distribution. Table 10.2 shows some of the characteristics of various size droplets. The area covered and the volume of liquid in individual droplets is important in achieving effective and efficient application. Smaller droplets of the same volume provide more coverage. For example, one 200 μ droplet when broken into 64 droplets of 50 μ diameter will cover four times more area than the 200 μ droplet. The droplet distribution is also important from the point of view of spray drift. As seen in Table 10.5 the smaller the droplet size the longer it takes for it to settle and the higher the probability of drift. Note also that droplets evaporate in flight, becoming smaller and thereby increasing the chances of drift.

Droplet size distribution can be represented by a plot of the number of particles of a given diameter, as in Figure 10.35. This kind of plot is called a histogram. A smooth curve through the center points of the maxima of each size class gives the distribution curve. This curve represented by a function, f(x), is commonly called a distribution function. If the distribution function is known explicitly, then only a few parameters (e.g., mean diameter and standard deviation) are needed to define a given distribution. Minimum and maximum size are additional parameters, often associated with a distribution. Sometimes, the surface area or the volume of a droplet is more relevant in certain applications rather than the diameter. If this is used as the ordinate then the curve in Figure 10.35 would skew to the right because of the weighting effect of the surface area or volume associated with a droplet diameter.

**Table 10.2. Spray droplet size and its effect on coverage for a
10 L/ha application rate (Bode and Butler, 1981).**

Droplet diameter, μ	Type of droplet	Area relative to a 10 μ droplet	Volume relative to a 10 μ droplet	No. of droplets per cm^2	Coverage relative to 1000 μ droplet
5	Dry fog	0.25	0.125	1,524,647	200
10	Dry fog	1	1	190,581	100
20	Wet fog	4	8	23,822	50
50	Wet fog	25	125	1,525	20
100	Misty rain	100	1000	191	10
150	Misty rain	225	3375	56	6.7
200	Light rain	400	8000	24	5
500	Light rain	2500	125,000	1.5	2
1000	Heavy rain	10,000	1,000,000	0.2	1

---

[1] Microns are also called micrometers and may be abbreviated μm. One micron is one millionth of a meter or 1/25,400 of an inch. A person with normal eyesight can see 100 μ without any magnification.
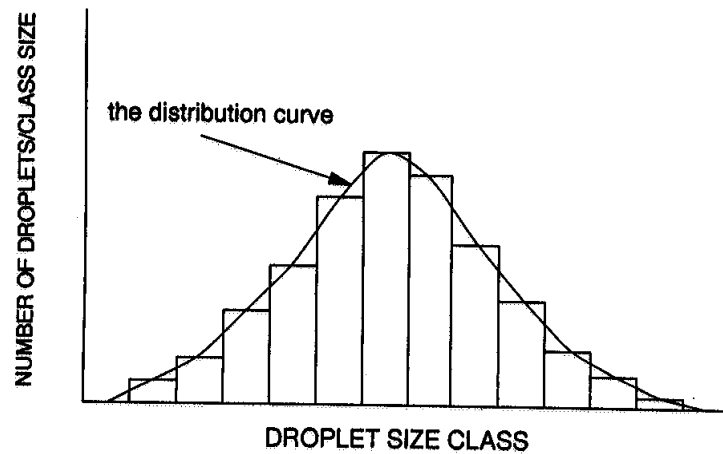
Figure 10.35 – A histogram of droplet sizes and associated frequency.

A more convenient method of representing a particle size distribution is to plot the cumulative fraction of the total number smaller than a given size against that given size. This plot is called a cumulative frequency plot and is shown in Figure 10.36. A more convenient way is to plot the data on a probability paper is shown in Figure 10.37. The droplet diameter is plotted on the ordinate (y-axis) and the abscissa is the cumulative percentage of droplet number, length, surface area, or volume. In pesticide application the cumulative number and cumulative volume are the most commonly used plot. The slope of the curve is an indication of the uniformity of the droplet size distribution.
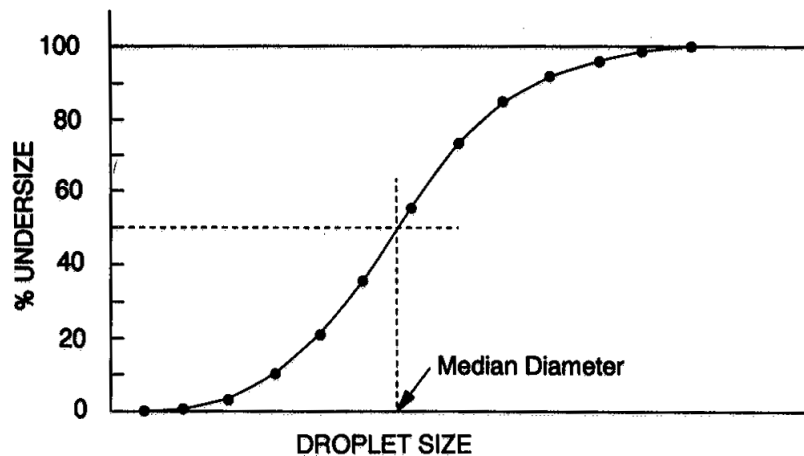
Figure 10.36 – A cumulative frequency plot.
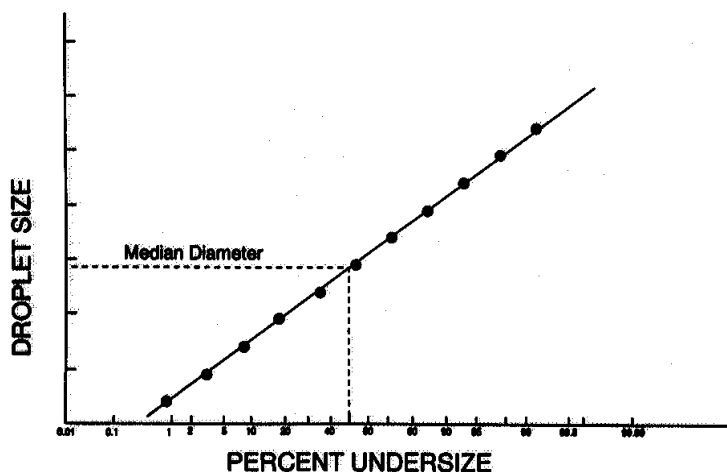
Figure 10.37 – A cumulative frequency plot on a normal probability paper.

The *median drop diameter* divides the spray into two equal parts by number, length, surface area, or volume. Number and volume median diameters are determined from the cumulative probability plots such as shown in Figure 10.38. A uniform method has been proposed to express the median diameters as D_{xf}. The subscript, x, can be V for volume, A for area, L for length, or N for number, and the subscript, f, is the fraction on the cumulative distribution plot. Thus, $D_{v.5}$ = volume median diameter (VMD) indicates that 50% percent of liquid volume is in droplets smaller than this diameter and 50% in droplets larger than this diameter.
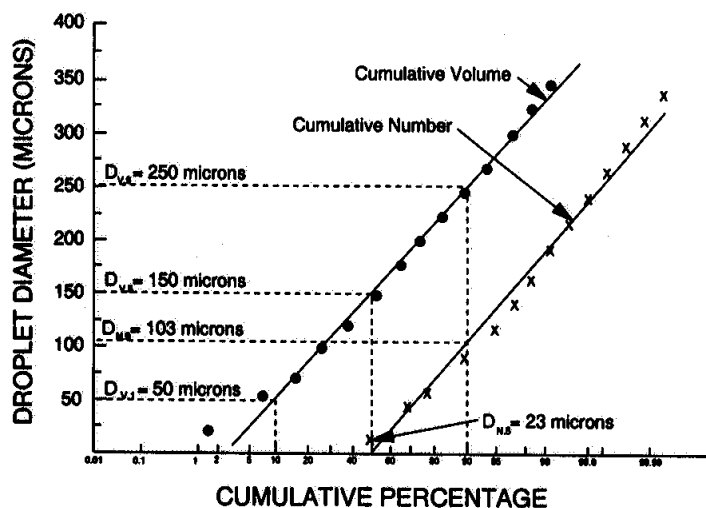
Figure 10.38 – Cumulative number and volume curves for a typical spray nozzle (after Bode and Butler, 1981).

Mean droplet diameters are weighted averages. Their names depend on the method used to compute the average. The following equation can be used to calculate the mean diameters:

$$\overline{D}_{pq}^{\,p-q} = \left(\frac{\sum\limits_{i-1}^{n} N_i D_i^{p}}{\sum\limits_{i=1}^{n} N_i D_i^{q}} \right)^{1/(p-q)} \tag{10.13}$$

where p,q = 1, 2, 3, or 4 and p > q

      D_i = droplet diameter for the *i*th size class

      N_i = number of droplets in the *i*th size class

      i = number of the size class

      n = total number of size classes

Various weighted averages may be computed based on the number of droplets in each class size. Commonly used means include: arithmetic mean ($\overline{D}_{10}$), surface mean ($\overline{D}_{20}$), volume mean ($\overline{D}_{30}$) and Sauter mean ($\overline{D}_{32}$). The arithmetic mean is computed by letting p = 1 and q = 0 in the above equation and it is the weighted average of all droplet diameters in the spray. Volume mean diameter (p = 3 and q = 0) is the diameter of the droplet whose volume times the number of droplets in the spray equals the total volume sprayed. Sauter mean diameter is calculated by equating p = 3 and q = 2 and it is an indicator of the volume to surface ratio of droplets in the spray. Similarly, the surface mean diameter, with p = 2 and q = 0, is the diameter of the droplet whose surface area times the number of droplets in the spray equals the total surface area of all droplets.

There is no general agreement as to which method of specifying droplet diameters is the best in agricultural chemical application. However, volume mean and Sauter mean diameters are most commonly used. Median diameters have a better physical significance in that they divide the droplet spectra equally based on the count, area, volume, etc.

Example 10.3

For the droplet size data given on the next page, determine the mean and median droplet diameters.

Class size range, μ	Number of droplets in each class size range
19 – 46	699
46 – 72	326
72 – 99	282
99 – 125	286
125 – 152	243
152 – 178	201
178 – 204	150
204 – 231	88
231 – 259	50
259 – 284	43
284 – 310	13
310 – 336	12
336 – 363	5
363 – 389	2
389 – 415	1

Solution

Mean droplet diameters are computed from the table below (Bode and Butler, 1981).

Size (diameter) class range, μ	Midpoint diameter, μ	No. in each size class, N	ND, μ	ND^2, μ^2	ND^3, μ^3
19 – 46	32	699	22,368	715,776	22,904,832
46 – 72	59	326	19,234	1,134,806	66,953,554
72 – 99	85	282	23,970	2,037,450	173,183,250
99 – 125	112	286	32,032	3,587,584	401,809,408
125 – 152	138	243	33,534	4,627,692	638,621,496
152 – 178	165	201	33,165	5,472,225	902,917,125
178 – 204	191	150	28,65	5,472,225	1,045,180,650
204 – 231	217	88	,19,096	4,143,832	899,211,544
231 – 259	245	50	12,250	3,001,250	735,306,250
259 – 284	272	43	11,696	3,181,312	865,316,864
284 – 310	297	13	3,861	1,145,717	340,574,949
310 – 336	323	12	3,876	1,251,948	404,379,204
336 – 363	349	5	1,745	609,005	212,542,745
363 – 389	376	2	752	282,752	106,314,752
389 – 415	402	1	402	161,604	64,964,808
	Totals	2401	246,631	36,826,178	6,880,181,431

Mean droplet diameters are: $\bar{D}_{10} = 102.7\mu$ $\bar{D}_{30} = 142.0\mu$

$$D_{20} = 123.8\mu \quad \bar{D}_{31} = 167.0\mu$$

$$\bar{D}_{21} = 149.3\mu \quad \bar{D}_{32} = 186.8\mu$$

To determine median diameters, complete the table as shown below and then plot the data on a probability paper as shown. Mean diameters are determined from the plot.

Size class midpoint, μ	No. in each size class	No. in each size class, %	Cum. % by number	Vol. in each size class, %	Cum. % by volume
32	699	29.1	29.1	0.3	0.3
59	326	13.6	42.7	1.0	1.3
85	282	11.7	54.4	2.5	3.8
112	286	11.9	66.3	5.8	9.6
138	243	10.1	76.4	9.3	18.9
165	201	8.4	84.8	13.1	32.0
191	150	6.2	91.0	15.2	47.2
217	88	3.7	94.7	13.1	60.3
245	50	2.1	96.8	10.7	71.0
272	43	1.8	98.6	12.6	83.6
297	13	0.5	99.1	4.9	88.5
323	12	0.5	99.6	5.9	94.4
349	5	0.2	9.8	3.1	97.5
376	2	0.1	99.8	1.6	99.1
402	1		99.9	0.9	100
			100		

$D_{N.1}$ = not applicable $D_{V.1} = 50\ \mu$

$D_{N.5} = 75\ \mu$ $D_{V.5} = 195\ \mu$

$D_{N.9} = 188\ \mu$ $D_{V.9} = 300\ \mu$

Cumulative Percentage (%)
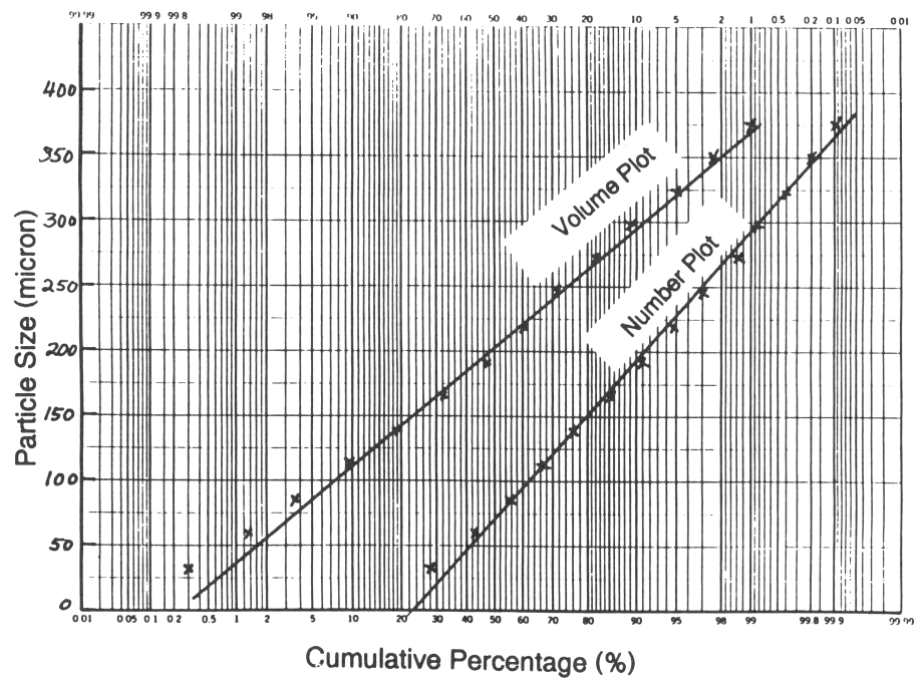
10.3 PERFORMANCE EVALUATION

10.3.1 Uniformity of coverage of granular chemical application

The performance of a dry chemical applicator is measured by the uniformity of coverage and the calibration accuracy. The uniformity of coverage is based on the uniformity of metering and on the spreading or distribution. Field variables affect the uniformity and calibration accuracy. Bumpy and sloping fields result in undesirable performance. The material being applied also affects the performance. Free-flowing materials produce a more uniform application, as opposed to the materials that tend to form clumps and do not meter well.

A typical metering uniformity for 24 outlets across the width of the applicator is shown in Figure 10.39. The coefficient of variation (C.V.) was 9.5%. The C.V. is a measure of the scatter in a data set and it is computed by dividing the standard deviation by the sample mean. The higher the C.V., the greater the scatter in the data.

The uniformity of spreading is expressed in terms of application rate at a given location across the width of the applicator. The distribution and C.V. shown in Figure 10.40 is typical.
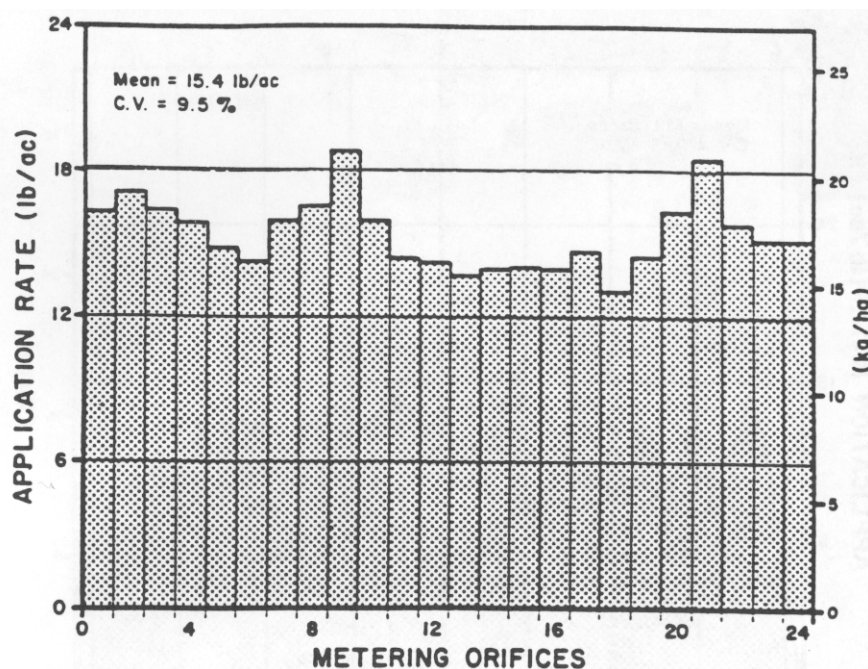
**Figure 10.39 – Typical variation in delivery rates from individual outlets
with the original set of hopper bottoms while applying Avadex BW
at 17.3 kg/ha (15.4 lb/ac) and 8 km/h (5 mph)
(courtesy of Prairie Agricultural Machinery Institute, Canada).**

In addition to the lateral uniformity of application, longitudinal uniformity also affects the applicator performance. The longitudinal uniformity usually is in the form of cyclic variations that are caused by the design of the metering mechanisms. Figure 10.41 shows different lateral distribution patterns for centrifugal spreaders. The overall uniformity is based on the individual pattern and the amount of overlap for each swath.

The performance of rotary broadcast-type fertilizer distributors is affected by the speed of the spinning disk and the size of fertilizer granules, among other factors. Crowther (1958) conducted a study of these effects. A commercial fertilizer was used in the study with size distribution such that 92% of particles pass through sieve opening 3353 μ, 36% at 2411 μ and 4% at 1190 μ. Figure 10.41 shows that as the speed of the disk increased the particles were thrown farther, which was expected. However, distribution of the spread density across the width of the distributor was also affected. Figure 10.42 shows the segregation of the particles at 400 rev/min. There is some segregation of particles according to their size; however, it is not likely to affect the overall distribution pattern.
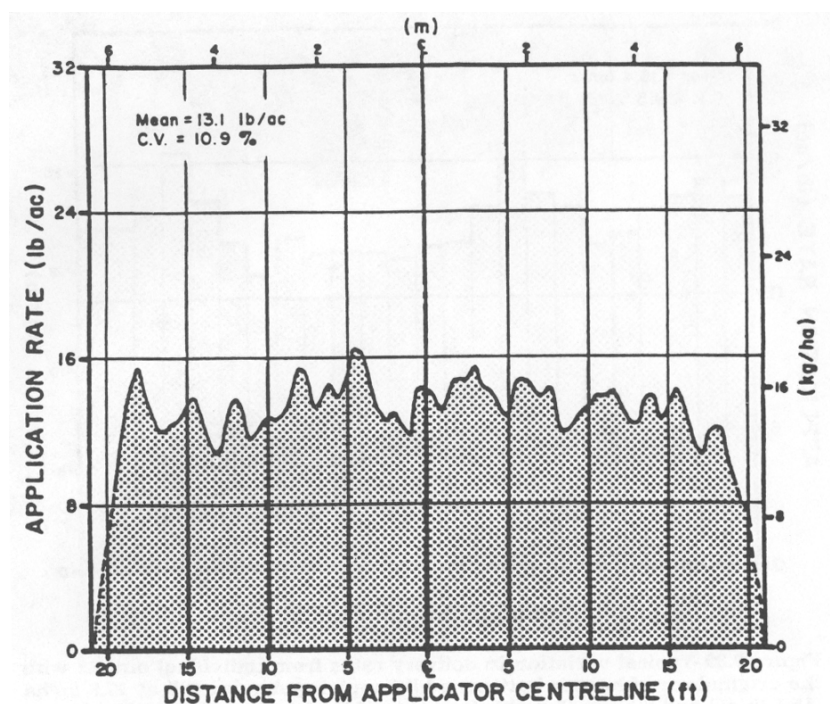
Figure 10.40 – Typical distribution pattern using the original hopper bottoms when applying 14.7 kg/ha (13.1 lb/ac) of Avadex BW at 8 km/h (5 mph) using 610 mm (24 in.) deflector spacing and a 610 mm (24 in.) deflector discharge height (courtesy of Prairie Agricultural Machinery Institute, Canada).
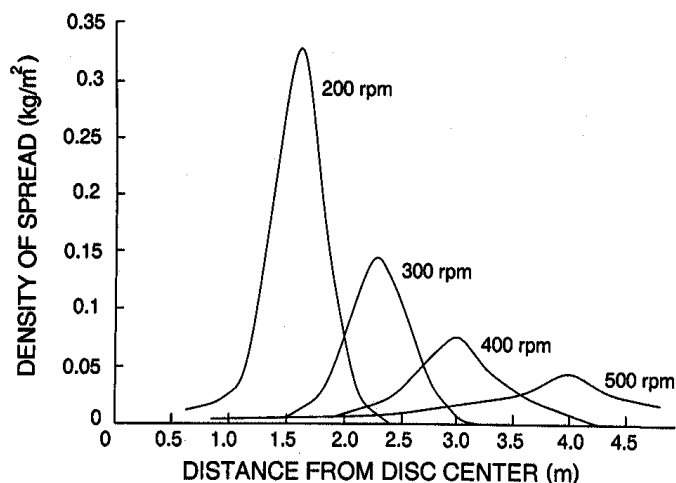
Figure 10.41 – The effect of disk speed on the distance the particles are thrown by the distributor (Crowther, 1958).
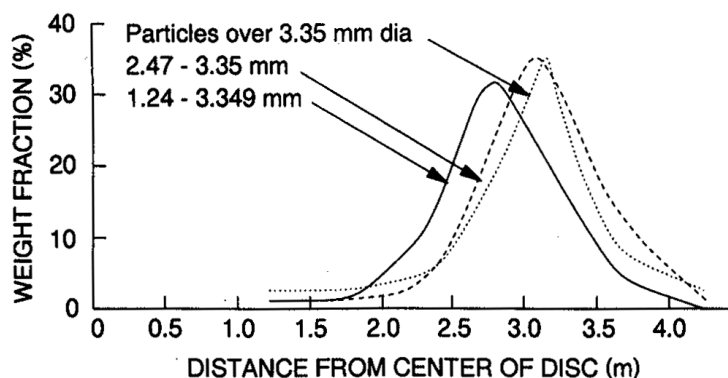
Figure 10.42 – Segregation of particles due to their size by the spinning disk (Crowther, 1958).

10.3.2 Calibration of fertilizer spreaders

10.3.2.1 Gravity spreaders

Calibration refers to the amount of chemical applied per unit area and is usually expressed as kilograms per hectare (kg/ha). The fertilizer (or other product) label indicates the recommended application rate. Sometimes the application rate is specified in terms of the amount of active ingredient to be applied per unit area since agricultural chemicals, particularly pesticides, are available in different formulations. In this case the product application rate can be computed using the following formula:

$$AR = \frac{AR_{ai}}{FR_{ai}} \tag{10.14}$$

where AR = product application rate, kg/ha
$\quad$ $AR_{a.i.}$ = application rate of the active ingredient in the formulation
$\quad$ $FR_{a.i.}$ = fraction of the active ingredient in the formulation

The rate of application is independent of the ground speed of the applicator as the metering rate is proportional to the rate of travel. This is accomplished by driving the metering mechanism by the ground wheel. Different fertilizers and pesticides require different application rates, so the applicator should be calibrated to the desired rate of application. The manufacturers of the applicators provide for the adjustment of the orifice to vary the application rate.

An applicator may be calibrated in the laboratory, although field calibration is recommended because ground roughness affects the rate. If the application rate is not correct, the applicator should be adjusted and the calibration should be performed again.

To calibrate in the field, fill the hopper with material and adjust the gage to the recommended setting. Pull the applicator forward until a steady stream is flowing from the tubes. Mark a distance at least 200 m. Remove the tubes and attach bags to collect the material. After traveling the marked distance at the desired speed, collect and weigh the material. The following formulas may be used to determine the application rate:

$$A = \frac{d\,w}{10,000} \tag{10.15}$$

$$AR = \frac{m}{A} \tag{10.16}$$

where A = treated area, ha
$\quad$ d = distance traveled, m
$\quad$ w = swath width, m
$\quad$ AR = application rate, L/ha
$\quad$ m = amount of material collected, kg

For laboratory calibration, the applicator is jacked up and the ground wheel is turned several times to simulate field travel. The granules are collected and weighed. The distance traveled in Equation 10.15 is then determined by:

$$d = \pi D_w N \tag{10.17}$$

where D_w is the ground wheel diameter (m) and N is the number of revolutions.

For banded applications, the rate of application in the band is the same as the recommended field application rate. Less total product is applied since the treated area is less than the total area. The following formula is used to compute the treated area in banded applications:

$$A_b = \frac{d_b A}{d_r} \tag{10.18}$$

where A_b = band treated area, ha
$\quad$ d_b = band width, m
$\quad$ d_r = row spacing, m

Table 10.3. Pan spacing for collecting samples to determine spread pattern.

Swath width (m)	Pan spacing, m, 9 pans	Pan spacing, m, 11 pans
9.144	1.143	1.066 on each side of center pan 0.991 between all other pans
10.668	1.321	1.066
12.192	1.524	1.219
13.716	1.727	1.372
15.240	1.905	1.524
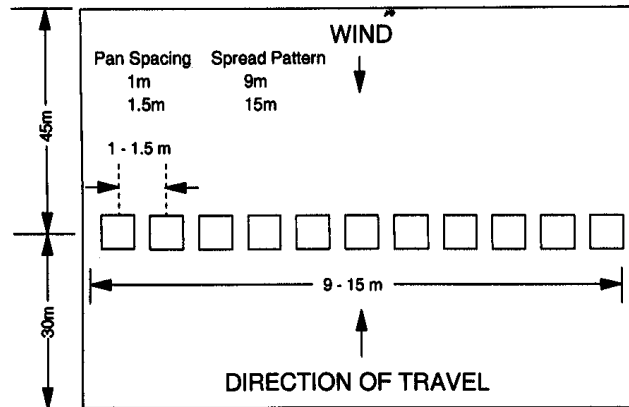
Figure 10.43 – Diagram showing the minimum requirements for a spread pattern test area.
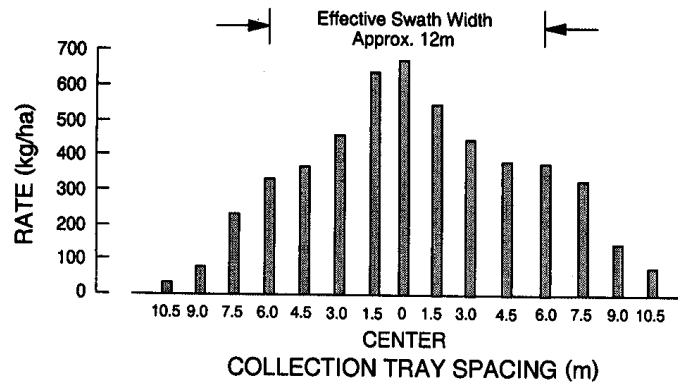
Figure 10.44 – Diagram showing the experimentally obtained distribution pattern and the effective swath width.

10.3.2.2 Rotary spreaders

The objective of calibrating a rotary spreader is to apply fertilizer at a desired application rate (kg/ha) and to obtain a uniform coverage. It is essential to establish the effective swath width and the spread pattern as they affect the amount of overlap. There are three acceptable spread patterns, flat-top, pyramid, and oval, that result in a uniform coverage if proper overlap is maintained.

Most spreaders come with a calibration kit and a set of instructions to establish spread pattern and swath width. These instructions should be followed carefully. Generally, a test area is set up as shown in Figure 10.43. Collection pans are placed according to the spacing as shown in Table 10.3. Position the row of pans so that the spreader is running at least 100 ft before it reaches them and continues to spread at least 150 ft beyond. Select the desired application rate for the fertilizer to be applied and perform the test. The application rate for each pan is then calculated based on the area of the pans and the weight of material collected in each pan. These data are then plotted in a manner similar to that shown in Figure 10.44. The effective swath width is computed from this data by locating the point on either side of the center where the application rate is one-half of that found in the center. The distance between these points is the effective swath width. The spread pattern can be visualized from the data given in Figure 10.44. If this pattern is not acceptable, necessary adjustments must be made according to the manufacturer's instructions. Finally, the application rate can be determined in field by keeping track of the amount of material applied and the area covered.

10.3.3 Liquid chemical application

Sprayer performance is evaluated by the uniformity of coverage and spray patterns, droplet size and size distribution, and target deposition and drift.

Uniformity of coverage. The uniformity of coverage is determined by (a) the type of nozzle, (b) the nozzle spacing, (c) the boom height, and (d) the angle of the spray nozzle. As shown in Figure 10.45, the most uniform coverage is produced with a flat-fan nozzle with a wide angle, with the boom height set at the minimum recommended height. Raising or lowering the boom results in over- or under-application. The figure also shows the effect of spray angle on the uniformity of the spray pattern. For narrow spray angle nozzles, the spray pattern is much more sensitive to changes in boom height. It is generally recommended that for flat-fan spray nozzles a 60% overlap should be obtained by adjusting the boom height. (The overlap is defined as the width covered by two adjacent nozzles divided by the width covered by a single nozzle, expressed in percent.) The boom height can be calculated for a given amount of overlap and nozzle spacing. However, manufacturers' recommended minimum boom height should be used because the actual spray width is somewhat less than the theoretical value as calculated by the spray angle and the boom height. The recommended amount of overlap for flooding flat-fan nozzles and some wide-angle hollow-cone nozzles is 100%.
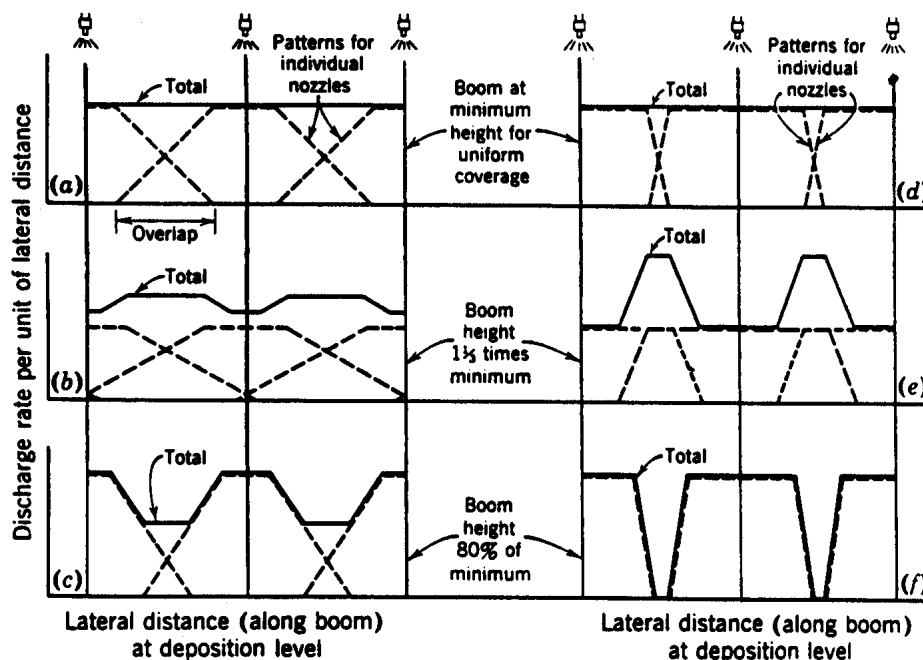
Figure 10.45 – Effect of nozzle distribution pattern and boom height on uniformity of coverage. Broken-line curves indicate distribution patterns (at the deposition level) for individual nozzles; the solid curve in each case shows the combined discharge pattern for all nozzles (i.e., the sum of the broken-line curves) (reprinted from Kepner et al., 1978).

According to the tests conducted at the Prairie Agricultural Machinery Research Institute (PAMI), Humboldt, Saskatchewan, Canada, the uniformity is affected by the nozzle pressure. Figure 10.46 shows a poor distribution pattern along the boom at low nozzle pressure corresponding to a forward speed of 8.3 km/h. The distribution became more uniform when the pressure was increased to maintain the same application rate for a forward speed of 14.6 km/h, as shown in Figure 10.47.

Other factors that result in unacceptable spray distributions include worn and damaged nozzles. Also, uneven ground causes boom height to vary thereby resulting in a non-uniform spray distribution.
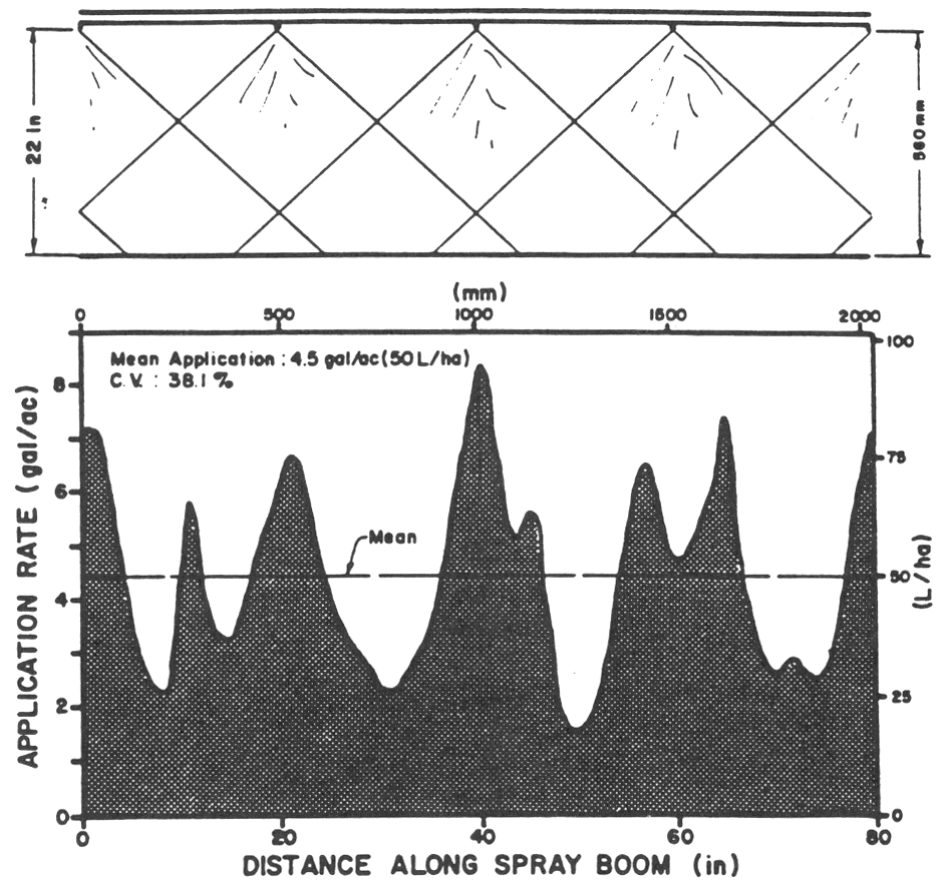
Figure 10.46 – Typical distribution pattern along the boom using number 3 nozzles at 8.3 km/h at a 560 mm nozzle height (courtesy of Prairie Agricultural Machinery Institute, Canada).
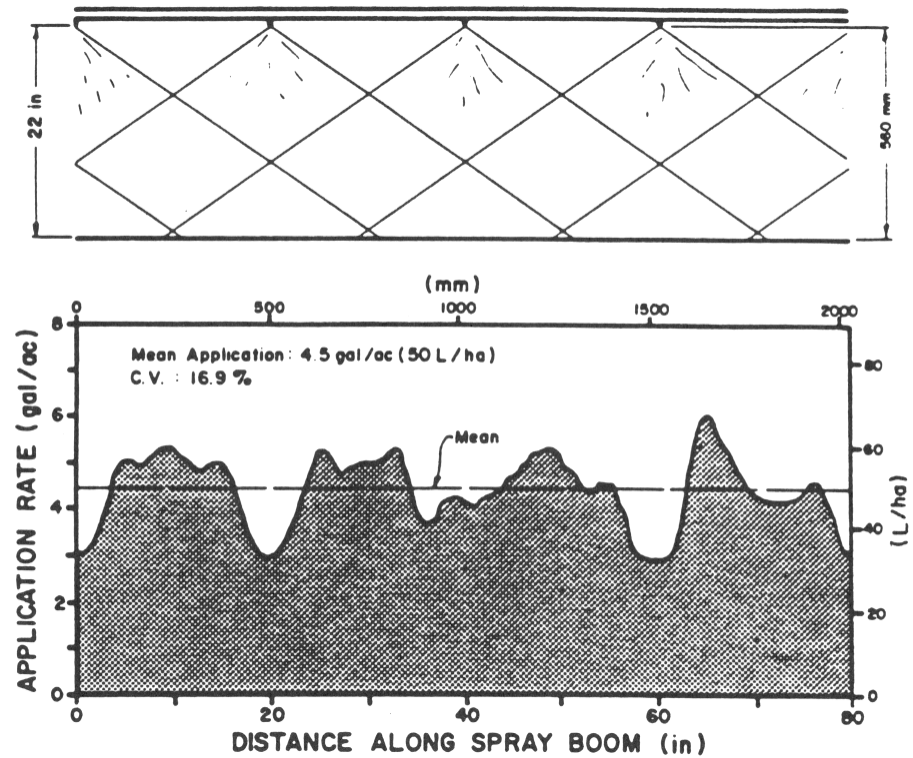
**Figure 10.47 – Typical distribution pattern along the boom using
number 3 nozzles at 14.6 km/h at a 560 mm nozzle height
(courtesy of Prairie Agricultural Machinery Institute, Canada).**

Droplet Size. Droplet size, often expressed as $D_{v.5}$ (volume median diameter), is affected by nozzle type, spray angle, flow rate, and operating pressure. Generally, the hollow-cone nozzles produce the finest droplets, flat-spray nozzles the next-finest, while the full-cone nozzles produce the coarsest spray. The droplets become finer as the width of spray increases, due to spreading of the liquid sheet to a greater angle, which produces more fines at the edges. For a given type of nozzle the smallest capacity nozzle produces smaller droplets and vice versa. Table 10.4 shows the effects of spray angle and flow rate on droplet size. As the operating pressure increases the droplet size decreases. It is, therefore, important to realize that while increasing the application rate by increasing pressure, the droplet size would decrease and may result in higher drift. Liquid viscosity and density have very little effect on droplet size in the range commonly found in agricultural application. Increasing the surface tension increases the volume median diameter (VMD).

Table 10.4. Effect of spray angle and flow rate on droplet size (Spraying Systems Co., 1991).

Spray Angle (°)	Nozzle Type (1.89 L min @ 275 kPa)	Volume Median Diameter (μ) (@ nozzle pressure of) (kPa)		
		103	275	550
40	4005 flat spray	900	810	780
65	6505 flat spray	600	550	530
80	8005 flat spray	530	470	450
110	11005 flat spray	410	380	360

Nozzle Type (275 kPa)	Volume Median Diameter (μ) (@ nozzle flow rate of) (L / min)		
	0.75	1.89	3
Std. TeeJet 80° Flat spray tip	390	470	560
XR TeeJet 80° Flat spray tip	360	460	560
TK-FloodJet Flat spray tip	370	450	540
FL-FullJet Full cone tip	—	680	770
TX ConeJet Hollow cone tip	220	360	—

Often manufacturers of spray nozzles give droplet VMD for a nozzle at a given pressure while spraying water. Droplet diameter may be estimated for a different pressure by the following equation:

$$\frac{D_{vm1}}{D_{vm2}}\left(\frac{p_2}{p_1}\right)^{1/3}$$ (10.19)

where D_{vm1}, D_{vm2} = VMD at pressures p_1 and p_2, respectively.

For similar nozzles and at constant pressure, the effect of different orifice size can be estimated from the manufacturers' data using the following equation:

$$\frac{D_{vm1}}{D_{vm2}}=\left(\frac{d_1}{d_2}\right)^{2/3}$$ (10.20)

where D_{vm1}, D_{vm2} = VMD at orifice diameters d_1 and d_2, respectively.

Often surfactants are added to increase the surface tension thereby increasing the droplet size and reducing drift. The effect of changing surface tension can be estimated from the following equation:

$$\frac{D_{vm.chemical}}{D_{vm.water}}=\left(\frac{\sigma_{chemical}}{73}\right)^{1/2}$$ (10.21)

where $\sigma_{chemical}$ = surface tension of the chemical, mN/m (dyne/cm).

Table 10.5. Spray droplet size and its effect on drift (Bode and Butler, 1981).

Droplet diameter, μ	Steady state fall rate, m/s	Time to fall 3.04 m in still air, sec.	Drift distance in 3.04 m fall with 4.82 km/h wind, m	Lifetime of evaporating water droplet, sec[a]	Fall distance of evaporating droplet in life-time, m[a]
5	0.00075	3960	4815	0.04	<0.025
10	0.003	1020	1372	0.2	<0.025
20	0.012	230	338	0.7	<0.025
50	0.076	40	54.25	4	0.076
100	0.122	11	14.63	16	2.44
150	0.457	8.5	7.62	36	12.2
200	0.9274	5.4	4.57	65	38.4
500	1.158	1.6	2.13	400	>380
1000	2.133	1.1	1.52	1620	>380

[a]Air temperature, 30°C; relative humidity, 50%.

Drift and coverage. Spray drift poses a significant hazard to the environment, as most pesticides, herbicides, and fertilizers are toxic or have other undesirable effects on unintended targets. Smaller droplets tend to drift more than larger ones, because smaller droplets take longer to settle (Table 10.5). Note that as the droplet size decreases settling time increases in a logarithmic manner. Droplets that take longer to settle are very prone to drift. Every nozzle produces droplets of different sizes, but if the size distribution is very wide, a lot of droplets will be undersize and be prone to drift. It is, therefore, best to produce a narrow distribution of droplet sizes near the desired size. Generally, a balance has to be struck between the large droplets and the small droplets. Large droplets give greater penetration of the plant canopy while smaller droplets give greater coverage. Table 10.2 shows the effects of droplet size on coverage. As the droplets become smaller the coverage increases for the same application rate. For systemic herbicides larger droplets would be acceptable, but for contact herbicides or fungicides, full coverage made possible by smaller droplets is more desirable. In addition, although smaller droplets give better coverage they evaporate at a faster rate adding to the drift. Table 10.5 shows evaporation rates for different size droplets.

Research is under way to improve sprayer efficiency and reduce drift. Electrostatic charging and air-curtain sprayers are two results of the efforts in this direction. Droplets are electrostatically charged to improve their tendency to adhere to the plants thereby increasing efficiency of coverage and reducing drift. In air-curtain sprayers, the droplets are introduced in a fast moving air stream to increase penetration into the plant canopy.

10.3.4 Sprayer calibration

Sprayer calibration refers to adjusting the chemical application rate in terms of L/ha. The application rate depends on the sprayer forward speed, effective sprayer width, and the nozzle flow rate. The following formula can be used to determine the required nozzle flow rating for broadcast applications:

$$Q_n = \frac{AR\, d_n S}{600}$$

(10.22)

where Q_n = nozzle flow rate, L/min
$\quad$ AR = application rate, L/ha
$\quad$ d_n = nozzle spacing, m
$\quad$ S = sprayer speed, km/h

Once the desired nozzle flow rate is determined an appropriate nozzle may be selected from the manufacturers' catalog. The next step is to adjust the system pressure to obtain the desired flow rate. The following formula may be used to determine the desired pressure (p):

$$p = \left(\frac{Q_n}{Q_r}\right)^2 p_r$$

(10.23)

where Q_r = rated nozzle flow rate (L/min)
$\quad$ p_r = rated nozzle pressure (kPa)

For banded application, use the spray-band width or swath width for spacing in Equation 10.22. For multiple-nozzle directed spray, the value to be used for spacing is the row width divided by the number of nozzles per row. Keeping a sprayer calibrated properly is very important to maximize chemical effectiveness and to minimize environmental hazards. Sprayer controllers are now available that monitor the tractor/sprayer speed and the flow rate, and continuously adjust flow to the desired application rate.

Example 10.4

Determine the nozzle flow rate for a hollow-cone nozzle for an application rate of 200 L/ha. The sprayer speed is 10 km/h and the nozzle spacing is 50 cm. The available 0.787 mm orifice diameter nozzle is rated at 0.473 L/min at 275 kPa pressure. Determine what pressure would be required to produce the desired nozzle flow. If the nozzle produces a VMD of 200 μ at 1000 kPa, determine the droplet size at the desired flow rate. If a VMD of 350 μ is needed, determine the surface tension that should be achieved by adding surfactants.

Solution

Determine the nozzle flow rate as:

$$Q_n = \frac{200(0.5)7.5}{600} = 1.24 \quad L/min$$

Now determine the desired pressure for the given nozzle as:

$$p = \left(\frac{1.24}{0.473}\right)^2 275 = 1889 \quad kPa$$

VMD at the above pressure is calculated next:

$$d_{vml} = \left(\frac{1000}{1889}\right)^{1/3} 200 = 162 \quad \mu$$

Surface tension has to be increased to get the desired droplet size of 350m. The necessary surface tension is calculated as:

$$\sigma_{chemcial} = \left(\frac{350}{200}\right)^2 73 = 223.5 \quad dynes/cm$$

Manufacturers of surfactants should be consulted to determine the appropriate compound and its proportion to achieve the desired surface tension.

HAY AND FORAGE HARVESTING

11

INTRODUCTION

Domesticated animals have been used as power sources and/or as food during the entire recorded history of agriculture. Through grazing, animals are able to make use of grasses, legumes, and other forage crops that people cannot consume directly. The climate permits year-around grazing in some parts of the world. Because grazing is selective and management intensive, however, *forages* are generally machine harvested and stored for later feeding. The two most common methods of preserving forage crops are as *direct-cut* or *field wilting*. With direct-cut harvest, silage is stored at the moisture level of the cut crop; field wilting allows the moisture content to decrease. *Ensilage* involves cutting the forage at 70% to 80% moisture, allowing it to field dry to 50% to 65% moisture, chopping it into short lengths to obtain adequate packing, and preserving it by fermentation in an airtight chamber. For *hay* harvest, the forage must be cut and allowed to dry to a moisture content of 15% to 23% before it can be stored. Hay has low bulk density and does not flow readily; *silage* has the same limitations, plus it will spoil if it is not fed soon after removal from storage. Thus, both hay and silage are often fed close to the point of production. There are, however, commercial hay farms that produce high-quality hay, bale it, and ship it considerable distances—even internationally—to customers.

Forages are unique because they are harvested with high moisture content levels. Because of the large volume of water that must be removed and the limited crop value, it is generally not feasible to dry forages by artificial means. Losses and storage properties are highly dependent on crop moisture (Figure 11.1).

11.1 METHODS AND EQUIPMENT

Figure 11.2 illustrates common activities for harvesting forage. For harvesting as silage, the standing or wilted crop is cut, field cured, and then chopped into short lengths by a forage harvester (Figure 11.3). The same machine conveys the chopped forage into a wagon or truck for transport to the silo. There, the chopped forage is dumped directly into a bunker or trench silo, bagged into horizontal bags, or blown into a tower silo with a forage blower (Figure 11.4). Most grass and legume forage is
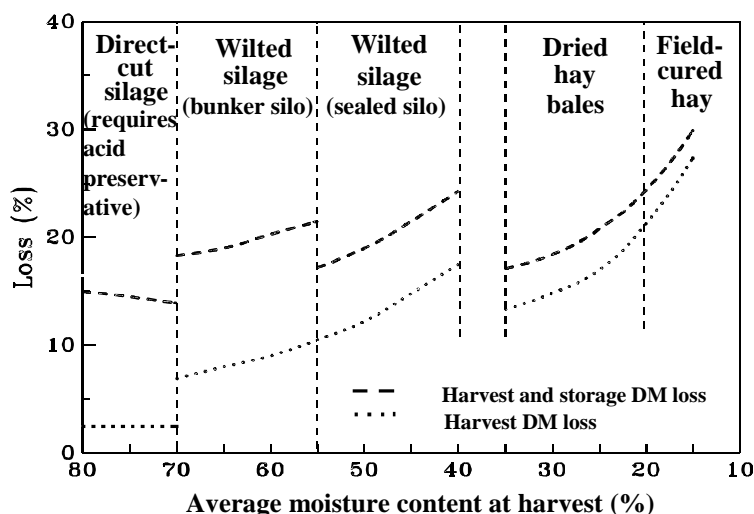
Figure 11.1 – Typical dry matter losses of forage during haycrop harvest and storage (Rotz et al., 1990).

allowed to partially dry by wilting before chopping; silage stored too wet produces effluents and causes poor fermentation. Silage that is too dry packs poorly and spoils. Therefore, once the crop has reached the proper moisture content (Figure 11.1), the forage harvester and its complementary equipment must provide for a rapid harvest. Direct-cut corn (maize) can be ensiled without drying, since the fermentation process prevents spoilage.

Forages are field dried in either a *swath* or a *windrow*. A swath approaches the width of the cut strip, generally leaving enough stubble uncovered to permit wheel traffic during subsequent operations. Swaths dry more rapidly due to greater area exposed to solar radiation, but they must be raked into a windrow for harvesting. A windrow is a narrow strip of forage that dries at a slower rate but does not require further manipulation before harvest. Forages to be made into dry hay are usually placed in a swath while those to be made into silage are placed directly into a windrow to control the drying rate. Tedding is sometimes used to spread the crop uniformly to increase the drying rate.

Leaves dry faster than stems with legume and grass-type forages. The leaves, especially in legumes, are higher in nutritional value than the stems. Brittle, dry leaves may be lost during raking and harvesting. To reduce such losses, the forage will be conditioned so that the stems dry at a rate approaching that of the leaves. *Conditioning* is a physical process of crushing or abrading the stems, or a chemical process that dissolves the waxy cutin layer of the stems. Either process increases the stem-drying rate by reducing the natural resistance to moisture removal from the stems.

Grass and legume forages are usually cut with a machine that combines the cutting and the conditioning process (Figure 11.5). The mower-conditioner can place the forage into either a wide swath or a narrow windrow. A windrower can be used to harvest either forages or small grains, but can only place the material into a narrow windrow.
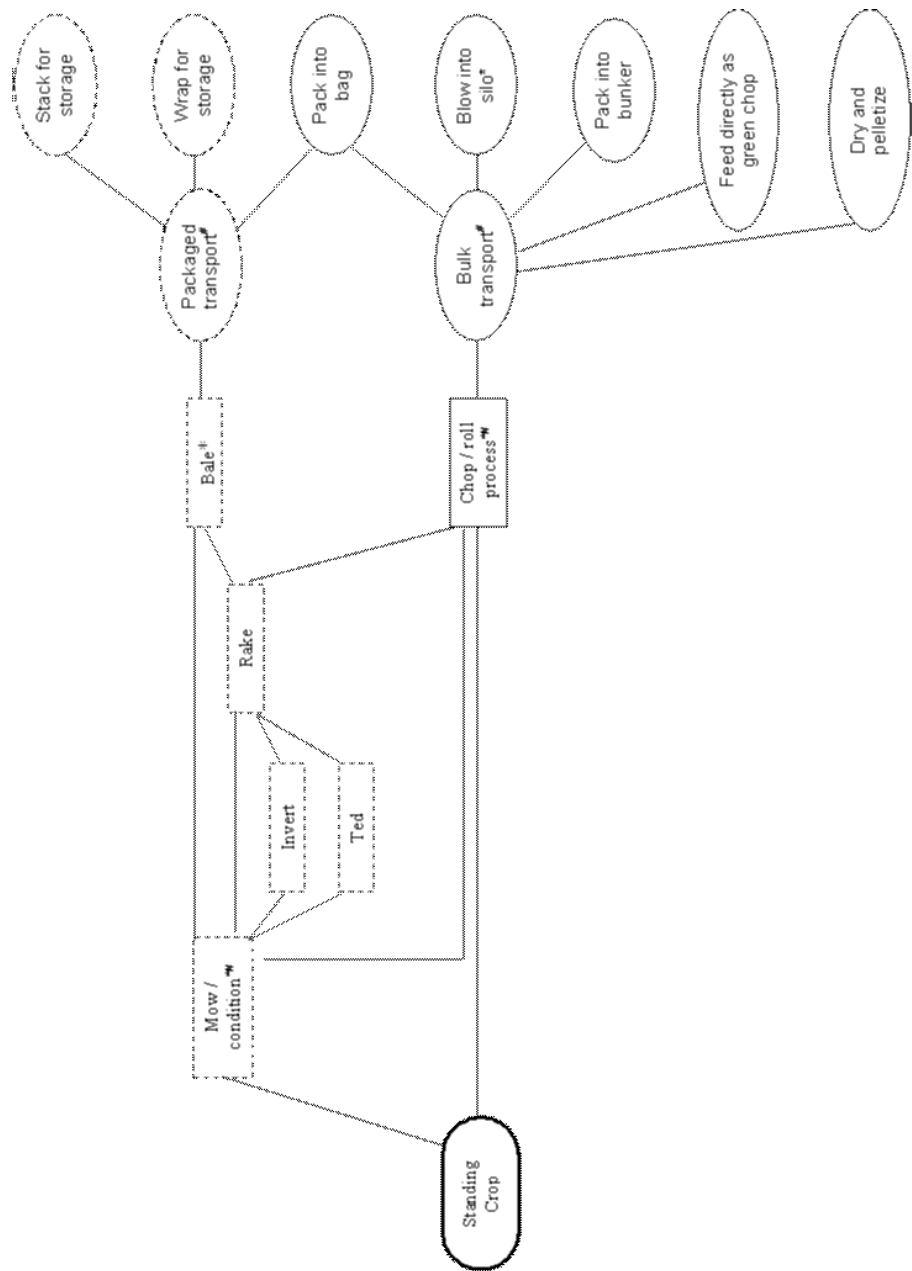
Figure 11.2 – Primary operations of forage harvest systems sequenced left to right (rectangles – harvest operations; ovals – non-harvest operations; dashed enclosures – wilted crops only; solid enclosures – wilted or direct-cut crops; * common points of chemical application; # sometimes self-propelled).

Figure 11.3 – Forage harvesters (Courtesy of CNH).
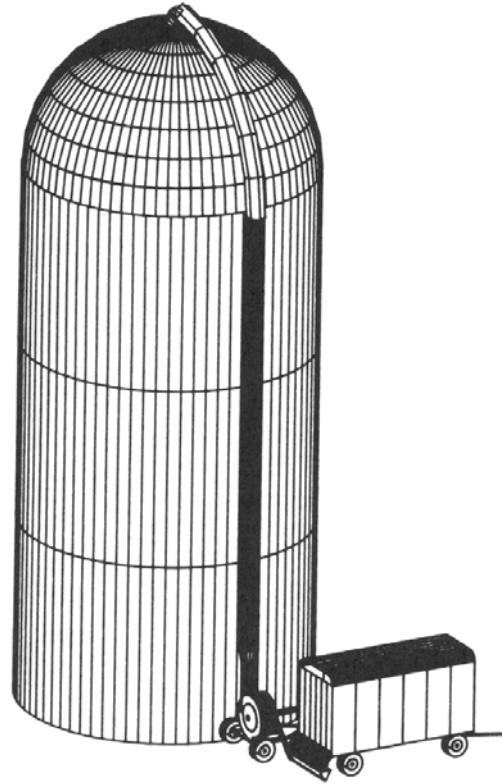
Figure 11.4 – Conveying forage into a tower silo.

After the forage dries to 23% moisture or less, it is usually compressed to some degree before being transported to storage. Baling the hay into small rectangular bales of 25 to 40 kg mass (Figure 11.6) provides hay packages that can are convenient to store and can be lifted by a single person or by machine. Because they do not resist water penetration very well, rectangular bales are usually transported and stored under a roof soon after baling. In another alternative, the hay is rolled into large round bales of 100 to 500 kg mass (Figure 11.7) that are more resistant to water penetration, especially if plastic wrapped, and are sometimes stored outdoors, although storage losses will be higher. The large round bales are too heavy to be handled by hand, so specialized powered equipment has been developed for handling and transporting such bales. Another approach is to package the hay into large rectangular bales that are similar in weight and density to large round bales. The large rectangular bales will not shed water and thus cannot be stored outdoors, but are better suited to shipping by truck than are large round bales.

In addition to those mentioned above, numerous other methods have been developed for harvesting hay. These include pelleting, stacking the hay into stacks in the field, compressing the hay into large loaves, and other methods. Specialized equipment has been developed to support each of these methods. Space does not permit an engineering analysis of all of this diverse equipment, so such analyses will be confined to mowing, conditioning, raking, forage chopping, and baling.
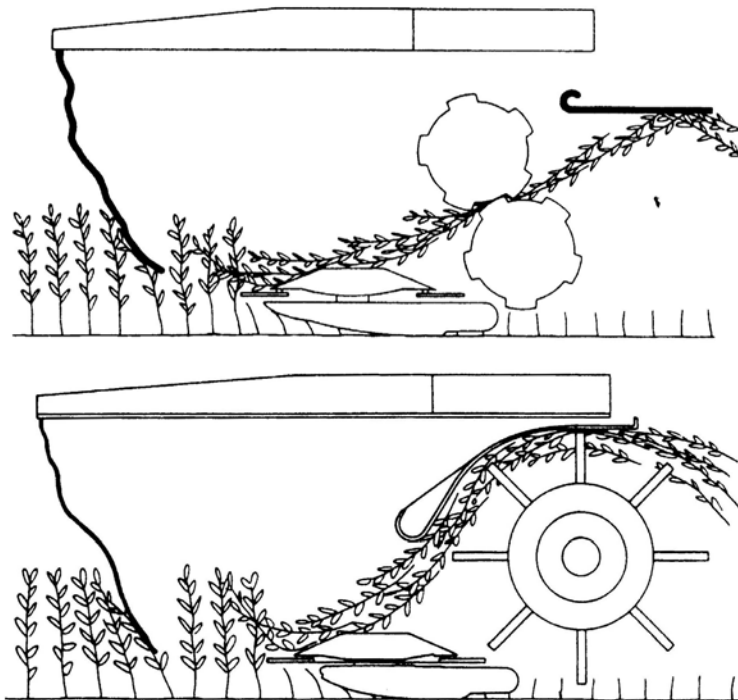
Figure 11.5 – Schematic, cross-sectional view of disk mower-conditioners (a) with roll conditioning, (b) with flail conditioning (Courtesy of CNH).
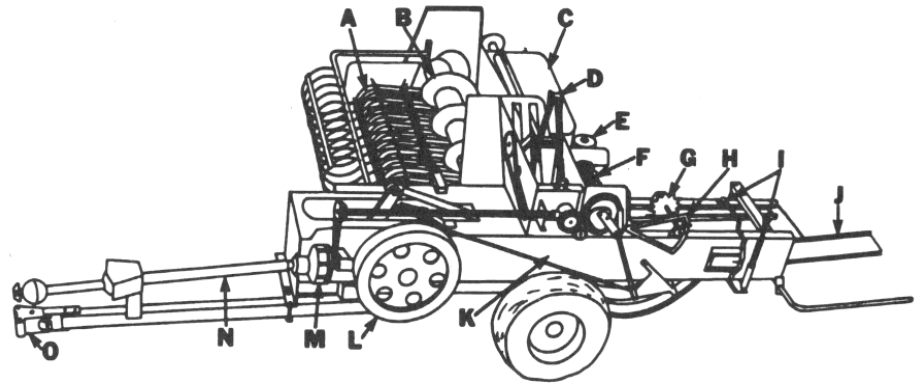
Figure 11.6 – A baler that compresses hay into rectangular bales: A = pickup, B = feed auger, C = twine box, D = feed fork, E = hydraulic pump for density control, F = knotter, G = metering wheel, H = metering arm, I = density control rams, J = bale chute, K = bale chamber, L = flywheel, M = slip clutch, N = PTO drive, O = hitch (courtesy of Prairie Agricultural Machinery Institute, Canada).
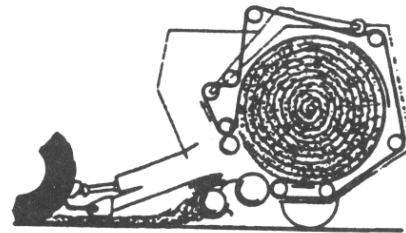
(a)
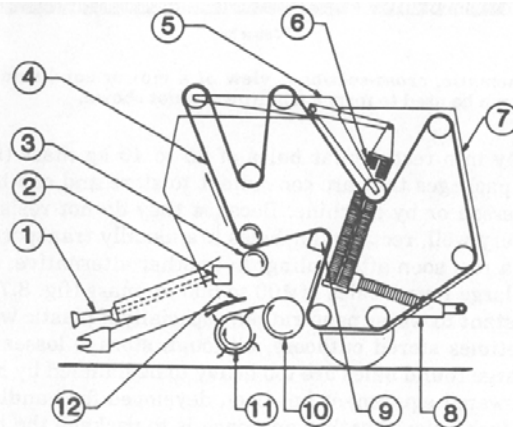
(b)

Figure 11.7 – Baler for large round bales showing (a) operation and (b) construction details: 1 = drive shaft, 2 = gear box, 3 = stripper roll, 4 = chamber belt, 5 = tensioning arms, 6 = tensioning springs, 7 = tailgate, 8 = bale ejector, 9 = core-forming cam idler, 10 = floor roll, 11 = pickup, 12 = wind guard (courtesy of Prairie Agricultural Machinery Institute, Canada).

11.2 FUNCTIONAL PROCESSES

11.2.1 Cutting mechanics and plant structure

Mowing and forage chopping involve the cutting of plant materials and cutting will be subjected to engineering analyses in this chapter. Those same analyses have wider application. For example, sickle bar mowers are used for cutting hay and forage, but similar sickle bars are included on the combines that harvest wheat, soybeans, and other crops. Thus theory learned in this chapter will be useful in understanding Chapter 12 and perhaps in analyzing machines not covered in this textbook.

11.2.1.1 Cutting geometry

In many agricultural machines, a knife is used to sever plant material. Often severing is accomplished by shearing the material between a moving knife and a stationary countershear. In designing equipment to accomplish the severing, the objectives are to maintain the quality of the harvested product while minimizing the force and energy needed to accomplish the task. The characteristics of both the cutting device and the plant must be considered in pursuing these objectives.

Figure 11.8 illustrates the geometry associated with a mower in which a knife (sickle section) moves with reciprocating motion. The plant material is sheared as the sickle section reaches and passes over the countershear (ledger plate) on the right. At the instant illustrated in Figure 11.8, the knife is just leaving the left end of its stroke and moving toward the ledger plate. Guards direct the plant material between the knife and ledger plate and also shield the blunt ends of the sickle sections while they reverse directions at the ends of their stroke.

Typically, in cutting theory, the x-axis of the coordinate system is in the direction of knife movement relative to the plant material. In Figure 11.8, the knife has a velocity component, v_{km}, relative to the mower and a component, v_f, due to the forward speed of the mower. The vector sum of these two components gives the knife velocity, v_{kg}, relative to the ground. Since the plants to be cut are attached to the ground, v_{kg} is also the knife velocity relative to the uncut plants. Therefore, the x-axis is in the direction of v_{kg}, the y-axis is in the plane of the paper but perpendicular to x, and the z-axis is perpendicular to the plane of the paper and points upward. Note that the orientation of the coordinate system in Figure 11.8 is for only one instant in time, since the magnitude of v_{km} varies during the cutting stroke and thus the coordinate system rotates about the z-axis as the direction of v_{kg} varies.

It is common knowledge that a sharp knife aids cutting. It is important, however, to distinguish between *sharpness* and *fineness*. A fine knife has a small bevel angle, ϕ_{bk}, while a blunt knife has a large bevel angle. Sharpness is defined by the edge radius, r_{ek}, of the knife, i.e., a sharp knife has a small radius while a dull knife has a larger radius. Initial penetration of the knife into the plant material is aided if the knife rake angle, ϕ_{rk}, is large. The knife clearance angle, ϕ_{ck}, is the angle formed between the bottom edge of the knife and the x-y plane. In general, the following relationship holds between the rake, bevel, and clearance angles:

$$\phi_{rk} + \phi_{bk} + \phi_{ck} = 90^\circ \tag{11.1}$$
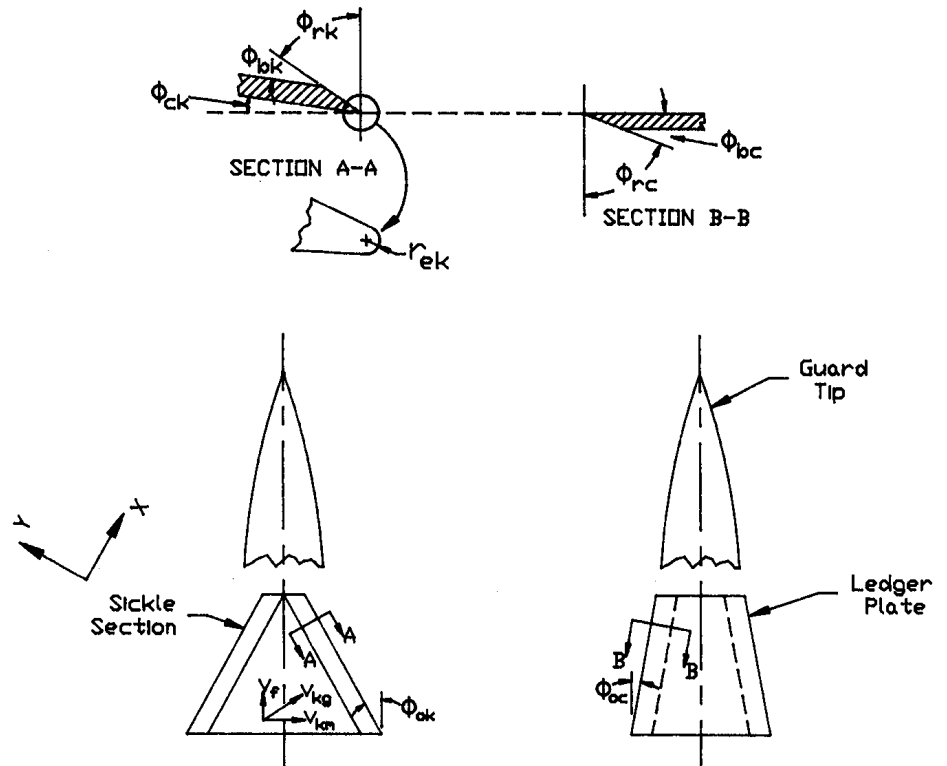
Figure 11.8 – Illustration of geometry of a knife and countershear.

The chip angle on the knife, ϕ_{chk}, is defined as follows:

$$\phi_{chk} = \phi_{bk} + \phi_{ck} \qquad (11.2)$$

The oblique angle of the knife, ϕ_{ok}, is the angle between the y-axis and the cutting edge. The ϕ_{ok} illustrated in Figure 11.8 is for the special case where $v_f = 0$. A straight cut is one in which $\phi_{ok} = 0$. Conversely, an oblique cut is one in which ϕ_{ok} is not equal to zero. Oblique cutting reduces the peak cutting force because the plant material is sheared progressively rather than all at once as in a straight cut.

The bevel, rake, clearance, and oblique angles all have their counterparts on the countershear, as shown in Figure 11.8. For each of these angles, the subscript k indicates that it relates to the knife, while a subscript c indicates the corresponding angle on the countershear. The clip angle, ϕ_{cl}, is the angle formed between the knife and countershear, i.e.:

$$\phi_{cl} = \phi_{ok} + \phi_{oc} \qquad (11.3)$$
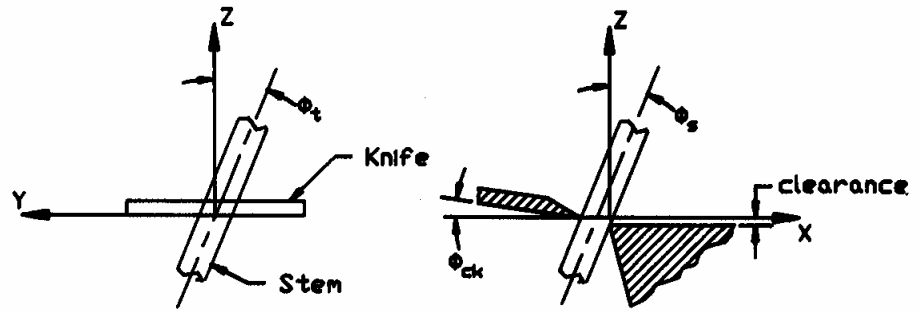
Figure 11.9 – Illustration of stem misalignment.

Frequently, plant stems are not parallel to the z-axis. Figure 11.9 illustrates the tilt angle, ϕ_t, and the slant angle, ϕ_s, which are used to define the orientation of such stems. The tilt angle is the angle between the stem axis and the z-axis projected into the y-z plane, while the slant angle is the angle between the stem axis and the z-axis projected into the x-z plane. Figure 11.9 also illustrates a positive clearance angle on the knife and the clearance that may be present between the knife and the counter-shear.

When ϕ_{ok} is not zero and the plant material is not yet in contact with the counter-shear, the possibility exists that the plant material may slide along the edge of the knife before or while being cut. The sliding is expected if the oblique angle is greater than the following maximum angle:

$$\phi_{ok,max} = \arctan f_{ek} \tag{11.4}$$

where f_{ek} = knife edge friction coefficient. The knife edge friction coefficient is the lateral force (parallel to the knife edge) imposed by the plant on the knife edge divided by the normal force imposed by the plant. When the plant is in contact with both the knife and countershear, sliding is expected if the clip angle is greater than the following maximum:

$$\phi_{cl,max} = \arctan \frac{f_{ek} + f_{ec}}{1 - f_{ek}f_{ec}} \tag{11.5}$$

where $\phi_{cl,max}$ = maximum value of ϕ_{cl} that will prevent sliding
    f_{ek} = friction coefficient for knife edge
    f_{ec} = friction coefficient for countershear edge

Since the forward motion of the mower helps to push the plants toward the rear of the knife sections, sliding is most likely to occur when v_f is small. To increase friction and thus prevent sliding, serrations may be cut into the edge of the knife and/or countershear. For example, values of $f_{ek} = 0.306$ for a smooth knife edge and $f_{ec} = 0.364$ for a serrated ledger plate were observed during cutting of flax straw.

11.2.1.2 Plant structure

   Cutting is a process that causes mechanical failure of plant stems and/or leaves and thus the structure and strength of plant materials are of interest. The engineering properties of plant parts are not as well understood as those of more common engineering materials such as steel, but some engineering studies of plant materials have been made. Living plants consist of solid material that surround air- and liquid-filled cavities. Fiber cells, with diameters of 10 to 50 µm and lengths exceeding 30 mm, provide the main strength of the plant material. Fiber cell walls include three basic layers: the middle lamella, the primary wall, and the secondary wall, with combined thicknesses on the order of 500 nm. The secondary wall lies inside the primary wall and provides the strength and flexibility of the structure. Cellulose chains, the main ingredient of the secondary wall, are bound together in parallel microfibrils of considerable length and with cross-sectional dimension of 2.5 to 20 nm (Figure 11.10). The microfibrils are oriented in spirals, and the angle of the spiral relative to the cell axis determines the elasticity of the cell wall. The cell wall density is approximately 1.45 g/mm^3, but makes up only a small proportion of the cross section. Some cell walls have strength approaching that of steel, but the numerous cavities greatly reduce the average strength of the plant cross section.

   Plant stems and leaves consist of large numbers of similar cells. Structurally, the stems can be viewed as materials with fibers of high tensile strength oriented in a common direction and bound together by material of much lower strength. The softer cells make use of their turgor (liquid pressure) to connect and support the fibers. Grasses, including small grains and corn (maize), and legumes are the materials most commonly involved in agricultural cutting processes, so their structure and strength
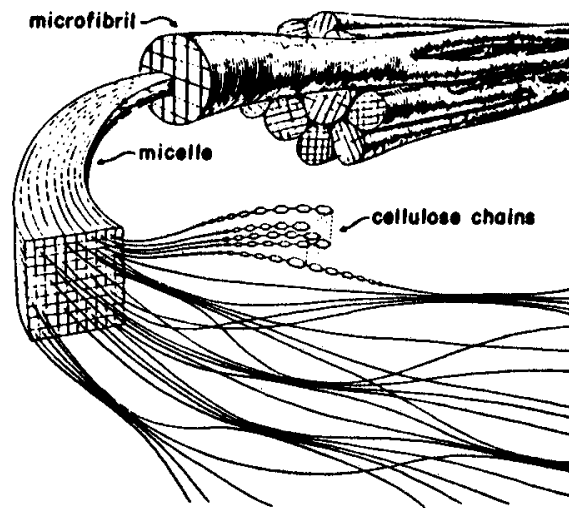
**Figure 11.10 – Arrangement and structure of microfibrils
(reprinted from Persson, 1987).**

are of special interest. Many grass stems have hollow internode sections joined by solid nodes (Figure 11.11). The internode sections are much weaker than the nodes and thus determine the stem strength. The corn stalk has internode sections which are not hollow but have a more uniform cross section. Figure 11.12 shows simplified models that were drawn to represent the actual cross section of a hollow stem for analyzing stem strength in bending. The strength is determined by the amount of structural fibers and their locations in the plant, rather than by the outside dimensions.
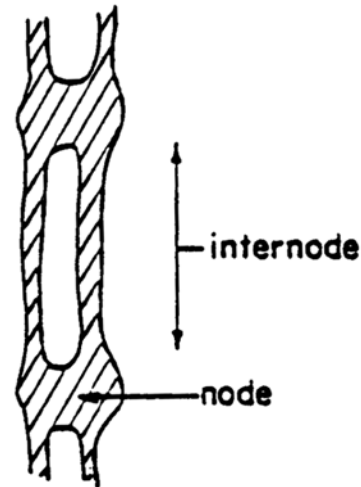
Figure 11.11 – Longitudinal section through a stem showing nodes and internodes (reprinted from Persson, 1987).

(a)   (b)
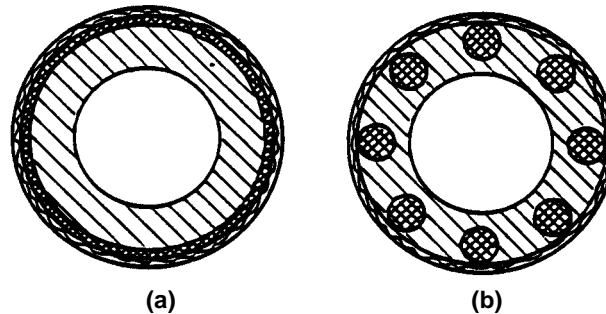
Figure 11.12 – Mechanical equivalents stem cross sections, showing the main structural components arranged as (a) a concentric cylinder, and (b) eight reinforcement rods. Drawn to approximate scale with regard to area and moments of inertia in bending (reprinted from Persson, 1987).

Secondary cell walls in their natural position have ultimate tensile strengths ranging up to 1100 N/mm², a modulus of elasticity (E) in the range from 10,000 to 100,000 N/mm², and ultimate strain (S_u) of 0.5% to 5%. Those subject to compression in the growing plant have lower tensile strength but greater elasticity. Other cell walls have much lower strength; for example, tensile strength of the outer layer (skin) ranges from 2 to 14 N/mm². Ultimate tensile strength of the solid portions of timothy or alfalfa stems ranges from 90 to 470 N/mm²; when the entire cross section of the alfalfa stem is used, the ultimate strength is only 8 to 35 N/mm².

The bending strength of a plant stem may be important during cutting. For example, some devices cut a plant in the absence of a countershear; the plant stem below the cutting plane is loaded as a cantilever beam. In other situations, the stem may be loaded as a simply supported beam. In either case, the direction of loading is radial (perpendicular to the longitudinal axis of the plant stem). The radial load that would cause failure in bending can be calculated using the following equation:

$$F_{bu} = \frac{I}{c}\frac{S_u}{L}$$ (11.6)

where F_{bu} = ultimate load at bending failure, N
   I = moment of inertia of the cross section, mm⁴
   c = radius from neutral axis of stem to most distant load-carrying fiber, mm
   or, alternately, I/c = section modulus, mm³
   S_u = ultimate stress of plant fibers, N/mm²
   L = distance from concentrated load to point of support, mm
The deflection of the stem is given by:

$$\delta_r = \frac{F_r L^3}{C_b EI}$$ (11.7)

where δ_r = radial deflection, mm
   F_r = radial concentrated load, N
   E = modulus of elasticity of stem fibers, N/mm²
   C_b = constant (3 for cantilevered stems, 48 for simply supported stems).
The moment of inertia of a homogeneous solid, circular section is:

$$I = \frac{\pi d^4}{64}$$ (11.8)

where d = diameter of the section, mm. For a hollow, thin-walled section, the moment of inertia is:

$$I = \frac{3\pi d^3 t}{32}$$ (11.9)

where t = wall thickness, mm. From comparing Equations 11.8 and 11.9, we note that the moment of inertia of a natural stem should be proportional to the section diameter raised to an exponent between 3 and 4. Similarly, assuming that the neutral axis is
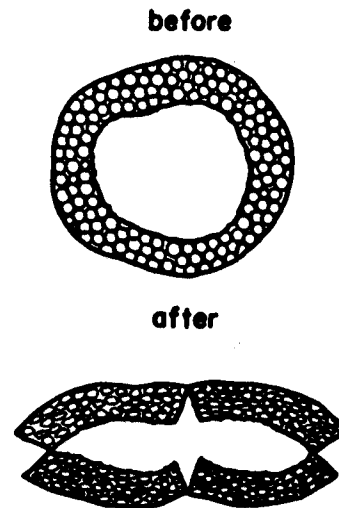
before

after

Figure 11.13 – Cross section of a stem before and after compression bending (reprinted from Persson, 1987).

centered in the stem, the section modulus should be proportional to the diameter raised to an exponent between 2 and 3. The appropriate section diameter is determined by the location of the cell wall fibers rather than the outside diameter (see Figure 11.12) and thus, if the outside diameter is used, the bending strength will be somewhat over estimated. If loading crushes a stem prior to cutting (see Figure 11.13), the circular cross section no longer exists; the moment of inertia and section modulus must then be calculated for the new geometry of the cross section.

The size and bending strength of plant stems increases with plant maturity (Persson, 1987). For example, the stem dry mass of timothy increased from 0.6 to 1.4 mg/mm of length as the plant matured; the corresponding stiffness (EI) increased from 1260 to 3900 N·mm^2. For red fescue (which has a much finer stem) at 67% moisture content, the corresponding figures were stem dry mass increasing from 0.017 to 0.083 mg/mm as the plant matured, while the stem stiffness increased from 0.53 to 5.7 N·mm^2. The stiffness of timothy stems was found to vary with diameter raised to an exponent between 2.66 and 2.99. For cotton stalks ranging in diameter from 7 to 16 mm, the stiffness varied with diameter to the 3.0 power. The modulus of elasticity of cotton stalks ranged from 600 to 3500 N/mm^2. Moisture content affects the strength of plants, since the turgor pressure in the cells affects stem rigidity and strength. Since plants must resist wind loading, strength also varies with height on the plant, i.e., most plants are larger and stronger near the ground than at the top. Near the base of rice straw at 62% moisture content, for example, the stems were 3.5 to 4 times heavier per unit length than near the top. Calculation of plant strength and deflection is illustrated in Example Problem 11.1.

Example Problem 11.1

A living alfalfa stem of 2.5 mm diameter is loaded horizontally at a distance 30 mm above the soil surface (as a cantilever beam). Based on the entire stem cross section, the modulus of elasticity is 1500 N/mm^2 and the ultimate tensile strength is 35 N/mm^2. (a) Calculate the horizontal force that would cause bending failure. (b) Calculate the horizontal deflection of the stem at point of failure.

Solution

(a) Before using Equation 11.6 to calculate the ultimate load, it is necessary to calculate the section modulus, I/c, of the stem. The value of c is half the stem diameter, or 1.25 mm. From Equation 11.8, the moment of inertia is:

$$\pi\ 2.5^4/64 = 1.92\ \text{mm}^4$$

The I/c = 1.92/1.25 = 1.53 mm^3. Then, from Equation 11.6, the ultimate bending load is:

$$F_{bu} = 1.53 \times 35/30 = 1.79\ \text{N}$$

(b) Now, Equation 11.7 can be used to calculate the stem deflection:

$$\delta_r = 1.79(30)^3/(3 \times 1500 \times 1.92) = 5.6\ \text{mm}$$

For this example, the stem would deflect 5.6 mm before the stem fibers failed in bending.

11.2.1.3 Mechanics of cutting

Several different modes of tissue failure can occur during cutting, depending upon the knife characteristics. Initial penetration of the knife results in localized plastic deformation (flow) of the plant material. In moist stems and with high knife speeds, turgor pressure in the stems limits initial compression of the plant. With further knife movement, considerable stem buckling and compression occurs (see Figure 11.13); depending on knife sharpness and speed, the compression can advance well ahead of and to the sides of the knife edge. The precompression before failure results in a gradual buildup of force on the knife and the energy for precompression can consume 40% to 60% of the total cutting energy. As the fibers are deflected ahead of the knife edge, the shear strength of the material is mobilized to produce fiber tensile stresses. These stresses become sufficiently large to cause the fibers to fail in tension, whereupon loading is transferred to fibers further ahead of the knife edge. For common crop materials, cutting occurs when the pressure exerted ahead of the knife edge exceeds 9 to 30 N/mm^2.

Figure 11.14a illustrates a knife and countershear cutting a bed of plant material. Forces on the knife are illustrated in Figure 11.14b. The force, F_x, in the direction of

(a) **(b)**
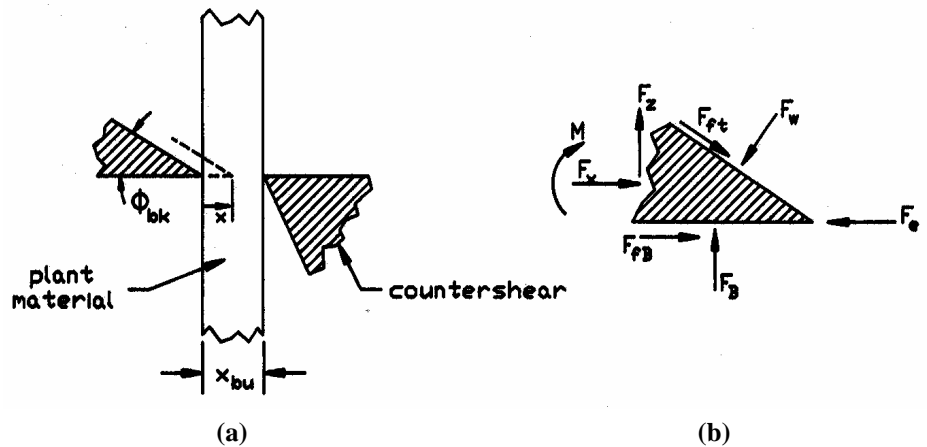
Figure 11.14 – Illustration of knife forces during cutting.

knife motion is the sum of the knife edge force plus x-components of forces imposed on the top and bottom surfaces of the knife as it compresses and penetrates the plant material. By assuming that only the material directly ahead of the knife is compressed and by use of the bulk modulus for the plant material, the following equation for knife force was derived:

$$\frac{F_x}{w} = \frac{F_{ek}}{w} + \frac{B_f x^\lambda}{2X_{bu}}(\tan \phi_{bk} + 2f) \tag{11.10}$$

where F_x = knife driving force in x direction, N
  F_{ek} = force imposed by plant on the knife edge, N
  w = width of knife, mm
  B_f = bulk modulus of forage, N/mm^2
  x = knife displacement after initial contact, mm
  λ = exponent
  X_{bu} = uncompressed depth of material between knife and countershear, mm
  ϕ_{bk} = bevel angle of knife edge
  f = coefficient of friction of forage on knife

Theoretically, $\lambda = 2$ in Equation 11.10. However, a smaller exponent gives a better fit to some experimental cutting data. In an experiment in which a thin ($X_{bu} = 8.9$ mm) bed of timothy at 20% moisture was cut at a very low (0.42 mm/s) knife speed, Equation 11.10 fit the data when $\lambda = 1.46$ and $B_f = 10$ N/mm^2. The knife edge force is calculated as the product of the projected frontal area of the knife edge times the pressure imposed on that edge by the forage. The approximate frontal area can be calculated from the following equation:

$$A_{ek} = r_{ek}[1 + \cos(\phi_{bk} + \phi_{ck})] \tag{11.11}$$

where A_{ek} = frontal area of knife edge per mm of width, mm^2
  r_{ek} = radius of knife edge, mm

Figure 11.15 shows the typical shape of the force-displacement curve when plant material is cut by a knife and countershear. In Section A, only compression occurs as the knife edge force is not yet high enough to cause cutting. After initial stem failure, some compression continues in Section B along with cutting. In section C, the material is fully compressed; cutting continues and then the force drops rapidly as the knife edge crosses the edge of the countershear. With suitable choice of parameters, the force in Sections A and B could be calculated using Equation 11.10. Section C does not involve compression so Equation 11.10 does not fit that section. The diagram in Figure 11.15 is for a straight cut, i.e., with $\phi_{cl} = 0$. For an oblique cut, the peak cutting force would be reduced and the duration of cut would be extended compared to Figure 11.15.

Figure 11.15 is useful in calculating the power requirement for cutting with a knife and countershear. The energy per cut is equal to the area under the cutting force curve; multiplying by the cutting frequency gives the power. The following equation can be used to compute the power requirement for cutting:

$$P_{cut} = \frac{C_f F_{max} X_{bu} f_{cut}}{60,000} \qquad (11.12)$$

where P_{cut} = power for cutting, kW

$\quad F_{xmax}$ = maximum cutting force, kN

$\quad X_{bu}$ = depth of material at initial contact with knife, mm (see Figure 11.15)

$\quad f_{cut}$ = cutting frequency, cuts/min

$\quad C_f$ = ratio of average to peak cutting force

C_f is always be between 0 and 1 and, for a typical force-displacement curve as illustrated in Figure 11.15, it is approximately equal to 0.64.
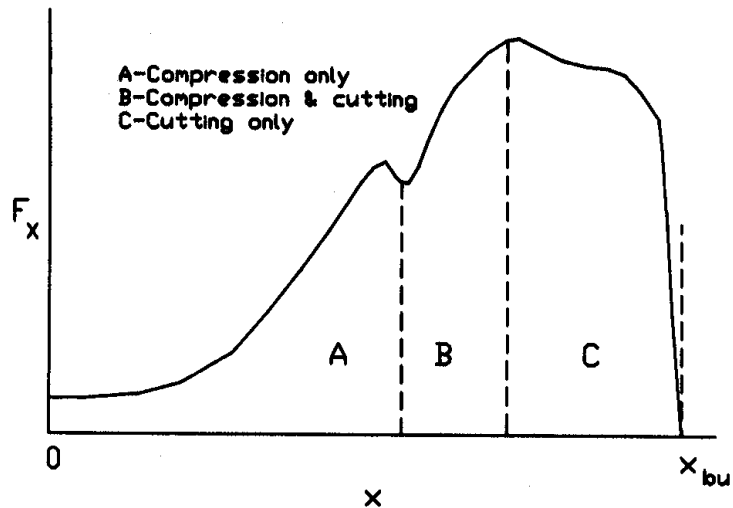
Figure 11.15 – Knife force-displacement curve for a straight cut against a countershear.

The cutting force, F_x, must be supported. If a countershear is present and clearance is small, the support force can be provided entirely by the countershear. When no countershear is present, the support force must be provided entirely by the plant itself through the bending strength of the stump below the cut and the inertia of the plant above the cut. The resulting cut is called, alternatively, an impact cut, an inertia cut, or a free cut. As clearance with a countershear increases, the plant strength and inertia come increasingly into play; thus, impact cutting is similar to countershear cutting with very large clearance. Figure 11.16 illustrates the forces and moments on the plant during impact cutting. The soil and the plant root system provide a force, F_B, and a moment, M_r, which tend to keep the stump upright. Acceleration of the stump is considered to be negligible. Force F_B represents the combined effects of the root system and stalk strength in providing bending resistance at the height of the cut. The center of gravity of the cut portion of the plant is at a height, z_{cg}, above the cut. The impact shown in Figure 11.16 tends to accelerate the cut plant to the right and counterclockwise; consequently, an inertia force and inertia moment appear on the plant at the center of gravity. The following equation results from summing moments about the center of gravity of the cut plant:

$$I_p \alpha_p = (F_x - F_b) z_{cg} \qquad (11.13)$$

where α_p = angular acceleration of plant, radians/s^2
$\quad$ F_x = cutting force, N
$\quad$ F_b = bending resistance of stump, N
$\quad$ z_{cg} = height of center of gravity of cut plant, m (see Figure 11.16)
$\quad$ I_p = centroidal moment of inertia of plant, kg m^2
$\quad\quad$ = $m_p r_g^2$ where m_p = mass of cut portion of plant, kg
$\quad\quad\quad\quad\quad\quad\quad\quad$ r_g = radius of gyration of cut portion of plant, m
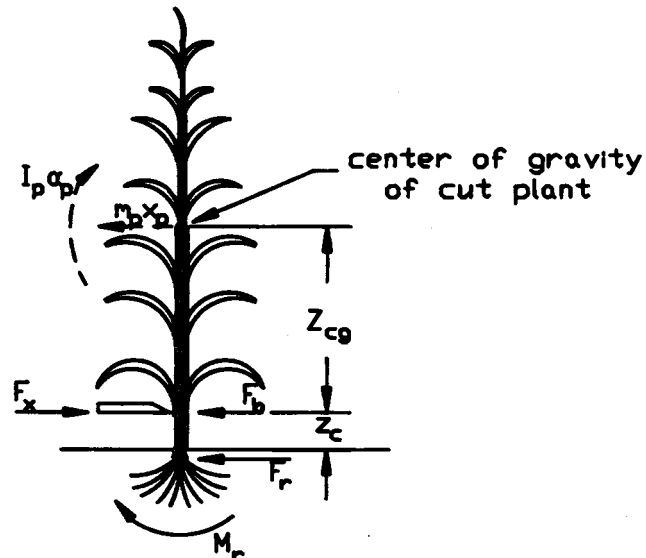
Figure 11.16 – Forces and moments in impact cutting.

An analysis of the kinematics (motions) of the plant gives the following equation for angular acceleration:

$$\alpha_p = \frac{a_c - a_{cg}}{z_{cg}} \tag{11.14}$$

where a_c = acceleration of plant at plane of cut, m/s^2
a_{cg} = acceleration of plant center of gravity, m/s^2

By assuming that the plant acquires knife velocity at the plane of cut, the following equation was derived:

$$a_c = \frac{1000v_k^2}{d_s} \tag{11.15}$$

where v_k = knife velocity, m/s
d_s = stalk diameter at plane of cut, mm

Equations 11.13 through 11.15 can be combined to give the following equation for minimum knife velocity for impact cutting:

$$v_k = \left[d_s \frac{(F_x - F_b)}{1000m_p} \left(1 + \frac{z_{cg}^2}{r_g^2} \right) \right]^{0.5} \tag{11.16}$$

When values for r_g and z_{cg} are not readily available, a simpler approximate equation can be obtained by assuming that $r_g = z_{cg}$. The simpler equation illustrates the key variables involved in impact cutting. If the stump bending resistance, F_b, is large enough to support the entire cutting force, F_x, the minimum required knife velocity is zero and cutting is equivalent to cutting with a countershear. Lowering the height of cut to increase F_b and reducing F_x by maintaining a sharp knife will both reduce the minimum required knife velocity. Tests of impact cutting of timothy, for example, have shown that cutting could be accomplished at knife velocities as low as 25 m/s but velocities of 45 m/s were required for reliable cutting of all stems. To assure reliable cutting over a wide range of knife sharpness and stem stiffness, minimum knife velocities of 50 to 75 m/s are generally recommended. Example Problem 11.2 illustrates the calculation of minimum knife velocity for impact cutting.

Example Problem 11.2

Impact cutting is to be used to cut the alfalfa stem of Example Problem 11.1 at a height 30 mm above the ground. The mass of the plant above the cut is 0.01 kg. Assume that cutting occurs when the pressure ahead of the knife edge reaches 25 N/mm^2. The knife has a bevel angle of 20°, zero clearance angle, and an edge radius of 0.3 mm. Calculate (a) the force imposed by the knife edge to achieve cutting, and (b) the minimum knife speed required for impact cutting.

Solution

(a) The frontal area of the knife edge can be calculated using Equation 11.11:

$$A_{ek} = 0.3[1 + \cos(20 + 0)] = 0.582 \text{ mm}^2/\text{mm width}$$

The width of knife is not known, but since only a single stem is being cut, the width will be assumed equal to the stem diameter, 2.5 mm. Then, using the critical pressure of 25 N/mm^2, the force required to initiate cutting will be:

$$F_{ek} = 0.582 \,(2.5)\, 25 = 36.4 \text{ N}$$

(b) Equation 11.16 is available for calculating the minimum knife velocity for impact cutting. Values for r_g and z_{cg} are not available, but we will assume $r_g = z_{cg}$. No value for F_b is given but we will assume it is equal to the ultimate bending load calculated in Example Problem 11.1, that is, $F_b = 1.79$ N. Then the minimum velocity is:

$$v_k = [2 \times 2.5 \times (36.4 - 1.79) / (1000 \times 0.01)]^{0.5} = 4.2 \text{ m/s}$$

Note: In this idealized cutting of a single stem, the minimum velocity was low. Typically, to allow for interaction of multiple stems during cutting, velocities of 50 to 75 m/s are recommended.

11.2.4 Windrowing

In some methods of forage harvesting, the forage is formed into windrows that can then be picked up directly by the harvester. This is common practice when harvesting forage for silage or where the climate is very dry. When dry hay is desired in humid climates, the forage is placed in a swath and then raked into a windrow. Tedders are sometimes used to spread swaths to fully and uniformly cover the field area. A side-delivery rake can be used to roll swaths left by the mower, or tedded forage, into windrows. Rakes can also be used to invert previously-formed windrows to promote faster drying, especially after rain has wetted the windrows. Dry matter losses during raking typically range from 3% to 6% and more leaves than stems are usually lost. Thus, gentle handling is an important goal in rake design. Popular types of side delivery rakes are the finger-wheel and rotary.

Definitions of symbols in Equations 11.46 through 11.54 are as follows:
α_1 = angle before bottom at which raking begins, radians (see Figure 11.33)
α_2 = angle at which raking ends, radians
β = angle between tooth bars, radians
γ = Acute angle between raking front and direction of travel, radians
θ_{tr} = angle between direction of travel and planes of reelheads, radians
θ_t = angle between v_t and direction of travel, radians
x_2 = horizontal distance traveled by teeth during nonraking, m
y_2 = vertical distance from lowest position of rake teeth to top of windrow, m
$L_1 + L_2$ = horizontal distance traveled by teeth during raking, m
r = reel radius, m
v_f = forward velocity of rake, m/s
v_{tr} = reel component = average horizontal velocity of teeth during raking, relative to rake, m/s
v_p = peripheral speed of reel, m/s
v_t = resultant tooth velocity = vector sum of v_f and v_{tr}, m/s
v_{hr} = average horizontal velocity of hay relative to rake, m/s
v_h = average resultant hay velocity = vector sum of v_f and v_{hr}, m/s
L_h = maximum theoretical distance travelled by hay during raking, m
w_r = width of rake, m

A parallel-bar (oblique-reelhead) rake is illustrated in Figure 11.33. The two reelheads are parallel but at an acute angle with the tooth bars. Thus, when one of the reelheads is driven, either by PTO power or by a ground wheel, every rake tooth follows a circular path in a plane parallel to the reelheads. All teeth automatically maintain parallel positions, usually vertical, but the pitch of the teeth can be changed by changing the tilt of the reelhead axes. Pitching the bottoms of the teeth forward gives a more vigorous raking action in heavy crops.

Figure 11.33 was used in deriving velocity relationships for a parallel-bar rake. Rake teeth contact the hay at angle α_1 from the lowest tooth position and release it at angle α_2 at the top of the windrow. Teeth are in contact with the hay during forward travel x_1 and out of contact during forward travel x_2. One expression for x_2 can be derived from Figure 11.33a, i.e.:

$$x_2 = (L_1 + L_2)\left(\cos\theta_{tr} + \frac{\sin\theta_{tr}}{\tan\gamma}\right) \tag{11.46}$$

Another expression for x_2 can be derived from Figure 11.33b, i.e.:

$$x_2 = r\frac{v_f}{v_p}(\beta - \alpha_1 - \alpha_2) \tag{11.47}$$

Then, since $L_1 = r\sin(\alpha_1)$ and $L_2 = r\sin(\alpha_2)$, Equations 11.46 and 11.47 can be combined into the following equation:
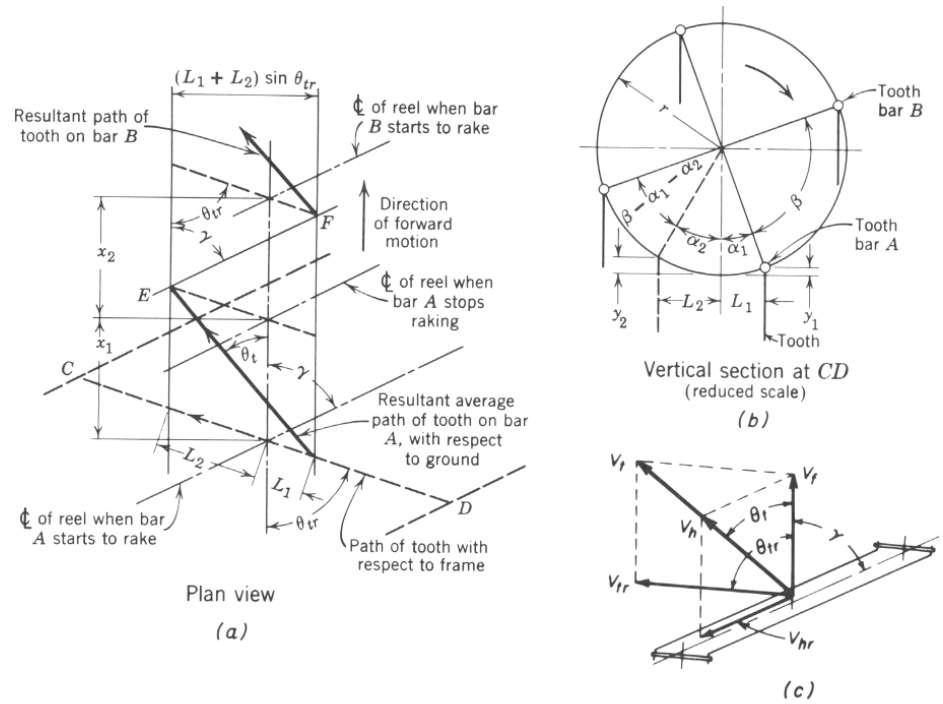
Figure 11.33 – A side-delivery parallel bar rake (courtesy of CNH).

$$\frac{\beta - \alpha_1 - \alpha_2}{\sin \alpha_1 + \sin \alpha_2} = \frac{v_p}{v_f}\left(\cos \theta_{tr} + \frac{\sin \theta_{tr}}{\tan \gamma}\right) \tag{11.48}$$

All terms in Equation 11.47 are design variables except α_1 and α_2, which are unknowns depending upon operating conditions. From Figure 11.33b:

$$\alpha_2 = \arccos\left(1 - \frac{y_2}{r}\right) \tag{11.49}$$

Distance y_2 can be determined as the height of the top of the windrow relative to the lowest position of the rake teeth. Then Equation 11.49 can be solved for α_2 and Equation 11.48 can be solved (iteratively) for α_1. Note that α_1 can be negative if the effective raking stroke begins beyond the lowest point of tooth travel. After α_1 and α_2 are known, the magnitude of vector v_{tr} can be calculated using the following equation:

$$\frac{v_{tr}}{v_p} = \frac{\sin \alpha_1 + \sin \alpha_2}{\alpha_1 + \alpha_2} \tag{11.50}$$

The direction of v_{tr} is parallel to the planes of the reelheads. After vector V_{tr} is determined, the direction and magnitude of v_t can be calculated. Angle θ_t can be calculated from:

$$\theta_t = \arctan\left(\frac{v_{tr} \sin \theta_{tr}}{v_f + v_{tr} \cos \theta_{tr}}\right) \tag{11.51}$$

and the magnitude, v_t, can be calculated from:

$$v_t = \frac{v_{tr} \sin \theta_{tr}}{\sin \theta_t} \tag{11.52}$$

The direction of v_h is coincident with v_t. The magnitude of v_h can be calculated using the following equation:

$$v_h = \frac{v_f}{\cos \theta_t + \sin \theta_t + \cot \gamma} \tag{11.53}$$

The theoretical maximum distance traveled by the hay during raking is given by the following equation:

$$L_h = \frac{w_r}{\sin \theta_t} \tag{11.54}$$

A finger-wheel side-delivery rake is illustrated in Figure 11.34. The action of one raking wheel is illustrated in Figure 11.34a, while velocity relationships for the complete rake are shown in Figure 11.34b. Raking teeth are carried on wheels whose planes of orientation allow each wheel to be ground driven. Thus, no separate drive train is required. As was true for the parallel-bar (oblique-reelhead) rake, the vector v_{hr} is parallel to the raking front and v_{tr} is parallel to the planes of the raking wheels.

(a)   (b)

Figure 11.34 – A finger-wheel side-delivery rake (courtesy of Deere and Co.).

Since the tooth wheels are each ground driven, the magnitude of v_p can be calculated from the following equation (see Figure 11.34a):

$$\frac{v_p}{v_f} = \cos(\pi - \theta_{tr}) = \cos\theta_{tr} \tag{11.55}$$

The reel component, v_{tr}, is proportionally less than v_p as shown in the following equation:

$$v_{tr} = \frac{r - y}{r} v_p \tag{11.56}$$

where y = half of the windrow height, m (see Figure 11.34a)

r = radius from center of tooth wheels to tooth tips, m

The angle, θ_t, of the resultant tooth and hay path is given by the following equation:

$$\theta_t = \arctan\left[\sin\theta_{tr}\left(\cos\theta_{tr} - \frac{v_f}{v_{tr}}\right)^{-1}\right] \tag{11.57}$$

The magnitudes of v_t and v_h can be calculated using Equations 11.52 and 11.53, respectively. The theoretical maximum length of hay travel for the finger wheel rake can be calculated using Equation 11.54.

The gentleness with which the hay is handled during raking is influenced by rake design variables. Gentleness is promoted by maintaining low hay velocity, v_h, by keeping v_t as close as possible to v_h to reduce tooth impacting on the hay, and by keeping hay travel, L_h, as small as possible. The ratio of v_h/v_t is closer to unity for the finger-wheel rake, thus providing a smoother raking action than for the parallel-bar rake. However, the finger-wheel rake has a somewhat longer hay path (compare Figures 11.33c and 11.34a). For the parallel-bar rake, reducing the ratio v_p/v_f lengthens the hay path but reduces the frequency of tooth impacts on the hay and also reduces the ratio v_t/v_h. Reducing v_f also provides gentler handing of the hay but decreases the raking capacity. The theoretical effects of the various raking parameters were determined analytically, but there is little published information on the effect of raking parameters on losses. Example Problem 11.7 illustrates calculations for a side delivery rake with oblique reel head.

Example Problem 11.7

A five-bar side delivery rake with an oblique reel head has a raking front angle, $\gamma = 65°$ (6.81 radians) and a raking width of 2.4 m. The reel radius is 0.3 m and the head angle is $\theta_{tr} = 72°$ (7.54 radians). The reel is ground driven with a speed ratio $v_f/v_p = 0.8$. When the rake is traveling at 8 km/h while raking a windrow of height 0.45 m, calculate the (a) direction and (b) magnitude of the resultant tooth path, (c) the average hay velocity, (d) the maximum theoretical distance travelled by the hay during raking, and (e) the ratio, v_h/v_t, of the average hay velocity to the resultant tooth velocity.

Solution

(a) Angles α_1 and α_2 must be calculated to begin the analysis. Since the angles and their trigonometric functions will be used, radians will be used instead of degrees in all of the trigonometric calculations. The value of α_2 can be calculated using Equation 11.49:

$$\alpha_2 = \arccos(1 - 0.45/0.3) = 2.09 \text{ radians}$$

then all variables in Equation 11.48 are known except for α_1. Because the reel has 5 bars, $\beta = 2\pi/5 = 1.26$ radians. Then:

$$\frac{1.26 - \alpha_1 - 2.09}{\sin \alpha_1 + \sin 2.09} = \frac{1}{0.8}\left(\cos 7.54 + \frac{\sin 7.54}{\tan 6.81}\right)$$

Solving the above equation by iteration gives $\alpha_1 = 5.45$ radians. The forward speed of the rake is $8/3.6 = 2.22$ m/s and the peripheral speed of the reel is $v_p = 2.22/0.8 = 2.78$ m/s. Equation 11.50 can be used to calculate the reel component, v_{tr}:

$$v_{tr} = 2.78 \; (\sin 5.45 + \sin 2.09) \; /(5.45 + 2.09) = 1.53 \text{ m/s}$$

Next, the direction of the resultant tooth path can be calculated using Equation 11.51:

$$\theta_t = \arctan[(1.53 \sin 7.54)/(2.22 + 1.53 \cos 7.54)] = 2.97 \text{ radians or } 28.4°$$

(b) From Equation 11.52, the magnitude of the resultant tooth velocity is:

$$v_t = 1.53 \sin(7.54)/\sin(2.97) = 3.06 \text{ m/s}$$

(c) Next, from Equation 11.53, the average hay velocity is:

$$v_h = 2.22/[\cos(2.97) + \sin(2.97) + \cot(6.81)] = 1.22 \text{ m/s}$$

(d) The maximum length of the hay path, from Equation 11.54, is:

$$L_h = 2.4/\sin(2.97) = 5.1 \text{ m}$$

(e) Finally, the ratio of hay velocity to tooth velocity is:

$$v_h/v_t = 1.22/3.06 = 0.40$$

The maximum hay path length is over twice the swath width and the average travel speed of the hay is only 40% of the tooth velocity. The teeth impact the hay repeatedly in moving it into the windrow and thus the leaves of legumes can be lost if the hay is very dry during raking.

Power requirements for side delivery raking are small and data are sparse. ASAE Data D497 suggests the following power requirement for hay rakes:

$$P_{rake} = C_1 \; w_{rake} \qquad\qquad (11.58)$$

where P_{rake} = PTO power requirement for raking, kW
$\quad$ w_{rake} = rake width, m
$\quad$ $C_1 = 0.4$ kW/m for side delivery rakes, 2.0 kW/m for rotary rakes

11.2.5 Baling

Hay can be harvested as loose hay in stacks or as chopped hay, but baling is the most popular method of hay harvest. The two types of balers in popular use are *rectangular balers* (Figure 11.6) and *round balers* (Figure 11.7). Although the discussion in this chapter relates to baling of hay, the same machines are used for baling straw and other fibrous materials. The principles of compression and packaging are applicable to many non-forage materials.

11.2.5.1 Rectangular balers

Virtually all rectangular balers have the baling chamber oriented in the direction of travel of the baler. A windrow pickup unit feeds the windrow into a cross conveyor which, in turn, feeds the hay into the baling chamber. There are three types of cross conveyors. In one type, an auger conveys the hay to a set of packer fingers that sweep the hay into the bale chamber. In a second type, linear moving packer fingers travel the full width of the pickup in conveying the hay into the bale chamber. In the third type, rotating finger wheels move the hay laterally to the packer fingers. The bale chamber is fed from the side or from below in current balers. Feeding from the bottom allows the baler to travel directly behind the tractor. In all feeder designs, the packer fingers must be timed to the movement of the reciprocating plunger so that the fingers are out of the bale chamber except when the plunger is in a forward position.

As the feeder delivers each charge of hay, a knife on the edge of the plunger and a countershear at the rear edge of the feed opening shear off the charge of hay as the plunger moves rearward. Continued movement of the plunger compresses the charge of hay and pushes previously accumulated compressed hay through the bale chamber. Controlled convergence of the bale chamber (Figure 11.35) provides resistance to bale movement and thus controls bale density. Fixed wedges and spring-loaded dogs extend into the bale chamber and minimize re-expansion of the compressed hay during forward movement of the plunger. During compression, a star wheel at the top of the bale chamber (the leftmost star wheel in Figure 11.35a) is driven by the moving bale to trigger the tying mechanism when a bale of sufficient length has been formed. When the plunger reaches its rearmost position after the tying mechanism has been triggered, needles (visible at bottom of Figure 11.35a) move through slots in the plunger face to deliver twine or wire to the knotter. The knotter completes the knots and the needles retract as the plunger begins moving forward.
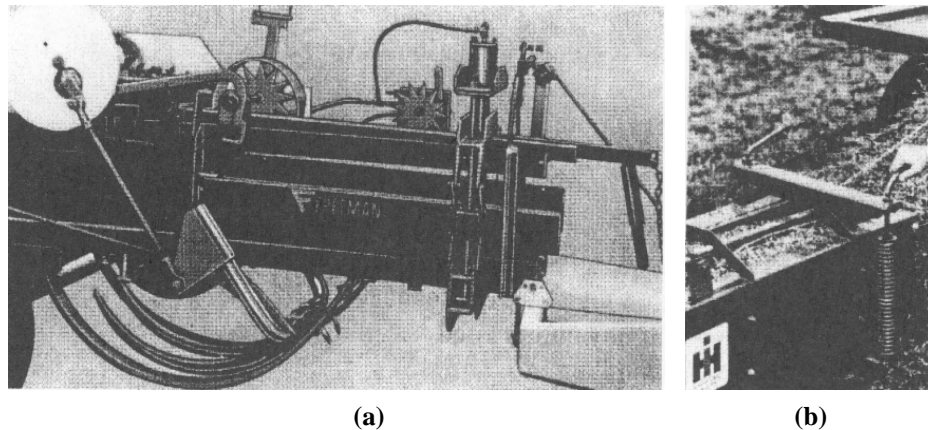

(a)   (b)

Figure 11.35 – Control of bale density (a) hydraulically and (b) with manually adjustable springs (reprinted from Kepner et al., 1978).

The density of hay in the bales is determined by the type of material being baled, its moisture content, and by the resistance provided by the convergence of the bale chamber. The convergence causes the hay to be compressed laterally as the bale moves through the chamber. Assuming the hay is an elastic material, the plunger force generated by convergence can be calculated using the following equation:

$$F_c = \frac{E_h y}{d_c} L_c w_c f_h \tag{11.59}$$

where F_c = compressive force supplied by plunger, N

E_h = effective modulus of elasticity of the hay, kPa

y = total convergence in converging section, mm

d_c = depth of bale chamber, m

L_c = length of converging section, m

w_c = width of bale chamber, m

f_h = coefficient of friction between hay and bale chamber

The quantity $E_h y/2d_c$ is the lateral pressure to compress the hay a distance y, and $2L_c w_c$ is the total area on which the lateral pressure acts assuming only two sides converge. Multiplying by the coefficient of friction gives the contribution of convergence to the plunger force. There will be some friction against the nonconverging sides. If all four sides converge, convergence of each pair of sides is usually controlled independently. In either case, the friction against all sides should be included in calculating F_c. Equation 11.59 is difficult to use to compute actual forces because of difficulty in determining values for E_h. However, the equation does provide insights into the problems of density control. Both E_h and f_h increase with moisture content of the hay, thus increasing the plunger force and the bale density. The tension-control springs in Figure 11.35b provide the lateral force for squeezing the bales in the convergence section. Hand cranks are provided to adjust the amount of spring tension and the tension must be adjusted to compensate for changes in moisture and crop. During operation, the springs extend when E_h increases and, although y declines, the lateral force increases. Zero-rate springs would be preferable and the equivalent effect is achieved by substituting a hydraulic cylinder to provide the convergence force (Figure 11.35a). The hydraulic pressure can be adjusted from the operator's station but remains at the set value, thus providing constant force. One large rectangular baler uses several load cells placed on the plunger face to monitor the compression force. The signals from the load cells are sent to a microprocessor. The microprocessor controls bale density by sending output signals to electrohydraulic valves that control oil pressure in hydraulic cylinders which regulate bale chamber convergence. The microprocessor system ensures uniform, constant bale density as crop conditions change.

Both twine-tie and wire-tie balers are available but the twine-tie balers are much more popular. ASAE Standards S229 and S315 provide specifications for baling wire and twine, respectively.

Figure 11.36 shows a twine knotter tying a bale. In a popular-sized baler, each bale is tied by two loops of twine and thus two knotters are included on the baler. When tying a bale, each knotter grips the cut end of its twine as the needles retract. As the
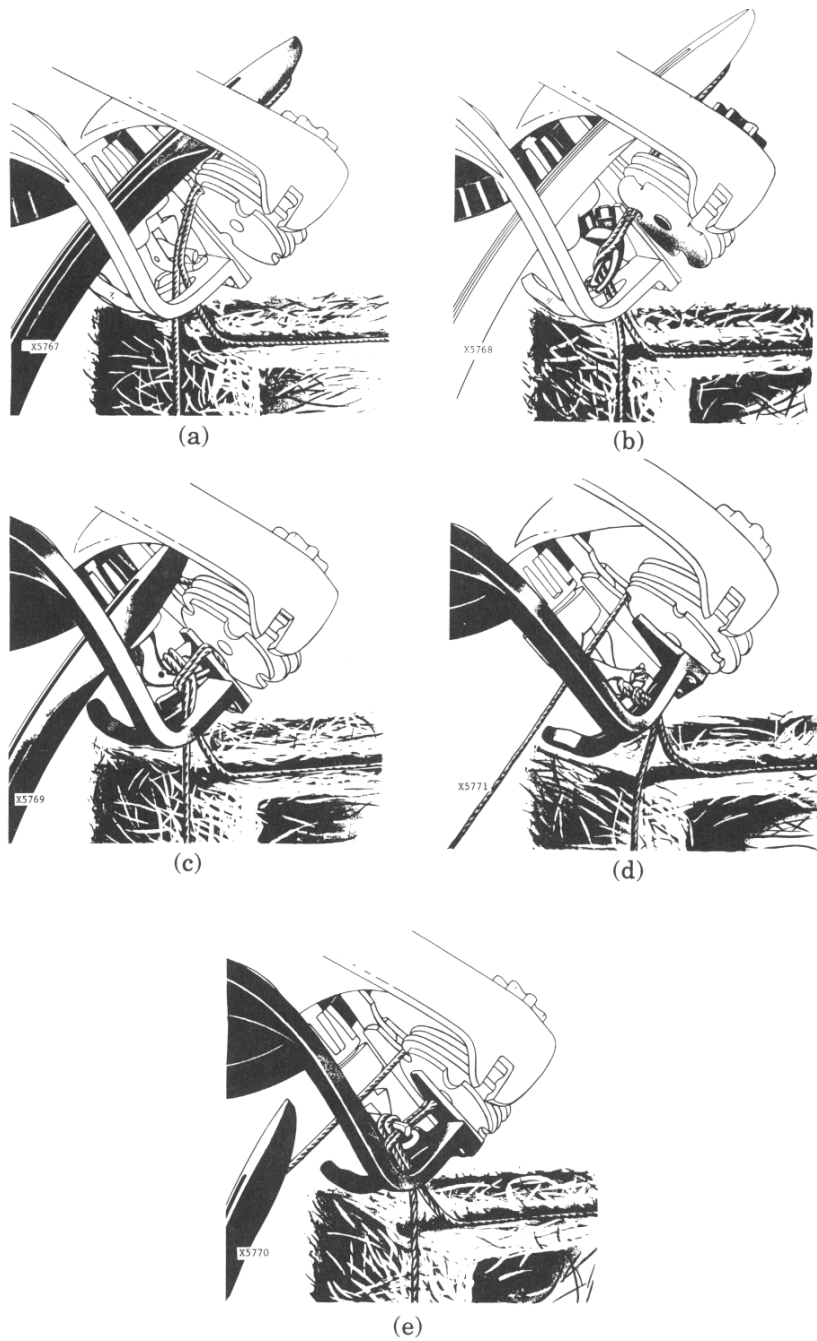
Figure 11.36 – Operation of a twine knotter (courtesy of Deere and Co.).

next bale advances through the chamber pushing the twine strands on its leading edge, twine is pulled from two twine balls though the needle eyes. When the bale tying mechanism is triggered by the star wheel through a limited-motion pawl clutch, the needles rise through the plunger slots, carrying the twine strands to the respective knotters. Figure 11.36a shows the start of the tying cycle. The needle has brought the twine around the bale and placed it in the twine holder. The two outside disks of the holder have rotated through the angle between adjacent notches while the center disk remained stationary, thus pinching the twine between the spring-loaded disks to hold it when the needle withdraws. The knotter-bill assembly in Figure 11.36b has begun rotating to form a loop in the string about the knotter bills. The loop is completed in Figure 11.36c, the knotter bills have opened and, with continued rotation, the bills close over the strings held by the twine holder. As the bills grip the strings, the knife attached to the stripper arm cuts the twine between the knotter and the twine holder, thus releasing the formed bale. The bills have gripped the strings and the knife has completed the cutting in Figure 11.36d and, in Figure 11.36e, the wiper has completed the knot by moving forward to push the loop from the bills over the twine held by the twine holder. Note that, in Figure 11.36d, the twine holder has already gripped the twine end for the next bale and continues to hold it while the current bale is being tied and the next bale is being formed.

Wires are tied around bales in a manner similar to that described above, except that the wire ends are twisted, not knotted. Thus a wire-tie baler has a wire twister instead of a twine knotter. Because of the greater tensile strength of wires, wire-tied bales can have greater density than string-tied bales.

The baling rate (in kg/s) can be limited by the rate at which forage is fed into the baler, by the design of the baler, or by available power. The following equation relates the first of these possible limits:

$$\dot{m}_f = \frac{d_c w_c \delta_s \rho_c \omega_c}{60} \qquad (11.60)$$

where $\dot{m}_f$ = baling rate or material feed rate, kg/s
  d_c = depth of bale chamber, m
  w_c = width of bale chamber, m
  δ_s = thickness of each compressed hay slice, m
  ρ_c = compressed density of hay in bale, kg/m^3
  ω_c = crank speed, rpm

A popular chamber size is w_c = 0.46 m and d_c = 0.36 m. However, much larger balers with chambers 1.2 m by 1.2 m are on the market and several intermediate sizes are also available. Densities of hay in bales, including moisture at time of baling, range from 130 to 225 kg/m^3 with the lower end of that range being the most popular. Use of low crank speeds limits capacity and increases stress loads. Tests by Burroughs and Graham (1954) have shown that, for a given feed rate and bale density, peak plunger force fell 20% as crank speed increased from 40 to 50 rpm but showed little decline with further increases in speed. Use of high speeds generates excessive inertia forces in the reciprocating plunger and causes greater losses of hay from the bale chamber. Practical crank speeds range from 45 rpm for some large balers to 100 rpm for smaller

balers. Each time the baler plunger moves rearward, it shears off the incoming hay and compresses the hay charge into a flake or slice. The flake thickness varies with the rate at which hay can be fed into the bale chamber. Typically, flake thickness is less than 20 cm. From Equation 11.60, for a baler with chamber dimensions of 36 by 46 cm, crank speed of 50 rpm, bale density of 225 kg/m^3, and flake thickness of 20 cm, the baling capacity would be 6.21 kg/s or 22.4 Mg/h. In NIAE (1965) tests of balers with the 36 by 46-cm bale chamber, rates as high as 22 Mg/h were recorded for short time periods, but maximum rates fell to 16.3 Mg/h for continuous tests.

Instantaneous crank torque varies widely on a baler and a flywheel is used to maintain a relatively constant crank speed; this also steadies the torque demand from the tractor PTO. Figure 11.37 shows two typical force-deflection curves for a baler plunger working with two different feed rates. The curves are similar except that compression starts earlier with the larger hay charge and the peak force is higher. The small peaks near 300 to 400 mm displacement are knife forces for shearing the hay charge; on most hay charges, these cutting peaks occur later and closer to the force
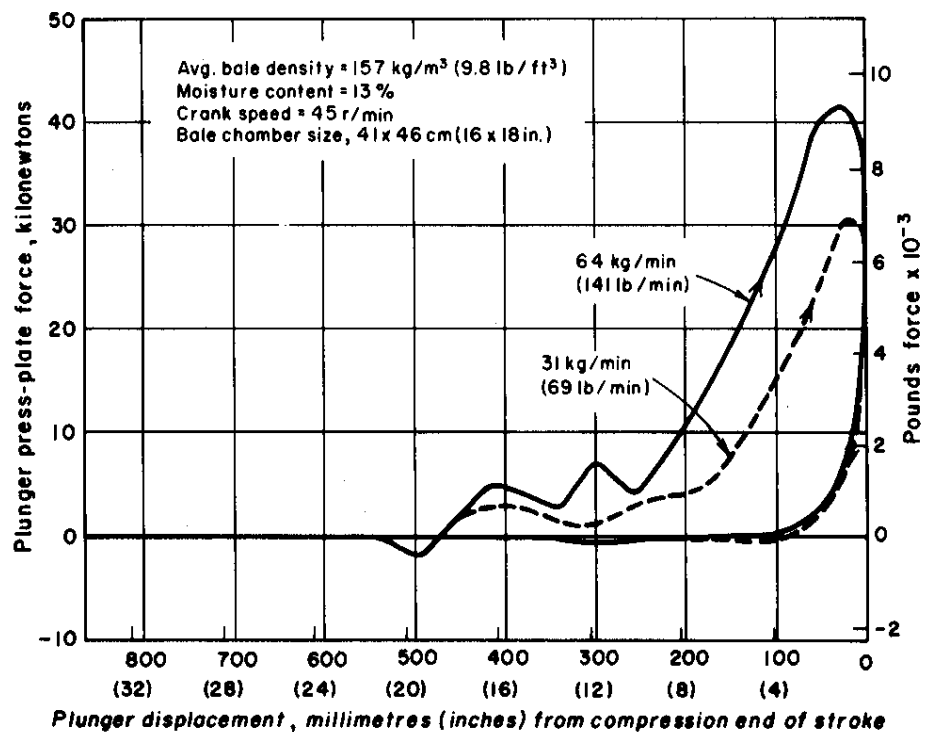
Figure 11.37 – Plunger work diagrams for two feed rates in alfalfa
(Burroughs and Graham, 1954).

peak. The force reaches a peak and begins declining when the hay compressed on ear-lier strokes begins moving in the chamber; the decline occurs because the sliding fric-tion is less than the static friction in the chamber. Both force curves merge after the plunger starts forward. The force is greater than zero during the first 100 mm of return travel only because the compressed hay re-expands somewhat. During the re-expansion, a small amount of potential energy in the compressed hay is returned to the plunger in the form of kinetic energy. A force-displacement curve (Figure 11.37) can be converted to a torque versus angular displacement curve for the crank. For any given crank angle, θ_c, the plunger displacement, x_p, can be calculated using the follow-ing equation from slider-crank theory (Figure 11.38):

$$x_p = r_c(1 - \cos\theta_c) + L_{cr} - \left(L_{cr}^2 - r_c^2 \sin^2\theta_c\right)^{0.5} \tag{11.61}$$

where x_p = plunger displacement, m (see Figure 11.38)
$\quad$ r_c = crank radius, m
$\quad$ L_{cr} = length of connecting rod, m
$\quad$ θ_c = crank arm displacement, radians

$\quad$ For the x_p corresponding to each θ_c, a force-displacement curve similar to the one in Figure 11.37 can be used to find the corresponding plunger force. Then the instan-taneous torque at that crank angle is given by the following equation:

$$T_c = \frac{-\dot{x}_p}{\dot{\theta}_c} F_p \tag{11.62}$$

where T_c = torque in crank arm, N·m
$\quad$ F_p = force on plunger, N

$\quad$ and $\qquad\qquad \dfrac{\dot{x}_p}{\dot{\theta}_c} = r_c \sin\theta_c \dfrac{r_c \sin\theta_c \cos\theta_c}{\left(\dfrac{L_{cr}^2}{r_c^2} - \sin^2\theta_c\right)^{0.5}}$ $\qquad\qquad$ (11.63)

where $\dot{x}_p$ = plunger speed, m/s
$\quad$ $\dot{\theta}_c$ = crank speed, radians/s (note: $\dot{\theta}_c = \omega_c\, 2\pi/60$)
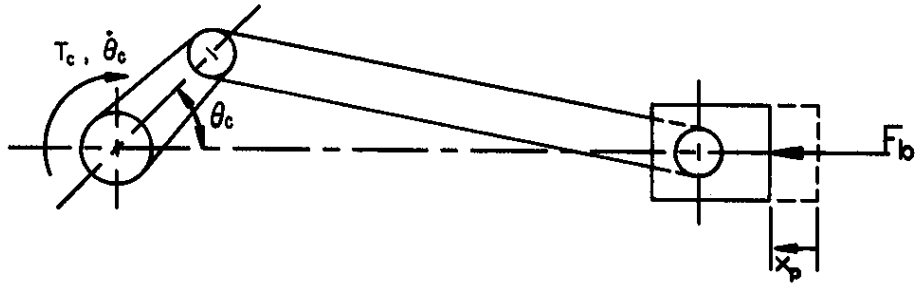
Figure 11.38 – Diagram of a slider-crank mechanism in a baler.

Figure 11.39 is an illustration of instantaneous crank torque. The small peak on the left is the cutting peak. The data representing instantaneous torque as a function of crank angle can be integrated numerically to obtain the average torque. The average torque, T_{cave}, that must be supplied by the engine is shown by the dashed line across the peak. The cross-hatched area represents energy that must be supplied by a flywheel when the instantaneous torque exceeds the torque output supplied by the engine. The required flywheel size can be calculated using the following equation:

$$I_f = \frac{\Delta E_k}{R_s \, \dot{\theta}_{cave}^2}$$
(11.64)

where I_f = mass moment of inertia of flywheel, kg m^2

ΔE_k = kinetic energy required from flywheel, J (see Figure 11.39)

R_s = speed regulation = (max speed – min speed)/average speed

$\dot{\theta}_{cave}$ = average crankshaft speed, radians/s, = (max speed – min speed)/2

The average power required to operate the plunger can be calculated from the product of the average torque and speed at the crankshaft. It can be shown that the average torque is proportional to the area within the plunger force-displacement diagram (Figure 11.37). Note that the average torque and thus the average power requirement increase with the feed rate. The power required by the pickup, conveyors, and packer also increase with feed rate (see Figure 11.40). The equation for the PTO power requirement of a baler thus has the following form:

$$P_{baler} = C_0 + C_1 \, \dot{m}_f$$
(11.65)

where P_{baler} = PTO power requirement of baler, kW

$\dot{m}_f$ = feed rate, kg/s

C_0, C_1 = constants that vary with baler design, type and moisture content of material being baled. Units are kW for C_0 and kW s/kg for C_1.
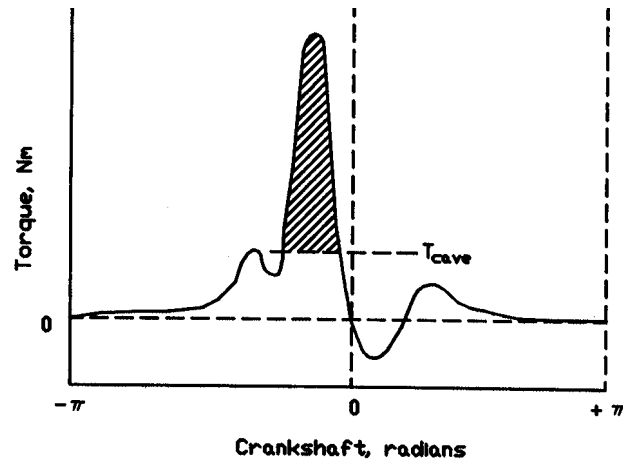
Figure 11.39 – Instantaneous torque in the crank arm.
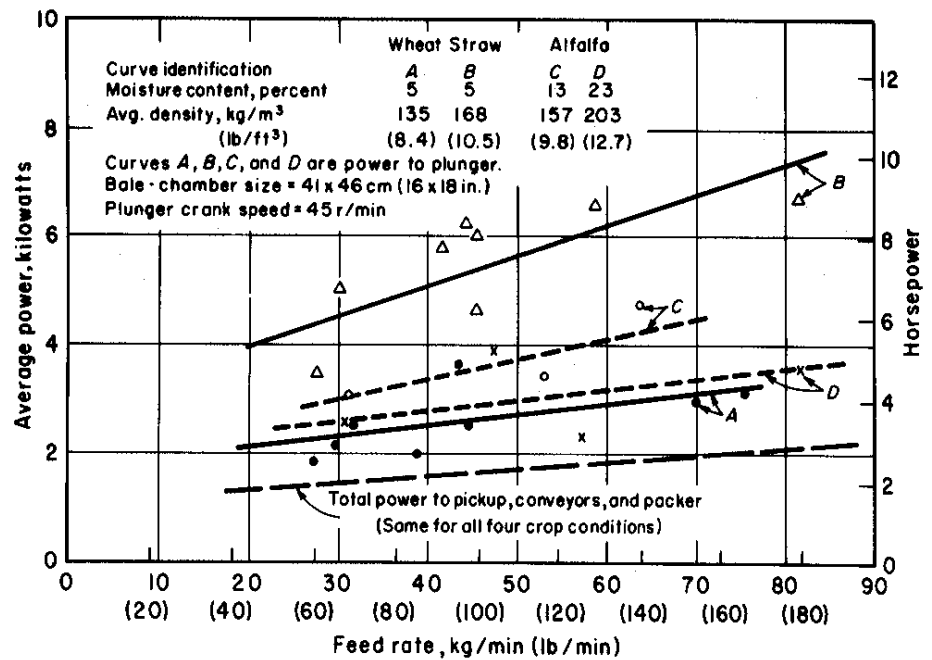
Figure 11.40 – Relation of average power requirements to baling rate (Graham, 1953).

Values for constants C_0 and C_1 can be determined from field tests of balers. From Figure 11.40, for example, values for (C_0, C_1) are (1.75, 1.17), (2.84, 3.37), (1.88, 2.23), and (1.97, 1.23) for curves A, B, C, and D, respectively. ASAE Data D497 suggests values of (2, 3.6) and (4, 4.7) for small and large rectangular balers baling hay, respectively. Calculation of baler capacity and power are illustrated in Example Problem 11.8.

Example Problem 11.8

A rectangular baler with chamber cross section of 0.36 m by 0.46 m is operated at a crank speed of 70 rpm. The feed rate is such that the thickness of each compressed slice is 0.15 m and slice density is 180 kg/m^3. Power constants are $C_0 = 2$ kW and $C_1 = 3.6$ kW s/kg. Calculate (a) the baler capacity and (b) the power requirement.

Solution
(a) From Equation 11.60, the capacity is:

$$\dot{m}_f = 0.36(0.46)(0.15)(180)(70)/60 = 5.2 \text{ kg/s or } 19 \text{ Mg/h}$$

(b) The baler conforms to varying feed rates by changing the slice thickness. For example, if the feed rate is increased by increasing the travel speed along the windrow, the slice thickness increases accordingly. The power requirement for the entire baler is:

$$P_{baler} = 2 + 3.6(5.2) = 21 \text{ kW}$$

Most of the power is used in driving the plunger.

11.2.5.2 Round balers

Machines to make large round bales (Figure 11.7) entered the marketplace in 1971. Early machines employed a variety of techniques for forming bales, including use of variable-geometry chambers (Figure 11.41), fixed-geometry chambers (Figure 11.42), and chambers without a floor (not shown) in which the forming bale is rolled on the ground. A pickup similar to those on rectangular balers but smaller in diameter is used to convey the windrow into the baler. When the windrow is narrower than the bale chamber, a certain amount of weaving is required by the operator to deliver hay to the full width of the chamber.

The variable-geometry chamber of Figure 11.41 is the most widely used design; it creates a bale of nearly uniform density whereas the other types create bales with a low-density core. In the design of Figure 11.41, a group of parallel, flat belts form the chamber. Typically, the belts are each 100 to 150 mm wide and have 50 to 100 mm wide spaces between them. The rollers on spring-loaded idler arms retract and allow the chamber to enlarge as the bale grows to full size. Power must be supplied to the chamber belts so that the moving periphery of the chamber will rotate the incoming

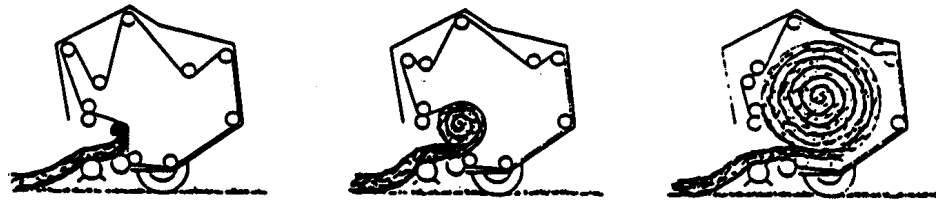**Figure 11.41 – A round baler with variable geometry
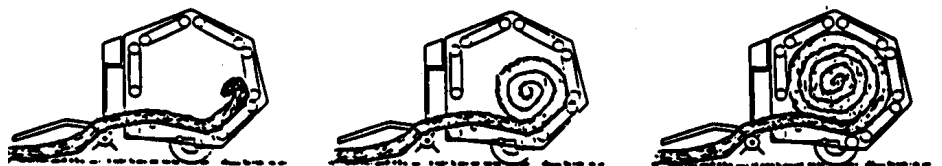(courtesy of Prairie Agricultural Machinery Institute, Canada).**

**Figure 11.42 – A round baler with fixed geometry
(courtesy of Prairie Agricultural Machinery Institute, Canada).**

hay and cause it to form into a tight roll. Peripheral speeds of the belts and floor conveyor typically range from 1.3 to 2.8 m/s. The chamber forms a bale with a low-density core. As additional layers are added, the density increases and is controlled by the belt tension. When the bale reaches the desired diameter, the operator stops forward motion and engages a wrapping mechanism as the bale continues to rotate. A manual or powered traversing guide spaces twine wraps at 150 to 200 mm intervals across the face of the bale. The twine is not tied; the twine end is inserted into the chamber, wraps on the bale as it rotates, is cut and left with a free end when the bale is completed. On some balers, dual-tying mechanisms allow both ends of the bale to be tied simultaneously for faster tying. As an alternative to tying with twine, the baler may be equipped with facilities for wrapping the bales in a full-width plastic netting. Only 1.5 to 2.5 turns of the bale are needed to wrap with netting, compared to 10 to 20 turns to wrap with twine. The netting gives the exterior of the bale a more closed structure, thus reducing leaf loss and improving weatherability compared to twine-wrapped bales. Although the netting is more expensive than twine, the improved productivity from faster wrapping, coupled with the reduced losses and improved weatherability, generally offset the higher cost of the netting. After tying, the operator backs the baler approximately 6 m and raises the tailgate to eject the completed bale onto the ground. The baler is moved ahead 6 m before lowering the tailgate to allow the gate to clear the discharged bale and then baling resumes.

Typical bale dimensions are 1.22 to 1.52 m in width and 1.22 to 1.83 m in diameter. Average densities range from 100 to 240 kg/m^3, giving bale masses ranging from 320 to 1050 kg per bale. Bale density varies with belt or chain tension and with belt-to-ground speed ratio. Increasing the belt speed relative to the ground speed causes thinner layers to enter the chamber and thus produces more dense bales. Good judgment must be used when ejecting bales on sloping land; ejecting bales while traveling up or down slope can allow the bales to roll downhill with great destructive potential.

Maximum instantaneous harvesting capacity of a large round baler is a product of the size of the windrow (in kg/m) and the allowable forward speed of the baler. Forward speed is typically limited by the pickup, i.e., pickup losses become excessive at very high speeds. Average travel speeds are generally in the range from 5 to 13 km/h, but speeds up to 19 km/h have been observed. Average capacity is reduced by the time lost in tying and discharging a bale. Depending upon the windrow size, formation of a bale can take from 1 to 15 or more minutes. The tying and unloading cycle typically requires about 1 minute with twine wrapping. Baling rates, accounting for the wrapping and unloading cycle, can reasonably reach 15 to 20 Mg/h. Since power requirements stay relatively high throughout the bale-forming process, the energy use per bale increases with the time required to form a bale (Figure 11.43). Thus, to save energy, it is advantageous to form the bales as quickly as possible.

Power requirements for operating a large round baler include PTO power to form and discharge the bales, and drawbar power to propel the baler. The PTO requirements follow the characteristic curve of Figure 11.44, in which point A is the end of the bale-forming cycle and point B is the end of the tying cycle. The PTO power requirements when the baler is running empty are typically 2 to 4 kW, but increase as the bale forms as shown in Figure 11.44. With a full bale in the chamber, PTO power requirements

range from 12 kW to 55 kW depending on bale density and baler design. Drawbar power requirements depend heavily on field conditions as well as bale size. On firm, level fields, drawbar requirements typically range from 2.5 to 10.5 kW but the requirements can increase by 50 kW in soft, hilly fields.
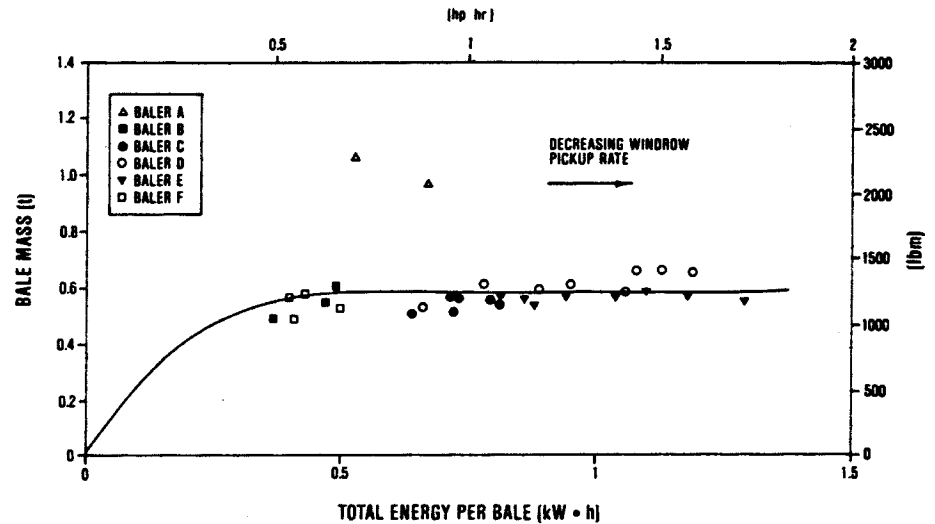

Figure 11.43 – Cumulative bale mass versus energy required to form a bale (Freeland and Bledsoe, 1988).
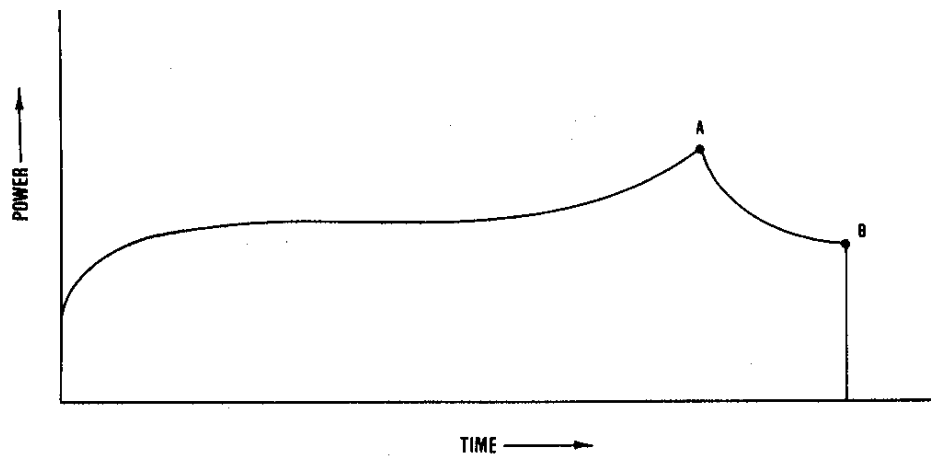

Figure 11.44 – Characteristic power curve of a variable-geometry baler (Freeland and Bledsoe, 1988).

11.3 PERFORMANCE EVALUATION

Techniques for evaluating performance can be specific to a particular machine and a wide variety of machines are used in hay and forage harvesting. For any machine, however, three types of evaluation are generally included. These are measurement of capacity, power requirements, and quality of the finished product. The Prairie Agricultural Machinery Institute (PAMI) of Humboldt, Saskatchewan, Canada, conducts independent tests of various farm machines under sponsorship of several Canadian provinces. The PAMI reports are an excellent source of performance data on selected hay and forage harvesting equipment.

Capacity measurements can be on the basis of area covered per unit time (in ha/h) or of material processed per unit time (in Mg/h). The amount of area that can be covered in unit time is called *field capacity* and is a product of the processing width and speed of the machine. Since width and speed are easily measured, field capacity measurements are not complex. For machines such as mowers, rakes, mower-conditioners, or windrowers, where the forage receives a minimum of processing, the material handling capacity is not important and only the field capacity is measured. Conversely, the *material handling capacity* is very important for forage harvesters or balers. Material handling capacity is the maximum feed rate that can be accommodated on a sustained basis. Forage harvester feed rate is the product of mass processed per unit travel distance (for example, in kg/m) times the forward speed of the harvester. The mass per unit distance can be measured before the material enters the harvester or as it leaves. As indicated by Equation 11.25, the former method involves measuring the crop yield and effective width processed by the harvester. In the latter method, the chopped material can be caught in a container for a given travel distance and then weighed. Baler feed rate can be determined by measuring the average time required to produce a bale and weighing to determine the mass in an average bale.

Power requirements of a machine include rotary power transmitted through the PTO shaft and drawbar power to propel the machine. Rotary power is the product of shaft speed and shaft torque. Accurate measurement of shaft speed can be accomplished by positioning a magnetic pickup to detect passage of teeth on a gear attached to the shaft in question. Digital data loggers are available for recording the tooth passage frequency, from which the shaft speed can be determined. Measurement of torque generally involves measurement of the deflection in a given length of shaft; since shafts are designed to work within their elastic range, the deflection is proportional to the shaft torque. From strength of materials theory, shaft torque causes both tensile and compressive strains to appear on the shaft surface (see Figure 11.45). Electric resistance or semiconductor strain gages can be attached to measure these strains and thus to measure the shaft torque. By proper positioning of the speed and torque transducers, the power demand of the various components of the machine can be measured during operation. When measuring power, it is important to simultaneously measure the other variables that affect the power requirement. Since feed rate affects the power requirement of forage harvesters and balers, the feed rate should always be measured and reported with power measurements. The moisture content of the forage should
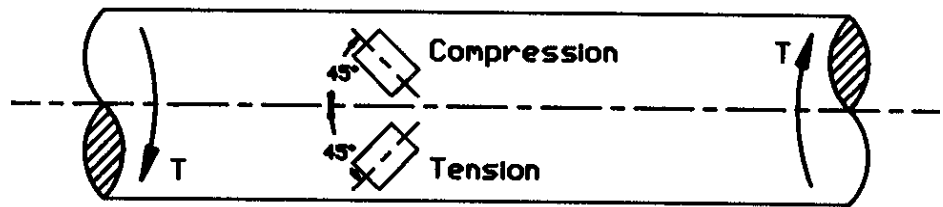
Figure 11.45 – Use of strain gages to measure shaft torque.

also be reported. Finally, values for all relevant machine parameters should be reported. In the case of a forage harvester, for example, the condition of the cutter knives has a large influence on the power requirement of the cutterhead. Drawbar power required to propel hay and forage machinery is usually much less than PTO power and is not always reported. If drawbar power is to be reported, it can be determined by measuring travel speed and drawbar pull. Radar units are available as optional or standard equipment on many tractors and can be used to determine travel speed. As in the case of torque measurement, strain gages can be used to make a drawbar force transducer and such transducers are commercially available.

Relevant measures of quality vary with the type of machine. As examples, uniformity of stubble height may be measured for sickle bar mowers, while length of cut is important for forage harvesters. ASAE Standard S424, which has been adopted by ISO as a technical report, provides methods for determining and expressing particle sizes of chopped forage. ISO Standard DP8909-1 deals with procedures for testing forage harvesters.

Forage loss is an important parameter for all of the machines. Koegel et al. (1985) used rolled plastic to evaluate losses. Plastic sheets 3.7 m in width by 30 m in length were folded along the length to a width of 2.2 m and rolled onto spindles. A spindle was attached to a mower-conditioner and, as the plastic was unrolled during operation, the swath was deposited on the plastic. Hedge shears were used to cut and a pitchfork was used to carefully remove sections of the swath. Material remaining after the swath was removed was gathered and weighed to determine mower-conditioner loss. Next, the part of the plastic sheet that was folded underneath was pulled out and the plastic was staked at its full 3.7 m width to provide space for raking on plastic. Again, hedge shears were used to cut and a pitchfork was used to remove sections of the windrow. Material remaining after windrow removal was gathered and weighed to determine mowing plus conditioning plus raking losses. Finally, a baler was used to bale the windrows from the plastic. Additional materials deposited on the plastic were attributed to baler losses. The technique did not permit separation of pickup and chamber losses from the baler. Minor damage sustained by the plastic during raking and baling was repaired with tape. The above method used by Koegel et al. (1985) may overestimate losses. One alternative to using plastic is to hand-pick losses from the ground in small (0.25 to 0.5 m^2) sampling frames placed in representative areas of the field. Buckmaster (1993) used artificial stubble put in place after mowing to measure subsequent harvester loss.

Length of cut is often measured when evaluating forage harvesters. Since 1 kg of chopped forage may contain over 500,000 pieces, a mechanical means of length analysis is essential (O'Dogherty, 1982). Sieving is the most common method used for length analysis, i.e., the chopped forage is passed through a series of sieves with increasingly smaller openings. A given sieve contains those lengths that passed through the sieve above but would not pass the given sieve, and the mass of that fraction is determined by weighing. The sieves must be able to size pieces which are long in relation to their cross-sectional dimensions, i.e., length to diameter ratios range up to 50:1. Sieves are oscillated to promote movement of the material; by keeping the screens horizontal and using a horizontal oscillation, the possibility of endwise movement of forage through the sieves is minimized. ASAE Standard S424 gives specifications for a lab standard sieving device. Kononoff et al. (2003) developed a simpler device commonly used on farms to determine forage and total mixed ration particle size distribution (Figure 11.46)

Figure 11.46. – Sieve set used to assess particle size distribution in forages and total mixed rations (Kononoff et al., 2003).

GRAIN HARVESTING

12

12.2.4.3 Cleaning performance

The performance of a cleaning shoe is expressed in terms of (1) grain loss or cleaning efficiency, (2) cleaner capacity, and (3) grain dockage. *Grain loss* is calculated by determining the percentage of lost grain on the basis of the total grain entering the cleaning shoe. The *cleaning efficiency* is the percentage of grain recovered by the shoe. The *cleaner capacity* is determined by first plotting a curve of grain loss against the material other than grain (cleaner MOG) feed rate passing through the cleaning shoe. A curve is fitted to the data, usually an exponential function, and the capacity of the cleaning shoe is determined corresponding to a given grain loss level. *Grain dockage* is the amount of chaff that is separated with grain. It is determined by taking a sample of grain from the grain tank of the combine and cleaning the sample to determine the percentage of chaff in the sample.

The cleaning shoe performance is affected by the following factors:
- Design factors such as sieve size, oscillation amplitude and frequency.
- Operating conditions including material feed rate, cleaning shoe slope, air flow, and chaffer openings.
- Crop properties including grain to MOG ratio, chaff and grain properties.

Design factors. Longer sieves would allow longer dwell time for more complete separation of grain. However, physical considerations limit the size of the cleaning shoe. Studies have indicated that the initial sieve length does not contribute much to the cleaning action. A cascade arrangement permits a more complete cleaning while keeping the length of the sieves short. The frequency and the amplitude determine the level of acceleration imparted on the crop. This determines the level of agitation necessary to provide the least resistance to grain separation. The material flow rate is also determined by these parameters. German and Lee (1969) reported on the effects of the frequency of oscillation on the shoe performance. The range of frequencies used were 260 to 460 cpm. Increasing the frequency of oscillation at 90 kg/min input rate reduced the grain loss significantly. However, they did not recommend increasing the frequency because of the increased mechanical vibrations.

Operating conditions. German and Lee (1969) also studied the effect of air volume on cleaning performance. The air volume has to be matched with the feed rate. They developed a relationship between the air volume and the debris found in the grain sample as follows:

$$Z = 2 - 50 \times 10^{-6} V + 0.4 \times 10^{-9} V^2 \tag{12.18}$$

where Z = amount of debris, kg/min

V = air flow rate, m^3/min

Bottinger and Kutzbach (1987) reported on the effect of fan speed and feed rate. Their results are shown in Figure 12.32. As shown in the figure, the grain loss increases somewhat exponentially with the fan speed and feed rate. Nyborg et al. (1969) found that the cleaning losses increase with MOG feed rate and with grain/straw ratio. The results are shown in Figure 12.33. As shown in the figure, the effect of feed rate becomes more significant at high grain/straw ratios and vice versa. Increasing the lip angle from 30° to 36° reduced grain loss according to a study reported by Lee and Winfield (1969). The lip angle effect is highly dependent on other factors such as the material feed rate.
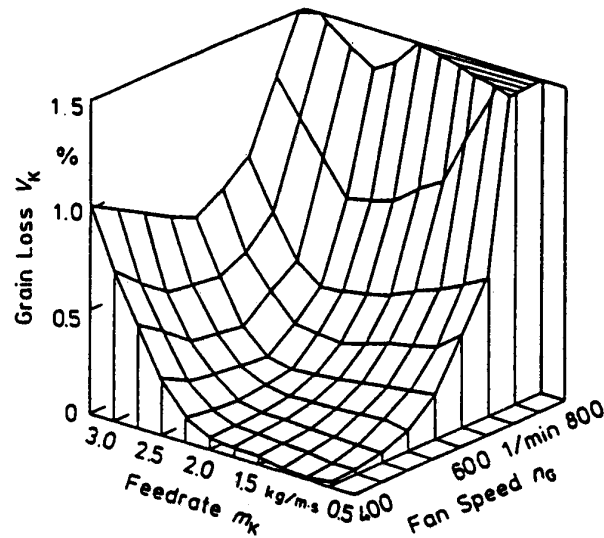
**Figure 12.32 – Performance characteristics of a cleaning shoe
(Bottinger and Kutzbach, 1987).**
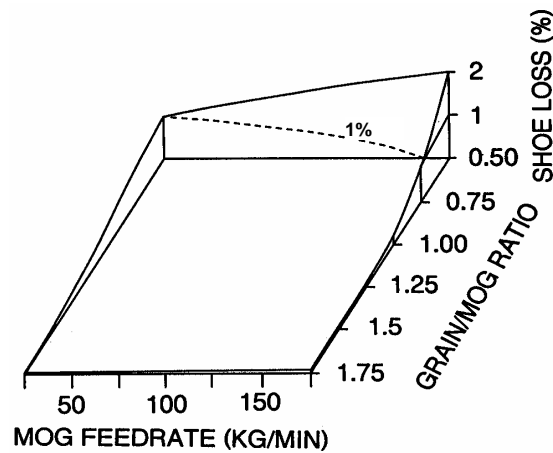
**Figure 12.33 – Shoe-loss surface for a standard combine in wheat
(Nyborg et al., 1969).**

   Crop properties. Srivastava et al. (1990) studied the effect of chaff and grain prop-
erties of wheat and barley on the capacity of the cleaning shoe. They found that the
grain angle of repose had a negative effect on the cleaner capacity. Increasing the
chaff friction also decreased the capacity. Increasing grain density increased the
cleaner capacity. Increasing chaff mean length tended to reduce the cleaner capacity.
Both grain and chaff moisture tended to decrease the cleaner capacity. Increasing
grain-to-MOG ratio decreased cleaner capacity.

12.2.5 Power requirements

Rotz et al. (1991) reported a simplified method for estimating rotary power requirements for agricultural machines by the following equation:

$$P_r = a + c\,F \tag{12.19}$$

where P_r = rotary power required, kW

F = material throughput rate, t/h

a, c = machine-specific parameters

Use a = 20 kW and c = 3.6 kWh/t for small grain self-propelled combines. The material flow rate is based on MOG flow rate. To estimate power for grain corn use a = 35 kw and c = 1.6 kWh/t. The throughput rate for corn is based on grain flow rate. For PTO-driven combines the value of parameter a should be reduced by 10 kW. A variation of as much as 50% can be expected in the value of b depending on the crop and the harvesting conditions.

If F is set equal to zero, Equation 12.19 can be used to estimate no-load or propulsion power. The cylinder generally accounts for a large portion of the total power. Power requirements for the separation and cleaning units are small and relatively independent of material flow rate. Short-time peak power requirements for the cylinder may be two to three times as great as the average requirement.

12.3 COMBINE TESTING

Combine testing is performed in the field as well as in the laboratory. Laboratory testing has the advantage of uniform crop and better control on test conditions. However, the crop has to be stored and that may cause changes in its properties, which affect the performance characteristics of the component being tested. The test engineer has to be aware of this.

The objectives of combine testing are to determine the performance characteristics of its functional components, power requirements, and durability. Only functional testing is discussed in this book. The objective of functional testing is to determine grain losses and capacity. Grain losses are expressed as percentages of total grain entering the combine. The capacity of a functional component is expressed as the MOG feed rate (t/h) through that component at a certain grain loss level.

Combine losses are divided into (1) header losses, (2) threshing losses, (3) separation losses, and (4) cleaning losses.

Header losses include lodging, shatter, and cutterbar loss. Lodged crop not cut by the cutterbar is considered lodging loss. Shatter loss is the grain that falls to the ground as the grain head is shattered due to the impact by the reel. Cutterbar loss is the cut grain heads that fail to land on the platform. The header losses may be expressed as kg/ha or as percentage of the crop yield. To determine the header losses, the combine is driven in the field and when the steady state operation is achieved, the combine is stopped. The combine is backed up a distance less than or equal to the longitudinal distance between the cutterbar and the discharge chute at the rear of the combine. A sample area is marked off in front of the combine and the losses collected from that area. Uncut grain heads still on the crop are considered lodging losses. Loose grain is considered shatter losses and the cut grain heads are considered cutterbar losses.

Threshing or cylinder losses are those unthreshed grain heads that escape the combine at the rear with straw and are expressed as the percentage of total grain entering the combine.

Separation losses, also called walker losses in conventional combines, are lost grain with straw expressed as the percentage of total grain entering the combine.

Cleaning losses, also called shoe losses, are the grain lost with chaff expressed as the percentage of the total grain entering the combine.

Discharge losses are the sum of threshing, separation, and cleaning losses. These losses are affected by the material-other-than-grain (MOG) flow rate through the machine. The plot of these losses at different MOG feed rates is referred to as the *machine performance curve*. The capacity of a functional component is the MOG feed rate at a certain loss level. This loss level is 1% to 2% for the separator capacity and 0.5% to 1% for the cleaner capacity.

To determine the discharge losses in field material, discharges from the separator and the cleaner are collected separately. A simple method of collecting the sample is to hang a canvas bag at the appropriate discharge chute at the rear of the combine. The combine is run in the field and when the steady state operation is reached the bag is opened to collect the material. At the same time, grain coming out of the clean grain auger is collected at the grain tank. When the bag is full it is closed and the sampling time is recorded. The material is weighed and the MOG flow rate is established. The grains are separated from the collected MOG and their percentage is computed. The procedure is repeated several times at different combine forward speeds and a curve is plotted as in Figure 12.34. To determine threshing losses the MOG collected from the separator is re-threshed in a stationary thresher after determining separator losses. Re-threshed grains are then separated to find cylinder losses. The separator and cleaner losses are often plotted against their own MOG feed rate rather than the total machine MOG feed rate. In this case it is necessary identify it as the separator MOG (primarily straw) and the cleaner MOG (primarily chaff). Various manufacturers have developed automated methods that save time and increase accuracy in developing loss curves.
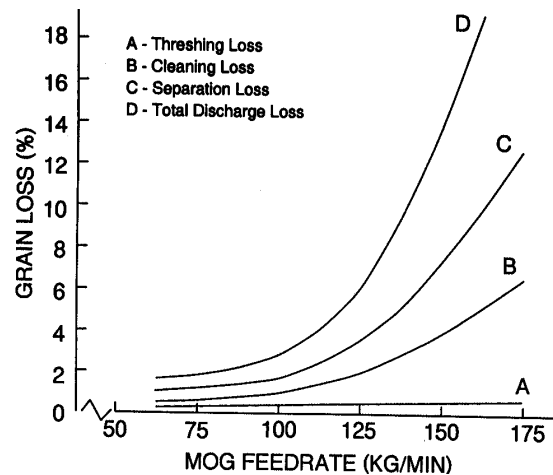

Figure 12.34 – Typical combine performance curves.

FRUIT, NUT, AND VEGETABLE HARVESTING

13

13.3 THEORETICAL CONSIDERATIONS

Several principles have been successfully utilized in solving mechanization problems in fruit, vegetable, and nut harvesting. Appropriate engineering analyses are often used to explore the feasibility of a possible design solution or understand why an existing machine element or process functions. In each section that follows, important problem conditions are stated along with the necessary assumptions for the theoretical analyses and definitions of all engineering variables.

13.3.1 Aerodynamic concepts

Often it is possible to effect an operational result based upon one physical parameter by implementing another. This concept is useful and effective as long as a high correlation exists between the operational property and the desired result. For example, the size of an object is often used to effect a separation of product by mass. Similarly, the color of product is used to indicate ripeness or maturity. The choice of physical property to utilize in the machine function is dependent upon several factors. First is the relative ease of implementation. It is much easier to subject products to sizing by falling through a dimensionally controlled opening, than to effect a mass balance measurement of each item. Secondly, the two properties must be in fact significantly related. In some cases this relationship is functional as in the case of physical size and weight where the product density is known to be constant or nearly constant. Thus, it is a common and accepted design practice to utilize a strongly related property to effect a unit operation based upon another property.

13.3.1.1 Aerodynamic properties of strawberries

Cleaning the leaves, severed stems, straw, and other lightweight trash from harvested strawberries depends upon being able to introduce the unsorted materials into an air flow field that has an average flow velocity component lower than the relative terminal velocity of the berries, but higher than the relative terminal velocity of the lighter materials.

Terminal velocity in air (V_t) is defined as the maximum free-falling velocity that is achieved by a body subject to gravitational acceleration. Relative terminal velocity in air (V_r) is defined as the velocity of air in a uniform flow field that, when directed vertically upward, will suspend or "float" a body that is subject to gravitational acceleration. Thus, the free-falling terminal velocity of a strawberry will be different from the average upwardly directed air velocity necessary to suspend a berry in mid-air within that flow field. The preferred units for both terminal and relative terminal velocities are meters per second.

In practice, terminal velocity can be measured by determining the time of free-fall from a given height as determined by Equation 13.1 (Bilanski et al., 1962):

$$S = \frac{V_t^2}{g} \ln \left[\cosh \left(\frac{g\,t}{V_t} \right) \right] \tag{13.1}$$

where S = free-fall distance, m
  V_t = terminal velocity in still air, m/s
  g = gravitational acceleration, 9.807 m/s^2
  t = time to free-fall a distance S, s
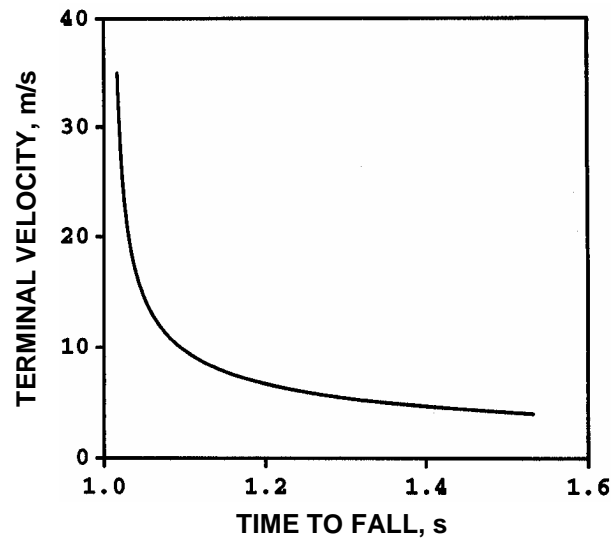
Figure 13.33 – Relationship between the terminal velocity of an object and the time to fall for a given drop height (Bilanski et al., 1962).

Equation 13.1, for a free-fall height of 5 m, is shown graphically in Figure 13.33. If the terminal velocity exceeds about 15 m/s, then the drop height must be increased above practical limits. Alternatively, the relative terminal velocity must be considered by establishing an airflow field with an average velocity that suspends the body. Often this process is complicated by the fact that the suspended body rotates or otherwise becomes unstable, thus making experimental observation of relative terminal velocities difficult.

The factors affecting the relative terminal velocity are the berry mass and the drag coefficient. The drag coefficient is a function of berry shape, size, and surface characteristics, as well as the Reynolds number of the fluid flow field. DeBaerdemaeker and Segerlind (1974) combined the technique of free-falling time measurement with a flow field that had an average upward velocity somewhat less than the terminal velocity of

**Table 13.1. Regression analysis coefficients for relative terminal velocity
(V_r) as a function of strawberry mass (m) for various maturities.**

$V_r = a + b \, m^{0.5}$			
Maturity	Mass, g	a	b
Green	1–11	9.52	2.51
White	2–12	10.18	2.52
White-pink	2–16	10.43	2.39
Pink	2–16	11.18	2.16
Red	3–19	11.98	1.92
Overall	1–19	10.08	2.53
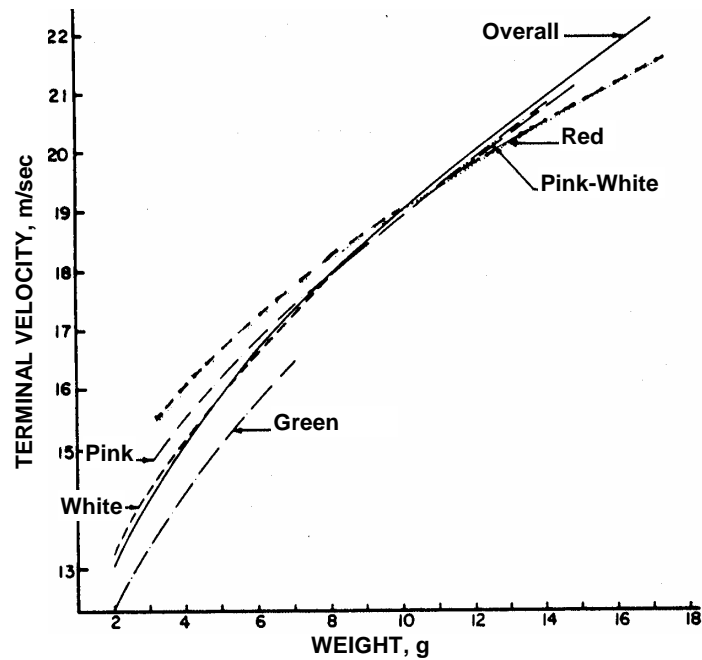
**Figure 13.34 – Terminal velocity of strawberries by mass for five color groups
(DeBaerdemaeker and Segerlind, 1974).**

the body to be measured. Thus, they were able to experimentally determine the relative terminal velocities of strawberries as a function of mass as given by:

$$V_r = a + b \, m^{0.5} \tag{13.2}$$

where V_r = relative terminal velocity, m/s

a, b = coefficients from Table 13.1

m = mass of individual berry, g

Table 13.1 gives the values of the coefficients a and b that were derived from experimental data and these computational results are shown in Figure 13.34. Clearly seen in this figure, the stage of ripeness has much less effect on relative terminal velocity than does the berry mass. With the exception of the green berries, little effect can be seen due to stage of ripeness.

13.3.1.2 Aerodynamic properties of blueberries

Low-bush blueberries are harvested by stripping the plants using either hand-held rakes (combs) or by a mechanized system of rakes. Both methods require removal of trash and leaves, which is most often achieved with the use of a vertical, upwardly directed air stream. If the mean velocity of the air stream is somewhat less than the relative terminal velocity of the berries, then the lighter trash with a lower relative terminal velocity will be removed. Since blueberries are nearly spherical, the drag coefficient can be expected to be nearly constant at 0.44 for fully developed turbulent

flow ($N_{Re} > 103$). Soule (1970) reported mean drag coefficients (C_d) between 0.483 and 0.525, depending upon berry shape. Berry suspension occurs in the air stream when the drag force (F_d) is equal to the force due to gravity reduced by buoyant effects (F_g) as given by:

$$F_d = C_d A_b \rho \frac{V_r^2}{2} \qquad (13.3)$$

and

$$F_g = g\, m_b \frac{\rho_b - \rho}{\rho_b} \qquad (13.4)$$

Combining Equations 13.3 and 13.4, the general equation for the relative terminal velocity becomes:

$$V_r^2 = 2g\, m_b \frac{\rho_b - \rho}{\rho_b \rho\, A_b C_d} \qquad (13.5)$$

where C_d = coefficient of drag, dimensionless
   A_b = berry cross-sectional area perpendicular to the air flow direction, m^2
   ρ = density of air, kg/m^3
   ρ_b = density of berry, kg/m^3
   m_b = mass of berry, kg

Example Problem 13.1

It is necessary to design a leaf removal station for a red tart cherry harvester using an upwardly directed vertical air stream. What is the maximum average air velocity needed to accomplish this function? Would you expect this cleaner to remove the very small cherries if they were also present, and why?

Solution
It is necessary to assume that all fruit and leaves are single, and that if stems are present their effects can be neglected. Furthermore, we assume that red cherries are similar enough in shape and surface characteristics that Equation 13.5 can be used after you determine appropriate numeric values for the variables in the equation.

The effect of small fruit can be determined by looking at the relative change in relative terminal velocity when the fruit size is, for example, reduced by 50%. Cross-sectional area is a function of radius squared, thus if the radius is reduced to $\frac{1}{2}$ its previous value, the area reduces by $(\frac{1}{2})^2$, or $\frac{1}{4}$. Similarly, the mass is proportional to the volume which is a function of the radius cubed, thus volume (and mass) are reduced by $(\frac{1}{2})^3$ or $\frac{1}{8}$. We see from Equation 13.5 that V_r^2 is proportional to m_b/A_b, or $\frac{1}{8} \div \frac{1}{4} = \frac{1}{2}$. Therefore, we conclude that reducing the cherry size to $\frac{1}{2}$ the original radius reduces V_r^2 to $\frac{1}{2}$ its original value, hence V_r is reduced to $1/(2)^{0.5}$ or $\frac{1}{1.414}$ or 0.707 times the original value. If the air velocity is set at 85% of the relative terminal velocity of the large cherries, then the small (50% size) cherries will be removed with the leaves.

13.3.2 Fundamentals of bush and tree shakers

Inertial vibrators have proven to be a simple and reliable means of imposing forced vibrational motion upon bush and tree structures. The purpose of transmitting the vibrational energy to the plant structure is to cause detachment of the harvestable material. In addition to the mechanics of the vibrator itself, there are additional questions of damage to the harvested product, damage to the remaining plant structure itself, and the actual mechanics of detachment. We shall treat each of these factors in subsequent sections.

13.3.2.1 A single moving mass shaker

A simple shaker with one moving mass (m) is shown in Figure 13.35. We assume that the axis of rotation (0, 0) is fixed in space and that the inertial shaker mass (m), rotates with constant angular velocity (ω) in a counterclockwise direction. The angle of rotation is equal to the product of time (t) and ω. At any time (t) the center of mass (m) is located at point (x, y) where:

$$x = r \cos(\omega t)$$

and
$$y = r \sin(\omega t) \tag{13.6}$$

where x, y, r are displacements, m

t = time, s

ω = angular frequency, radians/s

The centrifugal force (F) created by the circular motion of m about 0,0 can be resisted by the two component forces:

$$F_x = m\frac{d^2x}{dt^2} = -m\omega^2 r \cos(\omega t)$$

and
$$F_y = m\frac{d^2y}{dt^2} = -m\omega^2 r \sin(\omega t) \tag{13.7}$$
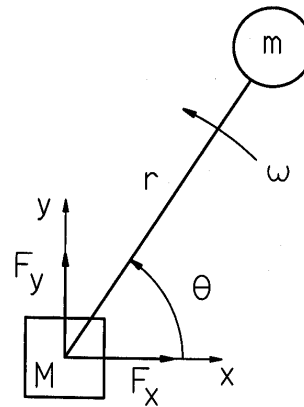
Figure 13.35 – A single rotating mass inertial shaker.

Power is the vector cross product of force times velocity. In this case, since the center of rotation has been assumed to be fixed, the power needed to operate the system is clearly zero. This model of a rotating mass is useful for predicting shaking forces, subject to the assumed limits. Another limitation of this model is that control of the direction of shaking force or the shaking pattern is not possible since the centrifugal force is constant in magnitude and its direction rotates uniformly.

Before proceeding, it is important to differentiate between the number of masses in a vibrational system and the number of degrees of freedom in that system. For each degree of freedom in the system, it is necessary to have one linearly independent equation in order to be able to solve the resulting system of equations. Each mass in the system is capable of producing six possible orthogonally independent motions, three mutually perpendicular linear displacements and three rotational displacements about axes that are at 90° to each other. Another way to consider the number of degrees of freedom of a system is to determine the number of independent engineering dependent variables needed to completely describe the system under consideration.

13.3.2.2 A double moving mass shaker

Control of both the direction and pattern of shaking can be achieved by the addition of a second rotating mass as shown in Figure 13.36. We also assume that the mass of the base, M, is very large such that the resulting "small" movements of M do not invalidate the inertial force summation calculations of F_x and F_y. Using the results of the single mass shaker, we have for Figure 13.36:

$$\Sigma F_x = M \frac{d^2x}{dt^2} = -m_1 \omega_1^2 r_1 \cos(\omega_1 t) - m_2 \omega_2^2 r_2 \cos(\Theta - \omega_2 t)$$

and

$$\Sigma F_y = M \frac{d^2y}{dt^2} = -m_1 \omega_1^2 r_1 \sin(\omega_1 t) - m_2 \omega_2^2 r_2 \sin(\Theta - \omega_2 t) \qquad (13.8)$$
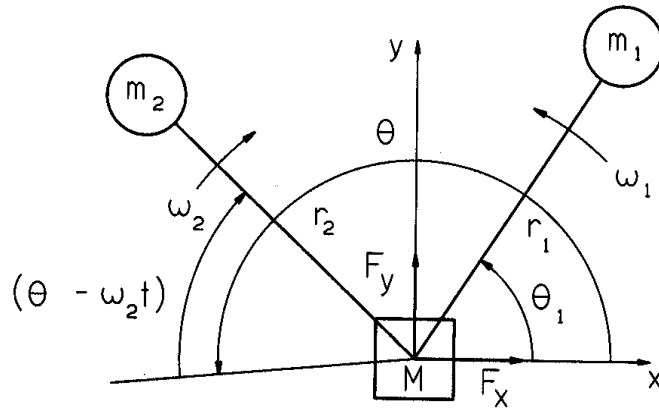
Figure 13.36 – A double rotating mass inertial shaker.

In the special symmetric case where $\omega_1 = \omega_2 = \omega$, $m_1 = m_2 = m$, $r_1 = r_2 = r$, and $\theta = \pi$, we have:

$$\sum F_x = 0$$

and
$$\Sigma F_y = -2m\omega^2 r \sin(\omega t) \tag{13.9}$$

Under these assumptions, the shaker is force-balanced in the x-direction with a pure sinusoidal excitation force in the y-direction.

If the y-direction force Equation 13.9 is divided by the mass (m) and twice integrated with indefinite limits of integration, then the y-direction displacement equation is given as:

$$y = (2\,m\,r/M)\,\sin(\omega t) \tag{13.10}$$

The general Equations 13.8 can also undergo double indefinite integration to yield the general displacement equations for the center of mass (M) that is also assumed to be the center of rotation of masses m_1 and m_2. These general equations of displacement are:

$$x(t) = (m_1/M)\,r_1\,\cos(\omega_1 t) + (m_2/M)\,r_2\,\cos(\theta - \omega_2 t)$$

and
$$y(t) = (m_1/M)\,r_1\,\sin(\omega_1 t) + (m_2/M)\,r_2\,\sin(\theta - \omega_2 t) \tag{13.11}$$

Example Problem 13.2

In the two rotating mass shaker analysis, the resulting motion was assumed to be "small." What conditions are necessary for the maximum displacement to be no more than 10% of the radius of the rotating masses in the case of the force-balanced shaker?

Solution
The amplitude of the resulting motion can be obtained from Equation 13.10 in the y-direction. Thus:

$$2\,m\,r/M < 0.10\,r$$

or
$$m < 0.05\,M \tag{13.12}$$

Therefore, if the rotating mass (m) is less than 5% of the shaken mass (M) the resulting maximum displacement of shaking will be less than 10% of the rotating mass radius (r).

Example Problem 13.3

Using Equations 13.11, subject to conditions of Equation 13.12, determine the values for m_1, m_2, ω_1, ω_2, r_1, r_2, and M that result in a three lobe shaking displacement pattern as shown in Figure 13.37.
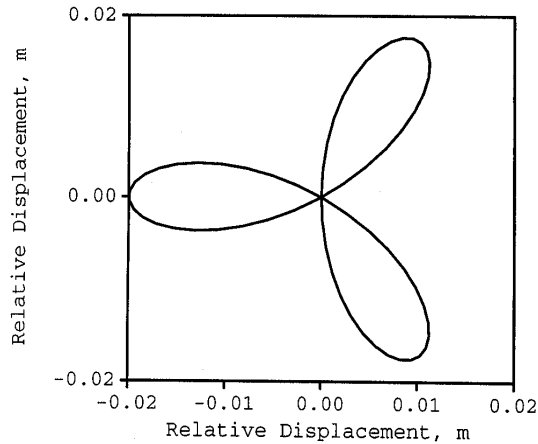
Figure 13.37 – Displacement of the center of a double rotating mass inertial shaker.

Solution

Equations 13.11 must be solved (by computer) for several incremental values of t between $t = 0$ and $t = 2\pi/\omega_1$ or $t = 2\pi/\omega_2$, whichever is the greater value of time. In this example TK Solver™ was used and the rule and variable sheets are shown in Table 13.2.

Table 13.2. TK Solver™ output sheets for Figure 13.37.

RULE SHEET For Academic Use Only
A1 = m1 • r1 / M
B1 = m2 • r2 / M
x = A1 • cos(w1 • t)+B1 • cos(theta-w2 • t)
y = A1 • sin(w1 • t)+B1 • sin(theta-w2 • t)

VARIABLE SHEET For Academic Use Only				
St	Input	Name	Output	Units
		A1	0.01	(m)
	10	m1		(kg)
	0.2	r1		(m)
		B1	0.01	(m)
	10	m2		(kg)
	0.2	r		(m)
	200	M		(kg)
L		x	0	(m)
	10	w1		(rad / s)
L	0	t		(s)
	3.1415927	theta		(rad)
	20	w2		(rad / s)
L		y	1.225E–18	(m)

13.3.2.3 A triple moving mass shaker

Figure 13.29 shows a triple moving mass shaker. All three masses rotate about a common axis. To this point, we have assumed the two moving mass shaker as being force-balanced in every direction except one. This is true, if the centers of gravity of the two masses rotate in a common plane perpendicular to the axis of rotation. In practice it is not so simple to achieve this result. A practical solution is to "split" one mass into two, placing one half above and the other half below the third mass in the middle, as shown in Figure 13.29. If equal masses (**1**) and (**2**) are synchronized to be in phase with each other at the same rotational direction and frequency, it should be obvious from symmetry that the resulting shaker is force-balanced in the plane perpendicular to the axis of rotation, but also moment balanced such that there are no unbalanced moments "rocking" this plane. Furthermore this shaker is clearly capable of producing the two-dimensional shaking patterns in the tree shown in Figure 13.28 if the entire mass of the shaker head (**1**) combined with the tree has an effective center of mass at the centerline of rotation of the three moving masses.

13.3.2.4 Shaker power

Consider the force-balanced shaker shown in Figure 13.38 where the forcing function F_y is given by Equation 13.9. The resulting differential equation of motion in the y-direction is:

$$M\frac{d^2y}{dt^2}+C\frac{dy}{dt}+Ky = 2mr\omega^2\sin(\omega t) \qquad (13.13)$$

where C = damping coefficient, N·s/m

K = stiffness, N/m

The transient (complementary) solution to Equation 13.13 is of little interest since it generally disappears relatively quickly. The steady state (particular) solution is of the form:
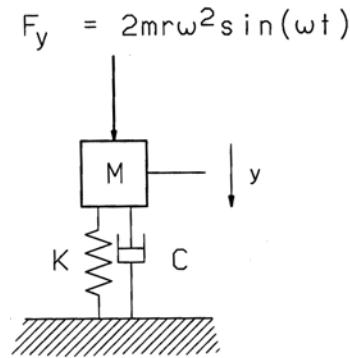
Figure 13.38 – Forced vibrational two-degree-of-freedom model excited with a force-balanced double rotating mass inertial shaker.

$$y(t) = \frac{2m\,r\,\omega^2}{\left[\left(K - M\omega^2\right)^2 + \left(C\omega^2\right)\right]^{0.5}} \sin(\omega t - \alpha)$$

where

$$\alpha = -\tan^{-1}\left(\frac{C\omega}{K - M\omega^2}\right) \tag{13.14}$$

If we define the natural frequency, $\omega_n^2 = K/M$, and the damping ratio, $\xi = C/(2M\omega_n)$, then,

$$y(t) = \frac{2m\,r\,\omega^2/K}{\left[\left(1 - (\omega/\omega_n)^2\right)^2 + 2(\xi\omega/\omega_n)^2\right]^{0.5}} \sin(\omega t - \alpha) \tag{13.15}$$

where

$$\alpha = \tan^{-1}\left(\frac{2\xi\omega/\omega_n}{1 - (\omega/\omega_n)^2}\right) \tag{13.16}$$

If the excitation frequency is much higher than the natural frequency, i.e., $\omega \gg \omega_n$, then Equation 13.15 reduces to:

$$y(t) = \left(\frac{2m\,r}{M}\right) \sin(\omega t - \alpha) \tag{13.17}$$

This result should be compared with Equation 13.10. The difference is that the damping effect has introduced a phase lag in the displacement with respect to the forcing function. The velocity is given by:

$$\frac{dy}{dt} = \frac{2m\,r\,\omega}{M} \cos(\omega t - \alpha) \tag{13.18}$$

Finally, the instantaneous power can be written as the product of the force times the velocity as:

$$P_{inst} = \left[2m\,r\,\omega^2 \sin(\omega t)\right]\left[\frac{2m\,r}{M}\right]\cos(\omega t - \alpha) \tag{13.19}$$

The average power can be obtained by integrating Equation 13.19 over the time required for one cycle of the slower rotating mass (T_f) as:

$$P_{avg} = 1/T_f \int_0^{T_f} P_{inst}\,dt$$

with the limits of integration being 0 to T_f. Thus, the average power is given by:

$$P_{avg} = \left[2m^2r^2\omega^3/M\right]\sin(\alpha) \tag{13.20}$$

Adrian and Fridley (1965) investigated the shaker power requirements under actual field conditions.

13.3.2.5 *LaGrange's equation*

Complex, forced vibrational problems with damping are often treated from the point of view of energy. Simply stated, LaGrange's equation is an energy balance applied to the entire vibratory system. Multi-degree-of-freedom systems are conveniently treated, but the resulting systems of differential equations often require a computer to solve. Closed-form (analytic) solutions to real, non-linear systems of equations that represent practical problems are virtually impossible to obtain. LaGrange's equation in generalized orthogonal coordinates (q_i) has the general form of:

$$\frac{d}{dt}\frac{\partial(K.E.)}{\partial q_i} - \frac{\partial(K.E.)}{\partial q_i} + \frac{\partial(P.E.)}{\partial q_i} + \frac{\partial(D.E.)}{\partial q_i} = Q_i \qquad (13.21)$$

where K.E. = kinetic energy of the system = $0.5\,M\,(dx/dt)^2$
P.E. = potential energy of the system = $0.5\,K\,x^2$
D.E. = dissipation energy of the system = $0.5\,C(dx/dt)^2$
Q_i = generalized external force acting on the system

Example Problem 13.4

Apply the LaGrange equation to the forced vibrational of a single-degree-of-freedom damped mass shown in Figure 13.38. The parameters M, C, and K are defined in Equation 13.13. Neglect gravity.

Solution

The kinetic energy of the system is $\text{K.E.} = 0.5M\left(\dfrac{dy}{dt}\right)^2$ $\qquad (13.22)$

The potential energy of the system is $\text{P.E.} = 0.5\,K\,y^2$ $\qquad (13.23)$

The dissipative energy of the system is $\text{D.E.} = 0.5C\left(\dfrac{dy}{dt}\right)^2$ $\qquad (13.24)$

The forcing function in the single degree-of-freedom direction of motion (y) is

$$Q = F_o \sin(\omega t) \qquad (13.25)$$

After calculating the appropriate partial derivatives and substitution, Equation 13.21 becomes $\qquad (13.26)$

$$\frac{d}{dt}\left[M\left(\frac{dy}{dt}\right)\right] - 0 + K\,y + C\left(\frac{dy}{dt}\right) = F_o \sin(\omega t)$$

and finally reduces to $\quad M\left(\dfrac{d^2y}{dt^2}\right) + C\left(\dfrac{dy}{dt}\right) + K\,y = F_o \sin(\omega t)$ $\qquad (13.27)$

13.3.3 Vibrational detachment during harvest

The LaGrange equation has been used to successfully analyze vibratory harvesting of olives (Tsatsarelis, 1987) and air-suspended strawberries (Ruff et al., 1980). A two-degree-of-freedom model for olives is shown in Figure 13.39a and a five-degree-of-freedom-model is shown in Figure 13.39b. Both of these studies looked at the resulting vibrational mode shapes that resulted from forced vibrations and confirmed with experimental observation that the tilting mode of vibration shown in Figure 13.40 is very important to fruit removal by causing detachment at the stem-fruit connection.
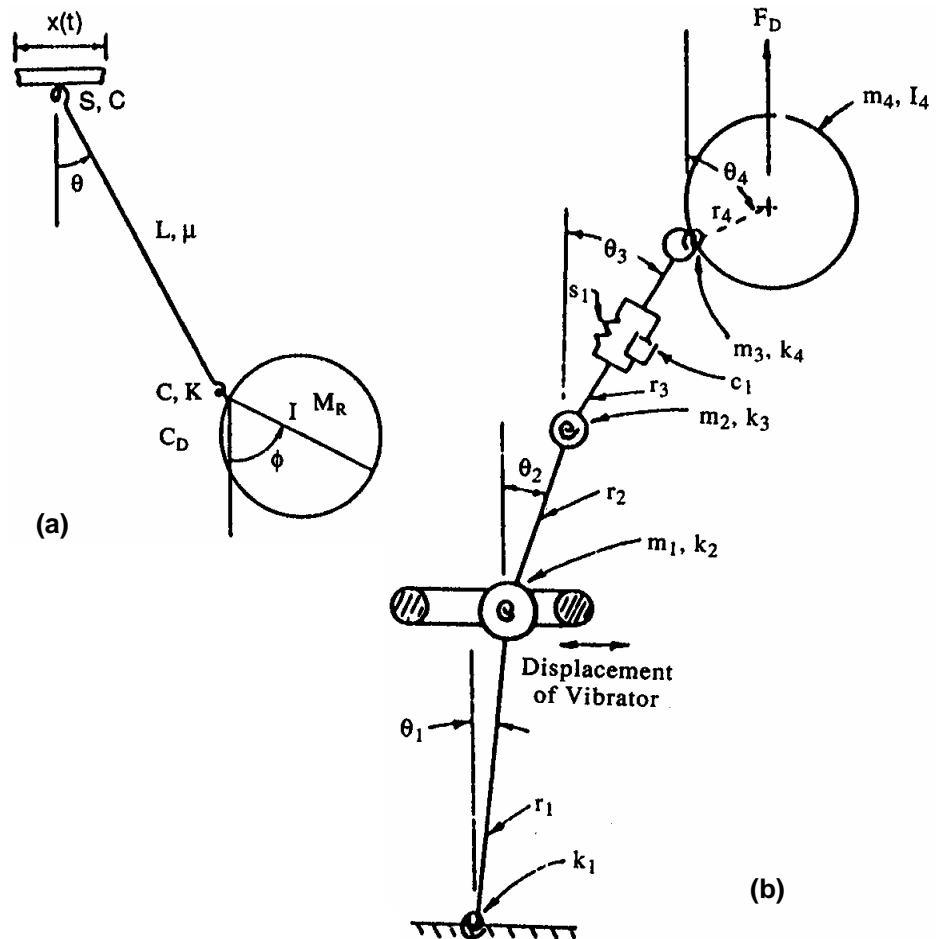
Figure 13.39 – (a) Two-degree-of-freedom fruit attachment vibrational model (from Tsatsarelis, 1987). (b) A five-degree-of-freedom vibrational model of an air-suspended depended, fruit-stem system (from Ruff et al., 1980).
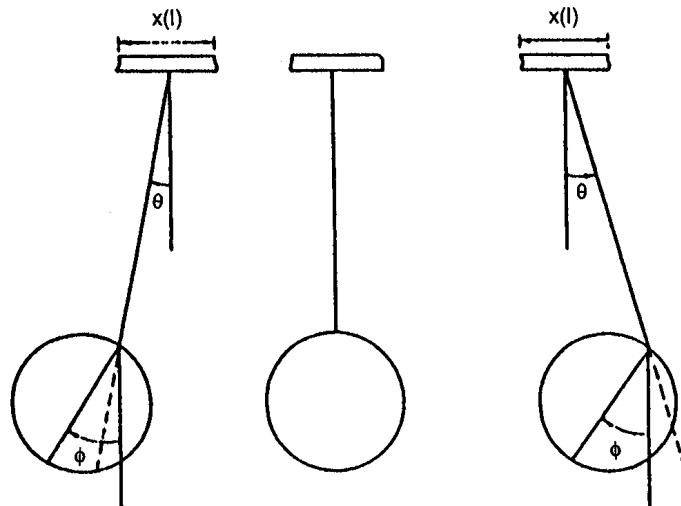
Figure 13.40 – Vibrational modes defined; pendular, left; rest, middle; and tilting, right (Tsatsarelis, 1987).

Three modes of vibration are important in understanding the mechanism of fruit detachment. The tilting mode is the most important and has been experimentally observed to be present at the time of detachment. This mode causes high tensile stresses to develop in the stem-calyx junction of the stem and the fruit. Under normal maturation processes this junction becomes weaker as the natural abscission layer develops. Furthermore, there is evidence that biological materials fatigue under repeated cycles of stress, each cycle of which is not individually capable of causing failure, but accumulatively will produce failure of the stem or stem-calyx junction.

The second important vibrational mode is the axial tension mode. This mode is the result of the application of forces directed along the axis of the stem itself. In the forced vibrational excitement of the plant structure, it is relatively easy to imagine how the vibrating fruit-stem could achieve a relative position such that the next cycle of vibration, by the assumed geometry, would result in a sudden imposition of a relatively high axial stem force. This situation can be recognized by the common expression of "crack the whip" which results in an amplification of tensile forces by sudden redirection of momentum forces.

The pendular mode is the third mode and is important to excite if the fruit is to be detached with the stem intact. It is much more difficult to excite this mode if the stems are relatively long than the tilting mode. In fact all three modes are present to varying degrees and as such combine to produce detachment.

13.3.4 Impact models and mechanical damage
Mechanical damage during harvesting operations can affect both the plant and the harvested product. In multiple-pick crops, unharvested product can also be damaged. The focus of this section will be on models that attempt to characterize damage to the harvested product. There are four principal components of failure in fruits and vegeta-

bles that contribute to reduced product value. These four components are compressive stress, shear stress, creep stress, and fatigue stress. Stress analysis in three dimensions in complex shapes with non-isotropic bodies is very difficult. The presence of a protective (usually tough) skin over a product is only one example of non-isotropic condition. Most loading conditions that are observed under practical conditions are a combination of the above four component loadings. For engineering purposes, useful information in equation form can be derived from empirical (physical) observations. Care should be exercised in applying empirical results to non-identical products or conditions.

13.3.4.1 Impact force response of a sphere on a flat plate

If a stationary flat plate is impacted with a spherically shaped object dropped under gravity, the resulting total force exerted on the plate is a function of the mass, impacting and rebounding velocities of the sphere. This results from the application of Newton's Second Law as given by:

$$I = \int_0^{t_c} f(t)dt = m(v_2 - v_1) \tag{13.28}$$

where I = impulse, N·s

$f(t)$ = contact force as a function of time, N

t = time during contact, s

t_c = total contact time, s

m = mass of sphere, kg

v_1 = velocity of center of mass, m/s, before contact, i.e., $t = 0$

v_2 = velocity of center of mass, m/s, after contact, i.e., $t = t_c$

The coefficient of restitution (r) is defined as:

$$r = -v_2/v_1 \tag{13.29}$$

where velocities v_1 and v_2 are defined as above and the minus sign reflects the fact that the direction of rebound is opposite the impact direction.

If one assumes r is greater than zero and considers two successive bounces, then on the first impact:

$$I_1 = m (v_2 - v_1)$$

and on the second impact, neglecting air frictional losses:

$$I_2 = m (v_3 - v_2)$$

If one assumes that the coefficient of restitution is constant for both impacts, then it can be shown that:

$$r = I_2/I_1 \tag{13.30}$$

Hence, by measuring the impulse of two successive impacts, the coefficient of restitution can be determined experimentally.

It is also possible to determine the fruit mass from the impact response by:

$$I_1 = m (v_2 - v_1) = m v_1 (v_2/v_1 - 1)$$

or $$m = -I_1/[v_1 (1 - r)] \tag{13.31}$$

The pre-impact velocity (v_1) can be estimated by knowing the free-fall height under constant gravitational acceleration. Thus, it is possible to experimentally determine the coefficient of restitution and the mass of a sphere dropped from a known height onto a rigid flat surface provided two consecutive impulses are measured and analyzed.

Until this point, the actual shape of f(t) has not been considered and, in fact, has no effect on the above equations. The shape of the impact force curve, f(t), is a function of the fruit firmness and damping as shown in the next section.

13.3.4.2 Impact models with firmness and damping effects

For ordinary engineering purposes, it is often assumed that the impact force and contact deformations within a convex fruit or vegetable product and a rigid flat surface can be modeled with one or two degrees of freedom. Two models are shown in Figure 13.41. The Kelvin model has a single degree of freedom with lumped parameter mass, spring, and damping characteristics. The Maxwell model contains the same lumped physical elements as the Kelvin model, but is based upon a different physical arrangement. Lumped parameter models are defined by parameter constants that represent invariant conditions. For example, in these models all mass is assumed to be "lumped" together and moves without internal deformations, hence the motion of the center of mass is assumed to be the motion of all mass.

Each model provides useful insights and engineering information. However, each model is also subject to certain restrictions and limitations. In addition to the lumped parameter assumption, the development of initial conditions, while physically justifiable, sometimes results in mathematical consequences that are not physically realizable. As each model is developed, further examples of differences between the physical and mathematical representations will be identified.

Before considering the equations of motion for the two models in Figure 13.41, an understanding of initial conditions will be developed. The models are considered at rest, without the effects of gravity, at times prior to "impact." This condition is assumed to exist for all time $t < 0$. At $t = 0^+$, the mass is considered to have an instantaneously achieved velocity of V_i in the direction noted in Figure 13.41. At this time, contact with the stationary surface exists and the initial displacements of all displacement variables are taken to be zero. Neither model is subjected to an external forcing function.
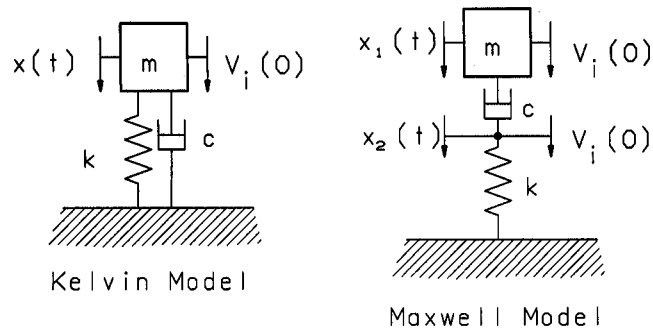
Figure 13.41 – Kelvin model and Maxwell model of a viscoelastic impact with a stationary surface.

Since contact continues to exist only if the contact force is positive, then the model equations of motion are only valid during the initial contact period. Once the contact force goes to zero, the initial impact event is considered to be complete and the velocity of the mass, if any, is considered to be the impact rebound velocity. The choice of units for the equations of motion can be made consistent with the equations themselves. Any consistent set of units may be used.

The Kelvin model, being a single-degree-of-freedom system, is described by the following equation of motion:

$$m\frac{d^2x}{dt^2} + c\frac{dx}{dt} + kx = 0 \tag{13.32}$$

while the general solution for this equation is of the form:

$$x = x_c + x_p \tag{13.33}$$

Only the complementary solution (x_c) is of interest since the particular solution (x_p) is, in this case, zero. The characteristic equation (or auxiliary equation) is:

$$m\lambda_2 + c\lambda + k = 0 \tag{13.34}$$

If $\omega_n{}^2 = k/m$ and $\zeta = c/(2m\,\omega_n)$, where ζ is called the damping factor, then,

$$\lambda_1 = \omega_n\left(-\zeta + \sqrt{\zeta^2 - 1}\right) \tag{13.35}$$

and
$$\lambda_2 = \omega_n\left(-\zeta - \sqrt{\zeta^2 - 1}\right) \tag{13.36}$$

The roots of the characteristic equation (λ_1 and λ_2) will be real and distinct, real and equal, or complex conjugates for ζ, being greater than one, equal to one, or less than one, respectively.

If ζ is greater than one the system is overdamped and oscillatory motion is not possible as given by the overdamped complementary solution:

$$x_c = Ae^{-\lambda_1 t} + Be^{-\lambda_2 t} \tag{13.37}$$

$$x_c = Ae^{-\lambda_1 t} + Be^{-\lambda_2 t}$$

where A and B are constants determined from the initial conditions.

Critical damping is a very special mathematical condition, seldom seen in the physical world, where $\zeta = 1$, and clearly $\lambda_1 = \lambda_2 = -\omega_n$. In this special case, the complementary solution is given by:

$$x_c = (C + Dt)e^{-\omega_n t} \tag{13.38}$$

again where C and D are constants determined from the initial conditions.

The underdamped condition, $\zeta < 1$, is often encountered in fresh, mature fruits and vegetables, and results in the complementary solution:

$$x_c = (A\cos\omega_d t + B\sin\omega_d t)e^{-\zeta\omega_n t} \tag{13.39}$$

ELASTIC CASE   PLASTIC CASE   ELASTIC-PLASTIC CASE
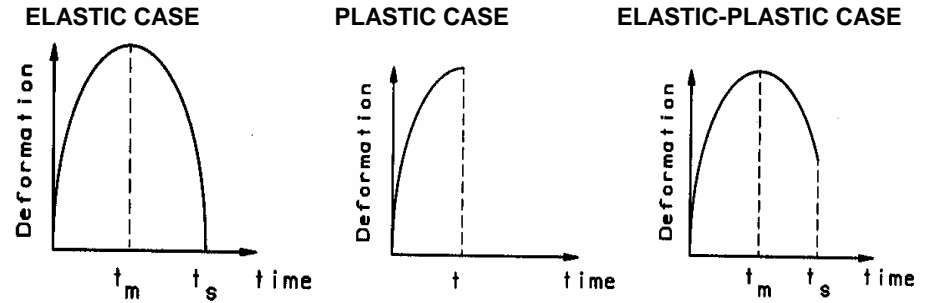
Figure 13.42 – Impact deformation curves for products with elastic, plastic, or elastic-plastic properties.

where the damped natural frequency $[\omega_d^2 = (1 - \zeta^2)\,\omega_n^2]$ is given by definition. If the initial displacement is taken as zero and the initial velocity is V_i, then $A = 0$ and $B = V_i/\omega_d$.

Maxwell's model is more complex because it has two degrees of freedom. By example problem, these equations will be derived using the LaGrange equations. The complementary solution can then be obtained by using a symbolic math package such as MAPLE [TM] resulting in rather than complex algebraic analytical solution. A TUTSIM [TM] computer solution to the differential equations could also be used.

Both the Kelvin and Maxwell models are useful in demonstrating the impact phenomena. Depending upon the relative mass, firmness, and internal energy absorption of the impacting body, elastic, plastic or elastic-plastic impact responses can be demonstrated as illustrated in Figure 13.42. The coefficient of restitution ($r = 1$ for elastic, $r = 0$ for plastic, and $0 < r < 1$ for plastic-elastic) characterizes the impact behavior.

Example Problem 13.5

Use LaGrange's equation to find the equations of motion for Maxwell's model shown in Figure 13.41. Neglect gravity.

Solution

The needed expressions and terms of the LaGrange's equations are written as follows:

$$\text{P.E.} = \frac{k\,x_2^2}{2} \tag{13.40}$$

$$\text{K.E.} = \frac{m}{2}\left(\frac{dx_1}{dt}\right)^2 \tag{13.41}$$

$$\text{D.E.} = \frac{c}{2}\left[\left(\frac{dx_2}{dt}\right)^2 - \left(\frac{dx_1}{dt}\right)^2\right] \tag{13.42}$$

and $Q = 0$ since there is no generalized forcing function.

After calculating the appropriate partial derivatives and substitution, Equation 13.21 becomes:

$$m\,x_1 - c\left(\frac{dx_2}{dt} - \frac{dx_1}{dt}\right) = 0 \tag{13.43}$$

and

$$k\,x_2 + c\left(\frac{dx_2}{dt} - \frac{dx_1}{dt}\right) = 0 \tag{13.44}$$

subject to $x_1(0) = x_2(0) = 0$ and $\dfrac{dx_1(0)}{dt} = \dfrac{dx_2(0)}{dt} = v$

The solutions to Equations 13.43 and 13.44 are:

$$x_1(t) = -\frac{v\,m}{c} - 2\frac{c\,v\,m^{0.5}e^{-kt/2c}\sinh(\beta)}{k^{0.5}(-4c^2 = m\,k)^{0.5}}$$

$$+ \frac{v\,m^{1.5}k^{0.5}e^{-kt/2c}\sinh(\beta)}{c(-4c^2 + m\,k)^{0.5}} + \frac{v\,m\,e^{-kt/2c}\cosh(\beta)}{c}$$

and

$$x_2(t) = -2\frac{c\,v\,m^{0.5}e^{-kt/2c}\sinh(\beta)}{k^{0.5}(-4c^2 + m\,k)^{0.5}}$$

13.3.4.3 Impact models results and applications

A Kelvin model (Bower and Rohrbach, 1976) and a double Kelvin model in series (Glass and Rohrbach, 1980) have been used to model blueberry fruit impacts. For a blueberry, the mass ranges from less than 1 g to nearly 3 g, the damping constant between 0.1 and 0.8 N·s/m, and the spring constant can take values between 500 and 8000 N/m. Actual model parameters were selected to match individual berry coefficient of restitution or contact force and velocity mechanical impedance criterion. Model berry mass is often found to be slightly less than actual berry mass.

Table 13.3 summarizes the impact parameters used in computer solutions of blueberry impact results for the Kelvin model shown in Figure 13.43 and the Maxwell model shown in Figure 13.44. In both cases the coefficient of restitution is 0.414 with the model mass being 1.54 g. The damping constant and the spring constant values were empirically adjusted in the Maxwell model to obtain equal coefficients of restitution for the two different models.

Table 13.3. Impact parameters and results for the solution of Kelvin and Maxwell equations of motion for blueberry models.

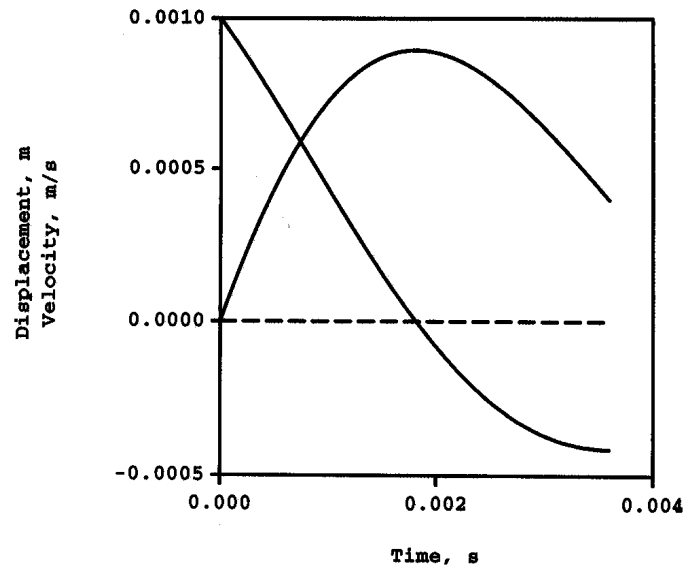| Model	m, g	c, N·s/m	k, N/m	F_{peak}, N	t_s, ms	r	See figure	d_p, mm
Kelvin	1.54	0.75	797	0.713	3.60	0.414	13.43	0.40
Maxwell	1.54	12.0	1000	1.27	3.85	0.414	13.44	0.28

**Figure 13.43 – Solution to Kelvin model of a blueberry.
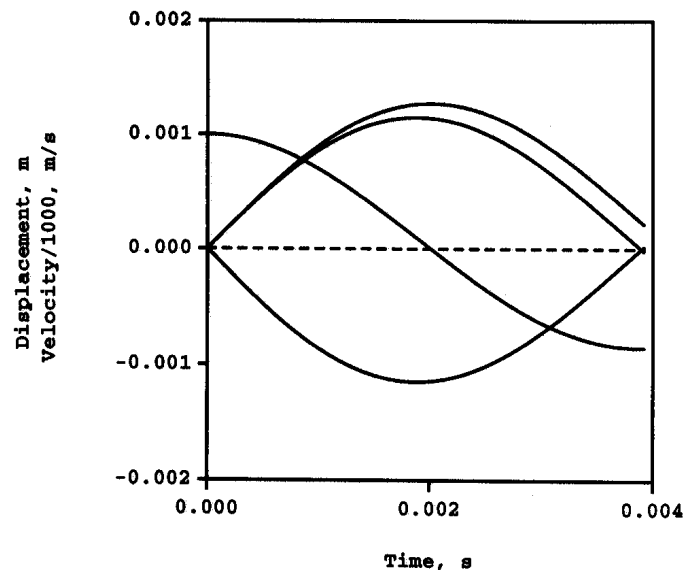See Table 13.3 for model parameter values and results.**

**Figure 13.44 – Solution to Maxwell model of a blueberry.
See Table 13.3 for model parameter values and results.**

Once the deformations within the spring model elements have been calculated, $x_1(t)$ for the Kelvin model and $x_2(t)$ for the Maxwell model, the impact force $f(t)$ is easily calculated as the product of the deformation and the spring stiffness (k). However, the Kelvin model predicts a non-zero impact force at the time of rebound or separation, which is not particularly useful, but, results from the model's "attempt" to restore the initial free length of the unstressed spring element. If one attempts to "correct" for the non-zero contact force prediction at the time of rebound by subtracting the force component associated with the viscous damping element, then the initial contact force becomes a step at $t = 0^+$ with a magnitude of $c(dx_1/dt)$. The Kelvin model does predict a permanent fruit deformation after separation in the case where separation does indeed occur.

The Maxwell model comes closer to predicting an impact force that exists during rebound, which is consistent with physical observation as well as a permanent fruit deformation (d_p) with a magnitude of $x_2(t_s)$, where t_s is the time at separation. The comparative results of the two impact models, in Table 13.3, show some differences between the predicted contact time, peak impact force, F_{peak}, and permanent fruit deformations after impact for identical coefficients of restitution. It is important to remember that engineering models are very useful to the extent that they help the engineer understand the physical situation represented and the engineering parameters of interest, but not all physical aspects of the real situation are accurately modeled.

In practice, most values for k are obtained from empirical force-deformation tests (Instron Universal Tester[TM]) or drop test data, and are only valid for the size and conditions of that test. The development of tri-axial contact stress during a fruit impact is beyond the scope of this text. Additional theoretical aspects of food rheology and physical properties are presented in Mohsenin (1970). Goldsmith (1960) is an excellent reference for additional discussion of impact events.

The coefficient of restitution in peaches has been reported to be successfully measured and used to identify individual fruit firmness (Meredith, Leffler and Lyon, 1988). The coefficient of restitution was determined from data collected from two consecutive bounces on an instrumented load cell. Neither variety, fruit size, nor drop height affected the determination of the coefficient of restitution within the range of the investigated variables.

An impact probe for determining apple and pear firmness was developed and tested by Delwiche et al. (1991). A small air cylinder moved an impact surface towards the side of a "stationary" fruit. Impact force was sensed by an accelerometer attached to the impact surface. A strong correlation between peak impact deceleration and fruit firmness was obtained by testing.

CONVEYING OF AGRICULTURAL MATERIALS

14

INTRODUCTION

There are several methods used to convey agricultural materials. The selection of conveying method depends upon the nature of application and on the type of material being conveyed. The agricultural material may be liquid, granular, powder, fibrous, or any combination of these. This chapter does not cover conveying of liquid material.

Generally, conveying is accomplished by a combination of mechanical, inertial, pneumatic, and gravity forces. Conveyors utilizing primarily mechanical forces are screw, belt, and mass conveyors. Oscillatory conveyors rely on the inertial and the friction forces. Pneumatic conveyors employ aerodynamic drag to accomplish conveying. Conveying by throwing combines both inertial and aerodynamic forces. Forage blowers utilize these principles.

14.1 SCREW CONVEYORS

Augers are used to convey materials that are free flowing, such as grain, as well as difficult fibrous materials and powders. For example, in a grain combine, augers are used to move cut crop on the platform to the feeder housing, clean grain from the bottom of the cleaning shoe to the grain tank, and to unload the grain tank onto a wagon or a truck. Augers are used at grain elevators and farmsteads to load grain storage bins and on feedlots for feed distribution.

14.1.1 Screw conveyor methods and equipment

The *screw conveyor* consists of a shaft that carries helicoid flightings on its outer surface. These flighting are enclosed either in a trough for horizontal augers or in a tube for elevating augers. The tube or the trough is held stationary while the rotation of the flightings causes the material to move longitudinally. Figure 14.1 shows the essential components of a screw conveyor. At the inlet side, the auger flightings extend beyond the tube. Generally, a hopper is provided to hold the material while it is conveyed into the tube. Augers can be permanently installed in a machine, or at a site, or they can be portable. The augers are driven either at the intake side or the discharge side. There are some center-drive augers but they are not common in agricultural applications.
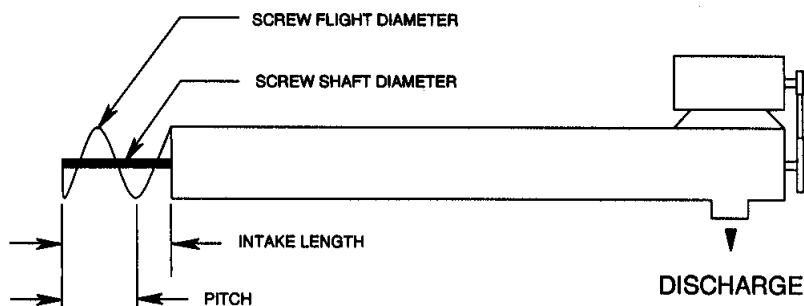
Figure 14.1 – A schematic diagram of a screw conveyor.

The auger length is defined as the length of the tube assembly including any intake but not including the intake hopper and/or the head drive. The intake length is the visible flighting at the intake of the auger. The outside diameter of the tube is referred to as the auger size. A standard pitch auger is the one whose pitch is approximately equal to the outside diameter of the helicoidal flighting. Generally, the pitch is not less than 0.9 and not more than 1.5 times the outside diameter. Standard pitch augers are used for horizontal and up to 20° inclination angles. For inclination angles greater than 20°, half-standard pitch screws are used. Double- and triple-flight, variable-pitch, and stepped-diameter screws are available for moving difficult materials and controlling feed rates.

14.1.2 Theory of screw conveyors

The *theoretical volumetric capacity* of an auger is expressed as:

$$Q_t = \frac{\pi}{4}\left(d_{sf}^2 - d_{ss}^2\right) l_p n \tag{14.1}$$

where Q_t = theoretical volumetric capacity, m^3/s
$\quad$ d_{sf} = screw flighting diameter, m
$\quad$ d_{ss} = screw shaft diameter, m
$\quad$ l_p = pitch length, m
$\quad$ n = screw rotational speed, rev/s

In reality the actual capacity of an auger is considerably less than the theoretical capacity. This results in loss of volumetric efficiency. The *volumetric efficiency* is defined as:

$$\eta_v = \frac{Q_a}{Q_t} \tag{14.2}$$

where η_v = volumetric efficiency
$\quad$ Q_a = actual volumetric capacity, m^3/s
Generally, the throughput rate in terms of mass (or weight) per unit of time, for example t/h or kg/min, is specified. The volumetric capacity is obtained by dividing the throughput rate by the bulk density of the material.

The power requirement of an auger is expressed by the *specific power,* defined as:

$$P' = \frac{P/L}{Q_a \rho_b} \tag{14.3}$$

where P' = specific power, W s/kg m

P = power requirement, W

L = auger length, m

ρ_b = material bulk density, kg/m^3

Thus, the specific power is the power required to convey a unit mass throughput rate per unit auger length.

The process of conveying by a screw conveyor is complex. It is difficult to develop analytical models to predict volumetric capacity and power requirements without making overly simplified assumptions. Purely empirical models, on the other hand, are not general enough in nature and cannot be used to predict auger performance in a variety of applications. Rehkugler and Boyd (1962) proposed the application of dimensional analysis as a tool to develop a comprehensive prediction model for screw conveyor performance. Table 14.1 shows a list of variables that are pertinent to the problem. These variables can be combined into ratios or dimensionless groups called the pi-terms using Buckingham's Theorem (see Chapter 1). The following equation includes the dimensionless terms:

$$\pi_1 = f\left(\frac{d_t}{d_p}, \frac{d_{sf}}{l_p}, \frac{d_{ss}}{l_p}, \frac{l_i}{l_p}, n\sqrt{\frac{l_p}{g}}, f(\theta), \mu_1\mu_2 \right) \tag{14.4}$$

where
$$\pi_1 = \frac{Q_a}{\frac{\pi}{4}\left(d_{sf}^2 - d_{ss}^2\right) l_p n} \quad \text{or} \quad \frac{P/L}{Q_a \rho_b g} \tag{14.5}$$

Table 14.1. A list of variables affecting screw conveyor performance.

Symbol	Variable definition	Dimensions	Units
Q_a	actual volumetric capacity	L^3/T	m^3/s
P	power requirement	ML^2/T^3	W
d_t	tube inside diameter	L	m
d_{sf}	outside screw diameter	L	m
d_{ss}	screw shaft diameter	L	m
L	screw length	L	m
l_p	screw pitch length	L	m
l_i	exposed screw intake length	L	m
n	angular speed	1/T	rev/s
θ	angle of conveyor inclination	–	degrees
ρ_b	material bulk density	M/L^3	kg/m^3
μ_1	material-metal friction	–	–
μ_2	material-material friction	–	–
g	acceleration of gravity	L/T^2	m/s^2

The first term in the right hand side of Equation 14.5 is the ratio of the actual volumetric throughput rate to the theoretical volume swept by the screw per unit of time. This has been regarded as the volumetric efficiency of the screw conveyor. The second term in the right hand side of the above equation is the power required per unit length per unit mass flow rate of the material being conveyed. It has been defined as the specific power or the power efficiency of the conveyor. The conveyor length does not affect the volumetric efficiency.

The dimensionless terms of Equation 14.4 were used to develop prediction equations using experimental data. Published data on the performance of auger conveyors conveying wheat, oats, and shelled corn were used to develop the performance equations. These equations may be used to estimate conveyor performance for similar materials.

$$\frac{Q_a}{\frac{\pi}{4}\left(d_{sf}^2 - d_{ss}^2\right) l_p n} = (4.332 \times 10^{-4})\left(2\pi n \sqrt{\frac{l_p}{g}}\right)^{-0.44}\left(\frac{l_i}{l_p}\right)^{0.31}\left(f_1(\theta)\right)^{1.35}\mu_1^{-4.59}\mu_2^{-3.72} \quad (14.6)$$

$$\frac{P/L}{Q_a\rho_b g} = 3.54\left(2\pi n \sqrt{\frac{l_p}{g}}\right)^{0.14}\left(\frac{d_{sf}}{l_p}\right)^{-10.12}\left(\frac{l_i}{l_p}\right)^{0.11}\left(f_2(\theta)\right)\mu_2^{2.05} \quad (14.7)$$

where $f_1(\theta) = 1 + \cos^2\theta$ $\qquad\qquad\qquad\qquad\qquad\qquad\qquad\qquad\qquad\qquad$ (14.8)

$\qquad f_2(\theta) = 6.94\,(1.3 - \cos^2\theta)$

$\qquad \theta$ = conveyor angle as measured from the horizontal, degrees

$\qquad 0.414 > \mu_1 > 0.374$

$\qquad 0.554 > \mu_2 > 0.466$

14.1.3 Screw conveyor performance

The performance of a screw conveyor, as characterized by its capacity, volumetric efficiency, and power requirements, is affected by the conveyor geometry and size, the properties of the material being conveyed, and the conveyor operating parameters such as the screw speed and the angle of inclination. The effect of these factors is discussed below.

14.1.3.1 Capacity

Screw length has no effect on the capacity of a screw conveyor. The effect of speed and inclination is given in Figure 14.2. As shown in the figure, there is a limiting value of speed beyond which the capacity does not increase. In fact, it may even decrease beyond a certain speed. It is also seen from this figure that the capacity decreases as the angle of inclination increases. The limiting value of speed is independent of the angle of inclination. It has been suggested that there may be two factors responsible for this behavior: (1) the maximum possible rate of grain flow through an orifice, and (2) the centrifugal force due to the rotation of the grain mass. Initially, the capacity increases directly with speed up to 250 rev/min. After this point the centrifugal force restricts the flow of grain at the intake and causes the slope to decrease. If the speed is increased sufficiently the centrifugal force may become so restrictive as to cause a decline in the capacity.
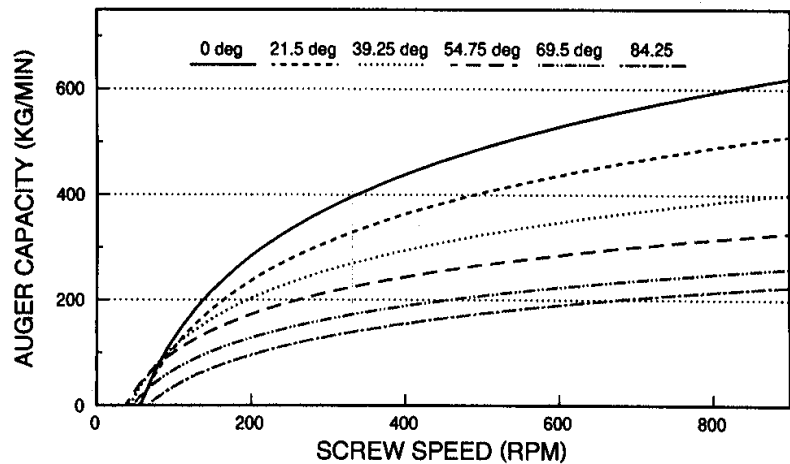
Figure 14.2 – Effect of screw speed and angle of auger inclination on conveying capacity (redrawn from Regan and Henderson, 1959).

Figure 14.3 shows the effect of screw angle of inclination on the capacity. The reduction in the capacity approximately follows the cosine function with two exceptions: (1) the capacity at higher speed is well below the cosine function, and (2) the capacity at 90° angle is about 30% of the horizontal capacity. This may be due to the restriction to grain flow into the intake of the conveyor at higher speeds and the fact that grain flows from a vertical orifice at one-third the rate from a comparable horizontal orifice.
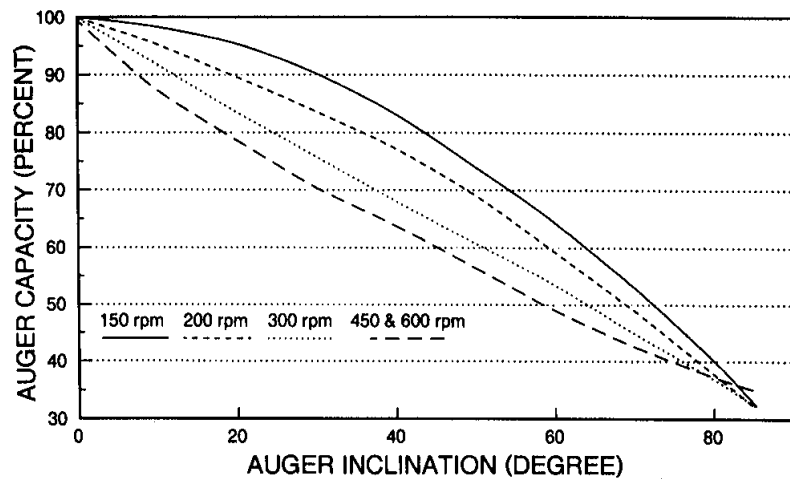
Figure 14.3 – Reduction in the auger conveying capacity as affected by the angle of inclination at different speeds (redrawn from Regan and Henderson, 1959).
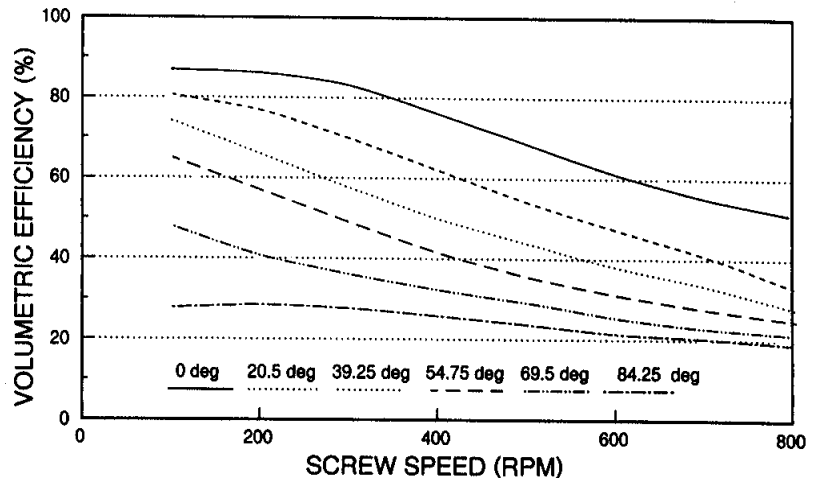
**Figure 14.4 – Effect of screw speed on volumetric capacity at various
angles of inclination (redrawn from Regan and Henderson, 1959).**

14.1.3.2 Volumetric efficiency

Screw length has no effect on the capacity and volumetric efficiency of a screw conveyor. The effect of screw speed and inclination on volumetric efficiency is given in Figure 14.4. Generally, volumetric efficiency decreases as the screw speed and the angle of inclination increase. Brusewitz and Persson (1969) reported that the screw clearance affects the volumetric efficiency. As shown in Figure 14.5, the diametral
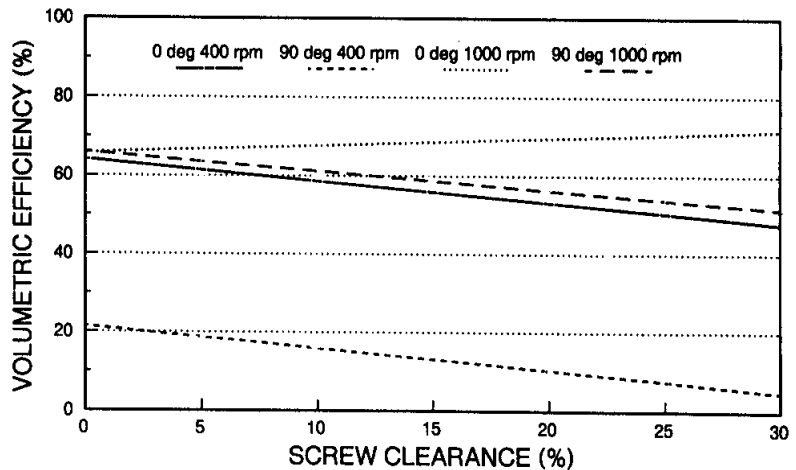
**Figure 14.5 – Effect of the clearance between screw flightings and
the tube inside diameter on the volumetric conveying efficiency
(redrawn from Brusewitz and Persson, 1969).**

clearances up to 5% to 7% have little affect on the volumetric efficiency, but a drop in efficiency of 0.7% per 1% increase in clearance can be expected. No interaction of the conveyor inclination and screw clearance is evident.

14.1.3.3 Power requirements

The effect of screw diameter on specific power, as defined earlier, is dependent on the speed of a screw conveyor. At low speeds there is a decrease in the specific power with increase in the screw diameter. The trend reverses with higher speeds. Screw length has no effect on specific power. There is a slight effect of the pitch on the specific power. An increase in pitch tends to reduce the specific power. For horizontal augers, an increase in the diametral clearance causes a slight decline in the specific power. However, for vertical augers, this results in a general increase in the power. An increase in screw speed results in an increase in the required power as shown in Figure 14.6. The hump in the power curve below 300 rev/min is due to the high torque value at lower speeds. Increasing the angle of inclination causes the power to increase initially but a decrease follows beyond a certain angle. This is due to the decline in the volumetric efficiency. Moisture content that is associated with increase in friction causes the specific power to increase significantly.

Presently, concise data are not available for individual design problems. The selection is based on data provided by the manufacturers. Most data provided by the manufacturers are for low-speed horizontal augers. However, the equations given above may be used for estimating auger capacity and power requirements for a given application.
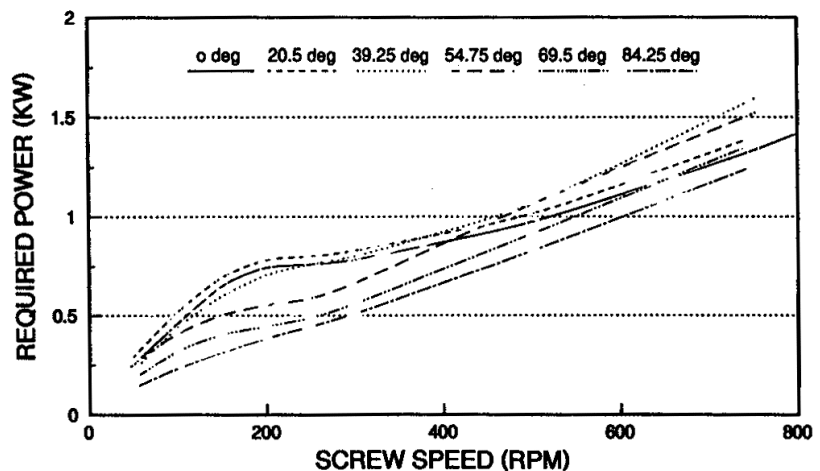
Figure 14.6 – Auger conveyor power requirements at different screw speeds and angles of inclination (redrawn from Regan and Henderson, 1959).

Example 14.1

Determine the efficiency, volumetric capacity, and power requirement of a horizontal standard pitch screw auger conveying wheat. The screw diameter is 15.24 cm (6 in.) and the shaft diameter is 2.54 cm (1 in.). The screw speed is 600 rev/min. The grain-metal friction may be taken as 0.414 while a value of 0.466 may be used for internal friction coefficient. The intake length of the screw is two times the pitch.

Solution

Given: d_{sf} = 0.1524 m (6 in.) μ_1 = 0.414
          d_{ss} = 0.0254 m (1 in.) μ_2 = 0.466
          l_p = 0.1524 m (6 in.)   n = 10 rev/s (600 rev/min)
          l_i = 0.3048 m (12 in.) θ = 0
          ρ_b = 769 kg/m^3 (Table 14.2)

Table 14.2. Grain properties related to pneumatic conveying (ASAE Data D241.2).

Material	Bulk density, kg/m^3	Particle density, kg/m^3	Equivalent particle diameter, mm
Wheat	769	1300	4.08
Oats	410	1050	4.19
Barley	615	1330	4.05
Soybeans	769	1180	6.74
Corn	718	1390	7.26

Use Equation 14.6 to determine the efficiency. The dimensionless groups are calculated as follows:

$$2\pi\, n\sqrt{\frac{l_p}{g}} = 2\pi(10)\sqrt{\frac{0.1524}{9.81}} = 7.83$$

$$\frac{d_{sf}}{l_p} = \frac{0.1524}{0.1524} = 1$$

$$f_1(\theta) = 2$$

$$\frac{l_i}{l_p} = \frac{0.3048}{0.1524} = 2$$

Substituting in Equation 14.6 we get:

$$\frac{Q_a}{\frac{\pi}{4}\left(d_{sf}^2 - d_{ss}^2\right) l_p n} = (4.32 \times 10^{-4})(7.83)^{-0.44}(2)^{0.31}(2)^{1.35}(0.414)^{-4.59}(0.466)^{-3.72}$$

$$= (4.32 \times 10^{-4})(0.404)(1.24)(2.55)(57.3)(17.12)$$

$$= 0.541$$

$$\eta_v = 0.541 \text{ or } 54.1\%$$

Volumetric capacity can be found as:

$$Q_a = 0.541\frac{\pi}{4}\left[(0.1524)^2 - (0.0254)^2\right](0.1524)(10) = 0.0146 \text{ m}^3/\text{s (or 40.5 t/h)}$$

Use Equation 14.7 to determine the power requirement.

$$\frac{P/L}{Q_a \rho_b g} = 3.54(7.83)^{0.14}(1)^{-1012}(2)^{0.11}(2.082)(0.466)^{2.05}$$

$$= 3.54(1.334)(1)(1.079)(2.082)(0.209) = 2.217$$

$$P/L = 2.217(0.0146)(769)(9.81) = 245 \text{ W/m}$$

14.2 PNEUMATIC CONVEYORS

Pneumatic conveyors move grain by imparting the kinetic energy of moving air to grain in conduits. Pneumatic conveyors are flexible in that they may be used to convey material to areas that are hard to reach by other mechanical conveyors. However, pneumatic conveyors require relatively higher specific power as compared to screw conveyors.

14.2.1 Pneumatic conveyor methods and equipment

14.2.1.1 Types of pneumatic conveying systems

The pneumatic conveying systems can be divided into three types: positive pressure, negative pressure, and combination negative/positive pressure systems. However, negative pressure systems are not common in agricultural applications.

Positive pressure systems. Material is introduced into the high-pressure stream of air by means of an air lock as shown in Figure 14.7. The material may be transported from a single point to many destination points. There is no need for a cyclone separator and a dust collector. High capacities may be obtained from a relatively smaller unit due to the higher operating pressures. The system is limited to 10 psig pressure.

Combination negative/positive systems. Some systems employ a combination of both vacuum and positive pressure. Vacuum is used to draw the material into the system and then the positive pressure is used to convey the material to its destination. The air mover for this system is larger than either of the above systems. A combination system is shown in Figure 14.8. The total range of pressure for the combination system is 33 cm (13 in.) Hg to 68.9 kPa (10 psig).
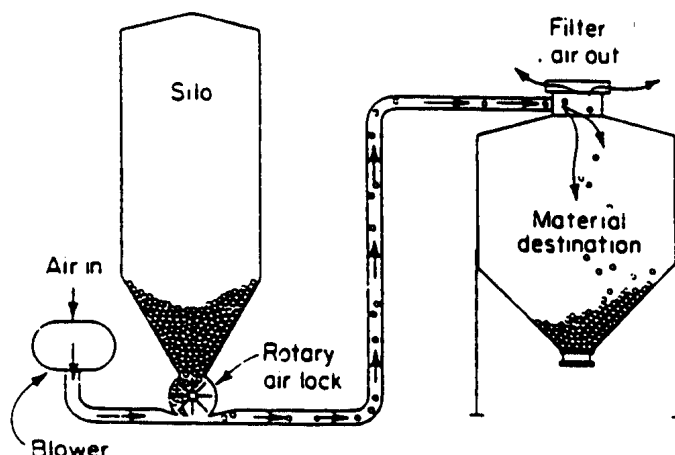
Figure 14.7 – A positive pressure pneumatic conveying system (reproduced from *Chemical Engineers' Handbook* by permission of McGraw-Hill Book Co.).
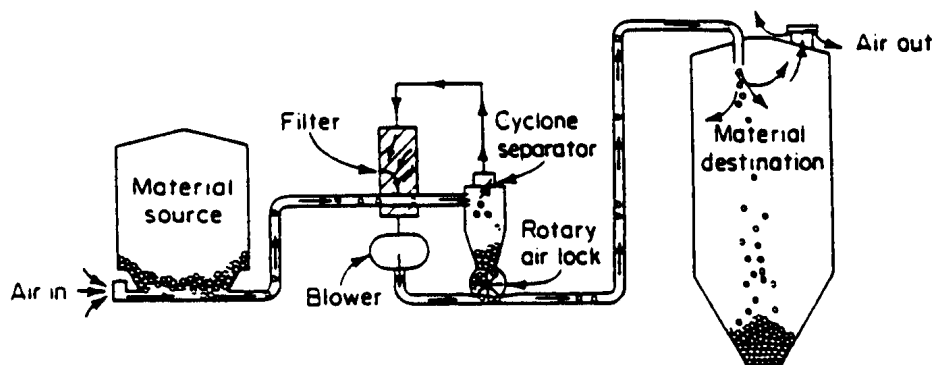
Figure 14.8 – A combination negative/positive pressure pneumatic conveying system (reproduced from *Chemical Engineers' Handbook* by permission of McGraw-Hill Book Co.).

14.2.1.2 Components of pneumatic conveying systems

The necessary components used to complete a pneumatic conveying system may be classified into the air moving system, the feeding system, the discharge system, and the piping and fittings.

Air moving system. The selection of the air mover depends upon the pressure and airflow requirements of the system. The air movers may be divided into low volume, high pressure or high volume, low pressure systems. Figure 14.9 shows a rotary posi-

(a)   **(b)**
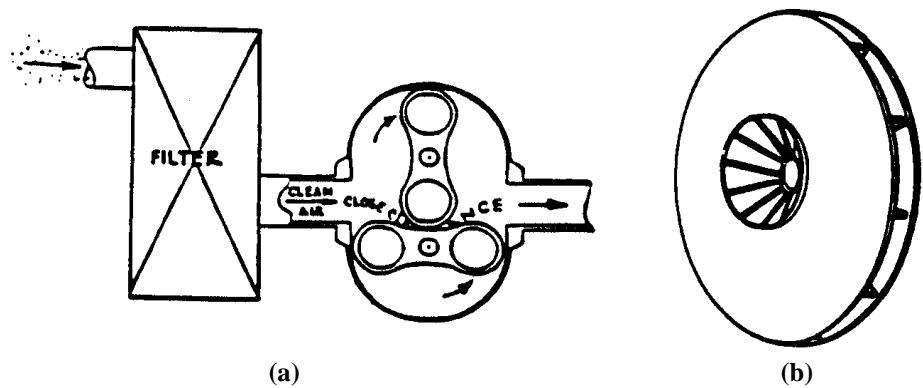
**Figure 14.9 – (a) A rotary positive displacement blower, (b) a centrifugal blower
(reprinted from Hellevang, 1985).**

tive displacement blower and centrifugal blower. As shown in the figure, a pair of
lobed rotors fitted inside a housing create the positive pumping action. These blowers
are suitable for pressures up to 68.9kPa (10 psig). A pressure relief valve and an air
filter are essential for a positive displacement blower. A centrifugal blower can gener-
ate a large volume of air but at relatively low pressures—usually less than 34.5 kPa (5
psig). However, the blowers may be connected in series to generate higher pressures.
Centrifugal blowers are more tolerant of dirt which is an advantage when used in a
negative pressure system.

   Feeding system. The design of a feeding system depends upon the type of the con-
veying system used. For a pipeline under vacuum the material may be metered in
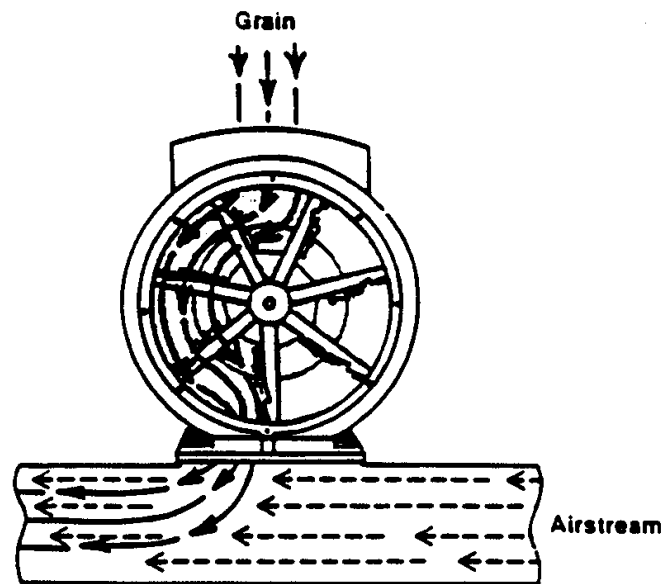
Figure 14.10 – A rotary air lock (reprinted from Hellevang, 1985).
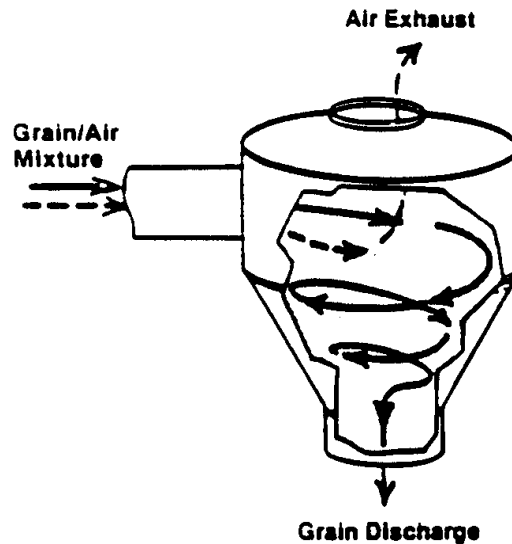
Figure 14.11 – A cyclone separator (reprinted from Hellevang, 1985).

through a rotary air lock, a controlled feed hopper, or a self-regulating pickup nozzle. For a pipeline under positive pressure the material must be metered in through a rotary air lock to keep back pressure to a minimum. A vent is provided in the feed hopper to relieve back pressure. Figure 14.10 shows a rotary air lock feeder. The speed of rotation is controlled to regulate the material flow rate.

Discharge system. For a pipeline under vacuum, the conveyed material must be separated from the conveying air. A *cyclone separator* is used to slow the grain in order for it to settle in the bottom and be separated from the air. A screen or a filter is needed to remove the dirt from the air before it enters the blower. For pipelines under pressure, the material may be discharged directly into the bins or silos. The discharge is tangential to create a cyclone effect. Often, in high velocity, low positive pressure systems, a cyclone separator is used to slow the material down to minimize damage to grain. A cyclone separator is shown in Figure 14.11.

Pipelines and fittings. Pipeline diameter, wall thickness, and the pipe material are to be determined while selecting a pipeline. The pipe material should be wear resistant. Most piping has smooth bores and couplings that butt the pipes to minimize grain damage. Long factory bends are preferred to minimize grain damage and pipe wear. It is recommended that the turning radius be six to eight times the tube diameter for bends of 45° or greater.

14.2.2 Theory of pneumatic conveyors

As solid particles are introduced in a flowing stream of air in a duct they are subjected to aerodynamic drag. If the air velocity is sufficiently high the particles accelerate and the drag is reduced, because the relative velocity between the particles and the
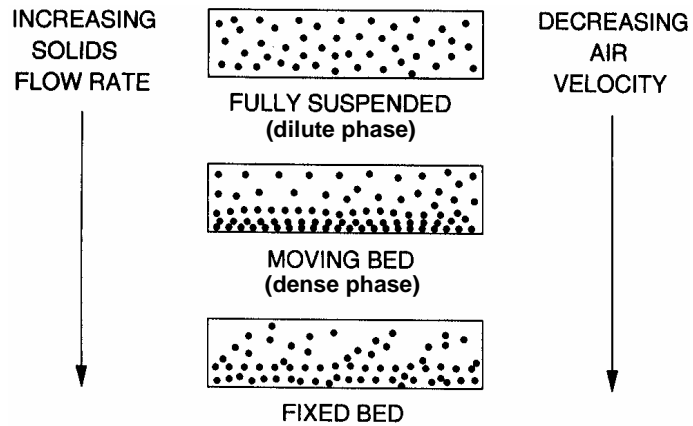
Figure 14.12 – Different phases of solids flow in pneumatic conveying.

air also is reduced. When the particles are being conveyed, the drag overcomes the forces of gravity, particle-to-particle interaction, and friction between the particles and the conduit wall. As the number of particles in the airstream are increased as a result of a higher conveying rate, the resistance to airflow increases. If the conveying rate of the solids continues to increase, there comes a point when the particles no longer behave as discrete particles. They may form clusters and eventually a plug if the flow rate of solids continues to increase. The phase when the solids are in a uniform suspension is called the *dilute phase* (also called the *lean phase*). The *dense phase* occurs when the particles begin to form clusters. Conveying of agricultural material is done in the dilute phase. Figure 14.12 shows the distribution of particles as the solids flow rate increases.

Figure 14.13 shows a plot of pressure drop per unit length versus superficial airflow velocity at different material flow rates. In the initial part of the curve, the pressure drop decreases as the velocity increases. Then, after a certain velocity the pres-
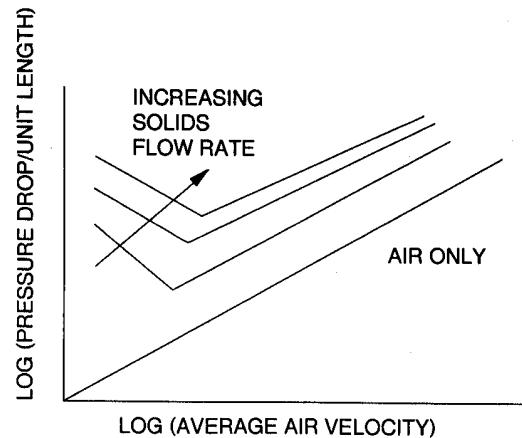
Figure 14.13 – A pneumatic conveying state diagram.

sure drop increases. The point of inflection of the curve essentially separates the dense phase from the dilute phase. The point that separates the two flow regimes is based on the mass flow rate of solids relative to that of the air. Generally, a solid/air mass flow ratio less than 15 would result in the dilute phase. The minimum point on the curve represents the minimum velocity required to produce the dilute phase for that mass flow rate.

During transport, the solid particles are in a suspension and may be treated as an aggregate of solids with void space. The void ratio (e) is defined as:

$$e = \frac{V - V_s}{V} = 1 - \frac{V_s}{V} \tag{14.9}$$

where V_s = volume occupied by solids, m^3
    V = total volume, m^3
The total volume occupied by solids is the sum of each solid particle and may be expressed as follows:

$$V_s = n\, V_p = \frac{\dot{m}}{\rho_p c} dL \tag{14.10}$$

where n = number of solids in the control volume
    V_p = volume of each solid particle, m^3
    $\dot{m}$ = mass flow rate of solids, kg/s
    ρ_p = density of solid particles, kg/m^3
    c = velocity of solid particles, m/s
    dL = elemental length of the conveyor tube, m
The density of solid particles may be determined from the data presented in Table 14.2. Substituting Equation 14.10 in Equation 14.9 we get:

$$e = 1 - \frac{\rho^*}{\rho_p} \tag{14.11}$$

where ρ^* = apparent bulk density of solids during transport, kg/m^3, calculated as:

$$\rho^* = (\phi_m v \rho)/c$$

where ϕ_m = mass flow ratio = $\dot{m}/(\rho Q)$
    where Q = volumetric flow rate of air, m^3/s
        v = velocity of air, m/s
        ρ = density of air, kg/m^3
        c = solids velocity, m/s
Marcus et al. (1990) have reported the following equation for estimating the solids velocity (c):

$$\frac{c}{v} = 1 - 0.68 d^{0.92} \rho_p^{0.5} \rho^{-0.2} D^{0.54} \tag{14.12}$$

where d = particle mean diameter, m.
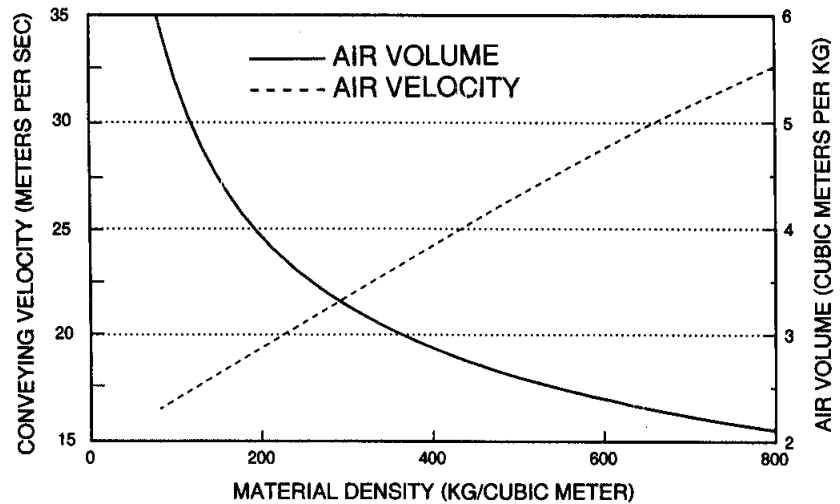
Figure 14.14 – Average velocities and air volume for low pressure pneumatic conveying of materials (redrawn from ASAE Data D273).

The design of a pneumatic conveying system involves determining the conveying air velocity, volume of conveying air, total pressure drop, and power requirement for the blower. The air velocity depends upon the size, shape, and density of the particles to be conveyed. The volume of air depends on the desired mass flow rate. Figure 14.14 shows the desired air velocity and volumetric flow rate that would produce dilute phase transport conditions. The pressure drop in the conveying system is a sum of many terms, as given by the following equation:

$$\Delta p = \Delta p_L + \Delta p_a + \Delta p_s + \Delta p_g + \Delta p_b + \Delta p_c \qquad (14.13)$$

where Δp = total system pressure drop, Pa

Δp_L = line pressure loss due to air only, Pa

Δp_a = pressure drop due to particle acceleration, Pa

Δp_s = pressure drop due to solids friction, Pa

Δp_g = pressure drop due to vertical lift, Pa

Δp_b = pressure drop in bends, Pa

Δp_c = pressure drop in accessories, Pa

Line pressure loss. The line pressure loss is the pressure loss due to only air flowing through the conveying ducts. It can be estimated from the following equation:

$$\Delta p_L = \lambda_l \frac{\rho}{2} v^2 \frac{L}{D} \qquad (14.14)$$

where λ_l = friction loss factor

L = length of the conveying duct, m

For turbulent flow the following equation given by Koo (as cited in Marcus et al., 1990) may be used to determine line friction loss factor:

$$\frac{\lambda_1}{4} = 0.0014 + 0.125 N_{Re}^{-0.32} \tag{14.15}$$

where the Reynolds number $N_{Re} = (\rho v D)/\mu$, and μ is the viscosity of air.

Acceleration pressure drop. As the solids are introduced into the air stream they are accelerated to the solids velocity (c). This acceleration requires an additional pressure drop. This pressure drop may be estimated from the following equation given by Marcus et al. (1990):

$$\Delta p_a = \phi_m v \rho c \tag{14.16}$$

Pressure drop due to solids. This pressure drop is due to solid particle interaction and wall friction. The following equation may be used to estimate this part of the total pressure drop:

$$\Delta p_s = \phi_m \lambda_s \frac{\rho}{2} v^2 \frac{L}{D} \tag{14.17}$$

Konno and Saito (Marcus et al., 1990) gave the following equation to determine the solids friction factor, λ_s, needed in the above equation:

$$\lambda_s = \frac{0.0285\sqrt{gD}}{c} \tag{14.18}$$

where g = acceleration due to gravity (9.81 m/s^2).

Pressure drop due to lift height. This pressure drop represents the potential energy change in lifting the solids through the desired height. The following equation is used to estimate this pressure drop:

$$\Delta p_g = \rho^* g \Delta z \tag{14.19}$$

where Δz = lift height, m.

Pressure drop due to bends. As the air/solid mixture goes around a bend, there is some loss of energy due to the friction of air and solids against the wall. The solids slow down as they go around the bend and an additional pressure is needed to accelerate them up to the conveying velocity. The pressure drop in a bend is computed separately for air and solids. The pressure drop due to air only is calculated by determining an equivalent length for the bend. An equivalent length is that length that produces the pressure drop in a straight pipe as that in the bend. The following equation is used to compute the equivalent length:

$$L_{eq} = \frac{K D}{\lambda_1} \tag{14.20}$$

where K = fitting loss coefficient.

The fitting loss coefficient (K) can be selected from Table 14.3. Equivalent length should be calculated for each bend and added to determine the total pressure loss due to the bends.

The pressure loss due to the solids can be calculated by the following equation:

$$\frac{\Delta p_{b,solids}}{\rho V^2} = 0.245 \left(\frac{\dot{m}}{\rho v D^2}\right)^{1.267} \left(\frac{R}{D}\right)^{-0.260} \tag{14.21}$$

where $\Delta p_{b,solids}$ = pressure drop due to solids in bends, Pa

R/D = bend radius to pipe diameter ratio

Pressure drop in accessories. The pressure loss in accessories is based on their design. No simple equations are available to estimate this pressure drop. Graphs are available in literature that can be used to determine Δp_c for different accessories. Often manufacturers provide pressure drop data which should be consulted. Table 14.4 gives pressure loss data for some common accessories.

Power requirements. The blower power requirement depends on the conveying air volumetric flow rate and total system pressure drop. The power requirement may be computed from the following equation for standard air. Correction should be made for altitude, temperature, and humidity.

$$P = \frac{\Delta p \, Q}{\eta_b} \tag{14.22}$$

where P = blower power requirement, W

Δp = total system pressure drop, Pa

Q = volumetric flow rate of air, m^3/s

η_b = blower efficiency, 0.5 to 0.7

The specific power or power per unit material flow rate may be calculated from:

Table 14.3. Some fitting loss coefficients, K, for turbulent flow (ASHRAE, 1972).

Fitting	Geometry	K
Entrance	Sharp	0.5
	Well-rounded	0.005
Contraction	Sharp ($D_2/D_1 = 0.5$)	0.38
90° elbow	Miter	1.3
	Short radius	0.9
	Long radius	0.6

Table 14.4. Presssure loss data for some common pneumatic conveying accessories (Noyes and Pfieffeer, 1985).

Accessory	Pressure drop, kPa
Blower suction	0.7
Inlet filter	0.7
Inlet filter and muffler	1.4
Outlet muffler and check plate	1.4
Discharge cyclone	0.7
Bin vent	1.4
In-line filter	1.4

508   CHAPTER 14 CONVEYING OF AGRICULTURAL MATERIALS

$$P' = \frac{P}{\dot{m}} \qquad (14.23)$$

where P' = specific power, W s/kg.

Example 14.2

Wheat is to be conveyed through a horizontal distance of 30 m horizontally and 10 m vertically at a rate of 30,000 kg/h. The transport line has four 90° bends and its diameter is 12.7 cm. Assuming standard air properties, determine total system pressure loss and blower power requirement.

Solution

From Table 14.2, wheat density, $\rho = 769$ kg/m^3. Corresponding to this value, it is recommended that the conveying velocity be 32 m/s (Figure 14.14).

Volumetric flow rate of air = Q = $(\pi/4)(0.127)^2(32) = 0.405$ m^3/s

Mass airflow rate, $\rho Q = 1.2(0.405) = 0.486$ kg/s

Converting the 30,000 kg/h conveying rate to kg/s, we get 8.33 kg/s.

Then, mass flow ratio, $\phi_m = 8.33/0.486 = 17.1$

This ratio is higher than the required 15 for lean phase conveying. The velocity of air must be increased to decrease the mass flow ratio.

Required air mass flow rate = 8.33/15 = 0.56 kg/s

Required air velocity, $v = \dfrac{0.56}{1.2\dfrac{\pi}{4}(0.127)^2} = 36.53$ m/s

Corresponding Reynolds number,

$$N_{Re} = \frac{\rho\,v\,D}{\mu} = \frac{1.2(36.53)(0.127)}{10^{-5}} = 5.57 \times 10^5$$

Line pressure loss, $\Delta p_L = \lambda_l \dfrac{\rho}{2} v^2 \dfrac{L}{D}$

$$\lambda_l/4 = 0.0014 + 0.125(5.57 \times 10^5)^{-0.32}$$

$$\lambda_l = 0.013$$

So $\Delta p_L = 0.013\dfrac{1.2}{2}(36.53)^2 \dfrac{(30+10)}{0.127} = 3240\,\text{Pa} = 3.24\,\text{kPa}$

Acceleration pressure loss (use Table 9.1, p. 266, for d, particle diameter),

$$\Delta p_a = \phi_m \, v \, \rho \, c$$

$$c/v = 1 - 0.68 \, d \, p^{0.92} \, \rho_p^{0.5} \, \rho^{-0.2} \, D^{0.54}$$

$$= 1 - 0.68 \, (4.10 \times 10^{-3})^{0.92} (1300)^{0.5} (1.2)^{-0.2} (0.127)^{0.54} = 0.951$$

$$c = 0.951(36.53) = 34.74 \text{ m/s}$$

$$\Delta p_a = 15(36.53)(1.2)(34.74) = 22843 \text{ Pa} = 22.84 \text{ kPa}$$

Pressure drop due to lift height, $\Delta p_g = \rho^* \, g \, \Delta z$

$$\rho^* = \frac{\phi_m v \rho}{c} = \frac{15(36.53)(1.2)}{37.74} = 18.91 \text{kg} / \text{m}^3$$

$$\Delta p_g = 18.91(9.81)(10) = 1860 \text{ Pa} = 1.86 \text{ kPa}$$

Pressure drop due to solids, $\Delta p_s = \phi_m \lambda_s \dfrac{\rho}{2} v^2 \dfrac{L}{D}$

$$\lambda_s = \frac{0.0285\sqrt{g \, D}}{c} = \frac{0.0285\sqrt{9.81(0.127)}}{34.74} = 0.92 \times 10^{-3}$$

$$\Delta p_s = 15(0.92 \text{x} 10^{-3}) \frac{1.2}{2} (36.53)^2 \frac{40}{0.127} = 3460 \text{Pa} = 3.46 \text{ kPa}$$

Pressure loss in bends, $L_{eq} = \dfrac{K \, D}{\lambda_l}$

Assuming K = 0.9 (Table 14.3), $L_{eq} = \dfrac{0.9(0.127)}{0.013} = 8.79$ m

Total equivalent length for four bends, $L_{eq} = 4 \, (8.79) = 35.2$ m

Pressure loss, $\Delta p_{b,air} = 3.24(35.2)/40 = 2.85$ kPa

Pressure loss due to solids (assuming R/D = 5),

$$\frac{\Delta p_{b,solids}}{\rho \, v^2} = 0.245 \left(\frac{\dot{m}}{\rho \, v \, D^2} \right) \left(\frac{R}{D} \right)^{-0.260}$$

$$= 0.245 \ \frac{8.33}{1.2(36.53)(0.127)^2} \ (5)^{-0.260} = 1.90$$

$$\Delta p_{b,solids} = 1.90(1.2)(36.53)^2 = 3040 \text{ Pa} = 3.04 \text{ kPa}$$

Thus, the total pressure drop is:

$$\Delta p = 3.24 + 22.84 + 1.86 + 3.46 + 2.85 + 3.04 = 37.4 \text{ kPa}$$

Note that the pressure drop is exclusive of the pressure drop due to the accessories, such as cyclones, etc.

The power requirement is then $P = \dfrac{\Delta p \, Q}{\eta_h} = \dfrac{37.4 \dfrac{\pi}{4}(0.127)^2 \, 36.53}{0.6} = 28.8 \text{ kW}$

14.2.3 Pneumatic conveyor performance

The performance of a pneumatic conveying system depends on factors related to the equipment, the material being conveyed, and the operating conditions. Proper design is important for efficient operation. The selection of the type of conveying system would depend upon the given constraints on material feeding and discharge. Material properties and the desired feed rate would determine the airflow rate and the power requirements. Figure 14.15 presents performance data for corn for a 11.12 kW (15 hp) positive pressure system. The figure shows the effect of vertical lift and the horizontal conveying distance on the volumetric conveying rate. Table 14.5 gives a comparison of performance of an 60 kW (80 hp) positive/negative pneumatic unit with a 15.2 cm (6 in.) screw conveyor (PAMI, 1979). It is evident that a screw conveyor is considerably more efficient than the pneumatic unit.

Grain damage is an important performance parameter. According to a PAMI test report (1977), 0.25% grain damage is caused for each pass through a pneumatic unit. It was also reported that the damage was comparable to that caused by a grain auger. Grain damage increases with conveying speed. Table 14.6 shows the effect of conveying speed on damage for white beans. Grain damage as caused by air lock is shown in Table 14.7 for two phases of conveying (Hellevang, 1985).
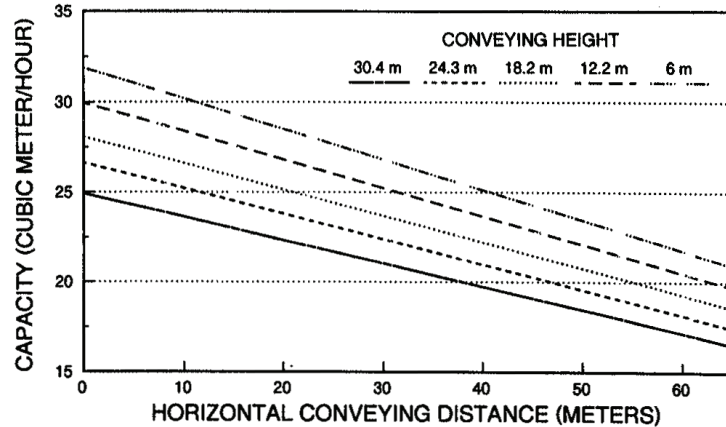

Figure 14.15 – Capacity of a pneumatic conveyor as affected by the vertical lift and the conveying distance (drawn using data by Hellevang, 1985).

**Table 14.5. Comparison of 60 kW, positive/negative pressure 20.32 cm (8 in.)
pneumatic unit to a 15.24 cm (6 in.) grain auger (Hellevang, 1985).**

Grain type	Maximum conveying rates				Specific capacities	
	Pneumatic unit		Auger		Pneumatic unit,	Auger,
	t/h	m^3/h	t/h	m^3/h	m^3/kWh	m^3/kWh
Wheat	25.1	28.5	37.6	42.7	0.87	10.60
Barley	24.2	34.4	27.9	39.7	1.04	11.77
Oats	33.5	67.1	21.8	43.8	1.79	16.00

**Table 14.6. Damage in conveying white beans
with a pneumatic conveyor (Hellevang, 1985).**

Seed velocity, m/min	Germination, %	Visible seed damage, %
0 (control)	93.5	0.00
198	91.0	0.40
292	89.7	0.49
440	83.5	0.59
505	82.7	0.70
689	73.5	1.62

**Table 14.7. Damage in conveying white beans
with a pneumatic conveyor (Hellevang, 1985).**

Breakage due to	Conveying Phase	
	Dense phase, %	Lean phase, %
Air lock	1.03	0.27
Transport	0.52	1.35
Total	1.55	1.62

14.3 BUCKET ELEVATORS

The bucket elevator is most commonly employed for vertical conveying of free-flowing materials such as small grain and pellets. A bucket elevator consists of equally spaced buckets mounted on a belt. The belt wraps around two pulleys located at the top and the bottom of a rectangular shaped housing as shown in Figure 14.16. As the belt rotates the buckets scoop some grain from the bottom and carry it up. At the top the buckets unload the material as they go around the top wheel and are made to turn upside down. Bucket size varies from 10.16 cm × 7.62 cm (4 in. × 3 in.) to as large as 35.56 cm × 20.32 cm (14 in. × 8 in.). Bucket spacing ranges from 11.43 cm (4.5 in.) to 30.49 cm (12 in.). The belt speed can vary from 1.2 m/s to 3.3 m/s. The capacity of the bucket elevator depends on the bucket size, bucket spacing, and belt speed. Commonly, the capacity of the elevators employed for agricultural applications is in the range of 7 m^3/h to 350 m^3/h.
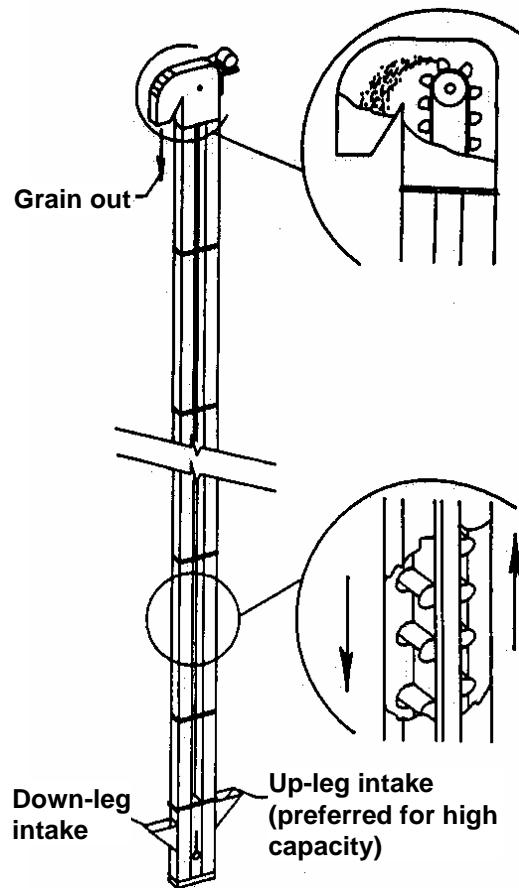
**Figure 14.16 – Schematic diagram of a bucket elevator
(reproduced with permission from *Grain Drying, Handling and
Storage Handbook,* 2nd ed., 1987 © Midwest Plan Services).**

14.3.1 Theory of bucket elevators

The relationship between head wheel speed and diameter is very important for satisfactory operation of this type of elevator. When the mass of grain in the bucket is moving around the head pulley it is subjected to the force of gravity acting vertically downward and the centrifugal force acting radially from the center of the head pulley. The resultant of these forces causes the material to be discharged from the bucket into the discharge chute. For clean emptying of the buckets, the start of the flow from the bucket must be delayed until after the bucket has passed its uppermost position on the head wheel. This situation will exist when the gravity and the centrifugal forces are equal. When the bucket reaches the top position on the head wheel, the resultant of the two forces will be zero, and there will be no discharging force on the material. It will neither be thrown vertically from the bucket nor fall out of the bucket.

Equating the weight of the grain to the centrifugal force acting on the grain, we get:

$$W = \frac{W}{g} \frac{v^2}{R}$$

or
$$v^2 = g\,R$$

or
$$v = \sqrt{g\,R}$$

Using $v = 2\pi Rn = (gR)^{0.5}$, the necessary wheel speed may be calculated as:

$$n = \frac{1}{2\pi}\sqrt{\frac{g}{R}} \tag{14.24}$$

where W = weight of material, N
  v = velocity of material, m/s
  g = acceleration of gravity, m²/s
  R = radius to the center of gravity of material in the bucket, m
  n = speed of head pulley, rps

  Figure 14.17 shows the relationship between the head wheel speed and the radius of the path of the center of gravity of the material in the bucket about the center of the head wheel. To find the diameter of the head wheel, deduct from this radius the thickness of the belt and the distance from the belt to the center of gravity of the material in the bucket.

  The trajectory of the material from the buckets is parabolic and can be determined from an equation of motion. It has been found that for high-speed elevators, those with head wheel diameters and speeds determined from the high-speed curve in Figure 14.17, the inner lip of the discharge chute should be located as close to the descending buckets as possible and at an angle of 15° to 20° below the center of the head wheel.
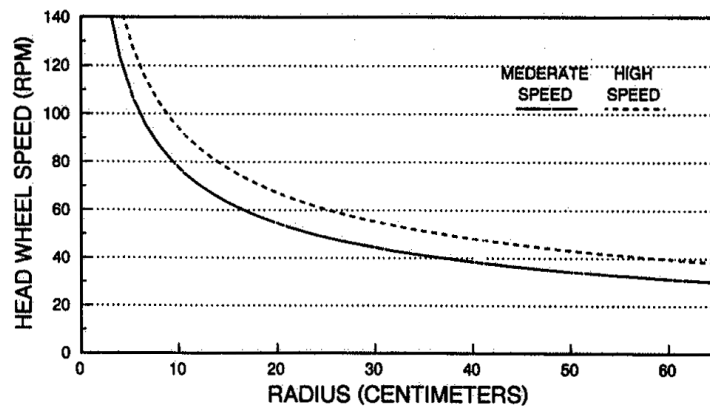

Figure 14.17 – Bucket conveyor vs. radius of the path of the center of gravity of the material in the bucket (redrawn from Millier, 1958).

14.3.2 Bucket elevator capacity

The capacity of bucket elevators depends upon the capacity of the individual buckets, the bucket spacing, and speed of the belt or chain carrying the buckets. Bucket spacing is governed by the shape of the bucket and its resulting discharge characteristics.

The capacity of a bucket is considered to be from 85% to 90% of the struck volume for high-speed elevators, if the feed is arranged to allow loading at or above the center of the foot shaft. If loading is below this point, the capacity may be reduced to 80% of the struck volume. On moderate speed elevators the bucket should be expected to fill 90% of its struck volume.

The following equation is used to determine elevator capacity:

$$Q = \frac{V\,v}{s} \tag{14.25}$$

where Q = elevator capacity, m^2/s
      V = bucket volume, m^3
      v = belt speed, m/s
      s = bucket spacing, m)

14.3.2 Bucket elevator power

The horsepower required to operate a bucket elevator is that required to lift the material, to scoop the material into the buckets, to discharge the material, to move a small amount of air, and to overcome friction in the bearings and other drive components. In general the bucket elevator has a high elevating efficiency. In practice it has been found that theoretical horsepower required to lift the material needs to be increased only 10% to 15% to obtain the actual power requirement. The following equation is used to obtain the theoretical power requirement:

$$P = \rho_b g\,Q\,h \tag{14.26}$$

where P = theoretical power, W
     ρ_b = material bulk density, kg/m^3
     h = material lift height, m

It is advisable to use the struck volume of each bucket in determining the elevator capacity. This will eliminate power failures in instances where feed rate is high and the buckets are filling well above the center of the foot wheel.

Example 14.3

Find the velocity of the material being conveyed if the radius to the center of gravity of the material in the bucket is 30.48 cm (12 in.). Then, find the speed of the head pulley in rev/min. Determine the power requirement of this bucket elevator.

Given: bucket capacity = 0.25 kg   bucket spacing = 20 cm
            belt speed = 1.25 cm/s   height = 15 cm

Velocity of material $= v = \sqrt{gR} = \sqrt{9.81 \times 0.3048} = 1.729 \text{m/s}$

Speed of the head pulley $= n = \dfrac{60}{2\pi} \sqrt{\dfrac{g}{R}} = \dfrac{60}{2\pi} \sqrt{\dfrac{9.81}{0.3048}} = 54.17 \text{rpm}$

Elevator capacity can be found as capacity $= \dfrac{\text{bucket capacity} \times \text{belt speed}}{\text{bucket spacing}}$

$$= \dfrac{0.25 \times 1.250}{0.2} = 1.5625 \text{kg/s}$$

Then, power requirement $=$ capacity $\times$ height $\times$ g

$$= 1.5625 \times 1.5 \times 9.81 = 22.845 \text{ W}$$

MACHINERY SELECTION AND MANAGEMENT

15

INTRODUCTION

Because of the seasonal nature of farm work, farm machinery is used during relatively short periods of the year. With growth in average farm size, machines of high capacity are required to accomplish their task during these short periods. Unlike factory machines, whose costs can be amortized over thousands of hours of annual use, farm machines are typically amortized over hundreds of hours of annual use. The need to amortize machine costs over low hours of annual use puts tight constraints on the manufacturing costs of farm machines. At the same time, since lost time is very costly during the limited periods of annual use, farm machines must be designed to have high reliability and high field efficiency. As early as 1924, it was noted that "time is the essence of farming" and that whatever helps to shorten the time required for planting and harvesting will help overcome the effects of adverse weather (Mount, 1924). Thus, machinery selection and management techniques are of great interest to both the designer and user of farm machinery. ASAE (now ASABE) has fostered research on machinery selection and management for many years and currently has three related documents in its annual standards book. They are Standard S495 on uniform terminology, Engineering Practice EP496 on machinery management, and D497 on machinery management data.

15.1 FIELD CAPACITY AND EFFICIENCY

15.1.1 Field capacity

Field capacity refers to the amount of processing that a machine can accomplish per hour of time and was first calculated by McKibben (1930). Field capacity can be expressed on a material or area basis. On an area basis, the field capacity is:

$$C_a = \frac{v \, w \, \eta_f}{10} \tag{15.1}$$

On a material basis, the field capacity is:

$$C_m = \frac{v\,w\,Y\,\eta_f}{10} \tag{15.2}$$

where C_a = field capacity, area basis, ha/h (C_{at} when η_f = 1.0)

C_m = field capacity, material basis, Mg/h (C_{mt} when η_f = 1.0)

v = travel speed, km/h

w = machine working width, m

Y = crop yield, Mg/ha

η_f = field efficiency, decimal

The term *theoretical field capacity* is used to describe the field capacity when the field efficiency is equal to 1.0, i.e., theoretical field capacity is achieved when the machine is using 100% of its width without interruption for turns or other idle time. For cultivators and other machines that work in rows, the machine working width is equal to the row spacing times the number of rows processed in each pass. An operator with perfect steering skills would be required to use the full width of mowers and other machines that do not work in rows. Since operators are not perfect, less than the full width of such machines is used in order to ensure coverage of the entire land area, i.e., there is some overlapping of coverage.

The travel speed of balers, forage choppers, and other machines that process a product may be limited by the C_{mt}, i.e., by the theoretical field capacity of the machine on a materials handling basis. For a given C_{mt}, W, and Y, Equation 15.2 could be used with η_f =1.0 to find the allowable forward speed. Equation 15.2 is not relevant to machines that do not process a product, e.g., tillage machines; the speed of such machines is limited by one or more other factors, including available power, quality of the work accomplished, safety, etc. Typical operating speeds for various machines are listed in Table 15.1.

15.1.2 Field efficiency

The theoretical time, τ_t, required to perform a given field operation varies inversely with the theoretical field capacity and can be calculated using the following equation:

$$\tau_t = \frac{A}{C_{at}} \tag{15.3}$$

where τ_t = theoretical time required to perform operation, h

C_{at} = theoretical field capacity, ha/h

A = area to be processed, ha

The actual time required to perform the operation will be increased due to overlap, time required for turning on the ends of the field, time required for loading or unloading materials, etc. Such time losses lower the field efficiency below 100%. The following equation can be used to calculate the field efficiency:

$$\eta_f = \frac{\tau_t}{\tau_e + \tau_h + \tau_a} \tag{15.4}$$

where $\tau_e = \tau_t/K_w$ = effective operating time, h

K_w = fraction of implement width actually used

τ_a = time losses that are proportional to area, h

τ_h = time losses that are not proportional to area, h

Table 15.1. Field efficiency, field speed , and repair and maintenance cost parameters (adapted from ASAE Data D497).

Machine	Effic. Range %	Typ. Effic. %	Speed Range, km/h	Typ. Speed, km/h	Est. Life, h	Total Life R & M[b] Cost, % of list price	RF1	RF2
Tillage and Planting								
Moldboard plow	70-90	85	5.0-10.0	7.0	2000	100	0.29	1.8
Heavy-duty disk	70-90	85	5.5-10.0	7.0	2000	60	0.18	1.7
Tandem disk harrow	70-90	80	6.5-11.0	10.0	2000	60	0.18	1.7
Chisel plow	70-90	85	6.5-10.5	8.0	2000	75	0.28	1.4
Field cultivator	70-90	85	8.0-13.0	11.0	2000	70	0.27	1.4
Spring tooth harrow	70-90	85	8.0-13.0	11.0	2000	70	0.27	1.4
Roller-packer	70-90	85	7.0-12.0	10.0	2000	40	0.16	1.3
Mulcher-packer	70-90	80	6.5-11.0	8.0	2000	40	0.16	1.3
Rotary hoe	70-85	80	13-22.5	19.0	2000	60	0.23	1.4
Row crop cultivator	70-90	80	5.0-11.0	8.0	2000	80	0.17	2.2
Rotary tiller	70-90	85	2.0-7.0	5.0	1500	80	0.36	2.0
Row crop planter	50-75	65	6.5-11.0	9.0	1500	75	0.32	2.1
Grain drill	55-80	70	6.5-11.0	8.0	1500	75	0.32	2.1
Harvesting								
Corn picker sheller	60-75	65	3.0-6.5	4.0	2000	70	0.14	2.3
Combine	60-75	65	3.0-6.5	5.0	2000	60	0.12	2.3
Combine (Sp)[a]	65-80	70	3.0-6.5	5.0	3000	40	0.14	2.1
Mower	75-85	80	5.0-10.0	8.0	2000	150	0.46	1.7
Mower (rotary)	75-90	80	8.0-19.0	11.0	2000	175	0.44	2.0
Mower-conditioner	75-85	80	5.0-10.0	8.0	2500	80	0.18	1.6
Mower-condition (rotary)	75-90	80	8.0-19.0	11.0	2500	100	0.16	2.0
Windrower (SP)	70-85	80	5.0-13.0	8.0	3000	55	0.06	2.0
Side delivery rake	70-90	80	6.5-13.0	10.0	2500	60	0.17	1.4
Rectangular baler	60-85	75	4.0-10.0	6.5	2000	80	0.23	1.8
Large rectangular baler	70-90	80	6.5-13.0	8.0	3000	75	0.10	1.8
Large round baler	55-75	65	5.0-13.0	8.0	1500	90	0.43	1.8
Forage harvester	60-85	70	2.5-8.0	5.0	2500	65	0.15	1.6
Forage harvester (SP)	60-85	70	2.5-10.0	5.5	4000	50	0.03	2.0
Sugar beet harvester	50-70	60	6.5-10.0	8.0	1500	100	0.59	1.3
Potato harvester	55-70	60	2.5-6.5	4.0	2500	70	0.19	1.4
Cotton picker (SP)	60-75	70	3.0-6.0	4.5	3000	80	0.11	1.8
Miscellaneous								
Fertilizer spreader	60-80	70	8.0-16.0	11.0	1200	80	0.63	1.3
Boom-type sprayer	50-80	65	5.0-11.5	10.5	1500	70	0.41	1.3
Air-carrier sprayer	55-70	60	3.0-8.0	5.0	2000	60	0.20	1.6
Bean puller-windrower	70-90	80	6.5-11.5	8.0	2000	60	0.20	1.6
Beet topper/stalk chopper	70-90	80	6.5-11.5	8.0	1200	35	0.28	1.4
Forage blower					1500	45	0.22	1.8
Forage wagon					2000	50	0.16	1.6
Wagon					3000	80	0.19	1.3

[a] SP indicates self-propelled.

[b] R & M is repair and maintenance.

τ_a and τ_h represent the two extremes for types of time losses and some losses may fall between these extremes. Examples of τ_a-type losses include unclogging of spray nozzles, adding filling fertilizer or seed boxes, or filling spray tanks. For a given yield, time spent in unloading harvested crop is proportional to area but unloading time also increases with yield. Many τ_h-type losses are proportional to effective operating time, τ_e; these include rest stops, adjusting equipment, and idle travel at field ends if such travel is at normal operating speed. Field shape can have an important effect on τ_h, i.e., τ_h will be much smaller relative to τ_e if the field is long and narrow. Then the machine will make fewer turns at the end for a given field area. Time required to move a machine to or from a field is not included in field efficiency calculations; else the field efficiency would vary widely depending upon distance between fields and distance from the machine storage site. Calculation of field efficiency and capacity is illustrated in Example Problem 15.1.

Example Problem 15.1

A self-propelled combine with a 12-row corn head for 75 cm row spacing travels at 5 km/h while harvesting corn yielding 12 Mg/ha. Losses proportional to area total to 5.2 minutes per hectare and are primarily due to unloading grain from the combine. Neglecting any other losses, calculate (a) the field efficiency and the field capacity on (b) an area basis and (c) material basis.

Solution
(a) In calculating the field efficiency, consider the time uses while harvesting one hectare. From the given information, $\tau_a = 5.2$ minutes and $\tau_h = 0$. To determine τ_e, note that a row crop header uses the full width, so that $K_w = 1.0$ and thus $\tau_e = \tau_t$. From Equation 15.1, the theoretical field capacity on an area basis is:

$$C_{at} = 5(12 \times 0.75)1.0/10 = 4.5 \text{ ha/h}$$

Then, from Equation 15.3:

$$\tau_e = \tau_t = 1/4.5 = 0.222 \text{ h or } 13.3 \text{ minutes}$$

Finally, from Equation 15.4, the field efficiency is:

$$\eta_f = 13.3/(13.3+5.2+0) = 0.72$$

(b) Now the actual field capacity on an area basis can be calculated:

$$C_a = 4.5(0.72) = 3.24 \text{ ha/h}$$

(c) Finally, by multiplying by the crop yield, the field capacity on a material basis can be calculated:

$$C_m = 3.24(12) = 38.9 \text{ Mg/h}$$

Machine breakdowns cause time losses and reduction of field efficiency if the breakdowns occur during planned working hours. The probability of machine down-time is equal to one minus the operational reliability of the machine. One useful way of expressing machine reliability is as the mean time between failures. As shown in ASAE EP456, the reliability of a group or components or machines with a serial relationship is the product of the individual reliabilities, i.e.:

$$R_m = \frac{100 r_1 r_2 ... r_\lambda}{100^\lambda} \tag{15.5}$$

where R_m = reliability of the entire machine, percent

r_1, r_2, etc. = reliabilities of individual components, percent

λ = total number of components in series

Components are said to be in series if the failure of any one of the components stops the operation of the entire machine. Conversely, reliability can be increased through redundancy, i.e., through use of components in parallel such that, when a component fails, a parallel component will take over the function. Equation 15.5 is valid for calculating the reliability of a single machine based on the reliabilities of its components, or for calculating the overall reliability of a group of machines based on their individual reliabilities. For example, if a successful hay harvesting operation requires the use of a mower, a rake, and a baler in sequence, the overall reliability of the harvesting operation is the product of the individual reliabilities of the mower, rake, and baler. The reliability probability for a machine or group of machines is essentially one for the next minute, but decreases with time. Thus, the probability that a large, complex machine will operate extensively over several seasons without a breakdown is essentially zero. Farmers repair machines during the off-season or trade old machines for new in order to maintain an acceptable level of reliability.

Careful consideration of Equation 15.4 leads to the conclusion that time losses are much more critical for a large machine than for a smaller one. As τ_e declines with increasing C_{at}, time losses τ_a and τ_h become larger relative to τ_e. Thus, as a company increases the theoretical field capacity of its combines, for example, it becomes essential to also increase the rate at which the grain tank can be unloaded, decrease the field time needed to service the machine, and decrease any other time losses. Similarly, in increasing a planter size from 4-row capacity to 12-row capacity, for example, it is important to provide a quicker means for refilling seed boxes on the larger planter. Otherwise, the field efficiency will decrease and the effective field capacity will increase less than the increase in theoretical field capacity. Table 15.1 provides a range of field efficiencies and a typical field efficiency for a variety of machines.

15.3 MACHINERY COSTS

Machinery costs include costs of ownership and operation as well as penalties for lack of timeliness. Ownership costs tend to be independent of the amount a machine is used and are often called fixed or overhead costs. Conversely, operating costs increase in proportion to the amount the machine is used. Total machine costs are the sum of the ownership and operating costs. Ownership, operating, and total machine costs can be calculated on an annual, hourly, or per-hectare basis. Total per-hectare cost is calculated by dividing the total annual cost by the area covered by the machine during the year. A custom cost is the price paid for hiring an operator and equipment to perform a given task. A farm operator can compare total per-hectare costs to custom costs to determine whether it would be better to purchase a machine or to hire the equipment and an operator to accomplish a given task. Per-hectare ownership costs vary inversely with the amount of annual use of a machine. Therefore, a certain minimum amount of work must be available to justify purchase of a machine and, the more work available, the larger the ownership costs that can be economically justified.

15.3.1 Ownership costs

Ownership costs include depreciation of the machine, interest on the investment, and cost of taxes, insurance and housing of the machine.

15.3.1.1 *Depreciation*

Depreciation is the reduction in the value of a machine with time and use. It is often the largest single cost of machine ownership, but cannot be determined until the machine is sold. However, several methods are available for estimating depreciation. One of these is to estimate the current value using various price guides for used equipment. Annual depreciation is generally highest in the first year of the life of a machine and declines each year. The sum-of-the-year digits and the declining-balance methods both give rapid depreciation in the early years and lower depreciation as the machine ages (Thuesen et al., 1971). Rapid early depreciation is used by many machine owners to obtain the income tax advantages associated with such methods. For simplicity in machinery management calculations, straight-line depreciation can be used. With straight-line depreciation, the difference between the purchase price and the salvage value is divided by the machine life to obtain the annual depreciation. Alternatively, the cost of depreciation and interest can be recovered through use of a capital recovery factor. The capital recovery factor is discussed in the Total Annual Ownership Costs section.

15.3.1.2 *Machine life*

The life of a machine can be terminated by wear out or by obsolescence. Wear out does not occur at a definite point in time. Rather, the repair costs required to keep the machine operational gradually increase until it becomes uneconomical to continue making repairs. Obsolescence occurs when the machine is out of production and repair parts are no longer available, or when it can be replaced by another machine or method that will produce a greater profit. Table 15.1 gives the estimated life of a number of machines based on total number of hours until the machine is worn out. The number of years of life until wear-out can be obtained by dividing by the annual hours

of use. In many cases, because of limited annual use, machines will become obsolete before reaching the wear-out lives given in Table 15.1. The term *economic life* is defined as the length of time after purchase of a machine that it is more economic to replace the machine with another than to continue with the first, whether because of wear-out or obsolescence. The economic life is then the appropriate life to use in calculating ownership costs.

15.3.1.3 *Interest on investment*

The money spent to purchase a machine is unavailable for other productive enterprises. Therefore, the cost of ownership includes the interest on the money that is invested in the machine. If a loan is used to purchase a machine, the interest rate is known. If a machine is purchased for cash, the relevant interest rate is the prevailing rate that could have been obtained if the money had been invested instead of being used to purchase the machine. The principal on which the interest is assessed is equal to the remaining value of the machine in any given year. For simplicity, when the straight-line method of depreciation is used, the annual interest cost is assumed to be constant over the life of the machine. It is calculated on the average investment, i.e., the average of the new cost and salvage value of the machine. Alternatively, it can be included in the capital recovery factor.

15.3.1.4 *Taxes, insurance, and shelter*

Taxes include sales tax assessed on the purchase price of a machine and property tax assessed on the remaining value in any given year. For simplicity, both kinds of taxes are distributed over the life of the machine. Some states have neither a sales tax nor property tax and, in such states, no tax cost should be included. The machine designer may not know which tax rate to use, especially if a machine can be used in any of a number of different states. If actual taxes are unknown, it is reasonable to estimate the annual tax charge at 1% of the purchase price of the machine.

Machines may be insured against loss by fire or other causes, in which case the cost of insurance is known. If no insurance policy is purchased, the owner has elected to carry the risk himself but an insurance cost should still be included. Insurance costs should be based on the remaining value of a machine. If insurance costs are unknown, a reasonable estimate of annual insurance cost is 0.25% of the purchase price of the machine.

There are no conclusive data to prove the economic value of sheltering farm machines. Nevertheless, providing shelter is often associated with better care and maintenance of machines that can result in longer life, improved appearance, and better resale value. If shelter is provided, the cost of providing that shelter can be calculated. If no shelter is provided, there is probably an economic penalty associated with reduced machine life and/or resale value. Thus, a shelter cost should be included whether or not shelter is provided. The annual cost of shelter is considered to be constant over the life of the machine. If shelter cost data are unavailable, it is reasonable to estimate annual shelter cost as 0.75% of the purchase price of the machine.

The total cost of taxes, insurance and shelter can be estimated at 2% of the purchase price of a machine unless more accurate data are available. Although taxes, insurance, and shelter are small relative to total ownership costs, they should be included.

15.3.1.5 Total annual ownership costs

The total annual ownership costs, as discussed above, can be expressed in the following equation:

$$C_{os} = \frac{C_{oa}}{P_u} = (1-S_v)\left[\frac{I_r(1+I_r)^{\tau_L}}{(1+I_r)^{\tau_L}-1}\right] + \frac{K_{tis}}{100} \tag{15.9}$$

where C_{os} = specific annual ownership costs, 1/yr
C_{oa} = total annual ownership costs, dollars/yr
P_u = purchase price of machine, dollars
S_v = salvage value as fraction of purchase price
I_r = real annual interest rate, decimal
τ_L = economic life of machine, years
K_{tis} = annual cost of taxes, insurance and shelter as percent of purchase price

As noted above, K_{tis} may be assumed to be 2% unless better data are available. The factor in the square brackets in Equation 15.9 is the capital recovery factor. The need for capital recovery is reduced to the extent that the machine has a salvage value at the end of its economic life. In the absence of better data, S_v is often assumed to be 0.1, i.e., the salvage value is estimated at 10% of the purchase price.

The real interest rate, as defined by Bartholomew (1981) is:

$$I_r = \frac{I_p - I_g}{1 + I_g} \tag{15.10}$$

where I_p = prevailing annual interest rate, decimal
I_g = general inflation rate, decimal

Equation 15.10 adjusts the prevailing interest rate for inflation. If there is no inflation, the real interest rate is equal to the prevailing rate. If the inflation rate is greater than or equal to the prevailing interest rate, the real interest rate is zero and the ownership costs are limited to the cost of taxes, insurance, and shelter. Purchasing a machine during times of high inflation tends to "lock in" costs and make machine ownership more attractive than leasing. Example Problem 15.4 illustrates the calculation of ownership costs.

Example Problem 15.4

The self-propelled combine of Example Problem 15.1 has a purchase price of $100,000, an expected economic life of 10 years, and an expected salvage value of 10% of new cost. At time of purchase, the prevailing interest rate is 6.0%, while the general rate of inflation is 3%. Calculate (a) the specific annual ownership costs and (b) the total annual ownership costs.

Solution

(a) No data were given concerning taxes, insurance, and shelter, so they will be assumed to be 2% of the purchase price, that is, $K_{tis} = 0.02$. From Equation 15.10, the real interest rate is:

$$I_r = (0.06-0.03)/(1+0.03) = 0.029 \text{ or } 2.9\%$$

Then, from Equation 15.9, the specific ownership costs are:

$$C_{os} = (1-0.1)\left[\frac{0.029(1+0.029)^{10}}{(1+0.029)^{10}-1}\right] + \frac{2}{100} = 0.125$$

(c) Finally, the total annual ownership costs are:

$$C_{oa} = \$100,000(0.125) = \$12,500/\text{year}$$

15.3.2 Operating costs

Operating costs are costs associated with use of a machine. They include the costs of labor, fuel and oil, and repair and maintenance. A constant hourly labor cost can be determined for hired operators. If the owner operates the machine, the labor cost is determined from alternative uses of the owner's time. If the cost of labor is unknown at the time of the analysis, a typical community labor rate can be used. Dividing the hourly labor cost by C_a gives the labor cost per hectare of land worked by the machine.

15.3.2.1 Costs of fuel and oil

For any given operation, per-hectare fuel (or oil) cost can be calculated using the following equation:

$$C_s = \frac{p_L Q_i}{C_a} \tag{15.11}$$

where C_s = per-hectare fuel (oil) costs, \$/ha
     p_L = price of fuel (oil), \$/L
     Q_i = fuel (oil) consumed by engine, L/h
     C_a = effective field capacity during the operation, ha/h

Of the three independent variables in Equation 15.11, Q_i is the variable for which it is most difficult to determine a realistic value. The first step is to estimate the engine power required to perform the operation. In Section 15.2, the power requirements of various operations was discussed. Power requirements computed at the drawbar must be converted into equivalent PTO power, as was done in Example Problem 15.2. After the total equivalent PTO power is calculated, the specific fuel consumption of the engine can be estimated. ASAE Data D497 provides specific fuel consumption equations for gasoline, diesel, or LPG engines, but since most farm tractors now have diesel engines, only the diesel equation is given here:

$$SFC_v = 3.91 + 2.64X - 0.203\sqrt{173 + 738X}$$

$$\text{If } X > 0.856, SFC_v = 0.411 \text{ L/kW h} \tag{15.12}$$

where SFC_v = specific fuel consumption, volume basis, L/kW h
   X = ratio of equivalent PTO power requirement to maximum available PTO power

Typical values of X range from approximately 0.2 for spraying operations to 0.85 for primary tillage. Multiplying SFC_v by the equivalent PTO power needed for the operation gives Q_i, the estimated fuel consumption to perform the operation.

The per-hectare cost of oil consumption can be calculated using Equation 15.11 with the word oil substituted for the word fuel. ASAE D497 gives equations for estimating oil consumption of gasoline, diesel, or LPG engines. The equation for diesel engines is:

$$Q_i = \frac{21.69 + 0.59P_r}{1000} \tag{15.13}$$

where Q_i = oil consumption, L/h
   P_r = rated engine power, kW

Equation 15.13 is based on replacement of oil in the crankcase at the manufacturer's recommended change intervals; it does not include oil that must be added between oil changes, nor does it include hydraulic/transmission oil or other lubricants. Total cost of all lubricants is approximately equal to 10% to 15% of fuel costs.

15.3.2.2 Costs of repairs and maintenance

Costs for repairs and maintenance are highly variable depending on the care provided by the manager of the machine. Some expenditures will always be necessary to replace worn or failed parts and/or to repair damage from accidents. Repair and maintenance costs tend to increase with the size and complexity, and thus with the purchase price of the machine. The following equation from ASAE EP496 can be used to estimate accumulated repair and maintenance costs:

$$\frac{C_m}{P_u} = RFl\left[\frac{t}{1000}\right]^{RF2} \tag{15.14}$$

where C_{rm} = accumulated repair and maintenance costs, dollars
   t = accumulated use, h
   RF1, RF2 = repair factors from Table 15.1

To correct for inflation, the purchase price in Equation 15.14 is multiplied by $(1+I_g)^n$, where n is the age of the machine in years. Note that the accumulated repair and maintenance costs vary from year to year. Average hourly costs of repairs and maintenance can be estimated by estimating the total economic life of the machine in
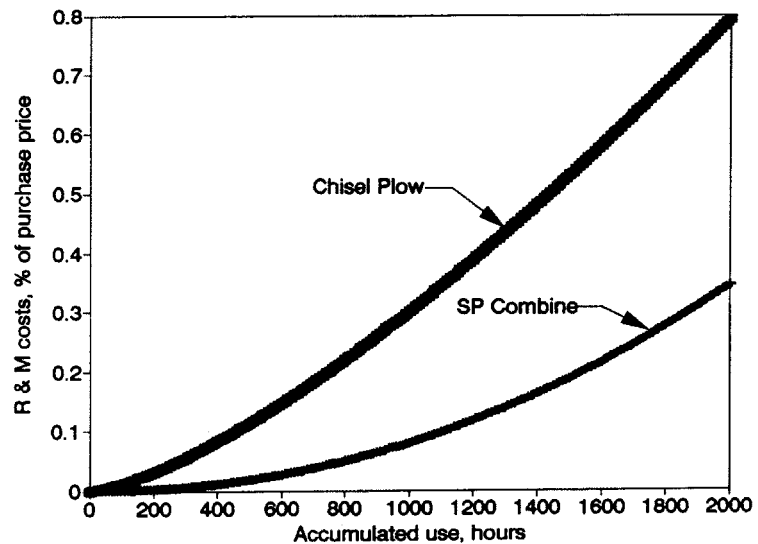
**Figure 15.2 – Accumulated repair and maintenance costs of two machines
as a percent of purchase price of the respective machines.**

hours, using Equation 15.14 to calculate the total repair and maintenance costs over
the life of the machine, and dividing the total by the economic life in hours. Then, by
dividing the average cost by C_a, one can obtain the average repair and maintenance
cost per hectare of area worked by the machine. Repair and maintenance costs are an
important component of total costs. For example, use of Equation 15.14 with the data
in Table 15.1 shows that, for a tractor, the total repair and maintenance costs over the
life of a tractor can equal the purchase price of the tractor. Figure 15.2 illustrates the
accumulation of repair and maintenance costs for two different machines. As a percent
of purchase price, the chisel plow accumulates repair and maintenance costs much
faster than the self-propelled combine. At the end of 2000 hours, for example, the ac-
cumulated repair and maintenance costs for the plow are 79.2% of purchase price. The
corresponding figure for the combine is only 34.3%. However, the purchase price of
the combine is about ten times that of the plow. Thus, in terms of dollars, the accumu-
lated repair and maintenance costs for the combine are over 4 times those of the plow.